MICROCOPY RESOLUTION TEST CHART

NATIONAL BUREAU OF STANDARDS-1963-A

AGARD-LS-124

AD A123450

AGARD

ADVISORY GROUP FOR AEROSPACE RESEARCH & DEVELOPMENT

7 RUE ANCELLE 92200 NEUILLY SUR SEINE FRANCE

AGARD LECTURE SERIES No.124

Practical Considerations of Design, Fabrication and Tests for Composite Materials

JAN 1 8 1983

A

NORTH ATLANTIC TREATY ORGANIZATION

DISTRIBUTION AND AVAILABILITY
ON BACK COVER

AGARD-LS-124

NORTH ATLANTIC TREATY ORGANIZATION

ADVISORY GROUP FOR AEROSPACE RESEARCH AND DEVELOPMENT

(ORGANISATION DU TRAITE DE L'ATLANTIQUE NORD)

AGARD Lecture Series No.124

PRACTICAL CONSIDERATIONS OF DESIGN, FABRICATION

AND TESTS FOR COMPOSITE MATERIALS

THE MISSION OF AGARD

The mission of AGARD is to bring together the leading personalities of the NATO nations in the fields of science and technology relating to aerospace for the following purposes:

— Exchanging of scientific and technical information;

— Continuously stimulating advances in the aerospace sciences relevant to strengthening the common defence posture;

— Improving the co-operation among member nations in aerospace research and development;

— Providing scientific and technical advice and assistance to the North Atlantic Military Committee in the field of aerospace research and development;

— Rendering scientific and technical assistance, as requested, to other NATO bodies and to member nations in connection with research and development problems in the aerospace field;

— Providing assistance to member nations for the purpose of increasing their scientific and technical potential;

— Recommending effective ways for the member nations to use their research and development capabilities for the common benefit of the NATO community.

The highest authority within AGARD is the National Delegates Board consisting of officially appointed senior representatives from each member nation. The mission of AGARD is carried out through the Panels which are composed of experts appointed by the National Delegates, the Consultant and Exchange Programme and the Aerospace Applications Studies Programme. The results of AGARD work are reported to the member nations and the NATO Authorities through the AGARD series of publications of which this is one.

Participation in AGARD activities is by invitation only and is normally limited to citizens of the NATO nations.

LIST OF SPEAKERS

Lecture Series Director: Professor B.Harris
School of Materials Science
University of Bath
Claverton Down
Bath AB2 7AY
UK

SPEAKERS

Dr A.R.Bunsell
Ecole Nationale Supérieure des
    Mines de Paris
Centre des Matériaux
Route Nationale 7, B.P. 87
91003 Evry Cedex
France

Professor R.Byron Pipes
Center for Composite Materials
University of Delaware
Newark
Delaware 19711
USA

Dr G.Dorey
Materials Department
Royal Aircraft Establishment
Farnborough
Hampshire GU14 6TD
UK

Dr J.J.Gerharz
Fraunhofer Institüt fuer
    Betriebsfestigkeit (IBF)
Darmstadt
Germany

Mr J.Huber
Advanced Manufacturing and
    Materials Development
Grumman Aerospace Corporation
Mail Stop A04-12
South Oyster Bay Road
Bethpage, New York 11714
USA

Dr J.M.Thomson
Flight Systems Department
Royal Aircraft Establishment
Farnborough
Hampshire GU14 6TD
UK

CONTENTS

THE NATURE OF FIBRE COMPOSITE MATERIALS

Bryan Harris

School of Materials Science
University of Bath
Claverton Down
Bath AB2 7AY
UK

1. THE IDEA OF A COMPOSITE

The concept is a familiar one even to those not acquainted with theoretical aspects of composites technology. Finely ground wood or silica or chalk are added to plastics moulding materials largely to make them cheaper. Crushed rock aggregate is used in concrete partly to reduce the cost per unit weight of the material and partly to improve its compression strength. Powered magnetic alloys of high coercivity are blended with rubbery polymers to make non-conducting, flexible magnets. The blending of air or gas with metals, with plastics, or with cements results in foamed products of low density. The bonding of plastic film onto steel sheet enables us to confer the natural chemical resistance of the polymer on a structural material which, for the most part, has little inherent resistance to environmental attack.

The purpose in each case is to optimise materials properties by the process of combination. In engineering practice, as indeed in nature, it is a common principle that two or more components may be profitably combined to form a composite material so as to make best use of the more favourable properties of the components while simultaneously mitigating the effects of some of their less desirable characteristics. The principle applies to all kinds of properties -- physical, chemical and mechanical -- and a concommittant benefit of making composites is that the density and perhaps the cost of the product are often lower, matters of importance to the engineers who use these materials.

The science of composites represents in several ways an epitomisation of the broader subject of Materials Science. Practitioners must understand the nature and behaviour of the gamut of substances -- metallic, ceramic and polymeric -- and the interactions between these characteristics. With this knowledge they may manipulate them in combinations whose properties, being determined by their microstructure, ought to be predictable if that microstructure can be adequately characterised. Clearly the properties of engineering materials must be reproducible and accurately known. And since satisfactory exploitation of the composite principle depends on the design flexibility that results from tailoring the properties of a combination of materials to suit a particular requirement, we also need to be able to predict those properties successfully. At the present time some of the more important engineering properties of composites can be well predicted on the basis of simple mathematical models, but many cannot. Elastic behaviour, for example, is successfully treated by existing composite mechanics theories, but toughness, fatigue response and time-dependent behaviour are not. For such properties as these, therefore, the designer must consult available experimental evidence and design with caution. As a result, the full potential for economic use of composites is often lost in the safety factors that are needed to accommodate this state of uncertainty.

The range of possible composites and their applications is enormous and it is not the intention, in this lecture series, to treat the subject exhaustively. Our aim is to concentrate largely on the physical and mechanical characteristics of the practical fibre composites that are most prominently of interest to structural and aeronautical engineers, and to discuss some of their applications in the aerospace field.

Over the past 30 years or so, for reasons that should become clear, the strongest incentive for technological advance in the composites field has been in the development of reinforced plastics. This is a comprehensive term which describes a multitude of materials of diverse character. It embraces high-performance laminates such as epoxide or polyimide resins reinforced with continuous carbon or boron filaments, as well as the humbler, bulk thermoplastic moulding compounds such as Nylon or polypropylene filled with chopped glass fibres. But perhaps the largest group of composites of this type consists of those referred to simply as GRP -- glass fibre reinforced thermoset resins, usually of the polyester variety -- that are currently finding applications in almost all general engineering fields, including transport, building technology, marine engineering, and in the chemical industry for plant and containers. Reinforced plastics (of all kinds) have probably been the subject of the majority of reported research investigations.

Much early experimental work, however, was carried out on metal matrix composites, many of them simply experimental model materials, and the foundation of the theory of composites lies firmly on this work. The practical development of metal matrix composites has been much more restricted, however, than that of the reinforced plastics and those that now seem most promising -- the directionally solidified superalloys containing grown-in fibres of refractory compounds like tantalum carbide, or composites of aluminium reinforced with carbon or boron filaments, for example -- have yet to find practical application on a reasonable scale.

Of reinforced ceramics in general relatively little can be said, for there are serious practical obstacles to the production of useful composites of this kind. The obvious exception is fibre reinforced cement in which there is a waxing interest for architectural purposes if not for structural applications. The jet engine manufacturers continue to hold a watching brief over the possibilities for fibre reinforced high temperature ceramics.

2. THE LIMITATIONS OF CONVENTIONAL ENGINEERING MATERIALS

It is profitless to try to draw up a table of comparative materials characteristics in order to assess their relative strengths and weaknesses. The reason for this is that the generic terms -- metals, plastics, ceramics -- each cover whole families of materials within which the range of available properties is sometimes just as broad as that which we associate with differences between the three classes. A comparison in the most general terms, however, can reveal some of the more obvious advantages and disadvantages of the different types of engineering materials, even though such generalisations can rarely be sustained in the face of more detailed examination. Such comparisons as may be

made are as follows:

- Plastics are all of low density; they lack thermal stability; they have good chemical resistance but only moderate resistance to environmental degradation; they possess relatively poor mechanical properties, but they are easily fabricated and joined.

- Ceramics may be of low density (although some, like TaC, are very dense); they possess great thermal stability and are resistant to most ordinary forms of attack; although intrinsically very rigid and strong, they are all extremely brittle; and they can be formed and shaped only with difficulty.

- Metals are mostly of medium to high density; many have good thermal stability and may be made corrosion resistant by alloying; they have generally useful mechanical properties and high toughness; and they are moderately easily shaped and joined. It is largely a consequence of their ductility and resistance to catastrophic crack propagation that metals, as a class, are the preferred engineering materials.

On the basis of such a superficial comparison it is apparent that each class has certain intrinsic advantages and disadvantages, although metals pose fewer problems for the designer than plastics or ceramics.

In making comparisons we cannot ignore economic aspects of the competition between materials, but the basis on which materials costs are compared will inevitably colour the results. Plastics industry statistics, for example, usually relate to volume production, whereas elsewhere output is discussed in terms of weight. But costs per unit volume, naturally, do not give the same picture as costs per unit weight. For a designer, however, costs are often more realistically related to the ability of a material to sustain a given load or resist a given deflexion. Thus, if the figure of merit chosen is the cost in pence of a component having a strength of 100 MPa, the following approximate league table would be appropriate for the early 1980's.

TABLE 1. COST OF MATERIALS IN TERMS OF STRENGTH

Material	Cost per 100 MPa of strength in pence*
Concrete	0.20—0.40
Timber	0.32—0.40
Wrought steel	0.45—0.84
Ferrous Castings	0.52—1.30
Aluminium	1.50—1.68
Zinc Castings	1.50—1.9
Plastics	1.80—6.50
Fibre Composites	2.26—6.00

*100p = £1 sterling

The figures in a table of this kind may fluctuate considerably over short periods of time, and the cost of hydrocarbon-based plastics is particularly unstable, but it is clear that the load-bearing composites represented in the table are not competing with conventional materials on a straightforward economic basis. Additions of 'cheap' particulate fillers like ground chalk or silica flour are often in order made to reduce the relatively high cost of plastics for applications which call for no reinforcement at all, but sometimes the cost of using even waste products -- like pulverised fuel ash -- is not as low as the consumer could wish. Even the use of air in low density foamed products often seems to require large energy expenditure the cost of which must naturally be passed to the consumer.

3   THE SCOPE FOR REINFORCEMENT OF CONVENTIONAL MATERIALS

In choosing to reinforce an ordinary engineering material, we are effectively selecting the matrix for a composite. This matrix is required to perform several functions, most of which are vital to the satisfactory performance of the composite. Bundles of fibres are, in themselves, of relatively little use to an engineer, no matter how strong or rigid they may be, and it is only the presence of a matrix or binder that enables us to make use of them.

3.1   Functions of the Matrix

(a) The matrix binds the fibres together, holding them aligned in the important stressed directions. Loads applied to the composite are then transferred into the fibres -- the principal load bearing component -- through the matrix, so as to enable the composite to withstand compression, flexural and shear forces as well as tensile loads. The ability of composites reinforced with short fibres to support loads of any kind is exclusively dependent on the presence of the matrix as the load transfer medium, and the efficiency of this transfer is directly related to the quality of the fibre matrix bond.

(b) The matrix must also separate the fibres so that they can act as separate entities. Most reinforcing fibres are composed of solids which are brittle and whose strength is therefore highly variable. When such materials are used in the form of an aggregate of fine fibres not only are the fibres stronger than the monolithic form of the same solid, but there is the additional benefit that the fibre aggregate does not fail catastrophically. The fibre bundle strength is also less variable than that of a monolithic rod of equivalent load-bearing ability. But these advantages of the fibre aggregate can only be realised if the matrix separates the fibres so that the cracks are unable to pass unimpeded through sequences of fibres in contact.

(c) The matrix should protect the reinforcing filaments from mechanical damage (e.g. abrasion) and from environmental attack. Since many resins which are used as matrices for glass fibres permit diffusion of water and certain ionic species this function is often not adequately fulfilled in many GRP materials, and the environmental damage that results is aggravated by the presence of stress. In cement the alkaline nature of the matrix itself is damaging to ordinary glass fibres and it has been necessary to develop alkali-resistant glasses to counter this. For composites operating at elevated temperature, the matrix would naturally need to protect

the fibres from oxidative attack.

(d) A ductile matrix will provide a means of slowing down or stopping cracks that might have originated at broken fibres. although conversely. a brittle matrix may depend upon the fibres to act as matrix crack stoppers.

(e) Through the quality of its grip on the fibres. manifested most directly in the interfacial bond strength. the matrix can be an important means of increasing the toughness of the composite.

(f) By comparison with the common reinforcing filaments most matrix materials are weak and flexible and their strengths and moduli are often neglected in calculating composite properties. But matrix materials like metals are structural materials in their own right and their inherent shear stiffness and compressional rigidity are important in determining the behaviour of the composite in shear and compression.

The potential for reinforcing any given material will depend to some extent on its ability to carry out some or all of these matrix functions. but there are often other considerations. We consider now the likely qualities of various classes of matrix materials.

3.2   Metals

Metals are (arguably) the most versatile of engineering materials and they owe this versatility to the fact that they can be plastically deformed and can be strengthened by a variety of methods which. by and large. act by inhibiting the motion of dislocations. Ironically. as a consequence of the non-directional nature of the metallic bond dislocations are highly mobile in pure metals which are therefore very soft. By controlling the number and distribution of defects. however. the materials scientist can adjust the properties of a metal or alloy system to suit his requirements. There are limitations. however. Increases in strength can usually be achieved only at the expense of the capacity to deform plastically. with the consequence that the strongest alloys lack the vital quality of toughness and are less tolerant of the presence of defects or stress-concentrating design features. Since brittleness is a drawback no designer can afford to underestimate. this leads to the use of large safety factors which. in turn. means that the full potential of high-strength alloys can often not be realised in practice.

Many solid-state hardening methods used in alloys involve producing a material in a metastable state which may subsequently tend to revert to the more stable but unstrengthened condition if sufficient driving force is provided. Thus. alloys strengthened by precipitation hardening. such as the strong aluminium alloys. those depending on phase transformations of the martensitic type. such as steels. and those depending simply on the presence of a high dislocation density. as in heavily cold-worked materials. will all tend to soften at elevated temperatures. The strongest aluminium alloys begin to lose their strength at temperatures little over $150^{\circ}C$. for example. Furthermore. in such metastable alloys the problem of fatigue is intensified because the cyclic deformation generates large quantities of point defects which enhance diffusion and can cause reversion of the metastable alloy structure even at room temperature.

Many conventional metallic systems have the disadvantage of being relatively heavy. For many land-based engineering projects this will be of no consequence. but economic arguments relating to pay-loads (in civil aircraft) and tactical arguments relating to manoevrability (in military aircraft) have always been a powerful driving force for the use of low-density materials in aerospace engineering. In the energy-conscious 1980's the economic incentive for lightening automobiles has already made considerable impact on the motor car designer. For structural applications involving compression or flexural design loads. as opposed to those which are predominantly tensile. the relevant structural stiffness index is not simply Young's modulus. E. or the modulus/density ratio. E/ρ . but may instead be the radios E/ρ^2 or E/ρ^3. For aerospace applications Biggs (1) has shown that modifications to materials that result in lowered density may be more profitable than attempts simply to improve their strength or stiffness. Ashby and Jones(2). discussing these effects in a series of illuminating case studies. show why. for a large telescope mirror. foamed polyurethane could be a serious alternative to the more obvious choice of carbon-fibre reinforced plastic (CFRP) if stiffness. density and cost considerations alone were the determining factors.

The foregoing arguments suggest that it would be worthwhile to attempt to use strong. stable fibres of low density to reinforce (without inducing brittleness) some of the lighter engineering metals and alloys.

3.3   Polymeric Materials

Few polymers are thermally stable by comparison with metals or ceramics and even the most stable. like polyimide. polyimidazole. polybenzoxazole or polyether ether ketone (PEEK) are degraded by exposure to temperatures above about $300^{\circ}C$. There is little that reinforcement can do to combat chemical degradation. but the associated fall in strength and increase in time-dependent (creep or viscoelastic) deformation -- a feature common to all polymers. though less serious in cross-linked resin systems than in thermoplastics -- can be delayed by fibre reinforcement.

A more serious problem in polymers is their very low mechanical strength and stiffness in bulk form: and like metals. the weakest plastics tend to be ductile (or even tough) but the strongest tend to be brittle. although there are exceptions.

Polymers are traditionally insulators and in their application as such strength is usually a secondary consideration. It is increasingly likely. however. that the enhanced electrical and thermal conductivity of plastics reinforced with carbon fibres will be of considerable importance in many aeronautical applications. Most polymers are already low density materials. and the addition of fibres cannot confer any advantages in this respect.

In such materials as these there is the greatest scope for improvement. and it is in the field of fibre reinforced plastics that the greatest successes have already been achieved. There is a thriving. international reinforced plastics industry. for which both the science and technology are highly advanced. although it appears that the general level of awareness of the merits of reinforced plastics on the part of designers in general engineering is very low. The same is not true. however. of the aerospace industry.

3.4   Ceramics and Glasses

Glasses have high chemical stability. but many lose their mechanical strength at relatively low temperatures as they pass through the glass transition (T_g). Special glasses have been developed with high T_g. however. and many are at least as resistant as some of the less stable steels. The principal problem with glassy materials is that they are

always brittle. The difficulty is not that glasses are not strong, for with careful preparation very high strengths can be achieved. The drawback is that they are highly notch-sensitive, and their measured strengths are in consequence subject to wide variation at ordinary temperatures. They are not able to relieve stress concentrations at crack tips by plastic deformation, as strong metals can, and they are not, therefore, fail-safe. A constant disadvantage, aggravated by low thermal conductivity, is that glass usually has poor thermal shock resistance unless, like quartz glass, it also has a low thermal expansion coefficient. Many of these difficulties can, in fact, be overcome by reinforcement with fibres like carbon, and with the added bonus of a saving in weight.

Most ceramics, whether the conventional whiteware and porcelains, or the pure ceramics like Al_2O_3, suffer from the same defects as glasses in the sense that though they are potentially high-strength solids, they are also brittle and highly notch-sensitive. Most ceramics retain their strength to very high temperatures, however, unlike glasses, and several have good thermal shock resistance. Improving toughness and reducing notch sensitivity are perhaps the only reasons for attempting to reinforce such materials, for as Bowen (3) points out the modulus of many ceramics is not very different from that of carbon fibre.

4. STRONG SOLIDS FOR REINFORCEMENTS

A search for materials that should theoretically have high strength and stiffness leads directly to elements or compounds possessing a high density of either pure covalent or mixed covalent/ionic bonds(4). Elements having these characteristics are carbon, boron and silicon; compounds that suggest themselves are ceramics like SiO_2, SiC, Al_2O_3, BN and Si_3N_4. It is of course not coincidental that these are all very brittle solids of low density.

Such materials are unpromising in the bulk form, and it is only when we convert them into fine fibres, eliminating as far as possible the strength-limiting defects normally present in brittle solids, that we obtain strong, rigid materials capable of being used as engineering materials. The most important fibres that are at all widely used in modern man-made composites are glass (SiO_2), carbon, boron and highly drawn polymers like polypropylene, polyethylene terephthalate (Terylene) and aromatic polyamides such as Kevlar 49. In many of these fibres it is possible to obtain strengths, characteristic of the strong covalent bond, which reach a high proportion of the theoretical tensile failure stress, approximately E/20. They are all available in the form of continuous filaments, which facilitates the manufacturing of high performance composites. Continuous fibres of $-Al_2O_3$ and SiC have also been produced in recent years (5). In the early days of composite materials development there was a great deal of interest in the properties of minute monocrystalline whiskers of almost theoretical strength and stiffness, but the problems of producing composites in which a reasonable proportion of this strength and stiffness could be economically utilised lead to early abandonment of their serious consideratrion as reinforcing fibres in favour of continuous filaments (6). Successful methods have, however, been developed for producing high quality laminates from chopped fibres such as carbon, glass and Kevlar-49 which have certain practical advantages over conventional composites (7). The properties of a range of modern reinforcing fibres are given in Table 2.

TABLE 2. MECHANICAL PROPERTIES OF REINFORCING FIBRES

Material	Relative density	Fibre diameter (μm)	Young's Modulus GPa	Tensile strength GPa
Carbon (PAN) HM	2.0	7–10	400	2.0–2.5 (5 cm)
HT	1.7	7–10	200	3.0–3.5 (5 cm)
A	1.9	7–10	220	2.4 (5 cm)
Carbon (mesophase)	2.02	~10	380	2.0–2.4
Boron	2.6	130	400	3.4
α–Al_2O_3(FP)	3.95	20	380	1.4–2.1
SiC (whisker)	3.2	1–50	480	up to 7.0
SiC (organosilicon precursor)	3.2	10	~400	6.0–8.0
		15	~245	3.0–3.5
E–glass (ordinary)	2.5	10	70	1.5–2.0
S–glass	2.6	10	84	4.6
$Fe_{80}B_{20}$(metallic glass)	—	—	100–150	3.6 (yield)
Polyethylene (extended chain, ultra high modulus)	—	—	60	—
Kevlar –29 (PPT)	1.44	12	60	2.7
Kevlar –49	1.45	12	130	2.7
High carbon steel	7.8	250	210	2.8

5. COMPOSITE MATERIALS

Apart from their use in ropes and cables in pure tensile structures fibres are of limited value in structural applications. For this reason, therefore, these strong filamentary materials must be combined with a matrix of metal, plastic, or (less frequently) ceramic so that a substantial proportion of their high tensile strength and rigidity can be utilized in stress systems more complex than simple tension. For composite matrices we may choose weak, ductile metals like aluminium; weak, brittle plastics like the thermosetting epoxides and polyesters; weak, ductile thermoplastics like Nylon; or weak (in tension), brittle ceramics like concrete.

If we choose a low-density matrix for reinforcement by light, strong fibres we can therefore expect to produce strong, rigid composites that are also light and tough, thereby fulfilling, to a greater or lesser degree, all of the engineers' requirements for a modern structural material. The most successful of modern rigid composites are glass and carbon-fibre reinforced plastics (GRP and CFRP), boron-fibre reinforced aluminium, Kevlar-49 reinforced resins, and polypropylene or steel-fibre reinforced cement (5). The most recent developments relate to the combination of two types of reinforcing fibres in a single resin matrix to produce materials known as hybrid composites which carry the opitmization principle even further.

In this lecture series we shall attempt to show the extent to which composites can provide aerospace engineers with satisfactory solutions to some of their design problems. Broadly speaking, three main aspects of the subject have been selected for detailed appraisal. First, we discuss the basic characteristics of the most familiar reinforcing fibres and matrix materials and we show how a knowledge of these characteristics can be used, together with

classical mechanics methods, to predict the strength and stiffness of laminates. Second, we study some longer term environmental effects relating to the use of composites in aerospace applications, discussing their damage tolerance, their fatigue response, and the effects of their exposure to other environmental conditions, including heat and moisture. Of particular importance to designers with this class of materials, by comparison for example with classical metals and alloys, is their response to electrical magnetic fields. And third, we attempt to give our subject practical relevance by discussing some of the manufacturing processes used for aeronautical structures, some of the methods available for non-destructive testing of laminates, and some specific aerospace applications of composite materials.

6.   REFERENCES

1.   Biggs, W.D., (1967), Contemporary Physics, Vol.8, 113.
2.   Ashby, M.F. and Jones, D.R.H, (1981), *Engineering Materials*, (Pergamon Press)
3.   Bowen, D.H., (1968), Fibre Science and Technology, Vol. 1, 85.
4.   Kelly, A., (1973), *Strong Solids*, (2nd Ed.), Oxford University Press.
5.   Watt, W., Harris, B., and Ham, A.,(Editors), (1980), Proc. Discussion Meeting on *Newer Fibres and Their Composites*, Royal Society, (London).
6.   Parratt, N.J., and Potter, K.D., (1980), Proc. Third International Conference on *Composite Materials*, Paris, (Pergamon Press), Vol.1,313
7.   Harris, B., (1981), Metallurgist and Materials Technologist, Vol. 13, 77.

CHARACTERISTICS AND SELECTION OF FIBRES FOR
AEROSPACE LAMINATES

A.R BUNSELL

Ecole Nationale Supérieure des Mines de Paris
Centre des Matériaux
B.P. 87

91003-EVRY CEDEX-FRANCE

SUMMARY

Synthetic fibres have appeared only in recent times, however in forming a new class of material they have also permitted the creation of fibre reinforced composites. Fibres are a form of matter which pocesses physical properties approaching closest to the maximum of those which are theoretically attainable. The physical properties required of the fibres used in composites are strength and rigidity, if possible linked with low density. The strength and Young's modulus of many synthetic fibres depend on their molecular structure and on its arrangement, which is produced during fibre manufacture. Each type of fibre has its advantages for certain types of composites but also some disadvantages including anisotropy and temperature dependance.

INTRODUCTION

The ultimate strength and Young's Modulus of a material depends on the forces which bind its   ic structure together. Materials almost never achieve this absolute strength because of internal defe   and irregularities which provide other mechanisms of failure or produce stress concentrations able to ·   ·me atomic forces with only a nominal stress applied to the material. Only in filamentary form are the·   ·heorical strengths approached. Whiskers which are fine filamentary monocrystals can be observed to attain a   ·re strain of 10% which is approximately the strain necessary to separate two atoms. The strength of w   is strongly size dependant, falling sharply as their dimensions are increased so increasing the proba ·.·   ·f the existence of defects.

Synthetic fibres although not attaining the strenghs predicted solely by atomic theory can be very strong. For example a glass fibre can be five hundred times stronger than the same glass in bulk form. This is because the fabrication process eliminates the irregularities and defects which weaken the bulk glass. These defects occur usually on the surface of a fibre and a simple calculation reveals how fibre production modifies the fibre surface. Fibre production usually involves a stretching process so that a relatively large diameter rod is transformed into a fine filament. If it is assumed that the volume of material does not change during fibre production then changes in surface area may be calculated.
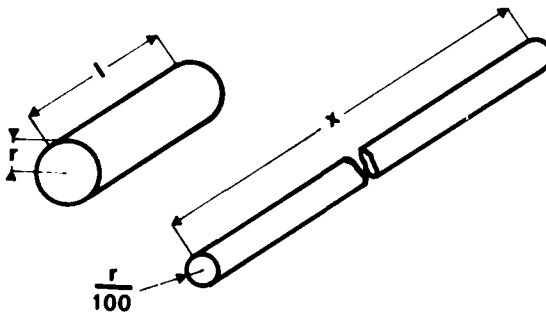

Figure 1 shows schematically the lengthening of the initial rod and the reduction of diameter to one hundredth of its original value. The two volumes can be equated so that

$$\Pi R^2 l = \Pi (\frac{R}{100})^2 x$$

therefore $x = 10000\ l$

The surface area of the rod before drawing is given by

$$(S.A)_1 = 2\ \Pi R l$$

and after drawing $(S.A)_2 = 2\Pi \frac{R}{100}\ 10000\ l$

so that $\dfrac{(S.A)_2}{(S.A)_1} = 100$

Drawing has increased the surface area of the cylinder and the plastic deformation required to produce the new surface has eliminated the mechanical defects which weakened the original bulk material. A dramatic fall in strength can however be produced simply by touching the newly draw glass fibre as the acids in the

skin are sufficient to damage the fibre.

Drawing is very important also for arranging the molecular structure of organic fibres so as to pre-ferentially align the macromolecules along the axial direction. As this alignment is increased so are the tensile properties of the fibre, at least in the axial direction but the structure also becomes increasingly anisc ropic.

The physical properties of organic fibres may be increased by making the basic molecular structures more rigid so that alignment and the use of molecules containing aromatic rings can produce high modulus fibres. Some fibres, such as Kevlar, are of this type and although related directly to textile fibres possess remarkable mechanical properties and are increasingly used in composites.

In order to obtain fibres which possess those properties most sought after for reinforcing composite materials it is useful to again consider the atomic processes involved. Strength and rigidity in a material are linked to the forces of interaction between atoms. These forces depend mainly on the outer valence electrons of the atoms and are not much effected by the atomic nuclei so that strength and rigidity are not related to atomic weight. This means that it is possible to create rigid and strong materials from some of the lightest elements which exist. From this sort of reasoning has emerged first boron and then carbon fibres and in particular the latter are in the process of revolutionising the aerospace industry.

FIBRE DEVELOPMENT

Fibres may be divided into three groups, natural, regenerated and synthetic. Natural fibres, such as cotton and wool, have been used by man throughout history. They can be found both in the plant and animal world and their existence reflects the fibrous nature of all living structures. Evolutionary forces have produced fibres and fibre reinforced structures but it is only recently that man has decided to follow the same line of development for structural materials. Natural fibres may also be found in the inanimate world and asbestos is an example. Although attempts had been made to produce synthetic silk, it was not until the end of the nineteenth century that the first regenerated fibres were made. A regenerated fibre is one which although made artificially uses the long macromolecules existing naturally in the form of cellulose which is usually obtained from wood. After treatement with caustic soda the cellulose is converted into alkali cellulose and then treated with carbon disulphide to convert it into sodium cellulose xanthate which is then disolved in a dilute solution of caustic soda. This solution, known as viscose, is then extruded through fine holes into a coagulating bath of sulphuyic acid to form viscose rayon (1). Altrough rayon has found many uses both textile and industrial it does not possess sufficiently interesting physical properties for it to be used in composites.

It was not until the end of the 1930 s that the first truly synthetic fibres were produced from short simple molecules. These first fibres were polyamides, quickly named nylon, and made by reacting a compound containing two amine groups with another two carboxylic acid groups. The resulting polymer contained re-peated amine groups ($- CONH-$) along the long molecular chains which is the characteristic of nylon fibres.

$$NH_2 \ (CH_2)_6 \ NH_2 \quad + \quad HOOC \ (CH_2)_4 \ COOH$$

hexamethylene diamine   adipic acid

$$\Downarrow$$

$$\dots\dots\dots\dots\dots\dots CONH(CH_2)_6 \quad NHCO \ (CH_2)_4 \dots\dots\dots\dots\dots$$
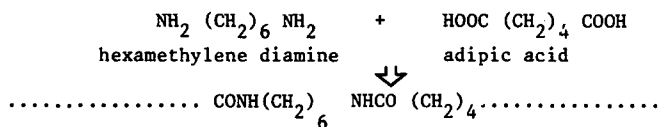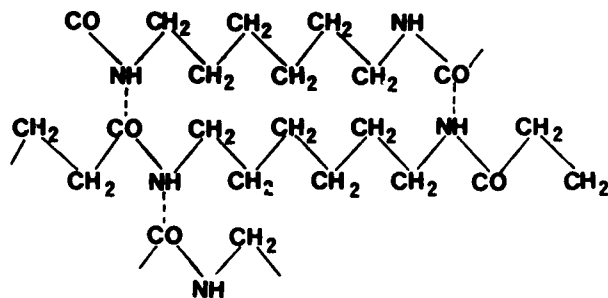
NYLON 66

FIGURE 2 : Molecular structure of Nylon 66 showing intermolecular hydrogen bonding between the CO.NH groups.

Figure 2 shows the linear and hence flexible structure of nylon 66 and also how neighbouring chains are attracted by hydrogen bonding between the $- CO.NH -$ groups. The regular repetition in the molecular chain and the attraction between chains promotes the existence of highly organised regions so the the structure of nylon fibres is about 60% crystalline. Molecular alignment which can be produced by drawing or stretching the fibre during production has a marked effect on final physical properties as is shown by Figure 3. As molecular alignment parallel to the fibre axis increases so does strength and Young's modulus but at the expense of strain to failure.

Drawing of nylon fibres takes place during fibre manufacture which begins with the melting of nylon chips so that the molten polymer can then be forced through the small holes of the spinneret. As the threads of molten polymer leave the spinneret they are cooled and solidified by contact with a stream of cold air and form solid filaments. These filaments are then drawn between two rollers rotating at different speeds so as to stretch the filaments into fine fibres.
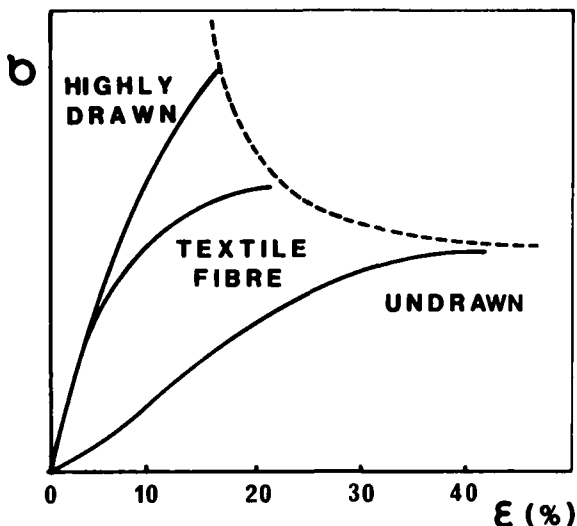
FIGURE 3: The stress (σ)-strain (ε) curves of undrawn, medium drawn and highly drawn fibres of the same polymer. As molecular orientation increases so does modulus but at the expense of breaking strain.

The polyamide molecule shown in Figure 2 is inherently flexible and a more rigid end product could be hoped for if a less flexible molecule were used for fibre manufacture. For this reason it is interesting to look at the second important synthetic fibre which was produced in the late 1940s which was polyetheylene terephthalate or simply polyester. The basic unit of the polyester molecule is shown in Figure 4 and it can be seen to contain a benzene ring which has the effect of stiffening the chain(2)Polyester fibres with similar drawing rates possess a higher Young's modulus than is found with nylon fibres.

POLYESTER (polyéthylénetéréphthalate)
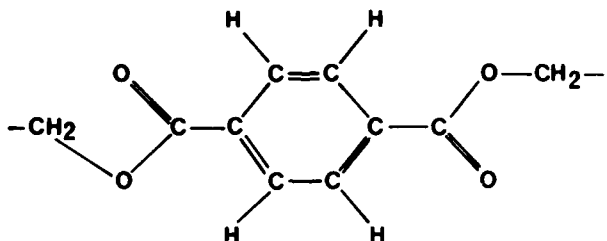
FIGURE 4 : The polyester molecular structure is not as flexible as the linear nylon molecule so that polyester fibres possess an inherently higher Young's modulus than do nylon fibres.

Following the production of the first synthetic fibres others have been produced with increasingly complex molecular forms. Aromatic polyamides such as "Nomex" were produced. These more complex polymers,based on more rigid molecular structures containing benzene rings, can be used at higher temperatures than is the case with nylon and polyester which melt around 260°C. Nomex can be used up to about 370°C and does not melt but carbonises.

As well as increasing thermal properties the more rigid molecular structure of aromatic polyamides has been used to create mechanically very strong fibres which have a high Young's modulus. The best known example of this ARAMID family of fibres is Kevlar made by Du Pont de Nemours. Figure 5 shows the tensile curves of several fibres and it soon becomes evident that the aramid fibre marks a remarkable departure from other organic fibres both in strength and Young's modulus.

ARAMID FIBRES

Aramid fibres of which the best known is the Du Pont's fibre Kevlar form a class of fibre which may be used as reinforcements in composites materials. Aramids do not melt so cannot be spun from the melt but can be dissolved in powerful solvents (3, 4). The molecular organisation of the solution which is formed is very important in determining the final fibre properties. In the case of Kevlar the solution is poly (p-phenylene Terephthalamide) or simply PPD-T. Dilute solutions are isotropic but as the solution concentration is increased spontaneous ordering of rod-like molecules takes place giving rise to an anisotropic mesophase.

The molecular structure of Kevlar is given in Figure 6 and it can be seen to be rigid with little possibility of bending occuring (5). It has been shown that the molecular structure of Kevlar fibres is in the form of radially arranged pleated sheets (6). The rod like molecules are greatly ordered to produce a highly crystalline structure having the basic unit of that shown in Figure 7.

The kevlar fibre is highly anisotropic being very strong and rigid in the axial direction but weak in axial (8) and radial compression (9). The high modulus form of the fibre Kevlar 49 does not creep very much and is not easily broken by tensile fatigue (10). Figure 8 shows the creep behaviour of a simple Kevlar-49
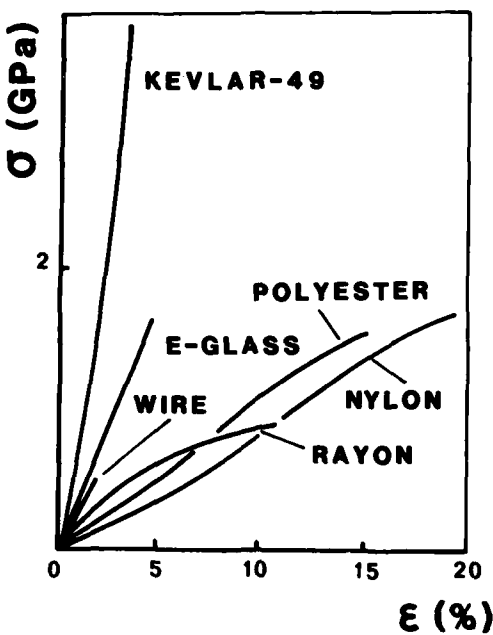
FIGURE 5: The aramid fibre Kevlar-49 has a much higher Young's modulus than other organic fibres

ARAMIDES

KEVLAR (p-phenyleneterephthalamide)
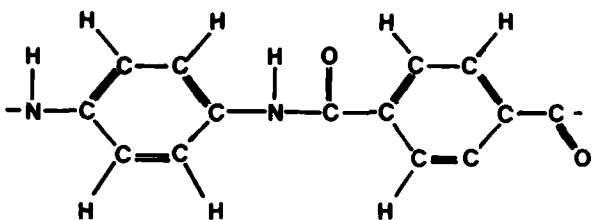
FIGURE 6 : The molecular structures of Kevlar.
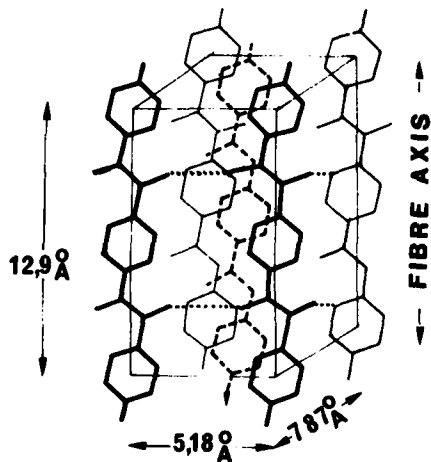
FIGURE 7: The basic crystalline structure of Kevlar.

fibre. Single Kevlar fibres have a diameter of about 13 μm and are circular in cross section. It is normal to find a wide scatter of physical properties when testing fibres and Kevlar fibres are no exception in this matter. The scatter in tensile properties of Kevlar fibres must be considered as a material property due to the defects which can be observed on the fibres, sometimes these defects are

large enough to be seen with the naked eye and probably exist at all scales down to the molecular level(11). Kevlar fibres fibrillate greatly on failure (10, 11) except when they have been bent. Bending produces kink bands in the fibre. These are lines of plastic deformation and the bending of Kevlar fibres seriously weakens them and can result in a more localised fracture point than is normally seen if subsequently tested in traction (12).
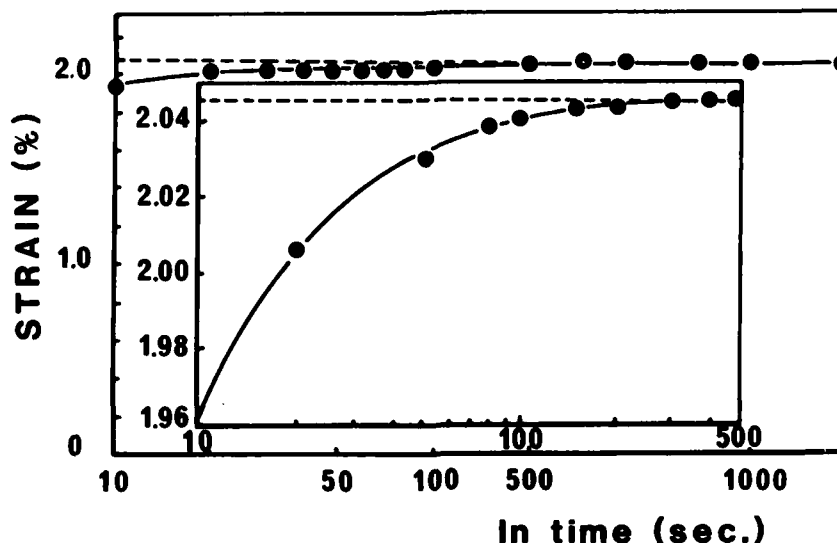

FIGURE 8 : The creep behaviour of Kevlar-49 loaded to 85% of breaking load.

There is no minimum bending radius of curvature for Kevlar fibres as the concave side of the bent fibre undergoes gross plastic deformation (8). In this way the fibre may be completely bent back on itself to a zero raduis of curvature without failing.An elastic fibre would of course break when the convex surface reached its breaking strain. The bending behaviour seen with Kevlar fibres reflects the basic weakness of the fibre in compression but does mean that the fibre has high tenacity which can be turned to an advantage. On the other hand the fibre is difficult to cut. The weak radial strength of the fibre also renders it sensitive to abrasion.

The Kevlar fibres are chemically inert in most environments although attacked by sulphuric acid and degrading in sunlight. The fibre is very stable up to 100°C with practically no change in strength or in Young's modulus. Both these parameters fall slowly up to 300°C at which the strength and the modulus have approximately 75% of their values at room temperature. Above 300°C an abrupt fall in properties is observed.
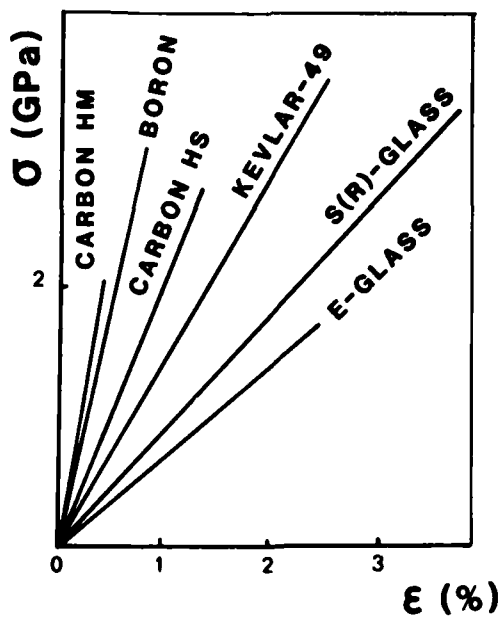
Figure 9 which compares the tensile curves of different reinforcing fibres shows that Kevlar-49 fibres are very well placed amongst the most common fibres used in composites. In addition its low density means that its specific properties (the property divided by the density) are particulary interesting as shown in Table 1. For the same weight a Kevlar fibre is five times stronger than steel when measured in air and thirty times stronger in water.

	Strength GN/m^2	Modulus GN/m^2	Breaking strain %	Density g/cm^3	Specific strength km	Specific modulus km
Kevlar 29	2.60	62.0	4.2	1.44	190	4300
Kevlar 49	2.70	130.0	2.0	1.45	190	9000
Polyester HiT	1.40	12	15	1.2	116	1000
Nylon T 728	1.00	5.6	18.5	1.14	88	500
Nomex	0.65	20.0	23.0	1.38	47	1450
Steel	2.80	200.0	2.0	7.83	36	2550
Boron	3.00	370.0	1.0	2.70	110	14000
Glass	3.50	70.0	4.8	2.54	137	2750
Carbon HS	2.70	270.0	0.8	1.80	150	15000
Carbon HM	2.00	400.0	0.5	1.95	108	20000

TABLE 1 : comparison of fibre properties.

The kevlar -49 fibre is finding increasing use in composites but the type of structure for which it can be used is restricted by the physical limitations of the fibre. The fibre may be handled like any other textile fibre and so may be wound around a preform without difficulty. One of the most successful uses of Kevlar-49 has been in filament wound pressure vessels whether rocket motors or other wise. This seems an ideal application for the fibre as it is subjected only to tensile forces due to the internal pressurisation of the vessel.

In other applications Kevlar is mixed with other usually more brittle fibres to form hybrid composites in order to increase the toughness of the composite structure and so reduce the problem of shock loading experienced with some composites. The inherent toughness of the fibre has been used in the production of flack jackets.

Kevlar 49 is a very interesting fibre and is increasingly used in composites. It is lighter and stiffer than glass but is priced between glass fibre and the higher modulus carbon and boron fibres. It will be used for secondary structures in the aerospace field, such as interior panels, access doors, flooring, rudder and fuselage skins. Kevlar 49 will be incorporated for example into helicopter blades and drive shafts probably combined with carbon fibre, Kevlar will not be used in primary structural parts, except in the case of the pressure vessel, because of its low compressive strength.

GLASS FIBRES

Glass fibres are the most widely used fibre in composite materials and were the first continuous fibre to be used for such a role. They come with different diameters and chemical compositions for a variety of purposes. The chemical structure of glass is based on that of silica (SiO_2) with additions of oxides of calcium, boron, sodium, iron and other elements. The structure of glass shows no long range ordering at the molecular level but consists of a three dimensional array of atoms.

Soda-lime glass used for windows and bottles can be drawn into filaments at temperature above 750°C but is weak and brittle so is rarely used in the form of fibres. The most commonly employed glass used for fibres is known as E-glass and typically has the following composition SiO_2 54.4%, Al_2O_3 14.4%, CaO 17,5% MgO 4.5%, B_2O_3 8.0%, K_2O 0.5%, Fe_2O_3 0.4% and F_2 0.3%. E-glass was originaly developed for its electrical properties but as it is relatively strong and stiff as well as drawing well it is widely used as a textile and reinforcing fibre. Some physical properties of E-glass can be seen in Table II together with details of other more specialised glasses (13).

Glass fibre types

Glass type	E	Sor R	D	C	M
Density	2.54	2.49	2.16	2.49	2.89
Strength (20°C) GPa	3.5	4.65	2.45	2.8	3.5
Youngs Modulus (20°C) GPa	73.5	86.5	52.5	70	111
Strain to failure %	4.5	5.3	4.5	4.0	3.1

TABLE II
A composition of the mechanical properties
of several different types of glass fibre.

Glass fibres are made by drawing from the melt as are many organic fibres. They are drawn at very high speed some hundreds of metres per second down to filaments which usually have diameters between 5 and 20 μm. This rapid cooling produces fibres which have a more open molecular structure than is found with bulk glass. For this reason reheating of glass fibres produces a slight increase in density. Glass fibres are easily damaged by abrasion, being brittle, so an integral part of fibre production is coating with a size which protects the fibre surface and holds the strands together. The coating may be permanent if for example the fibres are to be used for textile purposes or may be removed after handling of the fibre is completed when a coupling agent can be applied to help bonding to the matrix for making a composite.

Altrough E-glass is widely used for reinforcing fibres it has a low Youngs modulus when compared its some other fibres so that for some high performance applications other forms of glass are used. It is possible to increase the modulus of glass fibres by partial recrystallisation of the surface by redrawing through an oven (14). Usually however type S glass is used which has a composition based on 65% SiO_2, 25% Al_2O_2 and 10M MgO. It will be seen from Table II that S glass (known as R-glass in France) produces a fibre which has a higher Young's modulus and strength than has E-glass.

The other glasses shown in table II have been produced for very specialised applications and their composition decided upon so as to give : D-glass which is transparent to electromagnetic radiation having a particularly low dielectric constant; C-glass which has particularly good chemical resistance for use with corrosive material and M-glass which contains BeO which produces a particularly high elastic modulus.

Glass fibres may be obtained in a variety of forms. The least expensive form of continuous glass fibre is STRAND or ROVING which is a group of strands not twisted together but in the form of a ribbon. Roving can be used in filament winding processes. The fibres can also be cut into short lengths usually 5 mm to 50 mm in length. These chopped glass fibres can be sprayed immediately after chopping together with a liquid resin against a mould to build up a reinforced structure. Alternaively chopped fibre may be converted to a lightly bonded preform of the final object by collection of the short fibres with a small amount of resin. The preform can there be heated to cure the bonding resin and then impregnated with resin under pressure.

Chopped glass fibres can also be mixed with resin for to make dough or sheet moulding compounds (DMC and SMC) which may be press-moulded in the final product shape.
Continuous glass fibres may be allowed to fall randomly on to a moving belt to form a non-woven mat which may then be impregnated or alternatively and more expensively they may be woven into cloth. Woven glass fibre sheets allow high fibre volume fractions to be achieved.

Glass fibres are by far the most widely used reinforcing fibre for composites because of their ease of manufacture, relative low cost and ease of handling. The fibres suffer greatly however from a relatively low Young's modulus and high density producing composites with unimpressive specific properties as can be seen in Tables I and III.

	Density	Tensile strenth GPa	Young's Modulus GPa	Specific strength	Specific Modulus
35NCD16 Steel	7.9	1.85	200	0.24	25
Al ASG(6061)T6	2.7	0.35	70	0.13	26
Al AU4G1(2024)T4	2.8	0.59	73	0.21	26
Al A25G4(7075)TG	2.8	0.45	76	0.16	27
Ti TA6V	4.4	1.14	119	0.26	27
Be (sheet)	1.9	0.78	295	0.41	155
COMPOSITES					
Boron-Epoxy	2.1	2.0	270	0.95	129
Boron-Aluminium	2.7	1.25	225	0.46	83
Graphite-Epoxy	1.7	1.0	200	0.59	118
Carbon-Epoxy	1.5	1.3	140	0.87	93
Kevlar-Epoxy	1.35	1.5	80	1.1	58
Glass-Epoxy	2.2	1.09	39	0.5	18

TABLE III :

Comparison of mechanical properties of composites
and some metals alloys.

Glass fibres are of course insulators and composites based on these fibres have found important applications as such in electric motors, generators and as insulation for high voltage power lines. Both types E and S glass fibres are used in the aeronautic industry, increasingly with an epoxy resin matrix. Applications include, rocket motor casings made by filament winding, rocket launchers, aircraft flooring and a most important use in helicopter blades.

The replacement of metal helicopter blades by one made from composite materials has revolutionised helicopter blade technology. The average lifetime of such blades is now longer than the expected lifetime of the aircraft. In addition any damage to the blades becomes evident by a fall in their flexural rigidity which is easily seen. Although other types of fibre are now included in the make up of these blades glass fibres remain the most important element and the advantages of composites was demonstrated on wholly glass fibre reinforced resin blades. That composites have proved to be such an outstanding success in a structure which is subjected to extreme loading and vibration conditions and one which requires such high reliability

is a major achievement (15).

BORON FIBRES

Boron is the fifth element in the periodic table and is the second lightest element which is solid at room temperature. The lightest solid element, beryllium, is unsuitable for making fibres as it is very fragile, has less than remarkable specific properties and is toxic. In the early 1960s, it was therefore considered that boron, which could be made into fibres, had an assured future as reinforcement in advanced composites. Several years after the appearence of boron fibres came carbon fibres which have however replaced the boron fibre in nearly all the applications originally forseen for them. They are still used however in some structures and do possess remarkably high mechanical properties.

Boron is too hard and brittle to be drawn into filaments and so is made into fibres by interacting hydrogen and boron trichloride at 1500° K so as to deposit boron on to an electrically heated tungsten wire, as shown in Figure 10. The tungsten filament has a diameter of the order of 10 μm and is itself a costly item. The surface of the tungsten wire is not smooth and it is on the peaks of the irregularities that the deposition starts. This leads to the possibility of defects in the form of voids developing at the tungsten boron interface as the boron nodules develop (16). Fibres are produced at a speed of the order of 150 meters per hour and during the time that the tungsten wire passes in the deposition chamber a boron fibre of usually 140 μm or 200 μm is produced by the growth of boron nodules. The surface of the fibre reflects the nodular make-up of the fibres and the irregularities in the surface are the major source of breaks (17). It is for this reaon that precise temperature control is required during manufacture as the rate of a nodule growth would lead to greater local surface irregularities ans stress concentrations. This effect is particularly pronounced if a cheaper carbon fibre substrate is used as local hot spots occur on the carbon fibre during electrical heating.
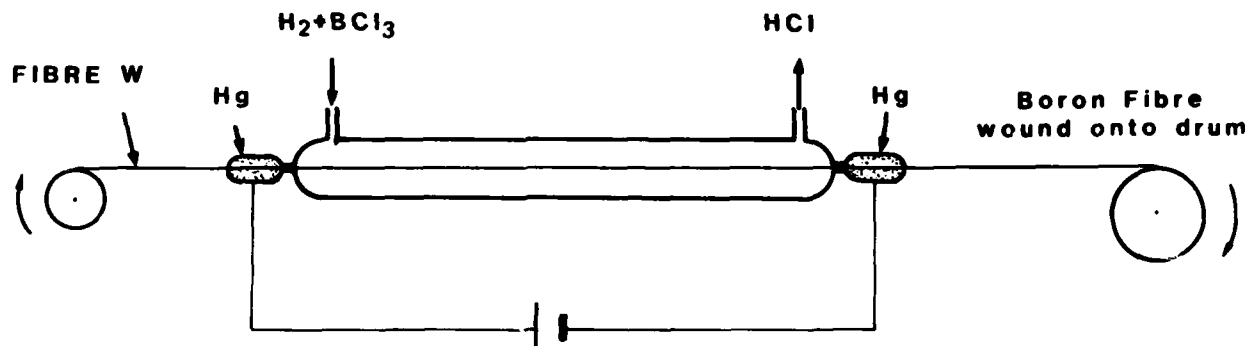

FIGURE 10: Schematic view of boron fibre production.

Early production techniques produced boron fibres of 100 μm diameter but these were found to split longitudinally (18). This problem was resolved by moving to the bigger diameters of 140μ m and 200 μm although if these fibres are compressed during composite manufacture they can also split (19).

The boron fibre is therfefore a composite structure in itself. The small boron atoms prenetrate the tungsten core during deposition to form tunsgten borides and the swelling which results puts the core into compression whilst the boron in the neighbourhood of the interface is put into tension. A final quenching stage puts the fibre surface into compression.

Boron fibres are particularly interesting for metal matrix composites and two versions of the fibre are produced for this purpose. These fibres either have a surface layer of boron carbide (B$_4$C) or silicon carbide (SiC) which prevents degradation of the boron by interaction with the metal matrix during hot pressing.

Boron fibres are by for the thickest fibres used normally for composites having a diameter of 20 times that of a carbon fibre. It is probably because of the difficulty of bending the fibres that they are so strong in compression. The fibres are also strong in tension and have a very high Young'sModulus as can be seen from Table 1.

Although boron fibres can be put into a wide variety of matrices and have reinforced epoxy resins for certain aircraft structures, their main interest is for metal matrix composites. There are no great difficulties in producing boron fibre reinforced aluminium or titanium as is the case with other fibres such as carbon. Boron fibre reinforced aluminium in the form of tubes plays a vital role in the structure of the American space shuttle and there is interest in using such tubes in aircraft undercarriages.

CARBON FIBRES

Since their introduction in the late 1960 s carbon fibres have not ceased to increase in importance in the aerospace industry and are now being studied closely by other types of industry.

Carbon fibres are in a sense one of the oldest types of synthetic fibres as the filaments in the earliest electric light bulbs were made by the carbonisation of cotton fibres. Present day high performance carbon fibres are made by the carbonisation of the organic fibre polyacrylonitrile which is not allowed to contract during the process.

Polyacylonitrile has a molecular make up as shown in the first stage of fibre production shown in Figure 11. It is a fibre which has an atactic structure but which never-the-less can be arranged by drawing so that the long chain molecules are almost parallel to the fibres axis. The fibre does not melt but carbonises on heating which is also the case of rayon, another fibre which has been used for carbon fibre manufacture but which is rarely now used.

(a)

(b)

(c)
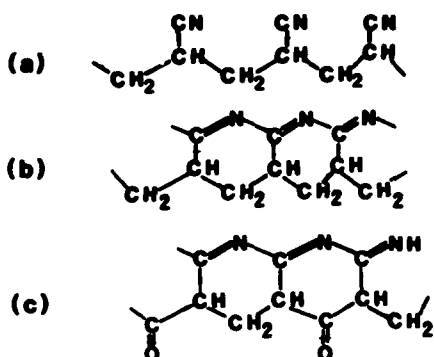
FIGURE 11 : Initial stages of the conversion of polyacrylonitrile into carbon fibre.

The polyacrylonitrile is heated in an inert atmosphere to around 250°C which produces the ladder type arrangement shown in the second stage of fibre production in Figure 11. Further heating up to about 600°C in air oxidises the structure as can be seen in Figure 11. Further heating still, above 1000°C, produces a carbon fibre. A final process is a surface treatement by oxidation to improve bonding with the matrix. Figure 12 shows that the final mechanical properties obtained are strongly dependent on the final temperature attained. The strength of the fibre passes through a maximum around 1500°C whilst the Young's modulus increases continuously with increasing temperature (20). In this way it is possible to obtain a family of fibres. In general two types of fibre are considered. Those which are produced around 1500°C are known as high strength fibres and those at 2000°C or above high modulus fibres. It is common amongst some research workers to speak of graphite fibres and to use the term indiscriminantely for both types of fibres. As graphite implies a certain type of structure it should only be used for the high modulus fibre which can be assumed to have a structure more closely resembling that of graphite than is the case for the high strength fibre.
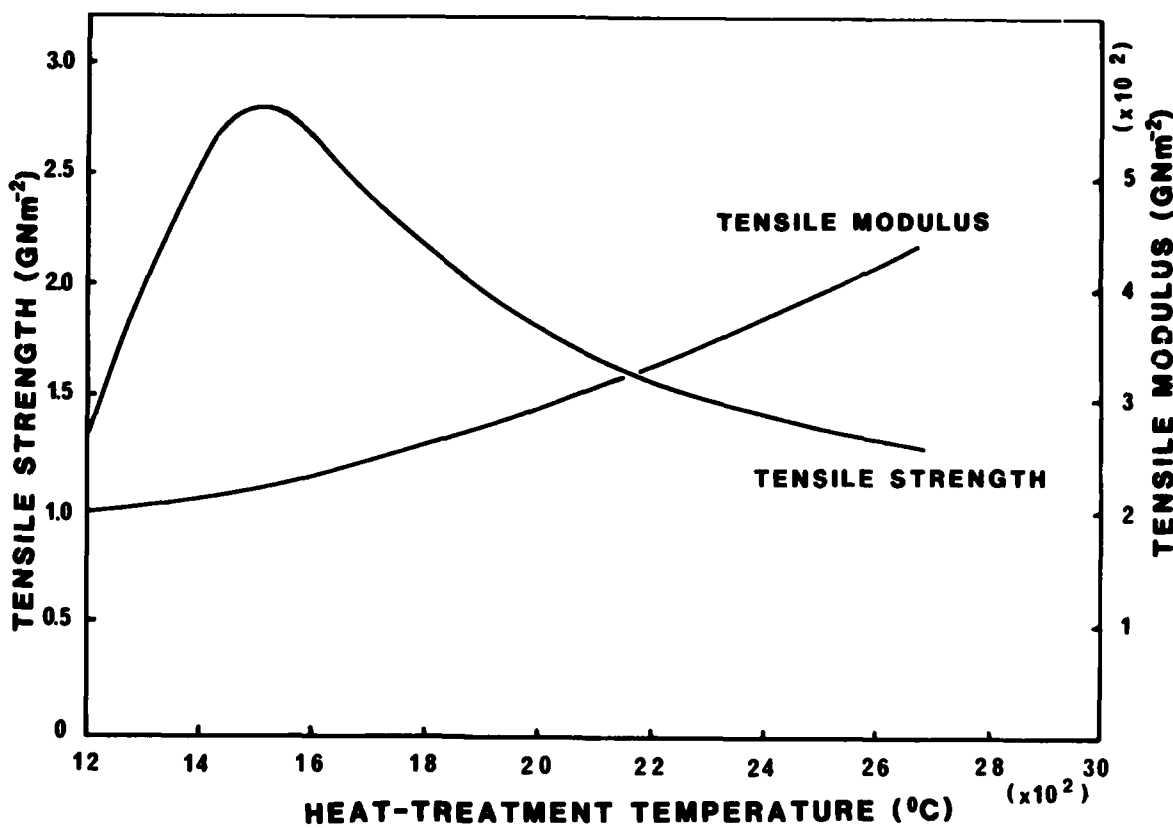

FIGURE 12 : The properties of carbon fibres depend greatly on the temperature of pyrolisis.

The possibility exists of making carbon fibres from the residue left after refining oil. These fibres made from pitch should become interesting if a large volume market develops for carbon fibres as under these conditions this type of fibre could be considerably cheaper than the fibres made from PAN (21). Carbon fibres are fine, having a diameter of about 7 μm and although this means that each individual fibre breaks at a low load it does mean that they are very flexible and can be wound around complex preforms. The fibres are made in bundler of 1000, 3000, 10000 fibres and for some uses in 160 000 or 320 000 fibre tows. Only the finer tows are normally used in the aerospace industry.

Carbon fibres are usually used together with organic matrices both thermosetting resins and thermoplastics and there is some interest in putting them into an aluminium matrix (22). Corrosion in the presence of

humidity is one problem where carbon-aluminium is concerned as a voltaic cell is set up between fibre and matrix. Carbon fibres can also be used to reinforce a carbon matrix and the carbon-carbon composite can be used to very high temperatures in excess of 3000°C.

The expansion coefficient of carbon is not constant but varies with temperature. In a direction parallel to the fibre axis the coefficient is negative being $-3 \times 10^{-7} K^{-1}$ at $-150°C$ and $-10 \times 10^{-7}K^{-1}$ at $150°C$. Variations in the radial direction are from $2 \times 10^{-5}K^{-1}$ at $-175°C$ to $7.5 \times 10^{-5}K^{-1}$ at $150°C$. These variations are not linear but follw S-curves. This gives the designer the possibility of producing a composite with a required expansion coefficient by using the fibre orientation to control the coefficient of expansion. In this way it is possible to envisage a carbon fibre composite with a zero expansion coefficient.

Carbon fibres are finding increasing numbers of applications in and outside the aerospace industry because of their high specific properties. The aerospace community now seems to have accepted carbon fibre reinforced plastics as an almost traditional material and it is being used in increasingly critical areas including fuselage and wing sections (23). The original uses of carbon fibres reinforced plastics in aircraft were as secondary components such as access panels, speed brakes, rudder and elevator components and wing tips. Now it is predicted that carbon fibre composites will make up 40% by weight of the next generation of military planes, leading to 20-25% weight saving and a cost saving of 5-10%.

HIGH TEMPERATURE AND CERAMIC FIBRES

It has already been mentioned that carbon fibres may be surrounded by a carbon matrix and that the resulting carbon-carbon composite can be used at extremely high temperatures in excess of 3000°C. There are two other main candidates as reinforcing fibres for composites for use in the temperature range around 1000°C. These are aluminia fibres and silicon carbide fibres.

Aluminia has a melting point at 2045°C and can be made into fibres of which one is the Du Pont's F P fibre. This fibre is one hundred per cent α-aluminia with a purity in Al_2O_3 of 99%. The manufacturers claim a Young's modulus of around 350 GPa, a breaking stress of about 1500 MPa and a density of 3.9. The fibres are extremely bittle and difficult to handle although they can be woven into a cloth (24).

They have a diamenter of about 20 μm. These aluminia fibres may be of interest in reinforcing metals for use at temperatures up to 700-800°C.

Nicalon is the name given by Nippon Carbon Company to their silicon carbide fibre made in an analogous manner to the carbon fibre by pyrolysis of an organic precursor which is a poly carbosilane, crosslinked at 200°C then heated in an inert atmosphere to 1300°C (25,26).
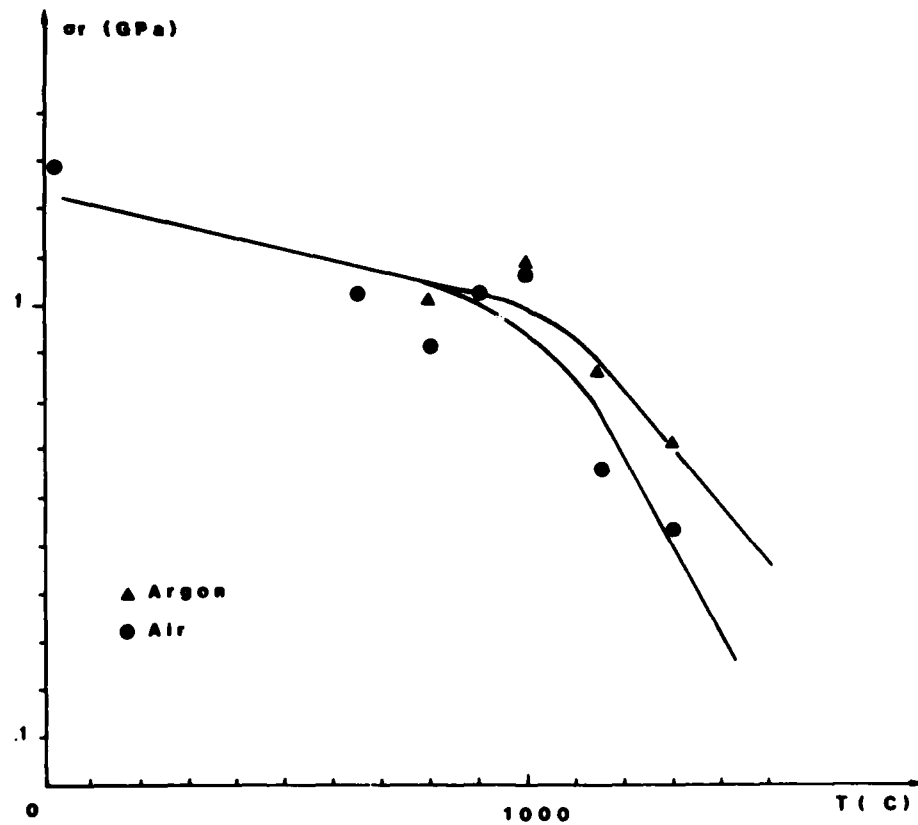
FIGURE 13 : The strength of SiC fibres as a function of temperature.

As Figure 13 shows the fibre retains most of its strength up to about 1000°C althrough above this temperature the fibre's properties fall off sharply (27). The behaviour of the fibre above 1000°C and an analysis of its structure shows that the fibre is not pure SiC however it is thought that it may well be of use in reinforced ceramics for high temperature applications.

REFERENCES

(1) A.M. Collier, Hanbook of textiles,2, Oxford, Pergamon (1974).

(2) W.E. Morton and J.W.S. Hearle, Physical Properties of Textile Fibres, 2, London, Heinemann (1975).

(3) P.L. Wagner. High Performance aramids, UMIST Symposium June 23-25 (1981).

(4) W.B. Black and J. Preston, High Modulus Wholly Aromatic Fibres, New York, Marcel Dekker (1973).

(5) T.T. Chiao, L. Penn and H.A. Newey, Chemical Characterisations of a high performance organic fibre J. Mat. Sci. Letters 11, 190 (1976).

(6) M.G. Dobb, D.J. Johnson and B.P. Saville, Supramolecular structure of a high modulus polyaromatic fiber. J. Poly. Sci. Polym. Phys. Ed. 15, 220 1 (1977).

(7) M.G. Northrolt, X-ray diffraction studies of poly (p-phenylene terephthalamide) European Poly. J. 10, 799, (1974).

(8) J.H Greenwood and P.G. Rose, "Compressive behaviour of Kevlar-49 fibres and composites". J. Mat. Sci 9, 1804 (1974).

(9) M. H. Lafitte and A.R. Bunsell " Comportement en torsion des fibres de Kevlar-29 " Colloque Int CNRS No. 319 Comportement plastique des solides anisotropes. 16-19 June 1981 in Villard-de-Lens-France.

(10) A.R. Bunsell " The tensile and fatigue behaviour of Kevlar-49 fibres " J. Mat. Sci. 10, 1300 (1975).

(11) M.H Lafitte and A.R. Bunsell " The fatigue behaviour of Kevlar-29 fibres J. Mat. Sci. To be published (1982).

(12) M. G Dobbs , D.J. Johnson and B.P. Saville " Compressional behaviour of Kevlar fibres " Polymer 22, 960 (1981).

(13) L.J. Broutman and R.H. Krock " Modern Composite Materials" Addison-Wesley Pub.Co. 1967   280-334.

(14) F.J. Trojer " High modulus glass-ceramic fiber ". Proceedings of ICCM-1 AIME (1975) 54-63.

(15) M. Torres " Les pales d'hélicoptères en composites : conception, réalisation et comportement en opération ". Advances in Composite Materials Vol II Ed. A.R. Bunsell, C. Bathias, A. Martrenchar, D. Menkes and G. Verchery . Pergamon Press (1980). 1465.

(16) J.Vegga-Boggio and J.D. Carlsson " The inital stages of growth and the origin of proximate voids in boron fibres . J. Mat. Sci. 12, 1750 (1977).

(17) J.Vegga-Boggoi and O. Vingsbo " Tensile strength and crack nucleation in boron fibres". J. Mat.Sci. 11, 273 (1976).

(18) C.I. Lyrch and J.P. Kershaw " Material Matrix Composites" CRC Press. (1972).

(19) A.R. Bunsell and T.T. Nguyen " The radial strength of boron fibres and fibre splitting in boron-aluminium composites ". Fibre Sci. Tech. 13, 363 (1980).

(20) D. Hull " An introduction to composite materials " Cambridge University. Press (1981) 9-15.

(21) H.N. Townsend "High-modulus, high performance carbon fibre from pitch precursor". Advances in Composite Materials Vol 1 Ed.A.R. Bunsell et al Pergamon Press (1980) 453.

(22) E.M. Trewin and R.F. Turner " Carbon fibre reinforced thermoplastics a cost effective material for the 80's". Advances in Composite Materials Vol II. Ed.A.R. Bunsell et al. Pergamon Press (1980) 1796.

(23) R.H. Hammer " Composites in the Boeing 767 ". Advances in composite materials Vol II. Ed A.R. Bunsell et al. Pergamon Press (1980) 1452.

(24) A.R. Champion, W.H. Krueger, H.S. Hartmann and A.K. Dhingra " Fiber FP reinforced metal matrix composites ". Proceding of the 1978 International Conference on Composite Materials B.R. Noton, R.A.Signorelli, K.N. Street and L.N. Phillips AIME (1978) 883.

(25) S. Yajima, Y. Hasegawa, J. Hayashi and M. Iimura " Synthesis of continuous silicon carbide fibre Part 1 synthesis of polycarbosilane as precursor ". J. Mat. Sci. 13, 2567 (1978).

(26) Y. Hasegawa, M. Iimura, S. Yajima " Synthesis of continuous silicon carbide fibre Part 2 Conversion of polycarbosilane fibre into silicon carbide fibres ". J. Mat. Sci. 15, 720 (1980).

(27) G. Simon and A.R. Bunsell " Caractérisation mécanique en traction de fibres de carbure de silicium pour la réalisation de composites à matrice céramique ". Compte renu des troisièmes journées nationales sur les composites (JNC-III). Ed. C. Bathias, A.R. Bunsell, A. Corvino, D. Menkes, E. Verchery AMAC (1982).
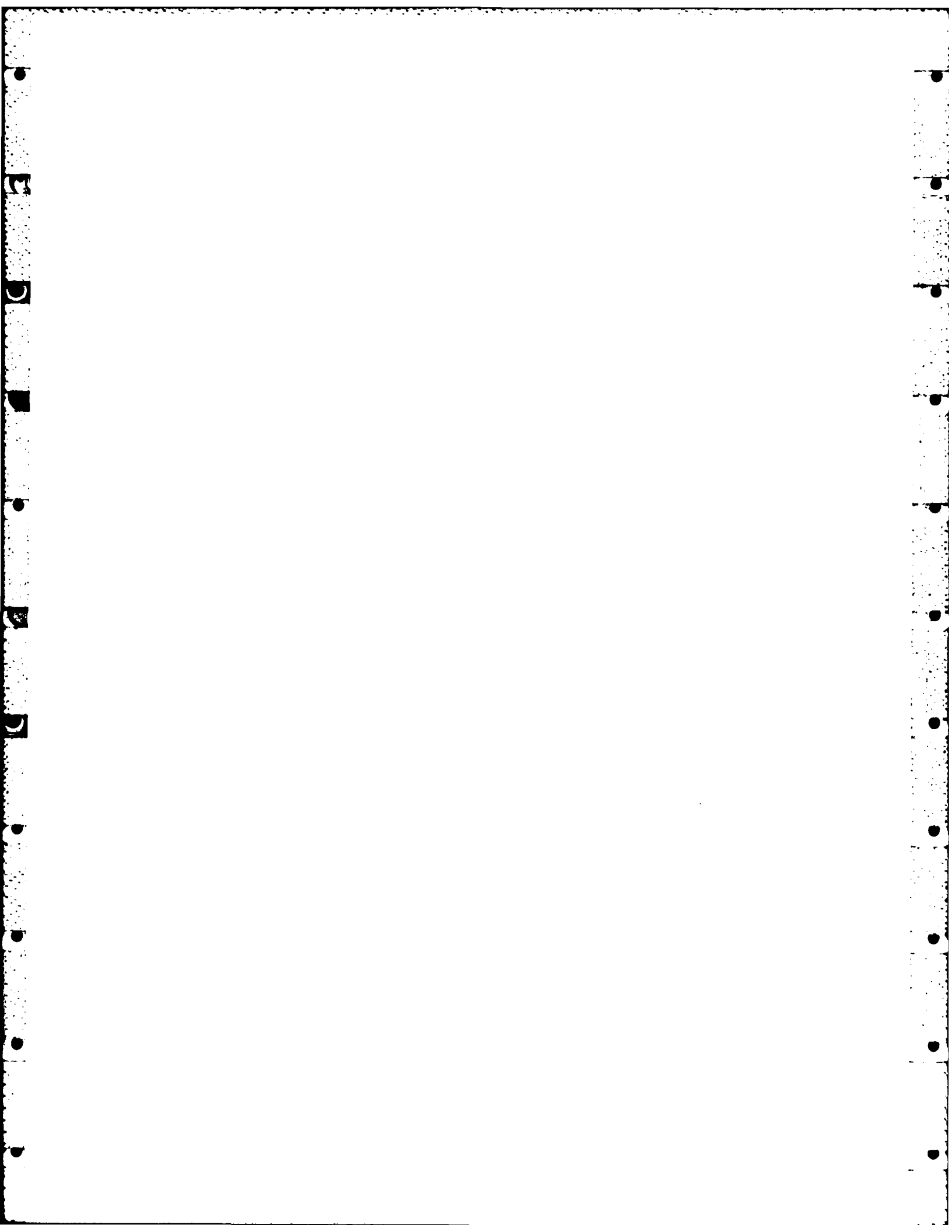
THE ROLE OF THE MATRIX

A.R BUNSELL

Ecole Nationale Supérieure des Mines de Paris
Centre des Matériaux
B.P. 87

91003-EVRY CEDEX-FRANCE

SUMMARY

A composite material is composed of fibres enbedded in a matrix. Usually, although not always, the mechanical properties of the fibres are greatly superior to those of the matrix which is usually weaker and more extensible. The role of the matrix is to transfer the load applied to the composite to the fibres and the matrix is rarely expected to support direct tensile loading. Load transfer into and between fibres is assured by shear deformation of the matrix around fibres. If the number of fibres in the composite is too low and the distance between fibres too great reinforcement does not occur. The quality of the adhesion between fibre and matrix plays an important role and the failure of this interface or of the matrix near the interface may be used as a crack stopping mechanism. In this way the fatigue properties of the composite may be influenced. Most composites are based on organic resin matrices but metal, carbon and ceramic matrices for higher temperature applications are also mentioned.

INTRODUCTION

Composite materials consist of fibres surrounded by a matrix. Usually it is the fibres which attract most attention as composites are often a means of making a structural material having as high performance properties as possible, which is to say attempting to approach those of the simple fibre. For this reason a high fibre volume fraction is used of about 60%. In order to calculate the maximum possible fibre volume fraction consider the two fibre arrangements shown in Figure 1. With an hexagonal arrangement it is theoritically possible to fill more than 90% of the composite volume with fibres and more than 75% with the square packing arrangement (1).
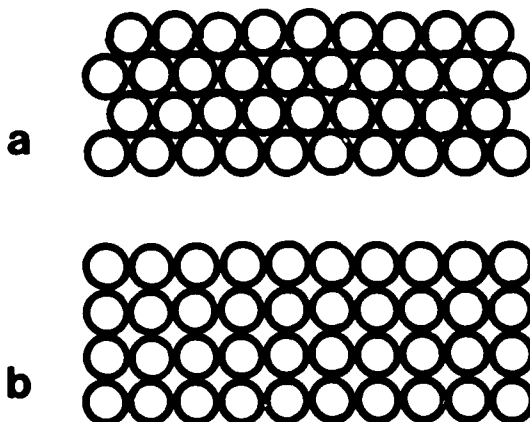

FIGURE 1: Ideal fibre packing arrangements. The hexagonal arrangement shown in
a) could lead to a maximum fibre volume fraction of more than 90% and the square arrangement
b) to more than 75%. The values are never attained however and 60% is more common.

Composite materials never have such high fibre volume fraction because of the difficulty of squeezing the matrix between the fine fibres due to surface tension effects. If such high volume fractions were attainable they would in any case be undesirable as at the points of contact between fibres there would in effect exist a small crack due to the absence of the matrix.

CONTINUOUS FIBRE COMPOSITES

If an unidirectional composite, reinforced by continuous fibres and loaded parallel to the fibres, is considered the roles of the matrix and fibres are clear. Figure 2 shows that the load is shared between the fibres and the matrix in proportion to their respective cross sections. Assuming a good bond between the fibres and the matrix the strain produced in the composite is that produced in the fibre and in the matrix so that :

$$\varepsilon_c = \varepsilon_f = \varepsilon_m \qquad (1)$$

and the load on the composite is the sum of the loads on the fibres and matrix so that:

$$\sigma_c \, A_c = \sigma_f A_f + \sigma_m A_M \qquad (2)$$

where the subscripts c, f and m correspond respectively to composite, fibre and matrix;

σ is stress
ϵ strain

and A the cross sectional area.

As the fibres are continuous in this case the volume fractions are given by

$$V_f = \frac{A_f}{A_c} \quad \text{and} \quad V_m = \frac{A_m}{A_c} \qquad (3)$$

From equations (1), (2) and (3) we can write

$$\sigma_c = \sigma_f V_f + \sigma_m (1-V_f) \qquad (4)$$

and from equations 1 and 4

$$E_c = E_f V_f + E_m (1-V_f) \qquad (5)$$

Where E is the Young's modulus.

Equation 5 is known as the law of mixtures (2).
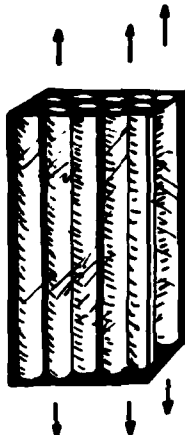
FIGURE 2 : Continuous fibres embedded in a matrix to make an unidirectional composite.

It can be seen from the above simple analysis that the matrix does not play a very important role. A typical epoxy resin is the Ciba Geigy 914 which has a Young's modulus at room temperature of about 4.0×10^3 MPa compared to the Young's modulus of a carbon fibre which is 2.4×10^5 MPa for the high strength fibre and 4.2×10^5 MPa for the high modulus fibre. The strength of this resin in 50 MPa compared to 28×10^2 MPa for high strength carbon fibres and 20×10^2 MPa for high modulus carbon fibres. Figure 3 shows schematically the shared loading between fibre and matrix.
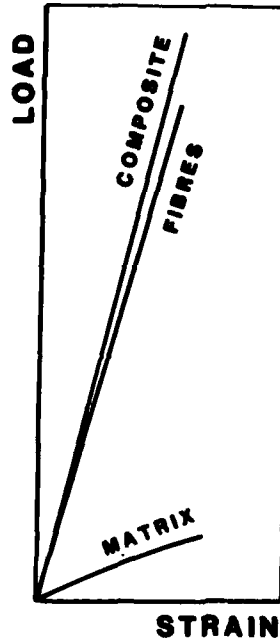
FIGURE 3 : Load sharing between the fibres and the matrix.

The analysis of stresses and strains given above is oversimplyfied as it does not take into account the Poisson's ratios of the compoments and a more detailed consideration to the deformation of laminates is given elsewhere (3).

The role of the matrix is not however only to fill in spaces between the fibres, but to assure load transfer between them. In the unidirectional composite this load transfer isolates fibre breaks in a small section of the composite.

In order to better understand this effect consider the behaviour of a simple fibre bundle with no matrix.

The behaviour of a simple fibre bundle is influenced by two probability distribution functions (4) the most important of which, when considering composite theory, is the distribution of strengths amongst the fibres making up the bundle. This is usually a Weibull distribution. The second distribution describes the variation of fibre lengths in the bundle which accounts for some fibres being loaded before others. Under applied load conditions the failure of one fibre results in the load previously supported by that fibre being transferred into all of the other fibres over their entire length and so the likelyhood of their failure occuring is increased. The next fibre to fail will do so at its weakest point. The breaking points of individual fibres are determined by the distribution of defects on or in the fibre and so the site of this second failure will be independant of the location of the first. The remaining intact fibres will be further loaded and again the probability of their failure is again increased. The sites of fibre breaks in a bundle will be randomly distributed over the whole bundle gauge length unless some interaction of fibres occurs which leads to load transfer between fibres.

If now a fibre bundle embedded in a matrix is considered, the adhesion between fibre and matrix and the shear stresses set up around a fibre break provide the means of transferring load to neighbouring fibres. The increase in load in a broken fibre due to this process is linear for an elastic fibre embedded in a plastic medium as will be discussed later.

The result of the effect of the break is therefore restricted to a section only of the composite. Rosen presented this picture of unidirectional composite failure and considered the case where all the fibres in the section shared in supporting the additional load (5). The composite can now be represented by a chain of fibre bundles in which failures occur but which are isolated from the effects of other failures in neighbouring sections. The effect of stress concentration in the section around a break was considered by Zweben (6).

Figure 4 shows schematically how the load transfer due to the shear of the matrix around fibre breaks allows more than one break to occur in a fibre

-a-   -b-   -c-

●   Fibre breaks

▲   Weak point
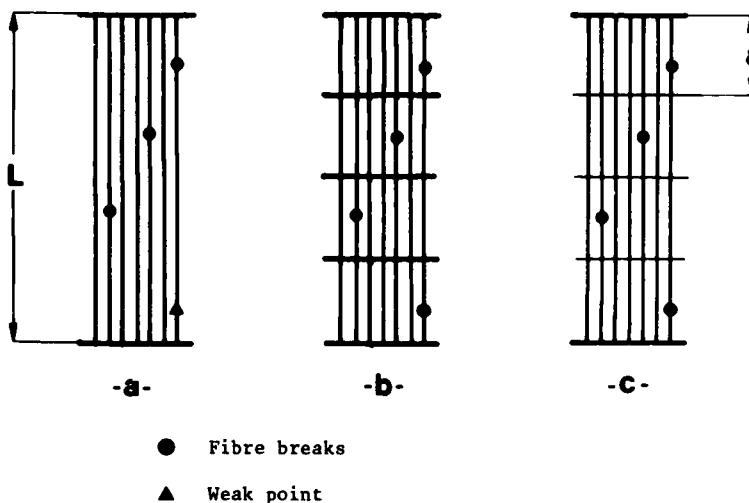
FIGURE 4:

a) Breaks of fibres in a fibre bundle lead to them playing no further role in load sharing over their whole length. As they are completely unloaded a second failure at the next weakest point is not normally possible. The remaining intact fibres are required to support the load previously taken by the broken fibres in an applied load test.

b) A chain consisting of fibre bundle links with mechanical joins between them behaves differently from a continuous bundle. Each break is isolated in its link and the stress increase in the remaining intact fibres in the link is that due to supporting the load carried in only one instead of all the fibres.

c) A composite can be considered to be analogous to the chain model in which load transfer due to the matrix defines the link length. As fibre breaks are isolated a fibre can fail more than once.

The effect of a viscoelastic matrix on Rosen's model was studied by Lifshitz and Rotem (7) who concluded that delayed failure could be explained by considering the viscoelastic behaviour of the matrix. Fibre breaks which are isolated in different sections could interact by relaxation of the shear stresses around breaks and the subsequent lengthening of the load transfer length. In this way the probability of fibre failure in two neighbouring sections would be increased as a function of time.
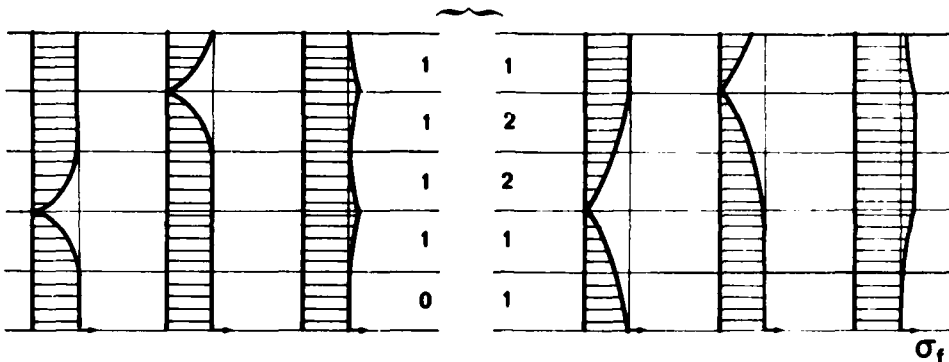
FIGURE 5 : Stress distribution at two instants of time in three neighbouring fibres two of which are broken. As the matrix relaxes the initially isolated fractures interact as the load transfer length increases and the third, intact fibre experiences increased stress over a longer length.

Fibre breaks which are initially isolated may interact after sufficient time because of viscoelastic relaxation of the matrix leading to longer load transfer lengths. This has the additional effect of spreading the load concentration on neighbouring fibres over a greater length so leading to an increased probability of additional fibres failures.

The derived equation for the composite strength F (σ) is a function of time (t) was given as:

$$\{1 - F (\sigma_f)\}^\beta \ln \{ 1 - F (\sigma_f) \} = -\frac{1}{\beta e} \{\frac{\sigma(t)}{\sigma^*}\}^\delta \qquad (6)$$

Where δ is the Weibull shape parameter for the strength distribution
σ^* the most probable failure stress in the weakest link elastic model
σ_f the stress on an intact fibre at time t.

It was found that this model could be applied to unidirectional glass reinforced epoxy resin, which was found to fail under creep and relaxation conditions as a function of time as described although at rather shorter life-times than predicted. It was suggested that the difference between theory and practice was most probably due to simplifications in the model.

An analogous line of reasoning is leading to a means of determining the minimum lifetimes of carbon fibre filament structures by taking into account the possibility of delayed fibre breaks occuring because of the viscoelastic behaviour of the matrix (8). It has been shown that unidirectional carbon fibre reinforced epoxy resion when subjected to steady or constant amplitude loading in the direction of the fibres can fail after some delay. Conventional means of detecting creep deformation such as by strain gauges or by extensiometry fail to reveal any evolution of the material although as failures sometimes occur it is clear that some form of degradation must be happening (9). Monitoring by acoustic emission does however reveal that activity continues under steady loading (10). These delayed failures must be due to the viscoelastic behaviour of the matrix as tests on simple carbon fibres reveal perfect elastic behaviour.

It is considered that in the unidirectional carbon fibre composites the principal source of emissions are the failure of fibres which initially occur all over the specimen (11). Under steady loading these emissions obey the following relation;

$$\frac{dN}{dt} = \frac{A}{(t+\tau)^n} \qquad (7)$$

Where N is the number of emissions
τ a time constant
n a power less than 1
A a constant which depends only on the applied load.

The value of n for undirectional specimens has been found to be very nearly 1 so that if n is put equal to unity we can write

$$\ln (\frac{dt}{dN}) = \ln (\frac{\tau}{A}) + \frac{N}{A} \qquad (8)$$

indicating a linear relationships between $\ln \frac{dt}{dN}$ and N under steady loading. Figure 6 shows that although the variations in strain are negligable and lie within the bounds of experimental error acoustic emission activity continues and reveal that internal damage accumulation continues to occur.
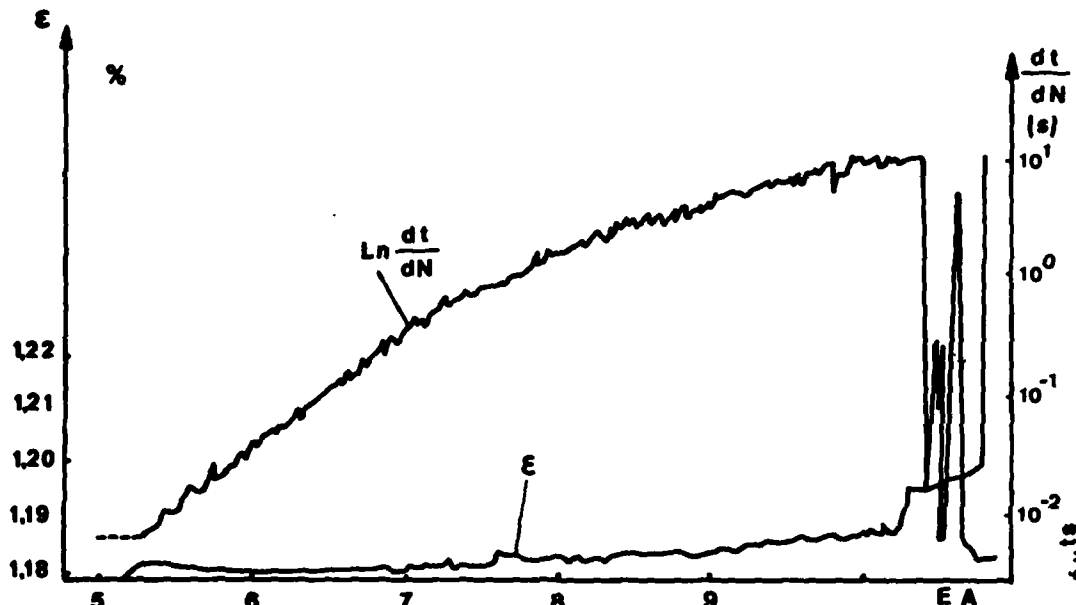
FIGURE 6:

Acoustic emission activity obtained with an unidirectional carbon fibre reinforced epoxy specimen under steady loading. Even though the variation in strain is negligable and lies within the bounds of experimental error the acoustic activity reveals that internal damage accumulation is occuring.

The use of acoustic emission technique allows the accumulation of internal damage to be monitored and quantified. If the fibre bundle chain model is taken as a reasonable picture of composite failure the emission must represent the integral failures occuring in all the sections or links. The strengths of the fibres in a bundle obey a Weibull distribution of the type

$$N_{(f)} = N_o \left(1 - e^{-\left(\frac{f-f_u}{f_o} \right)^\delta} \right) \qquad (9)$$

In which $N_{(f)}$ is the number of broken fibres

N_o the total number of fibres in the bundle

f the load applied to each fibre

f_u and f_o constants

δ the Weibull shape factor.

If the first fibre break occurs near to zero load which is a reasonable assumption then we can put $f_u = 0$ so that the load applied in order to break $N_{(f)}$ in the bundle is

$$f_{(N)} = f_o \left(Ln \left(\frac{N_o}{N_o - N_f} \right) \right)^{1/\delta} \qquad (10)$$

and the load applied to the bundle is P

$$P = (N_o - N_{(f)}) f_{(N)} = (N_o - N_f) f_o \left(Ln \left(\frac{N_o}{N_o - N_f} \right) \right)^{1/\delta} \qquad (11)$$

The form of this equation is shown in Figure 7 and passes through a maximum. The effect of the visco-elastic properties can best be seen by considering the result of applying a steady load Pl which is less that the breaking load Pmax. Fibres are broken during loading because of the spread of properties amongst the fibres. If the behaviour were completely dominated by the elastic fibres no further damage could be expected under the steady conditions however damage does continue to occur and accumulates at a rate given by equation 7. Under a loading of P max the critical damage level at which unstable failure occurs is at the level C. Under all loads less than P max the specimen can sustain greater damage and at level Pl it is necessary to attain damage level B for unstable failure to occur. The whole master curve given by equation 11 is difficult to obtain in practice however the curve up to failure at P max is given by acoustic emission. In this way a conservative measure of time to failure can be calculated by choosing damage level C as the maximum possible damage level.

It has seen that the role of the matrix under these steady loading conditions is to produce further damage accumulation and that this damage is that which could have occured at higher loads during a simple tensile test. This is shown when a creep test is interrupted and further tensile loading continued as no acoustic emission is recorded for a significant increase in load.
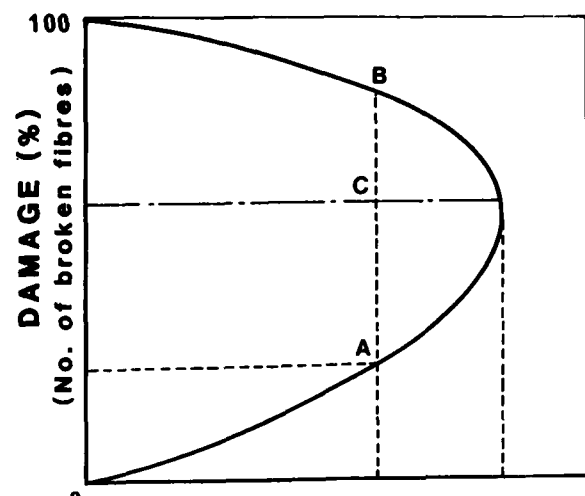
FIGURE 7:

Master damage curve tor a bundle or a section of an unidirectional composite. The load which the specimen can safely support passes through a maximum as damage increases.

LOW FIBRE VOLUME FRACTIONS

The properties od the matrix and of the reinforced fibres are very different and almost invariably the matrix has a greater strain to failure do the fibres. In composites where the fibres dominate the breaking strain of the composite is that of the fibres. The pysical mechanisms involved is that the matrix reaches its breaking strain locally around fibre breaks but that the breaking strain of the wole composite specimen is that of the fibres. In consequence at low fibre volume fractions the law of mixtures is not applicable. The resin is under a stress of σ_m at the breaking strain of the fibres but the unreinforced resin breaks at σ_u. Figure 9 shows that as the fibre volume fraction is increased the strength of the composite at first decreases as the fibres are too for apart to permit load transfer and reinforcement. In this way the fibres behave at first only as holes in the matrix and a critical fibre volume fraction must be reached before the composite attains the strength of the matrix.
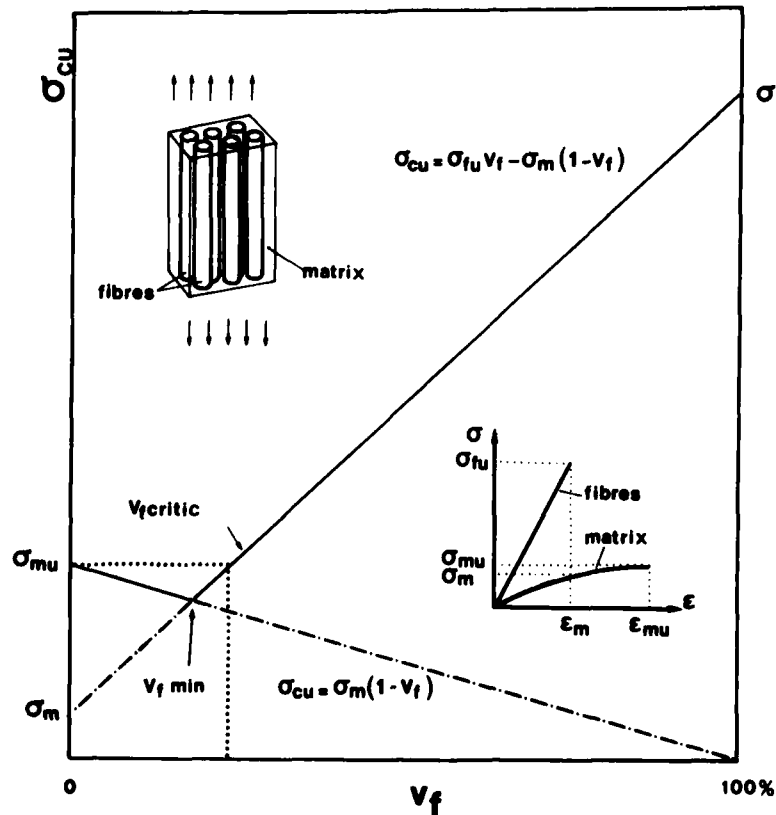

FIGURE 8 :

Composite strength as fibre volume fraction is increased.

SHORT FIBRE COMPOSITES

Composite materials may be composed of short stiff fibres embedded in a more extensible matrix (2). In order to understant the mechanism of reinforcement by short fibres consider the situation shown in Figure 9 which representes a short fibre surmounded by a cylinder of matrix. The unreinforced matrix when subjected to a given stress undergoes an uniform displacement of (V). The matrix at a distance from the fibre in Figure 9 undergoes this deplacement V but the matrix in the vicinty of the interface is prevented from deforming freely and follows the displacement of the fibre because of the interfacial bond.The fibre deforms very little because of its high Young's modulus.
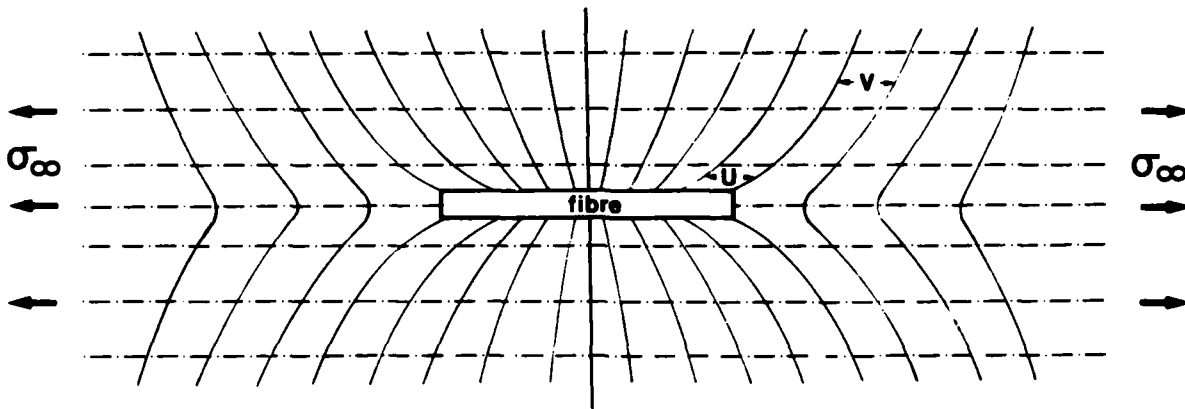

FIGURE 9:

Load transfer from the matrix into a short fibre due to shear of the matrix around the fibre.

The shear loading produced in the matrix around the fibre generates a load P in the fibre and produces a displacement u so that;

$$\frac{dP}{dx} = H \ (u-v) \qquad\qquad (12)$$

consider an elastic fibre embedded in an elastic matrix so that

$$P = E_f A_f \ \left(\frac{du}{dx} \right) \qquad\qquad (13)$$

Where x is the distance from the end of the fibre.For a steady load applied to the unreinforced matrix

$$\frac{dv}{dx} = e = constant \qquad\qquad (14)$$

From equations 12, 13, 14 we have

$$\frac{d^2 P}{dx^2} = H \ \left\{ \left(\frac{P}{E_f A_f} \right) - e \right\} \qquad\qquad (15)$$

Equation 15 can be resolved by the substitution

$$P = E_f A_f e + R \ Sinh \ \beta x + S \ Cosh \ \beta x$$

R and S and constants and P = 0 et x = 0 and 1

The stress in the fibre at point x is given by

$$\sigma_x = E_f e \ \left(1 - \frac{Cosh \ \beta(^1/2 - x)}{Cosh \ \beta \ ^1/2} \right) \qquad\qquad (16)$$

The relationship given by equation 16 shows that the load supported by the fibre increases from the ends of the fibre attaining a maximum at its centre at 1/2. Equation 16 shows that for the fibre to deform to the same degree as the composite and $\sigma x / E_f$ = e the function in brackets must reduce to unity. In this way it can be seen that only a continuous fibre can fulfil this condition and that short fibres cannot reinforce a matrix as efficiently as continuous fibres.

Continuing the analysis it can be seen that the shear of the matrix is a maximum at the fibre ends decreasing to zero at the central point of the fibre. The shear stress field is given by:

$$\tau_{(r)} = E_f \, e \, \left(\frac{Gm}{E \, 2\ln \left(\frac{R}{r_0}\right)} \right)^{1/2} \left(\frac{\text{Sinh } \beta(^1/2 - x)}{\text{Cosh } \beta^1/2} \right) \qquad (17)$$

Where $\tau_{(r)}$ is the shear at a radial distance r from the fibre axis

Gm is the shear modulus

It is possible to show that the parameter β is given by

$$\beta = \frac{Gm}{E_f} \left(\frac{2\pi}{A_f \, \ln (R/r_0)} \right)^{1/2} \qquad (18)$$

and that the greater Gm/E_f the greater the rate of load transfer into the fibre.

In the case of an elastic fibre embedded in a perfectly plastic matrix we can write by a simple equilibrium of forces

$$\frac{dP}{dx} = -2\pi r_0 \, \tau_{(r)} \qquad (19)$$

Assuring that the matrix has reached its elastic limit in shear τ_y we can write

$$P = 2\pi \, r_0 \, \tau_y \, x \, \Big]_0^x \quad \text{and} \quad \sigma x = \frac{P}{A_f} = \frac{2\pi r_0}{\pi r_0^2} \, \tau_y \, x$$

so that

$$\sigma_x = \frac{2\tau_y x}{r_0} \qquad (20)$$

From equation 20 we can see that in this case the stress tranferred into the fibre increases linearly from the fibre ends until it reaches the stress $\sigma\alpha$ applied to the composite as shown in Figure 10.
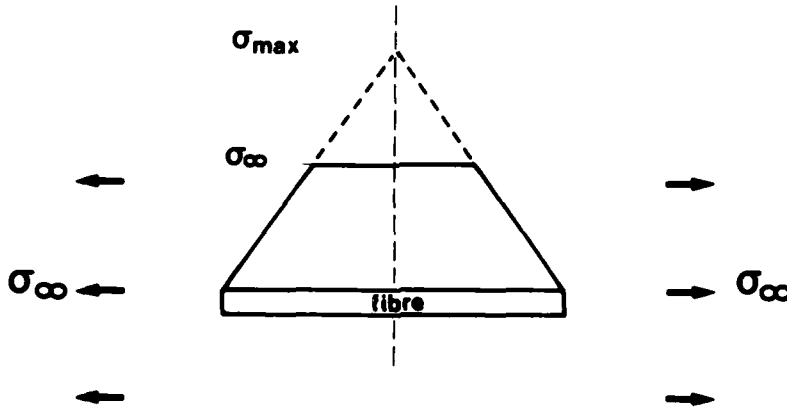
FIGURE 10

Load transfer into an elastic short fibre embedded in a perfectly plastic matrix

In the case of fibres which are longer than the load transfer length there exists a length of fibre which supports a steady load, chat load which a continuous fibre would support. This means that the fibre may break in the central portion if the applied stress reaches its breaking stress.

A critical length lc exists when the maximum load which can be transformed into the fibre is its breaking stress. All fibres shorter than the critical length are destined to be pulled out of the matrix during final failure of the composites. The critical case is described from equation 20 when

$$\sigma_f = \frac{2\tau_y l_c}{r_0}$$

which reveals the importance of the aspect ratio of the fibre for short fibre reinforced composites

$$\frac{l_c}{v_0} = \frac{\sigma_f}{2\tau_y} \qquad (21)$$

Short fibres are not necessarily added to a matrix material in order to produce a higher strength composite. In the case of fibre reinforced cement the fibre volume fraction is very low around 7% and, as is usually the case the fibres are randomly orientated at least in two dimensions. The role of the fibre in this type of composite is to increase the toughness of the matrix. This they do by bridging the micro-cracks and preventing them opening and so further propagating. On failure of the composites the fibres usually have to be pulled out which again increases the energy to failure (12).

SOME MATRIX MATERIALS

Polyester: the most widely used resins used as matrices for composites are the polyesters the structure of which is based on the recurring ester group -Co-O (13). Polyester is the main matrix material used with glass fibre reinforcement. They are still being developped and improved upon. They are a thermosetting resin and by modifying the way that cross linking is induced matrices of different properties may be produced so that a general impression of this type of resin is difficult to give. However polyester resins are amongst the cheaper resin systems available providing good mechanical and chemical resistant properties at moderate temperatures, usually not higher than 100°C. Polyester have low viscosity before crosslinking takes place and wet well glass fibres. The main weaknesses of these resins are, a generally high shrinkage rate during curing which can produce buckling of fibres and hence lower composite strengths especially in compression; sensivity to some aggressive solvents and chemicals especially alkaline and basic media, appreciable water absorption and resulting irreversible degradation.

Epoxy resin : the most common form of matrix for advanced composites are the epoxy resin systems. These resins are thermosetting materials based on reactions with the epoxide group. $-HC-CH_2$ and their properties may be greatly varied by modifications to the basic chemical structure. Hardening by crosslinking of the epoxy resin occurs through the reaction of the epoxy group with an added curing agent, hardener or catalyst. The type of hardener used may influence greatly the properties of the resulting composite. For example it has been shown that simply by changing the hardener used from a diamine to a dicyandiamide to an anhydride can greatly influence the water absorption behaviour of a composite (14). Epoxy resins have proved to be extremely versatile in processing and curing. They do not present the problem of shrinkage during curing, they are relatively strong provide good bonding with most fibres and are chemically resistant.

Higher Temperature Resins : the most wide known matrix materials for use at temperature above about 150°C are the polyimide resins which can be used up to around 300°C. As with most specialised resin systems polyimides are difficult or at least complicated to fabricate as they require very careful control during the fabrication proceedure.

Phenolic resins can also be used up to 300°C and for transient exposure up to more than 1000°C when reinforced with asbestos fibres. High moulding pressures and temperatures are required with these resins to achieve full cure and to eliminate void formation. Post curing at temperatures up to 250°C may follow . Phenolic resins are resistant to water solvents and most acids. They are sensitive to alkaline solutions.

Silicone resins are based on the polymer chain (-O-Si-O-) and can be used up to 250°C for long exposure times although their initial mechanical properties are lower than some other resins. Silicone resins have excellent resistance to water and oxidation.

Metal Matrices : Metals offer the possibility of creating composites which have inherantly greater matrix strengths than is possible with organic resins. In addition a metal matrix increases the toughness and temperature range of composites. The difficulties in making metal matrix composites are that few of the reinforcing fibres can be successfully embedded in them. By far the easiest type pf fibre for use in a metal matrix are the surface coated (B_4C or SiC) boron fibres but they are also the most expensive and least used at present. The most common metal matrices are aluminium alloys in particular the 6061 and 2024 alloys and boron reinforced composite may be made by hot pressing around 580 - 610°C. At these temperatures the aluminium is in a semi-liquid phase. Such a composite retains its room temperature properties at 300°C. Another possible metal matrix is the Ti6A14V titanium alloy which however requires hot pressing at 900°C.

Carbon fibres can be embedded in aluminim alloys but first are usually coated with nickel or silver to avoid galvonic corrosion between the carbon and the aluminium. The main interest of this type of composite lies in the avoidance of problems of outgassing under conditions of vacuum and also the possibility of creating composites with very low coefficients of expansion.

Very high Temperature Matrices : Fibre reinforced ceramics seem to offer the possibility of composites capable of withstanding temperatures up to 1300°C. The main candidates for this type of composite are the SiC and Si_3N_4 ceramics reinforced with SiC or Al_2O_3 fibres. The interest of this type of composite is yet to be proven as the role of the fibres may be very different from that which is the case for organic matrix composites. This is because it is no longer the case that the mechanical properties of the matrix are very different from those of the fibres. It may be that the principal role of the fibres is to hinder crack propagation.

Temperatures up to 4000°C can be supported by composites consisting of carbon fibres embedded in a carbon matrix. The matrix is produced either by pyrolisation of an organic matrix or by chemical vapour deposition. These composites have extraordinary thermal and mechanical properties althrough at high temperetures suffer from oxidation in the presence of oxygen.

REFERENCES

(1) M.R. Piggott, "Load Bearing Fibre Composites" Pergamon Press (1980) 85.

(2) A. KELLY " Strong Solids " Clarendon Press, Oxford (1966) 121-166

(3) S.W. Tsai and H.T. Hahn "Introduction to Composite Materials" Technomic Publishing Co,Westpoint U.S.A (1980).

(4) D.G. Harlow and S.L. Phoenix "The bundle chain probability model for the strength of fibrous materials" J. Comp. Mat. 12, 195 (1978).

(5)   B.W. Rosen "Tensile failure of fibrous composites" AIAA Journal 2, 1985 (1964).

(6)   K. Zweben "Tensile failure of fibre composites" AIAA Journal 6, 2325 (1968)

(7)   J.M. Lifshitz and A. Rotem "Time dependent longitudinal strength of unidirectional fibrous composites". Fibre. Sci.and Tech. 3, 1 (1970).

(8)   A. R. Bunsell, D. Laroche and D. Valentin "Damage and failure in carbon fibre reinforced epoxy resin". To be published in an ASTM-STP.

(9)   J.B. Sturgeon, R.I. Butt and L.W. Larke "Creep of carbon fibre reinforced plastics" R.A.E.Tech. Report 76168 (1976).

(10) M. Fuwa, B. Harris and A.R. Bunsell "Acoustic emission during cyclic loading of carbon fibre reinforced plastics "J. Phys.D. 8, 1460 (1975).

(11) M. Fuwa, A.R. Bunsell and B. Harris "Tensile failure mechanisms in carbon fibre reinforced plastics" J. Mat. Sci. 10, 2062 (1975).

(12) J.C. Lenain and A.R. Bunsell "The resistance to crack growth of asbestos cement "J. Mat. Sci. 14, 321 (1979).

(13) R. Kay "Principles of resin system selection""Fibre Composite Hybrid Materials" Ed.N.L. Hancox Applied Sci.Pub. (1981) 35-51.

(14) P. Bonniau and A.R. Bunsell " A comparative study of water absorption theories applied to glass epoxy composites " J. Comp. Mat. 15, 272 (1981).

Micromechanical Models for the
Stiffness and Strength of Fiber Composites

R. Byron Pipes

University of Delaware, U.S.A.

Introduction and Nomenclature

Combinations of fibrous materials in polymeric matrices yield composite materials with performance characteristics which cannot be achieved by the constituents acting individually. The properties of these "new" materials can be adjusted by modifying the properties of each phase or by changing the composition proportions. This yields families of materials possessing a variety of material properties and allows for simultaneous design of both material and structural geometry.

Design and analysis of composite materials and structures proceeds at several scales. First, the field of micromechanics examines the individual roles of fiber and matrix in determining bulk composite properties. Contemporary micromechanical models capable of predicting transport properties of composite materials consisting of collimated fibers in isotropic matrices (unidirectional lamina) will be discussed later in this lecture. The second scale of examination is often termed minimechanics. At this level the influence of the unidirectional lamina and its orientation upon the properties of the multidirectional laminates is investigated. By varying the orientation of laminae it is possible to produce laminates of widely varying properties. Finally, the multidirectional laminate is viewed as a homogeneous material at the macromechanical scale where the geometry of the structure is designed.

Since fibrous composite materials are made of high performance fibers and compliant polymeric matrices, it is not surprising that their effective bulk properties differ when measured parallel and perpendicular to the collimated fiber direction. Materials whose properties vary with direction are termed anisotropic. Anisotropic materials exhibit unexpected behavior which can be important in their analysis and design. Therefore, the next section of this lecture deals with the mechanics of anisotropic materials. One of the important consequences of material anisotropy is the dramatic increase in the number of parameters needed to describe the behavior of the material. For example, the elastic response of an isotropic material requires knowledge of only two elastic constants, while 21 constants must be measured for the generally anisotropic material, and nine constants describe an orthotropic material.

One of the major goals of micromechanical models is the prediction of anisotropic material descriptors required in the analysis and design of composite structures. The subsequent coupling of the various scales (micro, mini, and macro) of approach provides an overall design methodology which can fully exploit the potential for tailoring simultaneously material and structure to a given application.

Anisotropic Materials Descriptors

The elastic response of a generally anisotropic material is described through the constitutive relation (Hooke's law) which relates components of the stress and strain tensors.

$$\sigma_{ij} = \sum_{k=1}^{3} \sum_{\ell=1}^{3} C_{ijk\ell}\, \varepsilon_{k\ell} \tag{1}$$

where σ_{ij} are components of the stress tensor, $\varepsilon_{k\ell}$ are components of the strain tensor, and $C_{ijk\ell}$ are components of the fourth rank elastic constant tensor. The elastic constant array consists initially of 81 components, but symmetry of stress and strain tensors and the requirement that the strain energy density function be positive definite requires symmetry of $C_{ijk\ell}$ and reduces the number to 21. It is therefore appropriate to introduce contracted notation for purposes of simplification.

$$\sigma_{ii} = \sigma_i \qquad\qquad \varepsilon_{ii} = \varepsilon_i \qquad\qquad i = 1,2,3$$

$$\sigma_{23} = \sigma_4 \qquad\qquad \varepsilon_{23} = \varepsilon_4$$

$$\sigma_{13} = \sigma_5 \qquad\qquad \varepsilon_{13} = \varepsilon_5 \tag{2}$$

$$\sigma_{12} = \sigma_6 \qquad\qquad \varepsilon_{12} = \varepsilon_6$$

Thus, the constitutive relations may now be expressed in contracted notation

$$\sigma_i = \sum_{j=1}^{6} C_{ij}\varepsilon_j \tag{3}$$

The terms of the elastic constant array are termed stiffness constants since they relate strain to stress in the same manner a spring constant (stiffness) relates displacement to force. If we wish to examine the inverse relation, the compliance tensor, S_{ij} , may be defined:

$$\varepsilon_i = \sum_{j=1}^{6} S_{ij}\sigma_j \tag{4}$$

where $\qquad S_{ij} = C_{ij}^{-1}$ $\qquad$ (i,j = 1-6)

Thus the compliance array is also symmetric.

When materials possess elastic symmetry in material properties, the number of material descriptors (terms of the C_{ij} and S_{ij} arrays) are reduced. A single plane of elastic symmetry reduces the number of constants from 21 to 13, while three orthogonal planes of elastic symmetry (<u>orthotropic</u>) reduce the number of constants to 9. When collimated fibers are arranged in a random array, the plane transverse to fiber direction can be viewed as a plane of isotropy. Hence the number of descriptors is reduced to 5. However, in the interest of generality, it will be assumed that 9 constants are required to describe the unidirectional fiber composite material.

The terms of the stiffness and compliance arrays take on physical significance only when experiments are performed for their evaluation and engineering constants identified. Consider the expression (4) where $\sigma_i = 0$ (i = 2-6). The strain ε_1 is given as

$$\varepsilon_1 = S_{11}\sigma_1 \quad \text{or} \quad S_{11} = \varepsilon_1/\sigma_1 \qquad (5)$$

Hence, the term S_{11} is the inverse of the Young's modulus in the "1" direction, and it follows that:

$$S_{ii} = 1/E_i \qquad (i = 1,2,3) \qquad (6)$$

If in expression (4) $\sigma_i = 0$ (i = 1-5), then

$$\varepsilon_6 = S_{66}\sigma_6 \qquad (7)$$

Thus S_{66} is the inverse of the shear modulus in the 1-2 plane, $1/G_{12}$:

$$S_{66} = 1/G_{12}$$

and

$$S_{55} = 1/G_{13} \qquad (8)$$

$$S_{44} = 1/G_{23}$$

Finally, the off diagonal terms involve the Poisson's ratios, ν_{ij} of the material. For example:

$$S_{12} = S_{21} = -\nu_{12}/E_1 = -\nu_{21}/E_2$$

$$S_{13} = S_{31} = -\nu_{13}/E_1 = -\nu_{31}/E_3 \qquad (9)$$

$$S_{23} = S_{32} = -\nu_{23}/E_2 = -\nu_{32}/E_3$$

The stiffness constant array may be expressed in terms of the engineering elastic constants by inverting the compliance array. However, this action is tedious and will be deferred to consideration of plane stress conditions.

Many applications for composite materials involve relatively thin structures wherein the assumption of planar stress state is appropriate. Under this condition the normal stress, σ_3 , is assumed to vanish and the stiffness array takes on a new form:

$$\sigma_i = \sum_{j=1,2,6} Q_{ij}\varepsilon_j \qquad (10)$$

where the terms of the plane stress stiffness array may be expressed in terms of the original stiffness array constants as follows:

$$Q_{ij} = C_{ij} - \frac{C_{i3}C_{j3}}{C_{33}} \qquad (i,j = 1,2,6) \qquad (11)$$

The plane stress stiffness constants may now be expressed in terms of the engineering elastic constants, since inversion of the S_{ij} array involves only inversion of a 2×2 array.

$$Q_{11} = \frac{E_1}{1 - \nu_{12}\nu_{21}} \qquad Q_{12} = Q_{21} = \frac{\nu_{12}E_2}{1 - \nu_{12}\nu_{21}} \qquad (12)$$

$$Q_{22} = \frac{E_2}{1 - \nu_{12}\nu_{21}} \qquad Q_{66} = G_{12}$$

The plane stress and general compliance arrays are identical in the terms S_{11} , S_{12} , S_{22} , and S_{66} .

Since the components of stress and strain possess tensorial character, they may be transferred from one coordinate system to another. For example, it is possible to perform a

coordinate rotation, θ , about the "3" axis so that a new coordinate system 1'2'3' is defined as shown in Figure 1. The stress components in the new coordinate system may be expressed in terms of the stress components in the original coordinate system:

$$\sigma_i' = \sum_{j=1,2,6} T_{ij}\sigma_j \qquad (13)$$

where the stress transformation array is given as follows:

$$T_{ij} = \begin{bmatrix} m^2 & n^2 & 2mn \\ n^2 & m^2 & -2mn \\ -mn & mn & m^2-n^2 \end{bmatrix} \quad \begin{array}{l} m = \cos\theta \\ n = \sin\theta \end{array} \qquad (14)$$
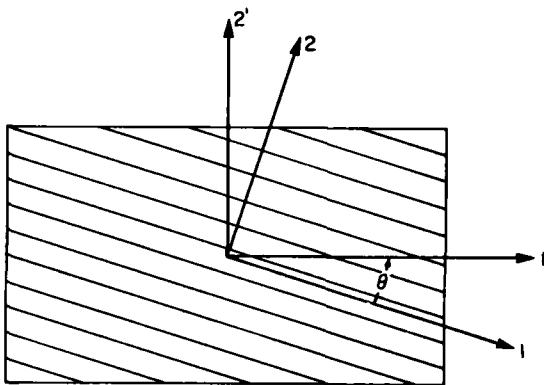

Figure 1. Rotation of Axes.

The components of strain also possess tensor transformation characteristics and the transformation array is identical to (14) for elasticity shear strain.

$$\epsilon_i' = \sum_{i,j=1,2,6} T_{ij}\epsilon_j \qquad (15)$$

For engineering shear strain, γ_6 , the transformation array must be modified since $\epsilon_6 = 2\gamma_6$.

$$T_{ij}^\epsilon = \begin{bmatrix} m^2 & n^2 & mn \\ n^2 & m^2 & -mn \\ -2mn & 2mn & m^2-n^2 \end{bmatrix} \qquad (16)$$

Once stress and strain transformation have been defined, it is possible to develop transformation relations for the terms of the stiffness array, Q_{ij} . Consider the constitutive relation given in (1). Substituting relations (13) and (15) into (10) results in the *following*.

$$\sigma_i' = \sum_{j=1,2,6} Q_{ij}'\epsilon_j' \qquad (i = 1,2,6) \qquad (17)$$

where

$$Q_{ij}' = \sum_{k=1,2,6,\ell=1,2,6} T_{ik}Q_{k\ell}T_{ij}^{\epsilon-1} \qquad (i,j = 1,2,6) \qquad (18)$$

$$Q_{11}' = Q_{11}m^4 + 2m^2n^2(Q_{12} + 2Q_{66}) + Q_{22}n^4$$

$$Q_{12}' = (Q_{11} + Q_{22} - 4Q_{66})m^2n^2 + Q_{12}(m^4 + n^4)$$

$$Q_{16}' = [(Q_{11} - Q_{12} - 2Q_{66})m^2 - (Q_{22} - Q_{12} - 2Q_{66})n^2]mn$$

$$Q_{22}' = Q_{22}m^4 + 2(Q_{12} + 2Q_{66})m^2n^2 + Q_{11}n^4 \qquad (19)$$

$$Q_{26}' = -[(Q_{22} - Q_{12} - 2Q_{66})m^2 - (Q_{11} - Q_{12} - 2Q_{66})n^2]mn$$

$$Q_{66}' = (Q_{11} + Q_{22} - 2Q_{12})m^2n^2 + Q_{66}(m^2 - n^2)^2$$

In a similar fashion, the plane stress compliance array may be transformed.

$$S_{11}' = m^4 S_{11} + (2S_{12} + S_{66})m^2n^2 + S_{22}m^4$$

$$S_{12}' = (S_{11} + S_{22} - S_{66})m^2n^2 + S_{12}(m^4 + n^4)$$

$$S_{16}' = -[(2S_{11} - 2S_{12} - S_{66})m^2 - (2S_{22} - 2S_{12} - S_{66})n^2]mn$$

$$S_{22}' = m^4 S_{22} + (2S_{12} + S_{66})m^2n^2 + S_{11}n^4 \qquad (20)$$

$$S_{26}' = [(2S_{22} - 2S_{12} - S_{66})m^2 - (2S_{11} - S_{12} - S_{66})n^2]mn$$

$$S_{66}' = 2(2S_{11} + 2S_{22} - 4S_{12} - S_{66})m^2n^2 + S_{66}(m^4 + n^4)$$

Mechanics of Materials Models

It is clear from the previous section that development of models for prediction of the bulk properties of a fibrous composite material in terms of constituent properties is a desirable objective. The central problem of a micromechanical analysis is the specification of an internal stress or strain field within the heterogeneous continuum which is consistent with the external field imposed on the macroscopic body. The internal stress and strain fields in a heterogeneous body such as a fibrous composite are influenced by

  i)   the relative magnitudes of the properties of the phases
 ii)   the size, shape and relative orientation of the phases
iii)   the packing geometry of the phase regions

However, since the small deformation elastic properties of the composite material represent the integrated behavior of the microscopic regions, it is possible to develop reasonable estimates of composite properties without detailed knowledge of the microscopic stress and strain distributions. The simplest models for predicting thermoelastic and transport properties may be developed intuitively by analogy. The properties parallel to the fiber direction (longitudinal) are taken to be determined by a parallel addition of constituent properties

$$P = \sum_{i=1}^{n} v_i P_i \tag{21}$$

where v_i is the volume fraction and P_i is the appropriate property of the "i" phase. Properties transverse to the fiber direction are determined by series summation of constituent properties

$$\frac{1}{P} = \sum_{i=1}^{n} \frac{v_i}{P_i} \tag{22}$$

These simple relationships have become popularly known as the "Rule of Mixtures." It has been demonstrated that the Rule of Mixtures estimates for the longitudinal properties are quite good, while the estimates for transverse properties depart significantly from measured values.

The mechanics of materials models are identical to the parallel and series models described above. Their derivation rests on the assumption of a uniform state of stress or strain within the heterogeneous composite, and therefore it is not surprising that predictions are inaccurate for the transverse properties. Consider the unidirectional composite material idealized in Figure 2. If a force is applied parallel to the fiber direction and the composite is assumed to experience a uniform axial strain, a force balance yields the Rule of Mixtures for the longitudinal Young's modulus, E_1 .

$$E_1 = E_f v_f + E_m v_m \tag{22}$$

where v_f = fiber volume fraction and v_m = matrix volume fraction. When the transverse strain is examined, the Rule of Mixtures for the major Poisson's ratio is determined

$$\nu_{12} = \nu_f v_f + \nu_m v_m \tag{23}$$

Figure 2. Idealized Mechanics of Material Model for Unidirectional Composites

Further, the longitudinal composite stress is

$$\sigma_1 = \sigma_f v_f + \sigma_m v_m \tag{24}$$

The effective transverse Young's modulus of the unidirectional composite can be determined by applying a force perpendicular to the fiber direction. A uniform state of stress, σ_2 , is assumed through the heterogeneous medium. By summing the transverse deformation of the fibrous and matrix phases and setting the total equal to that of the composite, we have

$$\epsilon_2 = v_f \epsilon_f + v_m \epsilon_m \tag{25}$$

Combining equation (25) with the assumption of uniaxial stress in the phases yields the Rule of Mixtures for the transverse Young's modulus

$$1/E_2 = v_f/E_f + v_m/E_m \tag{26}$$

The effective shear modulus in the 1-2 plane may be determined from the idealized model shown in Figure 3. Shearing forces, F_s , act to produce angular deformation within each

Figure 3. Idealized Mechanics of Material Model for In-Plane Shear

phase, the magnitude of which is dependent upon the phase shear moduli. The total shear strain is the volume average sum

$$\nu_{12} = v_f \gamma_f + v_m \gamma_m \tag{27}$$

If the state of stress within the phases is assumed to be equal to the applied shear traction, the Rule of Mixtures for the planar shear modulus is determined

$$1/G_{12} = v_f/G_f + v_m/G_m \tag{28}$$

In summary, the mechanics of materials models yield the classical Rules of Mixtures for the prediction of composite properties. Although the predictions for longitudinal properties have shown good agreement with experimental data, the gross simplifications required in derivation of relations for the transverse Young's modulus and shear modulus yield them to be crude estimates at best.

Rigorous Micromechanical Models

The inaccuracy and simplistic derivation of the mechanics of materials models led numerous researchers to seek improved models through more rigorous formulations. The next higher level of formulation may be termed the self-consistent field model. Here, detailed response of the phases are modeled, but gross simplifications in the phase geometry are introduced as shown in Figure 4. An elasticity formulation is developed for a single fiber embedded in a medium whose properties are taken as the overall average or effective properties of the composite materials. The doubly embedded model allows the fiber to be surrounded by a cylinder of pure matrix phase. A "self-consistent" stress field is identified and the effective properties of the composite determined:

(a) embedded

(b) doubly embedded
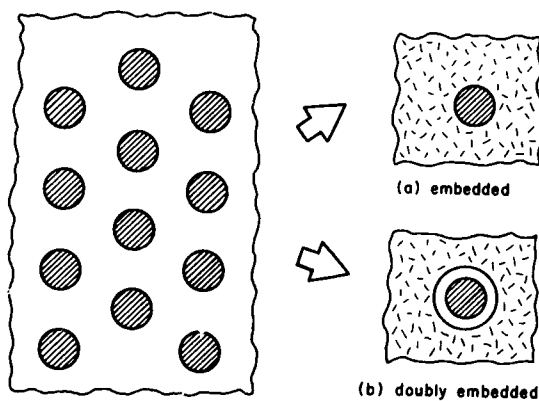
Figure 4. Simplification of the Geometrical Model for the Self-Consistent Field Approach

$$E_1 = E_{1f} v_f + E_{1m} v_m + \frac{4(\nu_{12m} - \nu_{12f})^2 k_{2f} k_{2m} v_m v_f}{(k_{2f} + G_{23m}) k_{2m} + (k_{2f} - k_{2m}) G_{23m} v_f}$$

$$\nu_{12} = \nu_{12f} v_f + \nu_{12m} v_m + \frac{(\nu_{12m} - \nu_{12f})(k_{2m} - k_{2f}) G_{23m} v_m v_f}{[(k_{2f} + G_{23m}) k_{2m} + (k_{2f} - k_{2m}) G_{23m} v_f]} \tag{29}$$

$$G_{12} = G_{12m} \frac{[(G_{12f} + G_{12m}) + (G_{12f} - G_{12m}) v_f]}{[(G_{12f} + G_{12m}) - (G_{12f} - G_{12m}) v_f]}$$

where k_2 is the plane strain bulk modulus. From expressions (29) it is clear that the predictions for E_1 and ν_{12} differ from the Rule of Mixtures only by the last terms. When the difference in Poisson's ratios of the fiber and matrix phases is small, the latter terms are negligible and hence the simple Rules of Mixture are shown to hold for these properties. In contrast the expression for G_{12} is seen to be quite different from the Rule of Mixtures predictions.

Perhaps the most significant rigorous models are those developed from the bounding approach. The bounding approach avoids the problems of specifying the explicit nature of the microstructure and the internal stress-strain fields by employing variational principles to establish upper and lower bounds on the properties. The results of these bounding methods can provide practical guides to material behavior only if the upper and lower bounds are reasonably close together so as to bracket the properties to within experimental error. The upper and lower bounds on longitudinal properties are very close and converge to the simple results for Rule of Mixtures. Unfortunately, the upper and lower bounds for the transverse properties and shear moduli are too far apart to be of practical value.

Semiempirical Models

The difficulties in obtaining tight bounds or rigorous predictions for other than highly simplified models lead to the development of semiempirical relations by Halpin and Tsai.

$$P = \frac{P_m(1 + \xi \chi v_f)}{1 - \chi v_f} \quad , \quad \chi = \frac{P_f - P_m}{P_f + \xi P_m} \tag{30}$$

where "P" denotes property and "ξ" is a scaling parameter. The central feature of the Halpin-Tsai relationship is the recognition that the properties of a composite material lie somewhere between the primitive bounds. The scaling parameter "ξ" serves to adjust the effective properties between these two limits. The role of ξ is best illustrated by rearranging equation (30) as follows

$$P = \frac{P_m[P_f + \xi P_m + \xi v_f(P_f - P_m)]}{[P_f + \xi P_m - v_f(P_f - P_m)]} \qquad (31)$$

For $\xi \to \infty$ (31) reduces to the parallel sum or Voigt bound

$$P = P_f v_f + P_m v_m \quad ; \quad \xi \to \infty \qquad (32)$$

Alternately as ξ becomes vanishingly small, the relationship reduces to the series sum or Reuss bound as illustrated in Figure 5.

$$1/P = v_f/P_f + v_m/P_m \quad ; \quad \xi \to 0$$

The reinforcing factor, ξ, may be treated as an adjustable parameter whose value can be obtained from experimental determination of the property of a composite at a given fiber volume fraction. Further, the reinforcing factor has been shown to be a function of fiber cross-sectional shape and packing geometry and to be different for each property predicted.
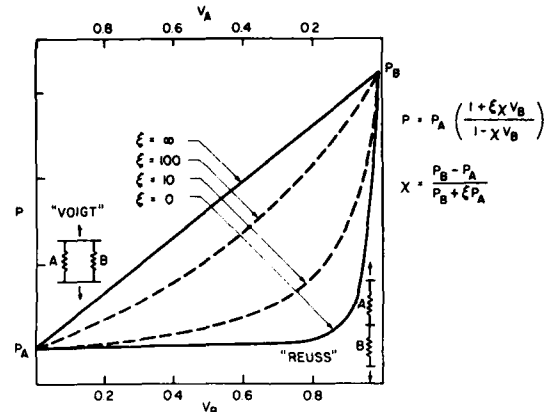
Figure 5. Illustration of the Role of Reinforcing Factor, ξ, of the Halpin-Tsai Equation

Biaxial Failure Models

The previous discussions have shown that fibrous composites are anisotropic in elastic properties. The fibrous phase is not only greater in stiffness than the matrix phase, but also fibers are typically stronger than the matrix. Therefore, fibrous composites typically exhibit anisotropy in strength characteristics. For example, the strength in the direction of the fibers is typically an order of magnitude greater than the transverse strength. Numerous models for the strength of anisotropic media subjected to biaxial (planar) states of stress have been developed to date; however, in this lecture only the maximum stress, maximum strain and quadratic criteria will be discussed.

Consider the maximum stress criterion. Failure is assumed to occur when any one of the stress components is equal to its corresponding intrinsic strength property. In mathematical form, the maximum stress criterion is given by:

$$\sigma_1 \geq X_1^T \quad , \quad \sigma_1 > 0 \quad ; \quad \sigma_1 \leq -X_1^C \quad , \quad \sigma_1 < 0$$

$$\sigma_2 \geq X_2^T \quad , \quad \sigma_2 > 0 \quad ; \quad \sigma_2 \leq -X_2^C \quad , \quad \sigma_2 < 0 \qquad (33)$$

$$\sigma_6 \geq X_6 \quad , \quad \sigma_6 > 0 \quad ; \quad \sigma_6 \leq X_6 \quad , \quad \sigma_6 < 0$$

where the intrinsic strength properties are defined as follows:

X_1^T = ultimate uniaxial tensile strength in the fiber direction,

X_1^C = ultimate uniaxial compressive strength in the fiber direction,

X_2^T = ultimate uniaxial tensile strength perpendicular to fiber direction,

X_2^C = ultimate uniaxial compressive strength perpendicular to fiber direction,

X_6 = ultimate planar shear strength under pure shear loading.

For most composite material systems, the planar shear strengths are equal for positive and negative shear stresses.

Consider the uniaxial strength of a tensile coupon wherein the fiber direction is rotated an angle θ with respect to the loading direction. The state of stress in the fiber coordinate system may be determined by an appropriate coordinate transformation.

$$\sigma_1 = m^2 \sigma_1'$$

$$\sigma_2 = n^2 \sigma_1' \qquad (34)$$

$$\sigma_6 = mn\sigma_1'$$

where $m = \cos\theta$ and $n = \sin\theta$. If the maximum strength criterion is applied, three potential failure modes are identified:

$$\sigma_1' = X_1^T/m^2 \quad \text{(fiber tension)}$$

$$\sigma_1' = X_2^T/n^2 \quad \text{(transverse tension)} \tag{35}$$

$$\sigma_1' = X_6/mn \quad \text{(planar shear)}$$

As the angle θ is varied from 0 to $\pi/2$, the failure mode will transition from fiber failure in tension to planar shear failure, and finally to transverse tensile failure as illustrated in Figure 6. Note that in the region of $\theta = \pi/4$ the data show poor agreement with predictions due to the <u>inter-action</u> in failure modes which act to <u>further degrade strength</u>.

The <u>maximum strain criterion</u> is totally analogous to the maximum stress criterion. Failure is assumed to result when any one of the strain components is equal to its corresponding intrinsic ultimate strain. In mathematical form the maximum strain criterion is given by:

$$\varepsilon_1 \geq e_1^T \quad , \quad \varepsilon_1 > 0 \quad ;$$

$$\varepsilon_1 \geq -e_1^C \quad , \quad \varepsilon_1 < 0$$

$$\varepsilon_2 \geq e_2^T \quad , \quad \varepsilon_2 > 0 \quad ;$$

$$\varepsilon_2 \geq -e_2^C \quad , \quad \varepsilon_2 < 0 \tag{36}$$

$$\varepsilon_6 \geq e_6 \quad , \quad \varepsilon_6 > 0 \quad ;$$

$$\varepsilon_6 \geq -e_6 \quad , \quad \varepsilon_6 < 0$$

where the intrinsic ultimate strains are defined as follows:

Figure 6. Off-Axis Tensile Strength of Boron Epoxy

e_1^T = ultimate tensile strain in fiber direction,

e_1^C = ultimate compressive strain in fiber direction,

e_2^T = ultimate tensile strain transverse to fiber direction,

e_2^C = ultimate compressive strain transverse to fiber direction,

e_6 = ultimate planar (engineering) shear strain under pure shear stress.

It was shown in Figure 6 that a biaxial state of stress can lead to strengths which are less than that predicted by the maximum stress criterion. The <u>quadratic interaction criterion</u> was developed to provide strength predictions wherein interaction among stress components could be considered in determining strength in a biaxial stress field. When a planar state of stress is considered this criterion may be expressed as follows:

$$F_1\sigma_1 + F_2\sigma_2 + F_6\sigma_6 + F_{11}\sigma_1^2 + F_{22}\sigma_2^2 + F_{66}\sigma_6^2 + 2F_{12}\sigma_1\sigma_2 = 1 \tag{37}$$

All of the failure constants of the quadratic failure criterion may be expressed in terms of the intrinsic strength properties of the composite, except F_{12}.

$$F_1 = 1/X_1^T - 1/X_1^C \quad , \quad F_{11} = 1/X_1^T X_1^C$$

$$F_2 = 1/X_2^T - 1/X_2^C \quad , \quad F_{22} = 1/X_2^T X_2^C \tag{38}$$

$$F_6 = 1/S_6^+ - 1/S_6^- \quad , \quad F_{66} = 1/S_6^+ S_6^-$$

Several researchers were able to correlate experimental data by choosing F_{12} to be zero. Actual determination of F_{12}, however, requires a biaxial test. In addition, most of the data to date show that biaxial predictions are only slightly modified by assuming $F_{12} = 0$.

Consider again the strength of the off-axis tensile coupon subject to a uniaxial stress, σ_1'. The stress state given in equation (34) may be substituted into (37) and the resulting quadratic equation solved for the ultimate strength $\sigma_1'_{(ultimate)}$.

$$\sigma_1'_{(ultimate)} = \frac{-B + \sqrt{B^2 + 4A}}{2A} \tag{39}$$

where

$$A = F_{11}m^4/4 + F_{22}n^4/4 + F_{66}m^2n^2/4$$

$$B = F_1 m^2/2 + F_2 n^2/2 + F_6 mn/2 \tag{40}$$

Results are shown in Figure 6 for the AVCO 5505 boron epoxy material. Intrinsic strength properties for this material system are given below.
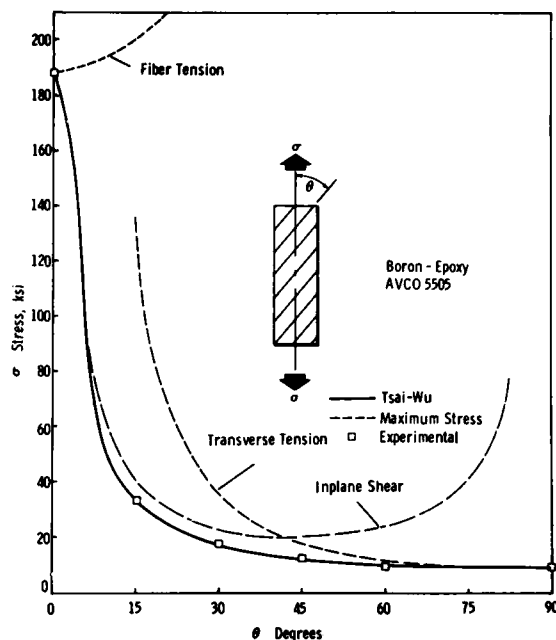
$$X_1^T = 27.3 \text{ MPa} \ (188 \text{ ksi})$$

$$X_1^C = 52.4 \text{ MPa} \ (361 \text{ ksi})$$

$$X_2^T = 1.3 \text{ MPa} \ (9 \text{ ksi})$$

$$X_2^C = 6.5 \text{ MPa} \ (45 \text{ ksi})$$

$$X_6 = 1.4 \text{ MPa} \ (10 \text{ ksi})$$

From these data it is possible to calculate the strength constants and to predict the coupon strength as a function of the angle θ as shown in Figure 6. Note the excellent agreement between theory and experiment.

Micromechanical Strength Models

The intrinsic strength properties required in the strength models discussed previously may be measured directly in the laboratory. However, just as there is a need for prediction of intrinsic composite elastic properties, it is desirable to develop methods for prediction of intrinsic strengths. One major difference between prediction of elastic and strength properties is that strength is a local phenomenon while stiffness is an average or integrated property. Hence, it should not be surprising to learn that techniques which model average material response are rather poor predictors of strength. Further, differences in tensile and compressive responses should be expected in fibrous materials since compressive failure may be controlled by microscopic instability of the fibrous phase, while tensile failure for brittle material systems is typically controlled by a local flaw in either fiber or matrix. For failures controlled by fiber stability the importance of the local geometry may not be understated. In this case, the existence of a single intrinsic compressive strength is doubtful. Nevertheless, in the spirit of completeness, simple micromechanical strength models will be presented here.

Consider the longitudinal strength of a unidirectional composite material.

$$X_1^T = (E_f v_f + E_m v_m) \epsilon_f^{ult.} \tag{41}$$

The relation (41) corresponds to a composite material wherein the fiber ultimate strain is less than that of the matrix phase and both fiber and matrix remain linearly elastic until failure. Further, the interfacial bond between fiber and matrix is assumed to be adequate for load transfer, while all fibers are assumed to possess a deterministic and uniform strength. Of course, these assumptions result in an oversimplified model of strength and many researchers are actively considering these important variables.

Unidirectional fiber composites are weak when stressed normal to the fiber direction since the matrix phase must support the transverse tensile stresses. Three possible modes of failure exist for transverse tension: matrix failure, interface failure, or fiber splitting. If discussion is limited to well bonded composites of fibers with transverse strength exceeding that of the matrix, then:

$$X_2^T = \sigma_m^{ult.} \tag{42}$$

where $\sigma_m^{ult.}$ is the ultimate tensile strength of the matrix. Experimental data have shown the composite transverse tensile strength to differ from the matrix tensile strength by a factor of 2.

If fiber instability controls the compressive strength of the unidirectional laminate then the properties of the matrix phase take on importance since the matrix provides the elastic foundation for the fiber and restrains it from buckling. If we assume the buckled fiber takes on the form

$$v = f \sin \frac{\pi x}{\ell} \tag{43}$$

where "v" is the lateral deflection and "ℓ" is the deflection half wave length, then moment equilibrium of the fiber requires

$$\frac{dM}{dx} - V + \sigma_1 A \frac{dv}{dx} = 0 \tag{44}$$

But both the moment and shear resultants in the fibers can be expressed in terms of the lateral displacement, v :

$$M = E_f I_f \frac{d^2 v}{dx^2} \quad , \quad v = AG_{12} \frac{dv}{dx} \tag{45}$$

where $I_f = A_f r_f^2$. Combining equations (43), (44) and (45) yields the prediction equation

$$X_1^C = G_{12}(1 - f_0/f_c) \tag{46}$$

where f_0 is the amplitude of the initial deflection in the fibers and f_c is the deflection at failure. When no initial imperfection exists ($f_0 = 0$), the compressive strength is predicted to be equal to the composite shear modulus, G_{12}. However, experimental results indicate that the compressive strength never achieves a level equal to this value. In addition to local imperfections in alignment (f_0) it is possible that the matrix phase initiates in the shearing failure mode. If equation (45) is solved for composite shear-

ing stress, S_6 then it is possible to determine the deflection amplitude at failure, f_c in terms of the initial imperfection and the ratio of shear stress and composite shear modulus

$$f_c = f_o + \frac{1}{\pi} \frac{S_6}{G_{12}} \tag{47}$$

It is also possible to determine the critical amplitude which corresponds to flexural failure of the fiber, assuming fiber tensile strain, $\varepsilon_f^{ult.}$ controls

$$f_c = f_o + \frac{2}{r_f} \left(\frac{\ell}{\pi}\right)^2 \varepsilon_f^{ult.} \tag{48}$$

where r_f is the fiber radius of gyration. Thus, two possible failure modes determine compressive strength for fiber instability

$$x_1^C = G_{12}/[1 + (\pi f_o/\ell)/e_6] \quad \text{(shear failure)}$$

$$x_1^C = G_{12}f_b/(f_o+f_b) \quad \text{(fiber flexural failure)} \tag{49}$$

and

$$f_b = \frac{2}{r_f} \left(\frac{\ell}{\pi}\right)^2 \varepsilon_f^{ult.}$$

The compressive strength predictions (49) suffer from several simplifying assumptions, the most important of which is the assumption of linear shear stress-strain response. Most polymeric composites exhibit highly nonlinear shear stress-strain response. Thus it is necessary to use the value of the secant modulus at failure rather than G_{12} initial.

Finally, the intrinsic shear strength S_6 is similar in nature to the transverse tensile strength in that three possible failure modes exist including matrix failure, interfacial failure and fiber shear splitting. Further, a reasonable estimate of composite shear strength is that of the matrix. However, since many matrices are brittle and exhibit tensile controlled failure, the shearing strength of the matrix is taken as equal to the matrix tensile strength. Stress concentrations due to the presence of the fibers may act to reduce the composite shearing strength below that of the matrix material in many cases.

Introduction to
Thin Laminate Theory

R. Byron Pipes

University of Delaware, U.S.A.

Laminate Theory

In contrast to micromechanical models which utilize fiber and matrix properties to pre-
dict properties of the equivalent homogeneous composite material, laminate theory pre-
dicts the behavior of multidirectional laminates from the properties of individual lamina
consisting of unidirectional, woven or discontinuous fibers. The lamina is viewed as
homogeneous and possessing orthotropic symmetry and as such is the building block for the
multidirectional laminate. Laminate theory offers a systematic way to analyze the lami-
nate for prediction of properties of an equivalent homogeneous material, state of stress
and strain within each of the lamina, and prediction of failure of any lamina within the
laminate. Thus laminate properties and behavior are considered in the macroscopic analy-
sis of a composite structure wherein the fiber and matrix properties are no longer iden-
tified. Yet through laminate theory and micromechanics .t is possible to trace the ef-
fects of constituent properties upon overall structural performance.

Laminate geometry can be precisely described for composite lamina of identical composi-
tion and thickness simply by listing the fiber orientations from the top of the laminate
to the bottom. For example, the notation $[0°/90°/0°]_T$ uniquely describes a three-layer
laminate with fiber orientations of 0° and 90° with respect to the laminate principal
axis (x) as shown in Figure 1. The subscript
T indicates that the laminae noted within the
brackets comprise the total laminate. For
laminates in which the laminae stacking se-
quence is symmetric about the laminate mid-
surface, the notation may be abbreviated by
using the subscript s for symmetry. For
example, the laminate configuration $[0°/90°$
$/90°/0°]_T$ may be rewritten as $[0°/90°]_s$.
Further, when a single lamina is repeated
in the sequence the nth repeat can be in-
dicated by subscript n for that lamina.
Thus the laminate $[0°/90°/90°/0°]_T$ becomes
$[0°/90°_2/0°]_T$. Angle ply laminates such as
$[0°/+45°/-45°]_s$ can be abbreviated as $[0°$
$/\pm45°]_s$. For an odd number of laminae the
midplane lies within the center lamina. A
bar is used over the central lamina to in-
dicate this; for example, $[0°/90°/0°]_T$ be-
comes $[0°/\overline{90°}]_s$.

Figure 1. Laminate Configuration.

Basic Assumptions

When laminate thickness is small relative
to its lateral dimensions, stress components
acting on interlaminar planes at interior
regions of the laminate (free edges will be treated later) are generally small and may be
neglected. Hence, the state of stress within each lamina is considered to be planar and
unique to the lamina. In addition we restrict our attention to deformations which are
small compared to the laminate thickness and inplane strains which are small compared to
unity. Further the Kirchhoff assumption that inplane displacements are linear functions
of the thickness coordinate is adopted, and therefore interlaminar shear strains are
negligible. With these assumptions the behavior of the laminate may be reduced to a two-
dimensional study of the laminate midsurface. Consider the strain-displacement relations
in the x,y,z coordinate system:

$$\varepsilon_x = \partial u/\partial x \quad ; \quad \gamma_{xy} = \partial u/\partial y + \partial v/\partial x$$

$$\varepsilon_y = \partial v/\partial y \quad ; \quad \gamma_{xz} = \partial u/\partial z + \partial w/\partial x \tag{1}$$

$$\varepsilon_z = \partial w/\partial z \quad ; \quad \gamma_{yz} = \partial v/\partial z + \partial w/\partial y$$

Where u,v,w are displacements in the x,y,z directions respectively. If the inplane dis-
placements are assumed to be linear functions in z, we have

$$u = u_o(x,y) + zF_1(x,y)$$

$$v = v_o(x,y) + zF_2(x,y) \tag{2}$$

where u_o, v_o are the midplane displacements. Since the shear strains, γ_{xz} and γ_{yz} are
known to vanish by Kirchhoff's assumption

$$\gamma_{xz} = F_1(x,y) + \partial w/\partial x = 0$$

$$\gamma_{yz} = F_2(x,y) + \partial w/\partial y = 0 \tag{3}$$

Therefore,

$$F_1(x,y) = - \partial w/\partial x \quad , \quad F_2(x,y) = - \partial w/\partial y \tag{4}$$

If the thickness strain ε_z is negligible then

$$w = w(x,y) \tag{5}$$

Substituting (4) into (2) and the result into (1) yields the strain-curvature relations for the laminate:

$$\varepsilon_x = \varepsilon_x^\circ + zK_x$$

$$\varepsilon_y = \varepsilon_y^\circ + zK_y \tag{6}$$

$$\gamma_{xy} = \gamma_{xy}^\circ + zK_{xy}$$

where

$$\varepsilon_x^\circ = \partial u^\circ/\partial x \quad ; \quad K_x = - \partial^2 w/\partial x^2$$

$$\varepsilon_y^\circ = \partial v^\circ/\partial y \quad ; \quad K_y = - \partial^2 w/\partial y^2 \tag{7}$$

$$\gamma_{xy}^\circ = \partial u^\circ/\partial y + \partial v^\circ/\partial x \quad ; \quad K_{xy} = -2(\partial^2 w/\partial x \partial y)$$

The stress-strain relations for the single orthotropic lamina was given in the previous section as equation (17). If the constitutive relation is combined with equation (6), the following results are developed for the individual laminae:

$$\sigma_x = Q_{11}'\varepsilon_x^\circ + Q_{12}'\varepsilon_y^\circ + Q_{16}'\gamma_{xy}^\circ + z(Q_{11}'K_x + Q_{12}'K_y + Q_{16}'K_{xy})$$

$$\sigma_y = Q_{12}'\varepsilon_x^\circ + Q_{22}'\varepsilon_y^\circ + Q_{26}'\gamma_{xy}^\circ + z(Q_{12}'K_x + Q_{22}'K_y + Q_{26}'K_{xy}) \tag{8}$$

$$\tau_{xy} = Q_{16}'\varepsilon_x^\circ + Q_{26}'\varepsilon_y^\circ + Q_{66}'\gamma_{xy}^\circ + z(Q_{16}'K_y + Q_{26}'K_y + Q_{66}'K_{xy})$$

where the x,y,z coordinate system is taken as the 1'2'3' coordinate system and $\tau_{xy} \equiv \sigma_6'$, $\gamma_{xy} = \varepsilon_6'$.

In order to describe the behavior of the laminate it is necessary to define the laminate force and moment resultants as shown in Figure 2.

Force Resultants:

$$N_x = \int_{-h/2}^{h/2} \sigma_x dz \quad ; \quad N_y = \int_{-h/2}^{h/2} \sigma_y dz$$

$$N_{xy} = \int_{-h/2}^{h/2} \tau_{xy} dz \tag{9}$$
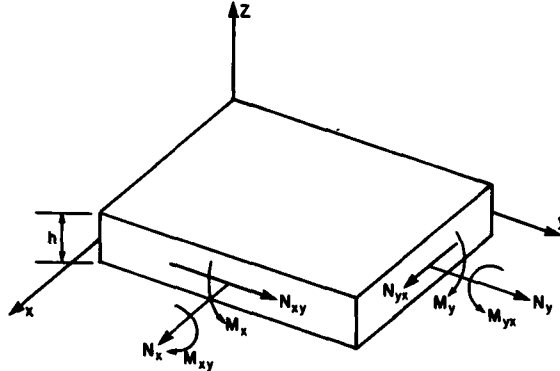
Figure 2. Force and Moment Resultants

Moment Resultants:

$$M_x = \int_{-h/2}^{h/2} \sigma_x z dz \quad ; \quad M_y = \int_{-h/2}^{h/2} \sigma_y z dz \quad ; \quad M_{xy} = \int_{-h/2}^{h/2} \tau_{xy} z dz \tag{10}$$

If equations (8), (9), and (10) are combined it is possible to express the force and moment resultants in terms of the midplane strains and curvatures:

$$N_x = A_{11}\varepsilon_x^\circ + A_{12}\varepsilon_y^\circ + A_{16}\gamma_{xy}^\circ + B_{11}K_x + B_{12}K_y + B_{16}K_{xy}$$

$$N_y = A_{12}\varepsilon_x^\circ + A_{22}\varepsilon_y^\circ + A_{26}\gamma_{xy}^\circ + B_{12}K_x + B_{22}K_y + B_{26}K_{xy}$$

$$N_{xy} = A_{16}\varepsilon_x^\circ + A_{26}\varepsilon_y^\circ + A_{66}\gamma_{xy}^\circ + B_{16}K_x + B_{26}K_y + B_{66}K_{xy}$$

$$M_x = B_{11}\varepsilon_x^\circ + B_{12}\varepsilon_y^\circ + B_{16}\gamma_{xy}^\circ + D_{11}K_x + D_{12}K_y + D_{16}K_{xy} \tag{11}$$

$$M_y = B_{12}\varepsilon_x^\circ + B_{22}\varepsilon_y^\circ + B_{26}\gamma_{xy}^\circ + D_{12}K_x + D_{22}K_y + D_{26}K_{xy}$$

$$M_{xy} = B_{16}\varepsilon_x^\circ + B_{26}\varepsilon_y^\circ + B_{66}\gamma_{xy}^\circ + D_{16}K_x + D_{26}K_y + D_{66}K_{xy}$$

The relations (11) may be inverted to yield the inverse relations:

$$\varepsilon_x^\circ = H_{11}N_x + H_{12}N_y + H_{13}N_{xy} + H_{14}M_x + H_{15}M_y + H_{16}M_{xy}$$

$$\varepsilon_y^\circ = H_{12}N_x + H_{22}N_y + H_{23}N_{xy} + H_{24}M_x + H_{25}M_y + H_{26}M_{xy}$$

$$\gamma^o_{xy} = H_{13}N_x + H_{23}N_y + H_{33}N_{xy} + H_{34}M_x + H_{35}M_y + H_{36}M_{xy}$$
$$K_x = H_{14}N_x + H_{24}N_y + H_{43}N_{xy} + H_{44}M_x + H_{45}M_y + H_{46}M_{xy}$$
$$K_y = H_{15}N_x + H_{25}N_y + H_{53}N_{xy} + H_{54}M_x + H_{55}M_y + H_{56}M_{xy}$$
$$K_{xy} = H_{16}N_x + H_{26}N_y + H_{63}N_{xy} + H_{64}M_x + H_{65}M_y + H_{66}M_{xy}$$

(12)

where the laminate stiffness terms are defined as follows:

$$A_{ij} = \int_{-h/2}^{h/2} Q'_{ij}dz \quad ; \quad B_{ij} = \int_{-h/2}^{h/2} Q'_{ij}zdz \quad ; \quad D_{ij} = \int_{-h/2}^{h/2} Q'_{ij}z^2dz \qquad (13)$$

$(i,j=1,2,6)$

The integration in relations (13) may be replaced by summations when it is recognized that the Q'_{ij} do not vary within a given lamina for a "n" layer laminate:

$$A_{ij} = \sum_{k=1}^{n} Q'^{k}_{ij}(h_k-h_{k-1})$$

$$B_{ij} = \frac{1}{2}\sum_{k=1}^{n} Q'^{k}_{ij}(h_k^2-h_{k-1}^2) \qquad (14)$$

$$D_{ij} = \frac{1}{3}\sum_{k=1}^{n} Q'^{k}_{ij}(h_k^3-h_{k-1}^3)$$

The h_k are defined in Figure 3.

The most important feature of the laminate constitutive relations (11) is that for the general laminate there are several coupling phenomena which are absent in laminates of a single fiber orientation or isotropic material. First, the B_{ij} stiffness terms, known as the bending-extensional coupling elements, relate midplane strains to moment resultants and midplane curvatures to force resultants. If the definition of B_{ij} is examined, it is clear that a symmetric $Q'_{ij}(z)$ yields $B_{ij} \equiv 0$. Hence the bending-extensional coupling phenomenon is only present for unsymmetric laminates. The second coupling phenomenon is that between extensional strains and shearing force resultant, and extensional force resultants and shearing strains. The terms A_{16} and A_{26} are known as the laminate shear coupling stiffnesses. Note should be made that when the shear coupling terms of the lamina constitutive relations are zero ($Q'_{16} = Q'_{26} = 0$) then the terms A_{16}, A_{26} also vanish. This is the case for laminates with lamina of only 0° and 90°. All other angles yield nonzero Q'_{16}, Q'_{26}. However, under the conditions that for every +θ° lamina there is a -θ° lamina within the laminate (termed a balanced laminate) the A_{16}, A_{26} terms also vanish. The final coupling phenomenon is between the twisting curvature K_{xy} and the moment resultants M_x, M_y, as well as the twisting moment, K_{xy} and the curvatures K_x and K_y. Here the coupling terms are D_{16} and D_{26}. Examination of the definition of D_{16} and D_{26} terms shows that only for antisymmetric $Q'_{ij}(z)$ do D_{16} and D_{26} vanish. However it can be shown that for laminates composed of only angle ply orientations $[\pm\theta°_n]$ the D_{16} and D_{26} terms are given as

$$D_{16} = \frac{h^3}{n} Q'_{16}(\theta)$$
$$D_{26} = \frac{h^3}{n} Q'_{26}(\theta)$$

(15)

Figure 3. Layer Nomenclature for Laminate

Hence, as the number of laminae, n increases, the terms D_{16} and D_{26} diminish in magnitude.

To illustrate the coupling phenomena consider a laminate subjected to a single force resultant, $N_x = N_o$. In addition, if it is assumed that the laminate remains planar during this loading the curvatures vanish, $K_x = K_y = K_{xy} \equiv 0$. Substituting these conditions into the first three equations of (12) yields the following midplane strains:

$$\varepsilon^o_x = H_{11}N_o$$
$$\varepsilon^o_y = H_{12}N_o$$
$$\gamma^o_{xy} = H_{13}N_o$$

(16)

Note that a nonzero shear strain γ^o_{xy} results from the application of a normal force resultant, N_o. This phenomenon is known as shear coupling and it characterizes one of the anisotropic properties of the general laminate. If the resulting strains described in (16) are substituted into the last three equations of (11) it is possible to determine the moment resultants:
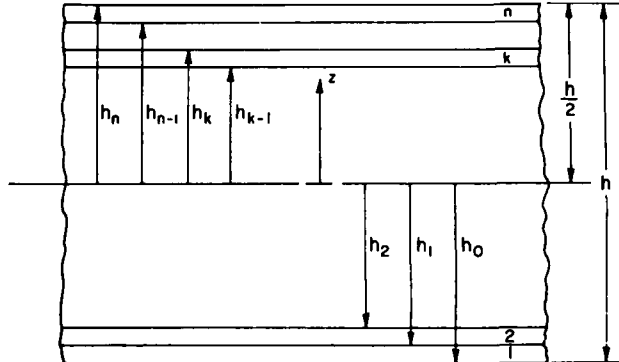
$$M_x = (B_{11}H_{11} + B_{12}H_{12} + B_{16}H_{13})N_o$$

$$M_y = (B_{12}H_{11} + B_{22}H_{12} + B_{26}H_{13})N_o \qquad (17)$$

$$M_{xy} = (B_{16}H_{11} + B_{26}H_{12} + B_{66}H_{13})N_o$$

The moment resultants are nonzero and must be applied to the laminate in order to restrain it to its initial planar shape when subjected to a uniaxial loading. This mathematical "experiment" clearly demonstrates the phenomenon of bending-extensional coupling. Finally consider the symmetric laminate subjected to a nonzero moment resultant, $M_x = M_o$ where $M_y = M_{xy} = 0$. The midplane curvatures may be determined from relation (12):

$$K_x = H_{44}M_o$$

$$K_y = H_{54}M_o \qquad (18)$$

$$K_{xy} = H_{64}M_o$$

Note that a nonzero twisting curvature, K_{xy} results from the application of the bending moment, M_x ; thereby illustrating the phenomenon of bending-twisting coupling.

Effective Laminate Properties

When dealing with composite laminates, it is often desirable to treat them as homogeneous. Therefore it is necessary to develop expressions for effective laminate engineering properties. For the balanced and symmetric laminates it is possible to express their effective enegineering properties as a function of the laminate extensional stiffnesses, A_{ij} and thickness, h.

Longitudinal Young's Modulus

$$E_x = (A_{11}A_{22} - A_{12}^2)/hA_{22} \qquad (19)$$

Transverse Young's Modulus

$$E_y = (A_{11}A_{22} - A_{12}^2)/hA_{11} \qquad (20)$$

Longitudinal Poisson's Ratio

$$\nu_{xy} = A_{11}/A_{22} \qquad (21)$$

Transverse Poisson's Ratio

$$\nu_{yx} = A_{12}/A_{11} \qquad (22)$$

Planar Shear Modulus

$$G_{xy} = A_{66}/h \qquad (23)$$

If the laminate is not symmetric, determination of effective properties is more complex in that all of the stiffness terms A_{ij} , B_{ij} and D_{ij} are involved. However, the inverted form of the stiffness array yields the needed results:

Longitudinal Young's Modulus

$$E_x = (hH_{11})^{-1} \qquad (24)$$

Transverse Young's Modulus

$$E_y = (hH_{22})^{-1} \qquad (25)$$

Longitudinal Poisson's Ratio

$$\nu_{xy} = -H_{12}/H_{11} \qquad (26)$$

Transverse Poisson's Ratio

$$\nu_{yx} = -H_{12}/H_{22} \qquad (27)$$

Planar Shear Modulus

$$G_{xy} = (hH_{33})^{-1} \qquad (28)$$

For lamina properties described in Table I, effective engineering properties are shown in Table II.

Table I. Transformed Stiffness Matrix*

$$E_1 = 20 \times 10^6 \qquad E_2 = 2.1 \times 10^6 \qquad \nu_{12} = 0.21 \qquad G_{12} = 0.85 \times 10^6$$

θ	Q'_{11}	Q'_{12}	Q'_{16}	Q'_{22}	Q'_{26}	Q'_{66}
0	2.009×10^7	4.431×10^5	0	2.110×10^6	0	8.500×10^5
45	6.622×10^6	4.922×10^6	4.496×10^6	6.622×10^6	4.496×10^6	5.329×10^6
90	2.110×10^6	4.431×10^5	-6.695×10^6	2.009×10^7	-3.611×10^6	8.500×10^5

*E_i, G_{12} and Q'_{ij} in psi. For S.I. units, 1 GPa = 6.895×10^6 psi

Table II. Typical Laminate Properties

Property	Laminate $[0°/45°/-45°]_s$	$[0°/45°/-45°/45°/-45°/0]$	$[0°/45°/45°]_s$
A_{11}	3.667×10^5 lb/in.**	3.667×10^5 lb/in.	3.667×10^5 lb/in.
A_{12}	1.132×10^5 lb/in.	1.132×10^5 lb/in.	1.132×10^5 lb/in.
A_{22}	1.685×10^5 lb/in.	1.689×10^5 lb/in.	1.689×10^5 lb/in.
A_{66}	1.266×10^5 lb/in.	1.266×10^5 lb/in.	1.266×10^5 lb/in.
A_{16}	0	0	9.891×10^1 lb/in.
A_{26}	0	0	9.891×10^4 lb/in.
B_{11}	0	0	0
B_{12}	0	0	0
B_{22}	0	0	0
B_{66}	0	0	0
B_{16}	0	-2.720×10^2 lb	0
B_{26}	0	-2.720×10^2 lb	0
D_{11}	4.822×10^1 lb/in.	4.822×10^1 lb/in.	4.822×10^1 lb/in.
D_{12}	5.301×10^0 lb/in.	5.301×10^0 lb/in.	5.301×10^0 lb/in.
D_{22}	1.032×10^1 lb/in.	1.032×10^1 lb/in.	1.032×10^1 lb/in.
D_{66}	6.520×10^0 lb/in.	6.520×10^0 lb/in.	6.520×10^0 lb/in.
D_{16}	2.992×10^0 lb/in.	0	3.989×10^0 lb/in.
D_{26}	2.992×10^0 lb/in.	0	3.989×10^0 lb/in.
E_x	8.82×10^6 psi**	8.78×10^6 psi	8.34×10^6 psi
E_y	4.06×10^6 psi	3.89×10^6 psi	2.64×10^6 psi
ν_{xy}	0.670	0.646	0.392
ν_{yx}	0.309	0.286	0.124
G_{xy}	3.84×10^6 psi	3.61×10^6 psi	1.97×10^6 psi

**For S.I. units, 1 NM/m = 1.751×10^{-4} lb/in., 1 GPa = 6.895×10^6 psi

Laminate Stress Analysis

When the laminate loading conditions N_x, N_y, N_{xy}, M_x, M_y, M_{xy} are known it is possible to determine the state of stress throughout the laminate through relation (6). Consider the case of the $[0°/\pm45°/90°]_s$ laminate subjected to a loading. Laminate strains and curvatures can be determined from equation (12). Next the stresses in the kth lamina are determined from the lamina consitutitive relation given in relation (8). Stress continuity at the interfaces z = constant is not required for the stress components σ_x, σ_y and τ_{xy} since they do not act on the interlaminar planes.

The stress distributions within the laminate are shown in Figures 4, 5 and 6. As expected the stress distributions show discontinuities at the laminae interfaces. This behavior reflects the significant differences between elastic stiffness properties of adjacent laminae. Since the Kirchhoff assumption of linear strain through the laminate thickness was invoked in the development of laminate theory, the stress discontinuities do not correspond to strain discontinuities. Rather the laminae remain intact and well bonded to near neighbors. The phenomenon of delamination will be discussed in a subsequent section.

Figure 4. Distribution of σ_x Within the $[0°/\pm45°/90°]_s$ Laminate

Hygrothermal Residual Stress and Strain

Since fibrous composite materials are processed at elevated temperatures and the polymeric matrices are hygroscopic, residual stresses are induced in the multiaxial laminate. In order to examine these phenomena, it is necessary to revise the lamina constitutive relations to account for hygrothermal strains:

$$\sigma_x = Q'_{11}(\varepsilon_x-\alpha_x T-\beta_x M) + Q'_{12}(\varepsilon_y-\alpha_y T-\beta_y M)$$
$$+ Q'_{16}(\gamma_{xy}-\alpha_{xy}T-\beta_{xy}M)$$
$$\sigma_y = Q'_{12}(\varepsilon_x-\alpha_x T-\beta_x M) + Q'_{22}(\varepsilon_y-\alpha_y T-\beta_y M)$$
$$+ Q'_{26}(\gamma_{xy}-\alpha_{xy}T-\beta_{xy}M) \qquad (29)$$
$$\tau_{xy} = Q'_{16}(\varepsilon_x-\alpha_x T-\beta_x M) + Q'_{26}(\varepsilon_y-\alpha_y T-\beta_y M)$$
$$+ Q'_{66}(\gamma_{xy}-\alpha_{xy}T-\beta_{xy}M)$$

where α and β are coefficients of thermal and moisture expansion, respectively, and T and M are change in temperature and moisture content, respectively. When the lamina consitutive relations including hygrothermal strains are employed in the development of the laminate constitutive relations, effective thermal and moisture force and moment resultants are identified:

Figure 5. Distribution of σ_y Within the $[0°/\pm45°/90°]_s$ Laminate

Thermal Force Resultants $\qquad (30)$

$$N^T_x = \sum_{k=1}^{n} (Q'^k_{11}\alpha^k_x + Q'^k_{12}\alpha^k + Q'^k_{16}\alpha_{xy})(h_k-h_{k-1})T$$

$$N^T_y = \sum_{k=1}^{n} (Q'^k_{12}\alpha_x + Q'^k_{22}\alpha^k_y + Q'^k_{26}\alpha_{xy})(h_k-h_{k-1})T$$

$$N^T_{xy} = \sum_{k=1}^{n} (Q'^k_{16}\alpha_x + Q'^k_{26}\alpha_y + Q'^k_{66}\alpha_{xy})(h_k-h_{k-1})T$$

Thermal Moment Resultants $\qquad (31)$

$$M^T_x = \frac{1}{2}\sum_{k=1}^{n} (Q'^k_{11}\alpha^k_x + Q'^k_{12}\alpha^k_y + Q'^k_{16}\alpha_{xy})(h^2_k-h^2_{k-1})T$$

$$M^T_y = \frac{1}{2}\sum_{k=1}^{n} (Q'^k_{12}\alpha_x + Q'^k_{22}\alpha^k_y + Q'^k_{26}\alpha_{xy})(h^2_k-h^2_{k-1})T$$
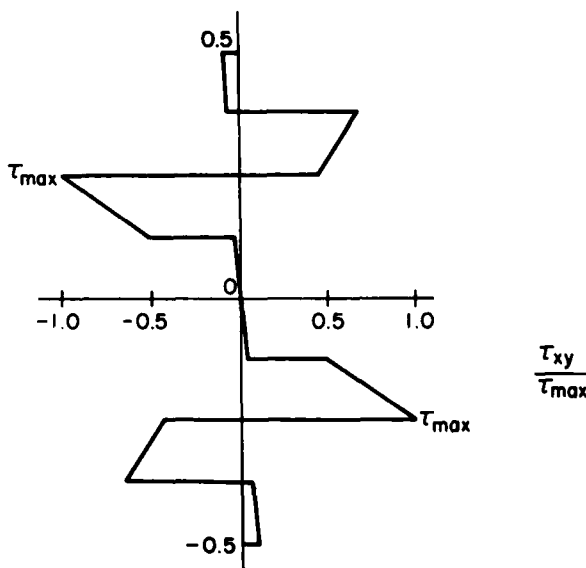
Figure 6. Distribution of τ_{xy} Within the $[0°/\pm45°/90°]_s$ Laminate

$$M_{xy}^T = \frac{1}{2} \sum_{k=1}^{n} (Q_{16}^{,k}\alpha_x + Q_{26}^{,k}\alpha_y + Q_{66}^{,k}\alpha_{xy})(h_k^2 - h_{k-1}^2)T$$

The expressions for moisture, force and moment resultants may be obtained by replacing α by β and T by M in equations (30) and (31).

Consider the general laminate which undergoes a change in temperature T. For example, the cooling of the laminate after processing results in negative thermal excursion. The laminate curvatures may be calculated in relation (12) if the loading is taken to be due to the thermal force and moment resultants. For example the curvature K_x is:

$$K_x = H_{14}N_x^T + H_{24}N_y^T + H_{34}N_{xy}^T + H_{44}M_x^T + H_{45}M_y^T + H_{46}M_{xy}^T \qquad (32)$$

For a xymmetric laminate, $H_{14} = H_{24} = H_{34} = H_{44} = H_{45} = H_{46} = 0$. Thus the as-processed symmetric laminate will exhibit no curvature. Yet the unsymmetric laminate will not be planar after processing, rather it will exhibit all curvatures, in general. Although the symmetric and balanced laminate exhibits no curvature after the thermal excursion it does exhibit inplane deformation:

$$\epsilon_x^\circ = \frac{A_{22}N_x^T - A_{12}N_y^T}{A_{11}A_{22} - A_{12}^2}$$

$$\epsilon_y^\circ = \frac{A_{11}N_y^T - A_{12}N_x^T}{A_{11}A_{22} - A_{12}^2} \qquad (33)$$

$$\gamma_{xy}^\circ = K_x = K_y = K_{xy} = 0$$

Note that the inplane strains induced by the thermal excursion, T enable the definition of the effective laminate coefficients of thermal expansion $\bar{\alpha}_x$ and $\bar{\alpha}_y$:

$$\bar{\alpha}_x = \frac{A_{22}N_x^T - A_{12}N_y^T}{(A_{11}A_{22} - A_{12}^2)T}$$

$$\bar{\alpha}_y = \frac{A_{11}N_y^T - A_{12}N_x^T}{(A_{11}A_{22} - A_{12}^2)T} \qquad (34)$$

Further thermal residual stresses are induced in the laminate by the effective thermal force and moment resultants. Consider the stresses in the kth lamina:

$$\sigma_x^k = [(Q_{11}^{,k}A_{22} - Q_{12}^{,k}A_{12})N_x^T + (Q_{12}^{,k}A_{11} - Q_{11}^{,k}A_{12})N_y^T]/(A_{11}A_{22} - A_{12}^2)$$

$$\sigma_y^k = [(Q_{12}^{,k}A_{22} - Q_{22}^{,k}A_{12})N_x^T + (Q_{22}^{,k}A_{11} - Q_{11}^{,k}A_{12})N_y^T]/(A_{11}A_{12} - A_{12}^2) \qquad (35)$$

$$\tau_{xy}^k = [(Q_{16}^{,k}A_{22} - Q_{26}^{,k}A_{12})N_x^T + (Q_{26}^{,k}A_{11} - Q_{26}^{,k}A_{12})N_y^T]/(A_{11}A_{22} - A_{12}^2)$$

Typical thermal residual stress distributions for the $[0°/\pm45°/90°]_s$ laminate are shown in Figures 7, 8 and 9.
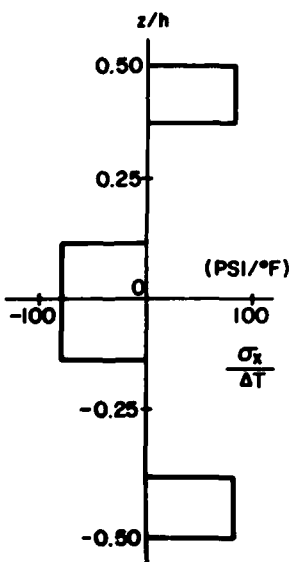
Figure 7. Thermal Residual Stress, σ_x Figure 8. Thermal Residual Stress, σ_y Figure 9. Thermal Residual Stress, τ_{xy}
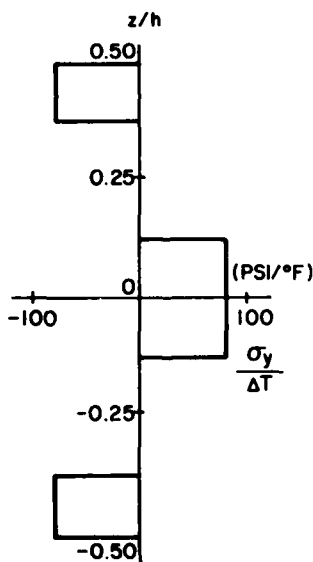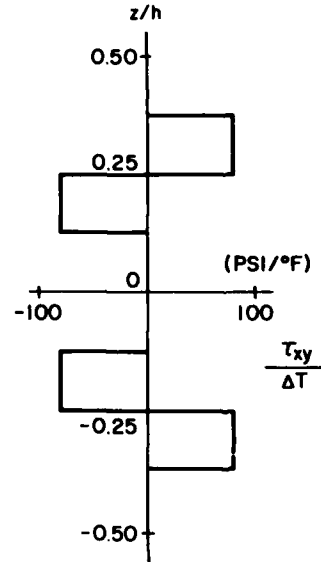
Laminate Strength

Prediction of laminate strength is accomplished by first determining the stress or strain distribution within each lamina of the laminate followed by a systematic application of a given failure criterion. Since the laminate stress state is a function of the laminate configuration, loading and laminae material properties, the elastic stress distribution can be determined only when all these factors are known. Furthermore, inelastic behavior of the laminae invalidates the stress field predicted by the elastic analysis. Therefore it should not be surprising to find that maximum strain criterion has received widespread adoption since the distribution of the strain through the laminate thickness (and hence in each lamina) is known when the surface strain components are known, regardless of material nonlinearity. Contemporary laminate strength models predict the first lamina failure, but do not consider the residual response of the surviving laminae. As such, this first failure model may be very conservative. Consider for example the laminate $[0°/\pm45°/90°]_s$. The first lamina to fail is typically the 90° lamina for most brittle matrices. However, since the stiffness of this lamina is quite low, it carries a proportionately small portion of the total laminate load and its loss is insignificant. Further, a single crack in the 90° lamina does not result in its global loss to the laminate. Rather, the stress in the vicinity of the crack is transferred to adjacent laminae and regions of the laminate removed from the failure are unaffected. However, first lamina failure provides a direct and conservative estimate of laminate strength.

Since the matrix materials of most contemporary fiber composites are thermosetting polymers, residual stresses are present in the laminate at room temperature. Thus, a complete strength analysis must include both thermal and moisture induced residual stresses.

Interlaminar Stresses

The existence of interlaminar stresses in the presence of bending loads which are functions of the inplane coordinates x,y are well known. For the case of inplane loading, lamination theory only predicts inplane stresses, i.e. each ply is in a state of plane stress. This result is accurate for interior regions removed from laminate geometric discontinuities, such as free edges. There exists, however, a boundary layer near the laminate free edge where the state of stress is three-dimensional. The boundary layer is the region wherein stress transfer between laminae is accomplished through the action of interlaminar stresses. The width of the boundary layer is a function of the elastic properties of the laminae, the laminae fiber orientation, and laminate geometry. A simple rule of thumb is that the boundary layer is equal to the laminate thickness, h.

The primary consequences of the laminate boundary layer are delamination-induced failures which initiate within the edge region and distortions of surface strain and deformations due to the presence of interlaminar stress components. Failures which initiate in the boundary layer region of a finite-width test specimen may not yield data which accurately represent the true laminate strength.

The mechanism of interlaminar stress transfer for the $[\pm\theta]_s$ angle ply laminate is termed the first mode mechanism (Mode I). The important feature of Mode I is the mismatch in shear coupling coefficients between $+\theta$ and $-\theta$ layers. Consider a balanced symmetric angle-ply laminate, $[\pm\theta]_s$, under the uniform load

$$\bar{\sigma}_x = N_x/h = \sigma_o = \text{constant}$$

$$\bar{\sigma}_y = N_y/h = 0 \tag{36}$$

$$\bar{\tau}_{xy} = N_{xy}/h = 0$$

A cursory examination of the transformation relations reveals that

$$Q'_{11}(\theta) = Q'_{11}(-\theta) \quad , \quad Q'_{22}(\theta) = Q'_{22}(-\theta)$$

$$Q'_{12}(\theta) = Q'_{12}(-\theta) \quad , \quad Q'_{66}(\theta) = Q'_{66}(-\theta) \tag{37}$$

Thus Q'_{11}, Q'_{22}, Q'_{12} and Q'_{66} are constant through the laminate thickness and the laminate midplane strains are:

$$\varepsilon^o_x = \frac{Q'_{22}(\theta)\,\sigma_o}{[Q'_{11}(\theta)Q'_{22}(\theta) - Q'^2_{12}(\theta)]}$$

$$\varepsilon^o_y = \frac{-Q'_{12}(\theta)\,\sigma_o}{[Q'_{11}(\theta)Q'_{22}(\theta) - Q'^2_{12}(\theta)]} \tag{38}$$

and since the laminate is balanced,

$$\gamma^o_{xy} = 0 \tag{39}$$

Substituting equations (38) and (39) into the lamina constitutive relation yields

$$\sigma_x(\theta) = \sigma_x(-\theta) = \sigma_o$$

$$\sigma_y(\theta) = \sigma_y(-\theta) = 0 \tag{40}$$

$$\tau_{xy}(\theta) = -\tau_{xy}(-\theta) = \frac{Q'_{16}(\theta) \, \sigma_o}{[Q'_{11}(\theta)Q'_{22}(\theta) - Q'^2_{12}(\theta)]} = \tau_o$$

Thus, each individual lamina is subjected to the axial stress σ_o and a shear stress τ_{xy} which is equal in magnitude, but opposite in sign for the $\pm\theta$ plies. This loading on the individual plies is illustrated in Figure 10b. The shear resultant, N_{xy} is zero, since the contributions from the $+\theta$ and $-\theta$ layers will cancel. The shear stresses τ_{xy} prevent inplane shear strains γ^o_{xy} from occurring which would be the case if each of the $+\theta$ and $-\theta$ plies were loaded individually by a uniaxial stress σ_o. At the free edge of the laminae these shear stresses cannot exist since an edge is traction-free. Thus, near the edge of the laminae the interlaminar shear stress τ_{xz} is required.

Both finite difference solutions and approximate analytical solutions of the exact equations of elasticity have been developed for the finite-width angle-ply laminate. Results for the interlaminar shear stress τ_{xz} at the interface between laminae of $+45°$ and $-45°$ fiber orientation are presented in Figure 11. These results show that the interlaminar shear stress is maximum at the free edge where it appears to grow without bound. In addition, the displacement of the laminate surface in the direction of the load increases near the free edge, resulting in antisymmetric surface displacements as shown in Figure 12. The distribution of axial displacement and interlaminar shear stress through the laminate thickness is shown in Figures 13 and 14. These rsults show that the maximum interlaminar shear stress occurs at the interfaces between the $+45°$ and $-45°$ layers.

Figure 11. Interlaminar Shear Stress, τ_{xz}

(a)   (b)

Figure 10. Uniaxial Loading of an Angle-Ply Laminate
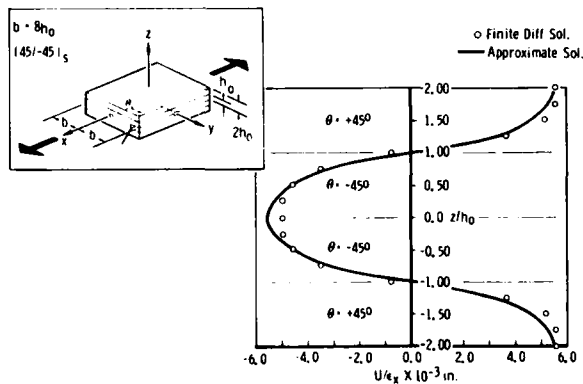
Figure 13. Distribution of Axial Dislplacement
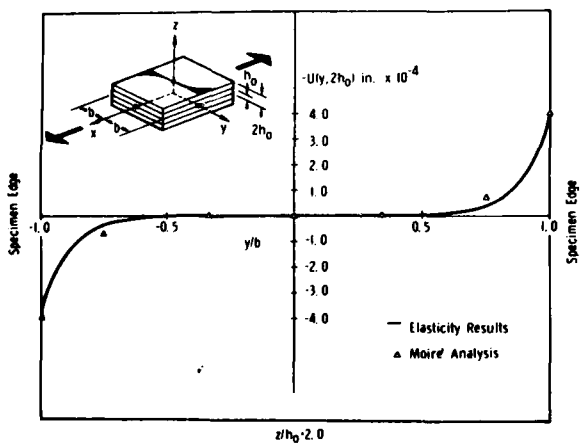
Figure 12. Surface Displacement
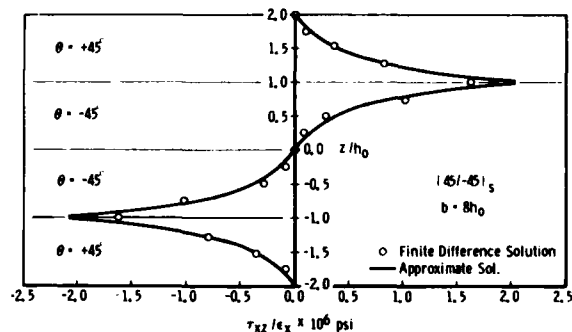
Figure 14. Distribution of Interlaminar Shear Stress Through the Thickness

The effect of the free-edge boundary zone on the inplane stresses σ_x and τ_{xy} is shown in Figure 15. It should be noted that the inplane shear stress vanishes at the free edge and coincides with the solution predicted by lamination theory at approximately one laminate thickness, h, from the edge.

An important point to bear in mind from this discussion is that the mechanism of the free-edge effect in angle-ply laminates is a mismatch in shear coupling coefficients between the $\pm\theta$ angle plies.

The mechanism of interlaminar stress transfer for the $[0°/90°]_s$ bidirectional laminate is termed the second mode mechanism (Mode II); its important feature is the mismatch in Poisson's ratios between 0° and 90° layers. Place a balanced, symmetric bidirectional laminate, $[0°/90°]_s$, under the same uniform load. For this laminate,

$$Q'_{12}(0°) = Q'_{12}(90°) = Q_{12} \tag{41}$$
$$= \frac{\nu_{12}E_2}{(1 - \nu_{12}E_2/E_1)}$$
$$Q'_{66}(0°) = Q'_{66}(90°) = G_{12}$$

Figure 15. Stress Results at Interface Between ±45° Laminae

Thus

$$Q'_{12} = Q_{12} \quad , \quad Q_{66} = G_{12} \tag{42}$$

In addition,

$$Q_{11} = Q_{22} = \frac{E_1 + E_2}{2(1 - \nu_{12}\nu_{21})} \tag{43}$$

Then the laminate strains are:

$$\epsilon_x^o = \frac{Q_{11}\sigma_o}{(Q_{11}^2 - Q_{12}^2)} = \frac{2(E_1 + E_2)(1 - \nu_{12}\nu_{21})\sigma_o}{(E_1 + E_2)^2 - 4\nu_{12}^2 E_2^2}$$

$$\epsilon_y^o = \frac{-Q_{12}\sigma_o}{(Q_{11}^2 - Q_{12}^2)} = -\frac{4\nu_{12}E_2(1 - \nu_{12}\nu_{21})\sigma_o}{(E_1 + E_2)^2 - 4\nu_{12}^2 E_2^2} \tag{44}$$

and there are no angle plies since $\theta = 0°$, 90°

$$\gamma_{xy}^o = 0 \tag{45}$$

Substituting equations (44) and (45) into the lamina constitutive relation yields

$$\sigma_x(0°) = 2\left[\frac{E_1(E_1 + E_2) - 2\nu_{12}^2 E_2^2}{(E_1 + E_2)^2 - 4\nu_{12}^2 E_2^2}\right]\sigma_o \quad , \quad \sigma_x(90°) = -2\left[\frac{E_1(E_1 + E_2) - 2\nu_{12}^2 E_2^2}{(E_1 + E_2)^2 - 4\nu_{12}^2 E_2^2}\right]\sigma_o \tag{46}$$

$$\sigma_y(0°) = -\sigma_y(90°) = \sigma_2 = \left(\frac{2\nu_{12}E_2(E_1 - E_2)\sigma_o}{(E_1 + E_2)^2 - 4\nu_{12}^2 E_2^2}\right) \tag{47}$$

$$\tau_{xy}(0°) = \tau_{xy}(90°) = 0 \tag{48}$$

In contrast to the state of stress for the angle-ply laminate, the inplane shear stress component vanishes for the bidirectional laminate due to the fact that the shear coupling terms Q'_{16} and Q'_{26} vanish at orientations of 0° or 90°. A mismatch in Poisson's ratios of 0° and 90° laminae leads to equal but opposite sign transverse stresses as illustrated in Figure 16. As in the case of the shear stress τ_o in angle-ply laminates, these transverse stresses, σ_2 , cannot exist at free edges in a $[0°/90°]_s$ bidirectional laminate. These transverse stresses are compensated for by interlaminar shear stresses τ_{yz} at the interface between the 0° and 90° layers. Further, the force vectors acting on the surface laminae due to the σ_y and τ_{yz} stresses are not colinear (see Figure 17) and hence result in a couple whose magnitude is given by

$$\text{Couple} = M_z = \sigma_y(h_o^2/2) \tag{49}$$

Figure 16. Uniaxial Loading
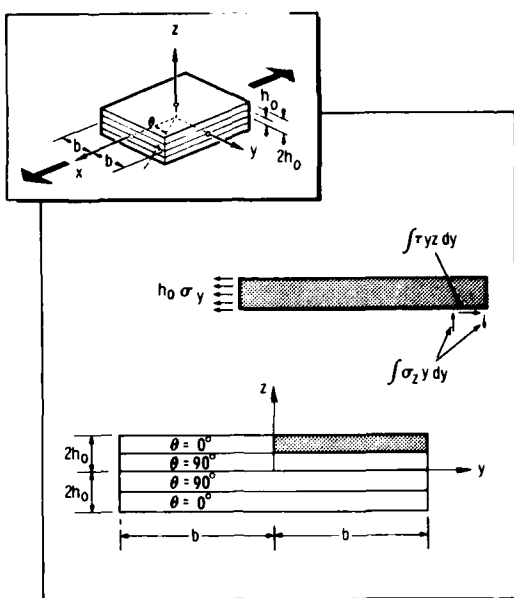
Figure 17. Transverse Normal and Inter-
laminar Shear Stresses

The couple is reacted by the interlaminar normal stress component, σ_z. The distribution
of the interlaminar normal stress must therefore result in a zero vertical force vector
while producing a couple equal in magnitude to that given in equation (49).

Solutions of equations of elasticity for the bidirectional laminate have been obtained
by numerical methods. These studies have revealed distributions of the interlaminar
shear and normal stresses at the interface between the 0° and 90° plies as shown in
Figures 18 and 19. Note the effect of stacking sequence on these stresses. Again the
free-edge boundary zone is approximately one laminate thickness from the edge. In addi-
tion, the interlaminar normal stress, σ_z , appears to be singular at the edge.

In the case of the [0°/90°]$_S$ bidirectional laminate, the mechanism of the free-edge
effect is a mismatch in Poisson's ratio between the 0° and 90° plies. Interlaminar nor-
mal stress in tension at the free edge can produce delamination.
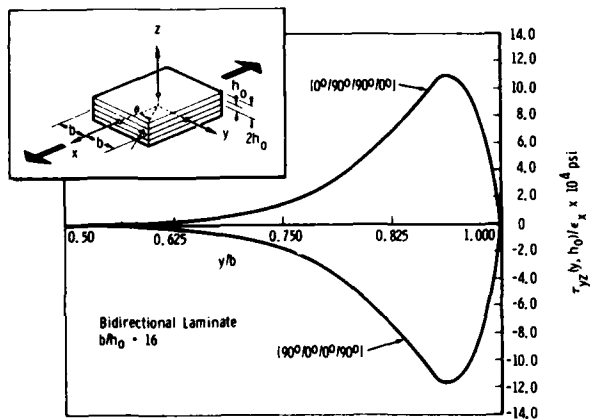
Figure 18. Distribution of Interlaminar
Shear Stress at the Interface
Between the 0° and 90° Plies
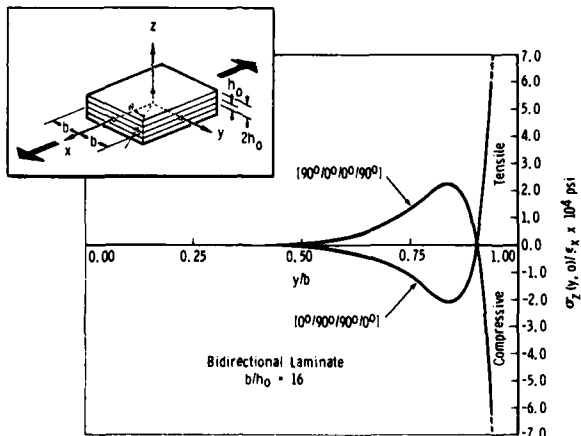
Figure 19. Distribution of Interlaminar
Normal Stress at the Interface
Between the 0° and 90° Plies

FRACTURE OF COMPOSITES AND DAMAGE TOLERANCE

by
Graham Dorey
Materials Department
Royal Aircraft Establishment
Farnborough
Hampshire, UK

SUMMARY

Composite materials are anisotropic in stiffness and in strength, and hence local stresses and strains within these materials are complex. They are also inhomogeneous and may have weak interfaces, which makes fracture more probable in certain directions. Fracture modes are therefore generally more complex than in isotropic homogeneous materials such as unreinforced metals and plastics. Advanced fibre composites tend preferentially to split parallel to the fibres, the initial fracture energy depending mainly on the matrix properties and the fibre-matrix interfacial bond strength; but, due to fibre misalignment, further fracture propagation depends on the fibre and interface properties. The three main stress modes to produce splitting are described. Fracture across fibres is more difficult and some of the energy absorbing mechanisms are discussed. In multidirectional laminates each ply still tends to split parallel to the fibres but the constraints of adjoining plies are significant and the fracture mechanisms and fracture energies depend on the ply orientations and stacking sequence (lay-up) and the ply thicknesses as well as on the usual fibre, matrix and interface properties. The strengths and toughnesses of advanced fibre composite laminates are continuously being improved.

In considering the impact behaviour of advanced composites for aerospace use there is generally more concern with the residual mechanical properties under realistic loading than with the energy absorption measured by conventional pendulum impact tests. The different forms of damage caused by dropped weights and high velocity projectiles are discussed, as well as the effects of material properties and structural geometry, on both the threshold energy and the extent of the damage. Although the incident energy of the projectile is one of the most significant parameters, its mass velocity and momentum also have important effects, especially in exciting various dynamic responses in the structure. The various types of impact damage have different effects on the residual shear, flexure, tension and compression properties and there are various methods such as 3-D reinforcement and hybrid laminates to improve composite impact performance; with important implications for the design of improved damage tolerant composite structures.

INTRODUCTION

Composite materials such as bone and some woods have evolved useful fracture characteristics whereby, under bending loads, they tend to split parallel to the grain and thus retain some integrity rather than snapping catastrophically across the grain. Some composite ceramics absorb damage by producing many micro-cracks throughout the damaged region rather than by forming a single critical crack. Man made materials such as brick and reinforced concrete have benefitted in certain applications from possessing specific characteristic fracture modes. In many of these cases the constituents of the composite material are inherently brittle and yet when combined they can produce a material that is remarkably tough.

Advanced composites for aerospace application, such as carbon,boron, glass or aramid fibres in epoxy resin, thermoplastic or carbon matrices, continue to make use of these characteristic fracture modes. Carbon, boron and aramid fibres have high specific stiffnesses and are useful to make lightweight air control surfaces, where maintaining the shape under aerodynamic loads is required. They also have high specific strengths and are finding increasing numbers of applications in primary load bearing structures. Glass fibres are strong but are more compliant and are damage tolerant, finding useful applications in rotary wing aircraft. Since aviation fuels increased markedly in price in the mid 1970's, weight saving has been more cost effective in civil aviation and carbon fibre and aramid fibre composites are being used more in relatively large secondary structures such as wing-to-body fairings in passenger aircraft. Advanced composites also allow the possibility of aeroelastic tailoring whereby the structure can respond to aerodynamic loading in such a way as to retain a greater efficiency; this could be useful in such applications as the forward swept wing. In all these different applications it is important to know the fracture characteristics of the materials under realistic loading.

Advanced composites will always contain "defects"; manufacturing defects such as delaminations and voids, machining damage especially at fastener holes, design cut-outs producing stress concentrations, accidental handling damage such as that caused by dropped tools and in-service damage such as that caused by runway stones, birds or weapons. In some instances the damage, although reducing the strength significantly, is barely visible and easily missed on inspection. Because of this notch sensitivity, carbon fibre reinforced plastics (CFRP) structures currently have a tensile strain design limit of about 0.4% even though the fibres have a breaking strain of over 1.3%. Similar design limits are applied in compression because of the micro-buckling fracture behaviour in hot-wet conditions. The micromechanics of the failure processes have important practical consequences. Even so, with these design limits, useful weight savings and cost savings have been demonstrated with CFRP and satisfactory performances in service have resulted.

Currently the carbon fibre manufacturers are managing to increase the failure strains to 1.5% and 1.7% and, as a result of pressure from aircraft constructors, are aiming at 2.0%. In making more efficient use of advanced composites and operating at higher stresses it is important to understand fully the failure modes and fracture characteristics. And as damage tolerant design philosophies become more widely applied it is necessary to detect flaws, to predict damage growth rates and to know when damage will become critical.

FRACTURE OF UNIDIRECTIONAL COMPOSITES

Fig 1 shows the effect of an elliptical notch in an infinite sheet of material subjected to a tensile stress σ_a. No tensile stress can be carried across the notch and load has to be shed onto the surrounding material, so that in Fig 1 the shaded areas above and below the dashed line are equal. This leads to a stress concentration at the tip of the notch given by

$$\sigma_x max/\sigma_a = 1 + 2 (a/\rho)^{\frac{1}{2}} \tag{1}$$

where 2a is the length of the notch and ρ is the radius of curvature of the notch tip. For a circular notch $a = \rho$ and the stress concentration factor is 3. Longer or sharper notches lead to greater values of $\sigma_x max$ and if this exceeds the tensile strength of the material it will fail locally. In a homogeneous (single phase) material it will either flow, leading to a greater value of ρ and hence reduce $\sigma_x max$ to less than the flow stress, or in a brittle material a crack will propagate in the y direction, perpendicular to the crack-opening tensile stress $\sigma_x max$.

There are however other stress maxima near the notch tip. The value of σ_y at the notch tip is zero but along the y axis ahead of the notch tip σ_y passes through a maximum tensile value. In the x direction from the notch tip there is a maximum shear stress τ_{xz}. In composite materials with weak interfaces it is possible for either of these local stress maxima to exceed the composite transverse strength and fracture can occur as illustrated in Fig 2. The effect again is to blunt the notch and reduce the stress concentration.

For sharp notches, where $\rho \to 0$, the value of $\sigma_x max$ becomes impossibly large and considerations of stress are insufficient to describe fracture. Considerations of fracture energy such as that of Griffith[1] are more useful; for crack propagation the energy released from the elastic strain field must exceed the energy needed to create the new fracture surface. Griffith calculated the critical applied stress for fracture to be

$$\sigma_c = (2\gamma E/\pi a)^{\frac{1}{2}} \tag{2}$$

where γ is the fracture energy per unit area of fracture surface and E is the Young's modulus. For single carbon fibres the fracture energy is approximately 10 J/m^2 indicating that the critical flaw size is in the range 0.1 μm to 0.5 μm. For glass fibres the figures are 0.3 J/m^2 and 2 nm. For epoxy resins used for aero-space applications the fracture energies are about 100 J/m^2.

For unidirectional composites fracture energies are usually least for cracks parallel to the fibres. This can be readily measured[2] using a double cantilever beam (DCB) technique (see Fig 3). A starting notch is machined in the end of the specimen and a tensile load is applied as shown. Extensions of the crack ΔA are measured and the energy or work being done on the specimen is measured directly from the areas under the load-extension curves for loading and unloading. Typical results for CFRP containing 60% by volume of fibres are shown in Fig 3. Initially the fracture energy is approximately 100 J/m^2 similar to that for the unreinforced resin. As the crack grows however misaligned fibres bridge the crack faces behind the crack tip. For the crack to propagate further the fibres in this tied zone have to be broken and, as the tied zone becomes established (after about 20 mm for a 2.5 mm thick beam) the fracture energy rises to about 1000 J/m^2 or 1 kJ/m^2 and then remains constant. This indicates that, even in splits parallel to the fibres, fibre fracture processes absorb most energy in the fracture of composites. For glass fibre reinforced plastics (GRP) the fracture energy rises from 100 J/m^2 to about 3 kJ/m^2 reflecting the greater strain energy to failure of glass fibres.

Fracture energies for different stressing modes can also be measured by using appropriate loading devices. Fig 4 shows the three main stress modes: mode I the opening mode under tension, mode II under a forward shear stress, and mode III under a tearing shear stress. For CFRP the values of fracture energy once the tied zone has been established are approximately 1 kJ/m^2 for mode I, 2 kJ/m^2 for mode II and 4 kJ/m^2 for mode III. Clearly friction between the fracture faces in the shear modes causes significant increases in fracture energy compared with the opening mode. For the DCB test to be applied to unreinforced materials, grooves have to be machined along the sides of the specimen to ensure that the crack propagates in the desired direction.

Fracture perpendicular to the fibres is considerably more difficult and requires more energy. Because of the tendency for the composite to split parallel to the fibres special test pieces have to be used. One commonly used to measure these fracture energies is shown in Fig 5. Under bending stresses, fracture can be initiated at the apex of the triangular section in the middle and the side grooves cause the crack to propagate across the fibres. Again the energy absorbed can be measured from the load-extension curve (using side grooves to guide the fracture could lead to restricted amounts of microsplitting and give slightly low values of fracture energy). For CFRP (60 volume % fibres) typical fracture energies are in the range 40 kJ/m^2 to 80 kJ/m^2. These values are markedly higher than for splitting parallel to the fibres and several energy absorbing mechanisms are responsible[3]: fibre-resin debonding, friction between fibre and resin as broken fibres are pulled out ("pull out energy") and straining the exposed fibres to failure (this strain energy is often not recovered because it is sufficient to shatter the fibre on fracture).

The two main energy absorbing mechanisms are fibre pull out and strain energy to failure in the fibres. The latter is governed by the area under the fibre stress-strain curve and since most reinforcing fibres are elastic to failure, this is equal to $\sigma^2/2E$ or for carbon fibres about 20 MJ/m^3. If this is absorbed over fibre lengths of about 1 mm the fracture energy for fibre breakage would be about 20 kJ/m^2. Similar values can be calculated for pull out energy. The distance over which the fibres debond depends on the fibre-matrix bond strength and this affects both the pull out energy and the fracture strain energy in the fibres. Thus to achieve tough composites one wants fibres with a high strain energy to failure and a low fibre-resin bond strength; this can lead to other problems such as fibre buckling under compression loading, as discussed later, and the fibre-resin bond strength needs to be optimized for a combination of mechanical properties.

FRACTURE OF MULTIDIRECTIONAL LAMINATES

In many applications the designer needs material with high strength and high stiffness in several directions in the plane of the sheet. This can be effected by moulding many thin plies (typically 0.125 mm thick) together at the required angles to form a multidirectional laminate; many practical laminates can be designed using combinations of 0°, 90° and 45° plies. Because the 0° plies have a much greater modulus than the 90° and 45° plies in the 0° direction (eg for CFRP, 140 GPa compared with 10-20 GPa) and the strains are equal, the 0° plies carry most of the applied load. The individual plies still tend to split parallel to the fibres, as in unidirectional composites, but this splitting is constrained by the stiffness of the fibres in the neighbouring plies.

When plain unnotched multidirectional laminates are loaded, the plies at 90° to the applied tensile stresses crack first[4]. For instance, for CFRP (0,90,0) laminates with thick 90° layers (8 plies, 0.5 mm thick), this transverse cracking occurs at tensile strains of about 0.3% but for a single 90° ply (0.125 mm thick) the constraints of the 0° plies postpone the onset of transverse cracking to strains >0.6%. These transverse cracking strains are affected by residual thermal strains, caused by differential thermal contraction of the plies on cooling from the moulding temperature, and by the uptake of moisture which tends to reduce the effect of the thermal strains. Laminates with plies at $+45^o$ can exhibit shear cracks in the 45 plies, parallel to the fibres, especially under fatigue loading, but the strains at which these occur and the extent to which they can travel depends on the details of the lay-up. Another form of splitting in multidirectional laminates is delamination in or between the plies, initiated at the free edge by the complex local stresses, again depending on the stacking sequence of the plies in the lay-up[5].

Multidirectional laminates are, in general, notch sensitive when loaded in tension, which means that the average stress at failure in the net section is less than the strength of the unnotched material[6]. This is illustrated in Fig 6 for a $[0,90,0,\pm45,0]_s$ CFRP laminate. The reduction in strength was not as much as would be expected from considerations of the stress concentration given by equation 1 indicating that there must have been some local failure at the notch tip resulting in a reduction in stress concentration. These local failure processes can be examined by means of a laser moire technique[7] that measures in plane strains round the notch tip. In experiments on two CFRP laminates[8], with [±45#0] and [0 ± 45]$_s$ lay-ups, small cracks were observed to form at the notch tip at loads of about 50% of the failure load; these were splits in the surface ply and are shown in Fig 7. As the load was increased further, the cracking extended in the surface ply and damage was observed in the adjoining ply indicating that in this ply too cracks were growing in the plies parallel to the fibres. The distance that these cracks can extend depends on the fibre matrix bond strength and on the thickness of the plies, which has already been shown to affect the interply constraints. These cracks growing in different directions in the different plies and delaminations between the plies form a "damage zone" that effectively blunts the notch. In GRP which is translucent the formation of damage zones can be studied using transmitted light[9]. The effects of biaxial loading on damage growth from notches has shown[10] that applied shear stresses make a significant contribution to the damage zone and to the ultimate failure load. In advanced composite laminates damage zones formed at sharp notches are typically a few mm in size before failure of the laminate occurs.

As the applied load is increased and the damage zone grows, the volume of highly loaded material near the notch tip increases, as shown in Fig 8 (it is assumed that σ_{xmax} remains equal to the material tensile strength). The individual fibres in advanced composites have a distribution of tensile strengths (coefficient of variation 15-20%), so that weaker fibres in the region of high stress near the notch will start to fracture. When sufficient fibres have fractured close enough together to form a critical crack extension the laminate will fail. (Substituting typical values for unidirectional CFRP into equation 2, the critical crack size would be about 2 mm, similar in size to the observed damage zones.)

Several mathematical models have been developed to predict the failure load for notched laminates[11]. Models based on a critical value of notch tip radius[12] or on a critical value of stress gradient at the notch tip[13] predict strengths of the form

$$\sigma_c = A/(1 + B (a)^{\frac{1}{2}}) \qquad (3)$$

where A and B are material constants. Models based on stresses integrated over a characteristic distance ahead of the notch[14] or on fracture mechanics[6] predict strengths of the form

$$\sigma_c = A/(1 + C a)^{\frac{1}{2}} \qquad (4)$$

where again A and C are material constants. Each model is semi-empirical and for every laminate the two material constants have to be measured. It is not yet possible to predict laminate notch sensitivity from fibre, resin and interface properties and lay-up. Although the four models are based on different physical mechanisms they all depend on the stress distribution ahead of the notch and it is not surprising that they all have an $(a)^{-\frac{1}{2}}$ dependency on notch length. A similar expression to equation (4) can be used[15] to predict the residual strength of damaged laminates using the total lateral damage (TLD) for notch length and a slightly greater value of toughness than for a sharp notch.

The notch sensitivity of composite laminates depends on a number of materials parameters. For (0,±45) CFRP laminates the notch sensitivity depends on the relative proportions of 0° and 45° plies[16] (see Fig 9). For laminates with less than 10% 0° plies the fracture is dominated by the shear splitting in the 45° plies and the laminate is relatively insensitive to notches. For laminates with more than 80% 0° plies the failure is dominated by the 0° shear splitting, similar to that shown in Fig 2, and again the laminates are not notch sensitive. For 0° ply contents between 10% and 80% however the interply constraints are sufficient to restrict the extent of the shear cracks and the laminates are notch sensitive. The actual value of the notch sensitivity can depend on the thicknesses of the layers in the laminate[12] as shown in Fig 10. In lay-up 1 $[(+45)n,(-45)n,(0)n]_s$ the layers were of varying thickness and in lay-up 2 $([+45,-45,0]_s)_n$ the laminate

thickness was varied but the layer thickness was kept constant. For high fibre-resin bond strengths the notch sensitivity did not vary because local fibre-matrix interactions dominated the fracture behaviour, which was rather brittle in nature. For lower values of interface bond strength, where shear cracks could run significant distances, the toughness increased with layer thickness, as the interply constraints became less effective. Further work has shown that the notch sensitivity also depends on the stacking sequence, that is on the relative orientations of neighbouring plies. The effect of the fibre-resin bond strength is further illustrated in Fig 11, where results[17] are given for laminates containing carbon fibres with varying levels of surface oxidation, which increases the interfacial bond strength as shown by the interlaminar shear strength. For (0 ± 45) laminates with 50% 0° plies the notched tensile strength decreases significantly for greater bond strengths. So with carbon fibre composites the bond between the fibre and the resin can be too strong resulting in brittle materials. This is not so for glass fibre and aramid fibre composites where at present efforts are still being made to increase bond strengths.

Materials properties are still improving, as illustrated in Fig 12 for CFRP laminates containing 50% 0° plies. In the past ten years the tensile strength of unnotched laminates has increased by 50% whereas the toughness has more than doubled. These improvements have resulted from increased fibre strengths and optimized fibre-matrix bond strengths. As the toughness of composite laminates increases, there has to be an increase in the size of centre notched panels for the measurement of toughness. This is shown in Fig 12 where lines have been drawn for two specimen sizes for

$$K_c = \sigma_o (1 - 2a/w)(\pi a)^{\frac{1}{2}} \qquad (5)$$

where K_c is the fracture toughness and σ_o is the strength of an unnotched panel. This line must be significantly above the test points to get a true value of notch sensitivity so that

$$\sigma_c < \sigma_o (1 - 2a/w)$$

as in Fig 6.

IMPACT DAMAGE IN COMPOSITES

Traditionally pendulum impact tests such as Izod and Charpy tests have been used to indicate the impact toughness of materials. They measure the total energy needed to break a specimen under impact loading. They have yielded useful information on notch effects in homogeneous materials and have indicated ductile-brittle transition temperatures. However, because of the complexity of composite failure processes, these tests are only of limited value for composite materials. For aerospace structures there is more concern with the extent of damage on impact and with the residual mechanical properties after impact[6,15]. Dropweight tests and ballistic tests have proved more useful, since they simulate in-service hazards.

A typical arrangement in an impact test is shown in Fig 13 together with the various forms of damage that can be produced. If the impact is at a relatively low velocity the laminate can respond by bending, and a critical condition is reached when a local stress exceeds a local strength. For small span-to-depth ratios this results in shear failures and delamination damage. The elastic energy in the beam prior to failure is

$$(2/9)(\tau_c^2/E))w\ell^3/t),$$

where τ_c is the interlaminar shear strength. For a CFRP laminate 2 mm thick and 25 mm wide with a span of 20 mm this gives approximately 0.3 J, which if it were all converted into fracture surface would result in a delamination of about 150 mm². For larger span-to-depth ratios, flexural failures are more likely and the stored elastic energy in this case is

$$(1/18)(\sigma_c^2/E)(wt\ell)$$

where σ_c is the flexural strength. For CFRP 2 mm thick 25 mm wide and a span of 50 mm the threshold energy would be about 1.5 J and with the greater fracture energy for this kind of failure the resulting fracture surface would be about 20 mm² in area.

At higher velocities different modes of flexural response may be excited[18] and embedded strain gauges have recorded complex stress wave propagation[19]. The impact produces a compression stress wave which travels from the impact surface through the thickness of the laminate. It is reflected from the back surface as a tension stress wave which can cause failure at the first weak interface, resulting in parts of the rear ply spalling off the back of the laminate.

At even higher velocities the laminate is effectively rigid resulting in shear out and complete penetration by the projectile (see Fig 13). The energy needed to do this is $\pi \gamma td$ where γ is the fracture energy and d the diameter of the hole which in many instances is similar to the diameter of the projectile. For CFRP 2 mm thick and a projectile 6 mm in diameter the penetration energy is about 3 J. The critical velocity for this kind of material failure can be estimated roughly by equating the shock wave energy density with the elastic strain energy density at failure. This gives

$$V_c = \sigma/(E\rho)^{\frac{1}{2}}$$

where ρ is the material density. For a CFRP laminate with 50% 0° plies this is approximately 70 m/s which for the 6 mm ball projectile is about 2 J incident energy; however, the projectile must have sufficient momentum to accelerate the material to the critical velocity quickly.

Fig 14 shows some of these threshold energies for CFRP laminates, with various geometries of specimen and supports, as a function of projectile diameter. It can be seen that large slow moving projectiles cause

shear or flexural failures whereas small fast moving projectiles are more likely to cause penetration. For extremely small particles the penetration is only partial and the damage takes the form of erosion of the surface.

In sandwich panels, the core material affects the damage in the laminate skins[20]. The core helps to reduce delamination damage and increasing the crushing strength of the core significantly improves impact resistance. Instrumented ballistic impact of sandwich panels[21] has shown clearly the loads and energies associated with penetrating the front skin, the core and the rear skin and this information can be used to design sandwich panels with improved penetration resistance.

RESIDUAL STRENGTHS OF DAMAGED LAMINATES

The various forms of impact damage described above affect the various mechanical properties to different degrees. Fig 15 shows the effect on residual interlaminar shear strength of CFRP laminates of delamination produced in dropweight and ball gun tests. The threshold energy for damage of 0.2 J is similar to the value of 0.3 J calculated above. Clearly the residual shear strength is related to the area of delamination and this can be fitted[22] to a simple fracture mechanics model

$$\tau_c = K_c/(\pi a)^{\frac{1}{2}} \simeq K_c(A)^{-1/4} \tag{6}$$

where A is the area of delamination and K_c is a fracture toughness. For the various laminates tested[22] K_c was 2.8 MPa$\sqrt{m}$ which gave a fracture energy for interlaminar shear failure of 1.1 kJ/m^2. similar to the values measured on DCB tests described earlier.

Fig 16 shows the effect of flexural impact damage on the residual tensile strength of a CFRP laminate. The threshold energy for damage was about 1 J, above which the residual strength was markedly reduced. Fig 17 shows the effect of the same damage on the residual flexural strength; the reduction in strength was even more marked because the impact damage was worse on the rear face of the laminate and this was the tension face in the subsequent bend test. For ball gun impact the minimum in residual strength coincided with the maximum amount of damage and occurred at incident energies close to that needed for penetration. Once the projectile can pass through the laminate less energy is absorbed by the material and relatively clean holes are produced with little associated cracking. The most marked reduction in strength in Figs 15, 16 and 17 occurs for similar incident energies for both the dropweight and ball gun impact even though the velocities and momenta were very different. This implies that the panels responded in flexure and that failure was determined by the maximum stresses in bend. This has been confirmed by slow indentation tests in a test machine using a similar geometry to the impact test - the stored energy at failure was similar to the threshold energies observed in the impact tests.

The shapes of these residual strength curves depend on the geometry of the specimen and supports, as indicated in the previous section. It also depends on the material properties, implicit in the energy density terms in the expressions given for threshold energies, and on the extent of the damage which is controlled by fracture energies. Figs 18 and 19 show residual flexural strength curves for laminates made from the same batch of carbon fibres in two different epoxy resins. Resin 1 was a standard epoxy system used in the aircraft industry and resin 2 was an experimental resin with high modulus and high density, that gave composites with superior compressive strengths, but with very brittle behaviour intension. The brittle resin clearly reduced the impact resistance of the composite. It is not so obvious that further improvements in resin properties will result in improvements in composite toughness, since this appears to depend more on fibre and interface properties. It can also be seen from Figs 18 and 19 that the stacking sequence has a marked effect on impact resistance; putting the 45° plies on the outside of the laminate reduces the flexural modulus and increases the elastic strain energy to failure $\sigma^2/2E$, as well as protecting the 0° fibres.

Further improvements in impact performance can be achieved by using hybrid laminates[22]. Glass fibres and aramid fibres have greater strain energies to failure than carbon fibres and benefits can be devised from incorporating plies of these materials into the laminate lay-up. Tests have shown[22] that surface plies of glass fibres and aramid fibres are the most effective (see for example Fig 20). Since these fibres have lower Young's moduli than carbon fibres this could be partly due to the increased flexural compliance seen with surface 45° plies. However, sections through the damaged laminates showed that more damage was caused in the surface layers and in delamination between the surface layers and the CFRP, thus protecting the load carrying CFRP underneath. Aramid fibres are lighter than glass fibres and, having a higher Young's modulus, can contribute more to the static load carrying capacity of the hybrid laminate. The hybrid concept has been carried further[23], to the design of super hybrid composite fan blades, comprising titanium foil outer plies over boron/aluminium plies and an inner core of carbon fibre/epoxy plies.

In Fig 12 it was shown that CFRP laminates have improved in recent years due to improved fibre strengths and optimized fibre/resin bond strengths. This "optimization" was achieved using static mechanical properties. Recently at RAE the impact performance was studied for CFRP laminates with a $[(0_2 \pm 45)_2]_s$ lay-up made from carbon fibres with various levels of surface oxidation treatment. The dropweight test was used and the laminates were supported over a 100 mm diameter support. Fig 21 is of a typical section through the damaged area for 2 J incident energy, showing that the damage consisted of multiple delaminations. At 4 J incident energy fibres were fractured. After impact, the laminates were scanned ultrasonically to measure the extent of the damage. Larger areas of damage were found for lower values of surface treatment. Specimens 250 mm x 50 mm were machined from the laminate so that the damaged area was at the centre of each specimen. Residual strengths were measured in tension and in compression using an anti-buckling guide that supported the edge of the specimen to prevent overall buckling but allowing local buckling at the damage site. Fig 22 shows the area of damage, for 1 J, 2 J and 4 J, in relation to the end tags and the side supports. Fig 23 shows the residual tensile and compressive strengths. The compressive strengths were significantly reduced

for incident energies of 1 J and 2 J. The damage consisted of relatively small areas of multiple delamination (as shown in Fig 21) with no sign of damage on either surface. This multiple delamination caused a local buckling instability under compressive loading. The tensile strength was not reduced until the damage included fibre fracture. Increasing the fibre-matrix bond strength resulted in greater reductions in residual tensile strength but was beneficial in compression because of the smaller areas of delamination. If delamination is a significant problem in a particular application improvements can be made by reinforcing the laminate in the third direction, that is through the thickness.

The reduction in strength depends not only on geometry and materials parameters, as discussed above, but also on any applied load at the time of impact[11,24]. Fig 24 shows the effect of applied tensile loads on the residual tensile strength of a CFRP laminate subjected to ball gun impact. For applied loads up to 35% of the tensile strength, the damage and residual strength were little affected. But at 40% UTS impacts above 2 J in energy produced complete failure. This might be expected since the residual strength of unloaded specimens was only about 45% UTS for these incident energies. However at 50% UTS applied load, complete failure occurred for an incident energy of only 0.5 J, which for unloaded specimens resulted in only a 25% reduction in strength. Similar tests, impacting compression loaded panels, have shown that out-of-plane deformation caused by the impact can cause local buckling to occur if the compression load is high enough.

It has already been noted that the residual strengths measured in coupon tests depend on the size of the specimen, on its dynamic response, on the design of the supports and in compression on the details of the anti-buckling device. Great care needs to be exercised therefore in interpreting the significance of this information for predicting the impact performance of advanced composite structural components.

CONCLUDING REMARKS

Damage that results in broken fibres reduces the tensile strength. Damage that results in delamination reduces the compressive and interlaminar shear strengths. Impact damage can include both broken fibres and delamination, depending on material properties such as fibre, resin and interface properties, on laminate stacking sequence and on structural details such as laminate thickness and supporting substructure.

Improvements in impact resistance can be produced by third direction reinforcement and by using hybrid laminates. Further improvements will be produced if the strain energy to failure of the fibres can be increased.

In designing damage tolerant laminates the aim should be to allow splitting parallel to the fibres, so as to avoid brittle failures, but to absorb as much energy as possible in propagating these splits so as to restrict the volume of damage.

REFERENCES

1   A A Griffith   Phil Trans Roy Soc A221, 163 (1920)

2   G R Sidey   Some investigations on carbon-fibre-reinforced plastics under impact loading,
     F J Bradshaw   and measurements of fracture energies.
                         Proceedings of the International Carbon Fibres Conference
                         London (1971) Paper 25

3   B Harris   Micromechanisms of crack extension in composites.
                         Metal Science, August-September (1980) 351-362

4   J E Bailey   On the transverse cracking and longitudinal splitting behaviour of glass
     P T Curtis   and carbon fibre reinforced epoxy cross ply laminates and the effect of
     A Parvizi   Poisson and thermally generated strain.
                         Proc R Soc Lond A366, 599-623 (1979)

5   P T Curtis   The effect of edge stresses on the failure of (0°, 45°, 90°) CFRP laminates.
                         RAE TR 80054 (1980)

6   G Dorey   Damage tolerance in advanced composite materials.
                         RAE TR 77172 (1977)

7   M Marchant   An interference technique for the measurement of in-plane displacements of
     S M Bishop   opaque surfaces.
                         Journal of Strain Analysis 9, 1, 36-43 (1974)

8   S M Bishop   Deformation near notches in angleplied carbon-fibre composites.
                         RAE TR 77093 (1977)

9   J F Mandell   The extension of crack tip damage zones in fibre reinforced plastic laminates.
     S Wang
     F J McGarny

JOURNAL OF COMPOSITE MATERIALS 9,266 (1975)

10   I M Daniel   Biaxial testing of graphite/epoxy laminates with cracks, in Test methods
                       and design allowables for fibrous composites.
                       ASTM STP 734, 109-128 (1981)

11   G Dorey   Relationships between impact resistance and fracture toughness in advanced
                       composite materials.
                       AGARD Conference Proceedings No 288 Effect of service environment on
                       composite materials.
                       Athens (1980) Paper 9

12   S M Bishop   Thickness effects and fracture mechanisms in notched carbon fibre composites.
     K S McLaughlin   RAE TR 79051 (1979)

13   R T Potter   On the mechanism of tensile fracture in notched fibre reinforced plastics.
                       Proc R Soc Lond A361, 325-341 (1978)

14   R J Nuismer   Uniaxial failure of composite laminates containing stress concentrations,
     J M Whitney   in Fracture mechanics of composites.
                       ASTM STP 593, 117-142 (1975)

15   J G Avery   Comparisons of the ballistic impact response of metals and composites
     T R Porter   for military aircraft applications in Foreign object impact damage to composites.
                       ASTM STP 568, 3-29 (1975)

16   R T Potter   The structural significance of failure mode in notched fibre reinforced
                       plastics under tension.
                       RAE TR 82009 (1982)

17   D V Dunford   The effect of surface treatment on type 2 carbon fibre on CFRP properties.
     J Harvey   RAE TR 81096 (1981)
     J Hutchings
     C H Judge

18   E J McQuillen   Low velocity transverse normal impact of graphite epoxy composite laminates.
     L W Gause   Journal of Composite Materials 10, 79-91 (1976)

19   N Takeda   Wave propagation experiments on ballistically impacted composite laminates.
     R L Sierakowski   Journal of Composite Materials 15, 157-174 (1981)
     L E Malvern

20   M V Rhodes   Impact fracture of composite sandwich structures.
                       ASME/AIAA/SAE 16th Structures, Structural Dynamics and Materials Conference
                       Denver (1975) Paper 75-748

21   M W Wardle   Impact damage tolerance of composites reinforced with Kevlar(R) aramid fibres.
                       Proceedings of DuPont Technical Symposium III on Design and Use of
                       Kevlar(R) Aramid in Aircraft (1981)

22   G Dorey   Impact properties of carbon fibre/Kevlar 49 fibre hybrid composites.
     G R Sidey   Composites 9, 25-32 (1978)
     J Hutchings

23   C C Chamis   Superhybrid composite blade impact studies.
     R F Lark   ASME Paper 81-GT-24 (1981)
     J H Sinclair

24   M D Rhodes   Low velocity impact damage in graphite-fiber reinforced epoxy laminates.
     J G Williams   34th Annual Technical Conference, SPI (1979)
     J H Starnes
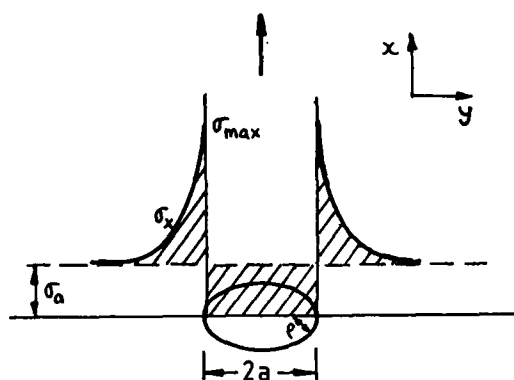
Fig 1 Stress concentration at an elliptical notch
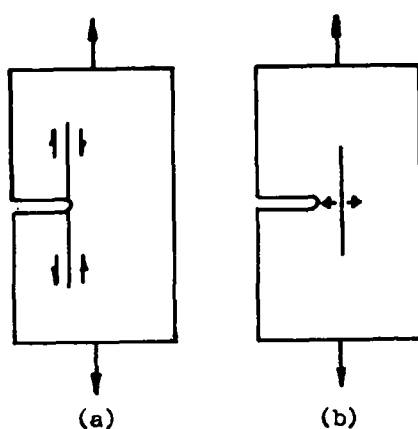
Fig 2 Splits parallel to the fibres in a unidirectional composite due to local stresses
(a) shear (b) transverse tension
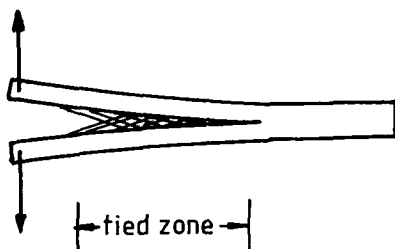
Fig 3 Misaligned fibres forming a tied zone and its effect on mode I fracture energy
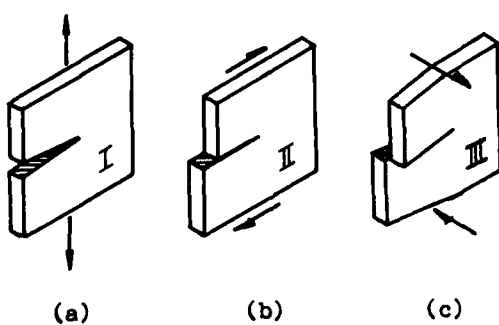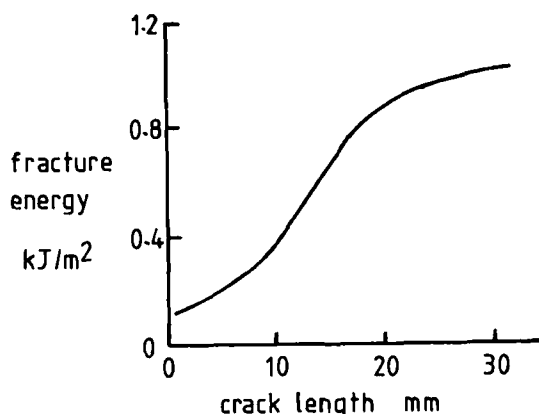
Fig 4 Three principal modes of fracture (a) opening mode (b) forward shear (c) tearing shear
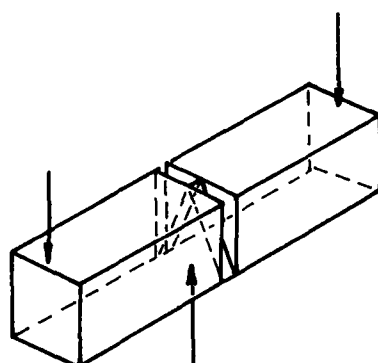
Fig 5 Specimen for the measurement of the fracture energy perpendicular to fibres in a unidirectional composite
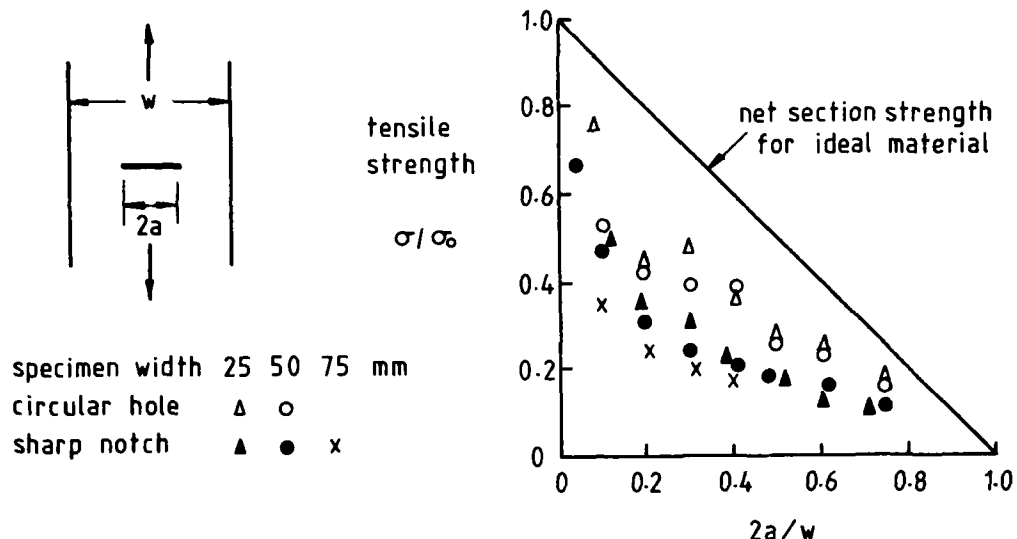
Fig 6 Notch sensitivity of a $[0\ 90\ 0\ \pm45\ 0]_s$ CFRP laminate
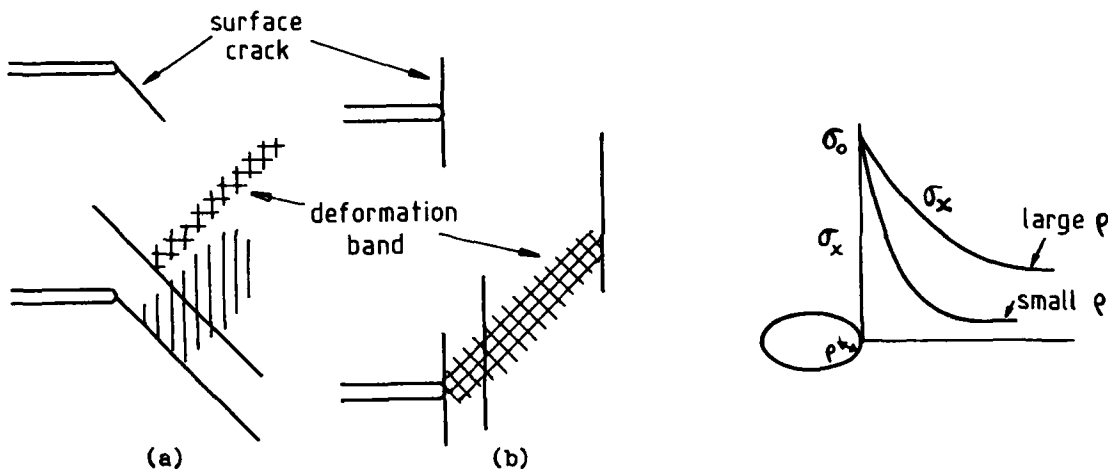
Fig 7 Damage zone formation at notch tips in CFRP laminates (a) $[\pm45\ 0]_s$ (b) $[0\ \pm45]_s$ observed by laser moire method

Fig 8 Increased volume of highly stressed material as damage zone grows
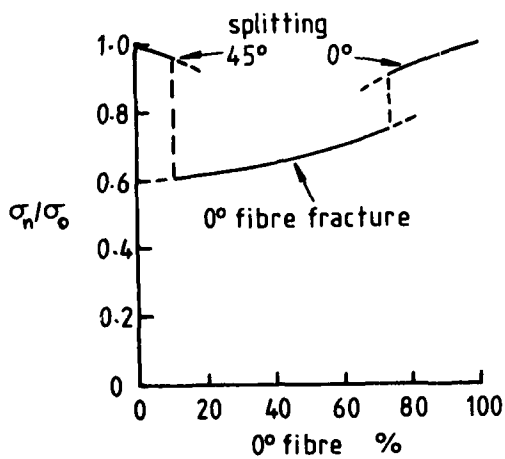
Fig 9 Effect of fibre lay-up on notch sensitivity of CFRP (0 ± 45) laminates (After ref.16)
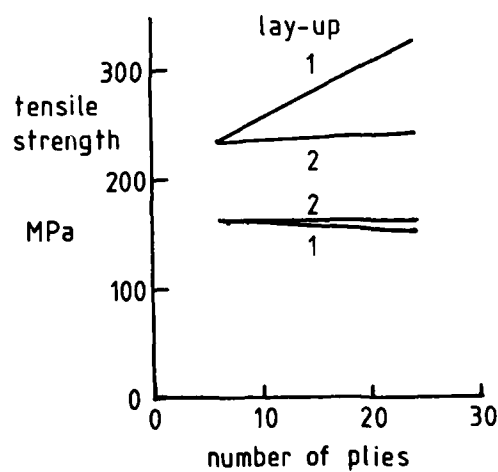
Fig 10 Effect of ply thickness on notch sensitivity of CFRP laminates 1$[(+45)_n(-45)_n0_n]_s$ 2$([\pm45\ 0]_s)_n$
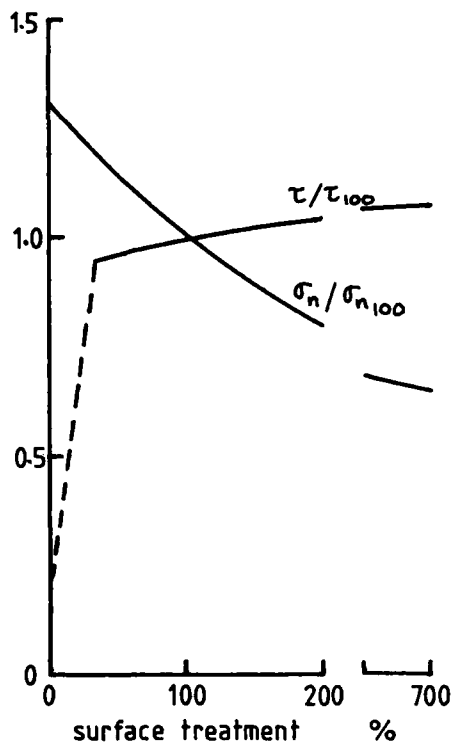
Fig 11 Effect of carbon fibre
surface treatment on notch
sensitivity of $[0_2+45_2-45_20_2]_s$ CFRP
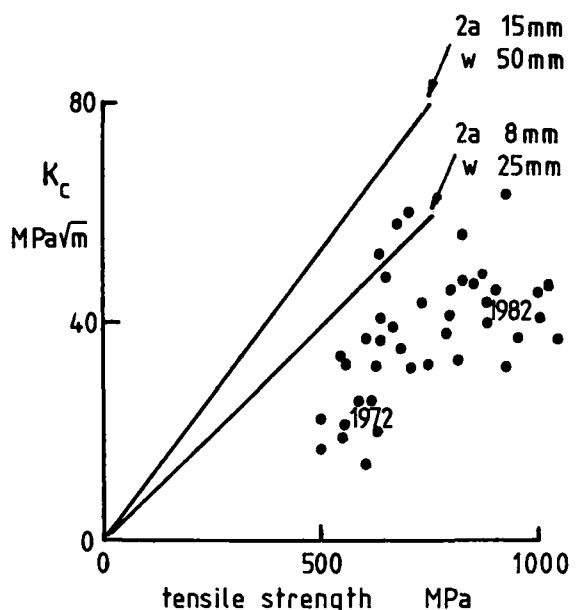
Fig 12 Strength and fracture toughness
of CFRP laminates with 50% 0° plies
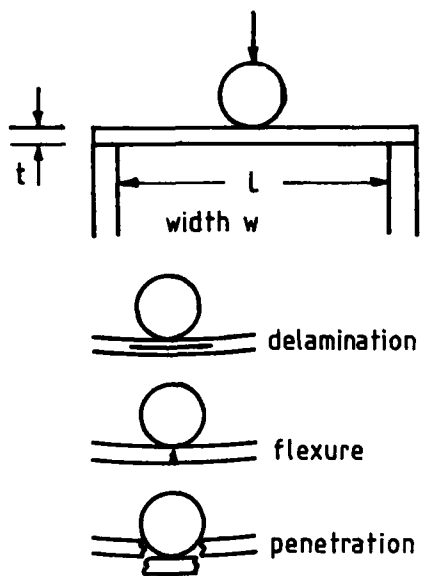
Fig 13 Geometry of impact test
and primary failure modes
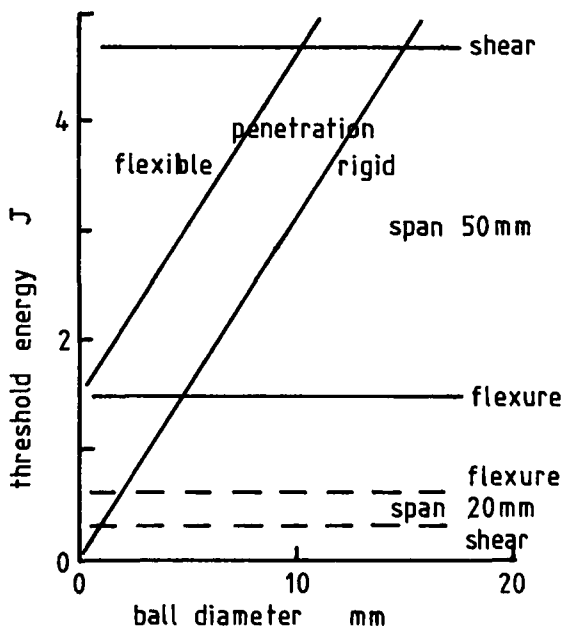
Fig 14 Threshold energies for different
failure modes in 2 mm thick CFRP
laminates
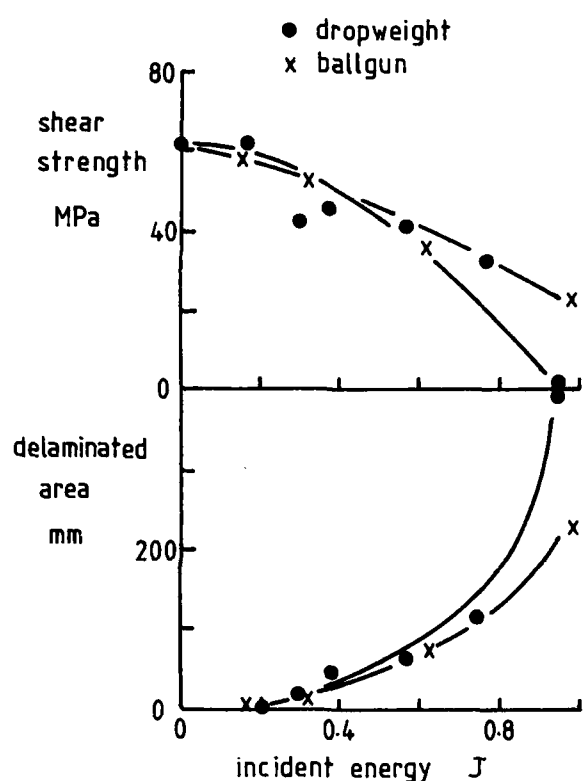
Fig 15 Effect of impact damage on
residual interlaminar shear strength
of [(0 90)₃]ₛ CFRP laminate
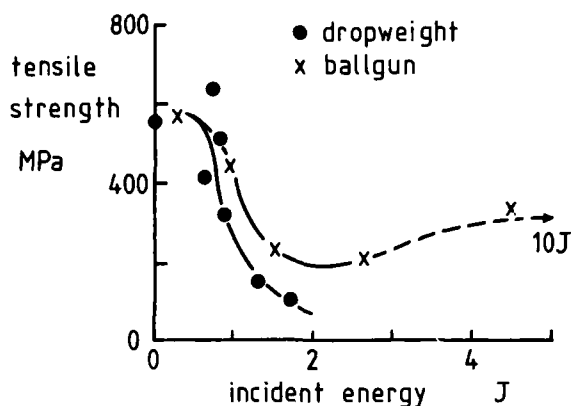
Fig 16 Effect of impact damage on
residual tensile strength of [(0 90)₃]ₛ
CFRP laminate   50 mm span
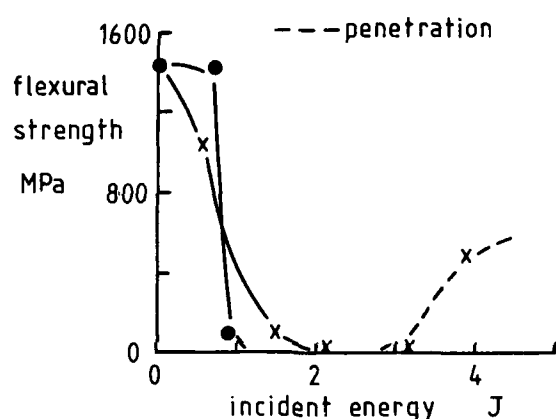
Fig 17 Effect of impact damage on
residual flexural strength of [(0 90)₃]ₛ
CFRP laminate   50 mm span
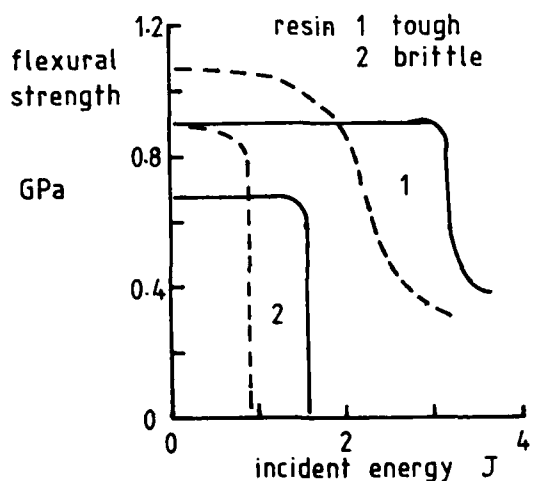
Fig 18 Effect of resin on residual
strength of CFRP - dropweight impact
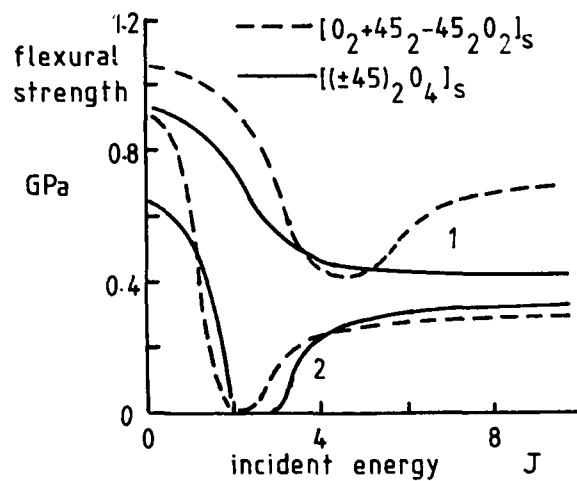
Fig 19 Effect of resin on residual
strength of CFRP - ballgun impact
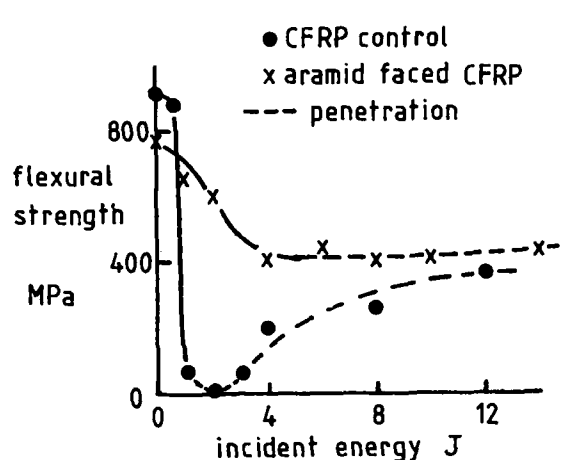
Fig 20 Effect of aramid fibre surface layers on [0 90 0±45 0]$_s$ CFRP laminate
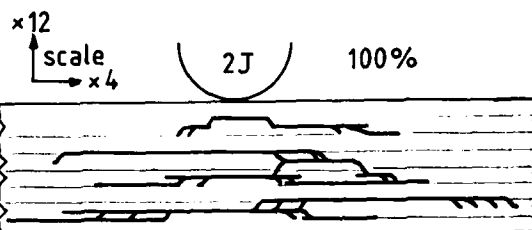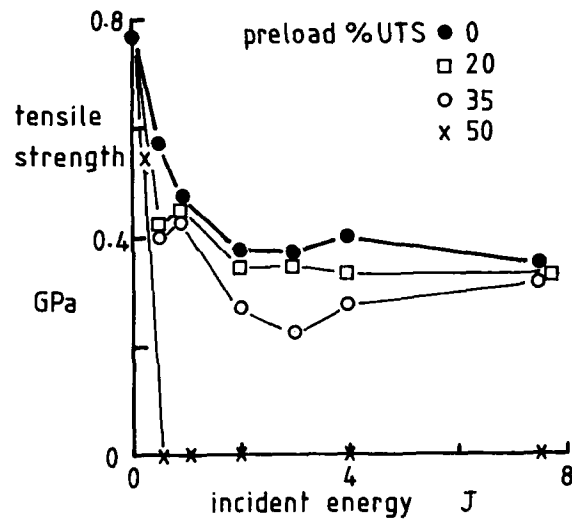
Fig 21 Multiple delamination in CFRP [(0$_2$±45)$_2$]$_s$ laminate - dropweight impact - 100% surface treatment
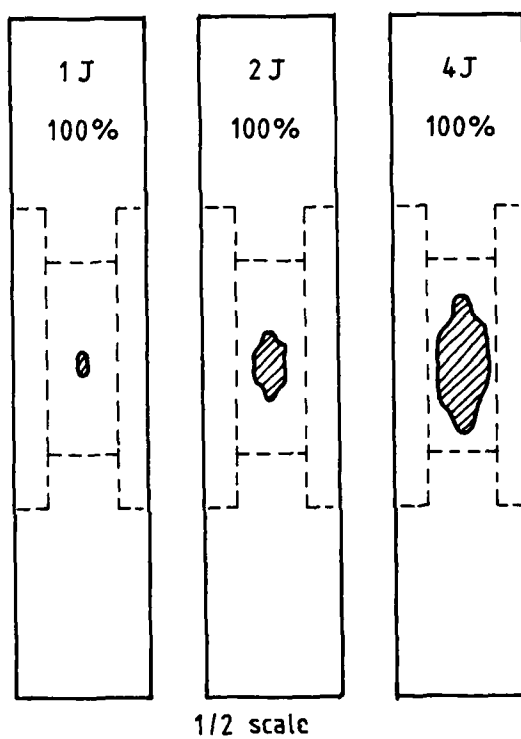
Fig 22 Impact damage in relation to compression test arrangement
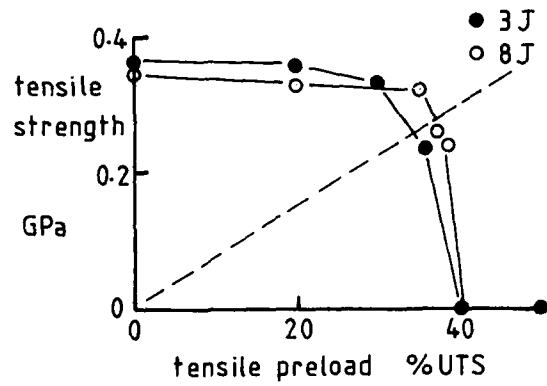
Fig 24 Effect of tensile preload on residual tensile strength of CFRP laminate - ballgun impact
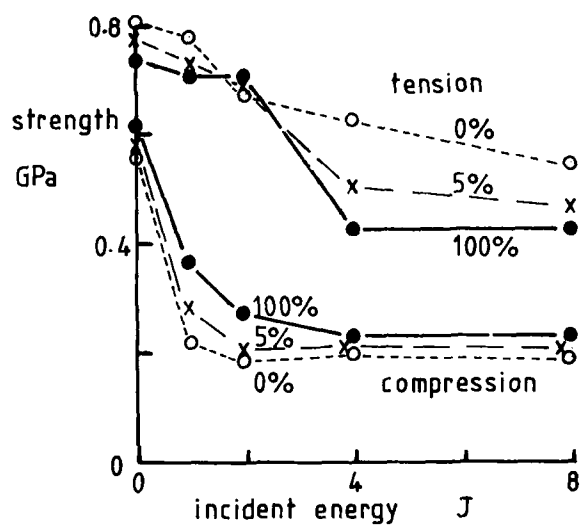
Fig 23 Effect of fibre surface treatment on residual strength of CFRP [(0$_2$±45)$_2$]$_s$ laminate - dropweight impact

MECHANISMS OF FATIGUE DAMAGE AND FATIGUE TESTING

J. J. Gerharz,

Fraunhofer-Institut für Betriebsfestigkeit (LBF), Darmstadt, Germany W.

I INTRODUCTION

Early investigations in the fatigue response of advanced fibre composites started with tension-tension constant amplitude loading at constant environmental conditions. Still today many studies on the field of composite fatigue have this experimental base. Improving experimental techniques and most of all the increasing use in engineering designs has demanded a broadening the field of activities on this subject. Fatigue testing has spread to tension-compression and compression-compression, variable amplitude loading, and testing with combined sequences of load- and environmental conditions. More effort is lately directed to examine the fundamental fatigue mechanisms, and fatigue of fibre composite materials under biaxial loading has opened a new area of investigation.

The increasing acceptance of the advanced fibre composites in engineering design has forced the designer to use analytical tools based on the presently avaible but incomplete knowledge of failure mechanism. Thus more or less empirically derived relationships are incorporated in the analysis as for example in the prediction of static strength of laminates containing holes or similar discontinuities, and prediction of fatigue life and residual strength. Because of the empirical nature of the models a large amount of testing is required until the time the understanding that is looked for emerges from research.

Designing against fatigue requires experimentally derived laminate fatigue data for various composite structural features. During fatigue loading the mechanical properties vital to the integrity of the structure should be recorded, as for example deformation, compliance, strength, etc. Constant amplitude fatigue data covering service life load conditions will provide the base for life prediction methods. Of course, it would be better to use variable amplitude loading to be closer to reality. But the available standardized load programmes (FALSTAFF, TWIST) providing comparability include assumptions and simplifications admissible to metals and metal structures. Still more investigations are needed to determine the allowable simplifications (of in service load- and environment-history) for composite structures mandatory for economical laboratory testing. Therefore, at present most of the fatigue testing for the evaluation of mechanical response during repeated loading is done with constant amplitude loading.

The following presentation the fatigue response of fibre composite materials containing various details of a composite structure. Besides the plain feature, open holes, bolted and bonded joints with differing configuration parameters are covered, see Fig. 1. The majority of data shown stem from a program to establish design data [1, 2]. All test samples had the same material and laminate structure namly graphite/epoxy 914C/T300 and the laminate built-up $[(0_2/\pm 45)_2 \overline{90}]_{s,n}$. Two paragraphs of this lecture deal with response of fibre composites to constant amplitude loading of plain and notched materials. This division of the subject is natural because of the significant difference in failure mechanisms. Besides the demonstration of fatigue behaviour within each section

- an overview in present knowledge of failure mechanisms is given;
- examples of fatigue data analysis are presented;
- the deformation behaviour under cyclic loading is explained;
- problems in testing technique concerning the comparability of coupon and structure behaviour are exposed; and
- differences between metal- and composite behaviour are pointed out.

A third paragraph deals with the behaviour of a cfrp-laminate under realistic fatigue loading and considers:

- evaluation of load spectrum modifications,
- effect of service environment simulation in realistic fatigue testing, and
- strength degradation.

II UNNOTCHED FIBRE COMPOSITE BEHAVIOUR

Overview on Failure Mechanisms during Fatigue Loading

In fatigue loaded unnotched fibre composite specimens final fracture occures when $0°$-plies have failed. Preceding the transverse fibre breakage required for final fracture various failures are observed, see Fig. 2, occuring with or without interaction. The presence of a particular failure depends to a certain degree on composite constituent materials and laminate type as shown in Fig. 3. For carbon fibre reinforced plastics (cfrp), for instance, transverse matrix cracking and delamination are the most prevalent, matrix dominated failures in multidirectional laminates.

Many publications on laminate damage experiments as for example Ref. [4] contain photomicrographs or C-scan and X-ray pictures demonstrating these failures. Fig. 4 shows schematic illustrations of the transverse and delamination crack in a $90°$-ply. For these failure mechanisms the important findings of laminate (multidirectional) damage investigations are summarized in Figures 5 and 6.

In multidirectional laminates cracks in $90°$-plies occur in many practical situations on the first loading cycle, and increase in density with number of cycles until a stable density for a particular laminate configuration is reached,

see Fig. 7, Ref. [4]. In this damage state no further transverse cracks occur in spite of additional loading; instead delamination continues at an increasing rate.

A dependency of the maximum crack density state on the onset of delamination cracking was noticed, Fig. 7. When delamination started early in life as observed in the [0/+45/90]-laminate, less transverse cracks developed compared to the case where delamination begins late in life as observed in a [0/90/+45]$_s$-laminate. Furthermore the increase in number of transverse cracks was largest in the pre-delamination phase. It seems that only a few additional transverse cracks develop in the 90- and 45°-layers after delamination had begun. Transverse ply cracks generally start in 90°-laminate when the threshold levels are reached, which vary with the thickness of the 90°-layer, see Fig. 5.

Delamination is observed to initiate at free edges where it is generated by interlaminar stresses in the presence of uniaxial in-plane loading. The determination of these stresses has received extensive discussion based on linear elastic analysis, see for example Ref. [5]. These interlaminar normal and shear stresses concentrate at the free edge but are thought to follow the delamination crack tip. One should also be aware of interlaminar shear stress concentration at the tip of a transverse crack expanding over the total specimen width, thus superposing the free edge interlaminar stresses [6].

The distribution of interlaminar stresses over the laminate thickness is governed by the stacking sequence. For example, at tensile loading interlaminar normal stresses at free edges are tensile in the [0/+45/90]$_s$ laminate and compressive in the [0/90/+45]$_s$ laminate. The latter stacking sequence also has the 90-layer with first transverse cracking outside the range of maximum interlaminar stresses. Thus, in contrast to the [0/+45/90]$_s$-laminate, the [0/90/+45]-laminate did not show any delamination under static tensile loading to failure, and it seems that interlaminar shear stresses were not critical. But during tension-tension fatigue loading delamination was observed between 45°-layers [4] starting at transverse crack tips, where interlaminar shear stresses are large. Generally, it is believed that static loading and fatigue loading cause similar damage. However, significant differences should be expected in damage development when interlaminar normal stresses are compressive, see Fig. 8. The compressive interlaminar stresses will change to tensile interlaminar stresses corresponding to a change of sign of the external in-plane loading. Thus external tension-compression fatigue loading always generates tension-compression cycling of the interlaminar normal stresses by which delamination cracking is enhanced. When increasing delamination size becomes critical (stability) the delaminated plies buckle out of plane under compression load and fracture occures at compression when, for example, the remaining cross section ceased being able to carry the load [7].

Crack opening and closing are easily visualized during cyclic loading at the specimen edges when peel-off and compressive interlaminar stresses are effective. It is often observed that a delamination crack will stay open at zero load due to residual stresses introduced during cool-down from curing temperature. The effectiveness of the interlaminar stresses is also demonstrated by fatigue test results from flat specimens and tubes, see Fig. 9. The interlaminar stresses acting at the longitudinal edges of the flat specimens reduce the fatigue strength in correlation to the tubes. In case a hole is drilled through the tube wall interlaminar stresses would be introduced at the hole edge and consequently delamination would occur around the hole during fatigue loading.

As in metals the propagation of the single dominant crack in composites the increase of multiple cracks in size and number reduces the residual strength and increases the deformation. This relationship has been observed many times [4, 8], and Fig. 10 gives just an example. The increase in deformation may be transformed into loss of stiffness or increase in compliance when the stress-deformation behaviour during cyclic loading is known. Data on increase in deformation and decrease in residual strength are needed by the designer. Derived by analytical tools or by tests they are essential to achieve economical and reliable engineering designs.

Fatigue Behaviour

Initially observed fatigue behaviour of fibre controlled laminates with high stiffness fibres gave the impression that these materials were not prone to fatigue. As can be seen by a family of constant life curves for a fibre controlled cfrp laminate, see Fig. 11, this is true at tension-tension loading which was applied in early fatigue testing. At this load condition the fatigue strength is close to ultimate tensile strength (F_{tu}) and even at high numbers of cycles not less than 2/3 of F_{tu} (design limit stress). But attention-compression loading serious fatigue damage develops so that fatigue strength at lives $\geq 10^5$ drops below the design limit stress, see Fig. 11. An extrapolation of the tension-tension fatigue strength of composites analogous to metal fatigue behaviour has proven to be incorrect. As demonstrated in Fig. 12 the fatigue strength of a metal is steadily increasing with decreasing mean stress whereas the fatigue strength of the composite materials decreases when compression becomes a larger part of the load cycle.

Schematically the constant life curves in Fig. 12 exhibit some differences in fatigue behaviour between composite materials. For the afrp laminate (aramide fibre reinforced plastic) this difference is related to the low compressive strength of it's fibres being 1/5 to 1/4 of the tensile strength. For the gfrp laminate the difference in fatigue behaviour, indicated by the shape of the constant life curve, is related to the lower stiffness of the glass fibre (E-glass) being 1/3 and 1/2 of that of the graphite (T 300) and aramide (Kevlar 49) fibre, respectively. Furthermore the strain at fracture of the glass fibre is larger by factor of 3 and 1.8 compared to the graphite and Kevlar fibre, respectively with the ultimate tensile strength being alike. Generally this difference in mechanical properties of the fibres is responsible for higher loading of the matrix in gfrp laminates. Correspondingly, damage developing in the matrix of gfrp laminates is believed to be more intense, consequently a damage state critical to the fibres is reached earlier in gfrp than in stiff fibre composites. On the other hand stress analyses reveal lower free edge interlaminar stresses. This might be the reason for the gfrp behaving more and more like the cfrp composite with increase in compressive loading, where interlaminar stresses were observed to be more effective to fatigue damage.

The sensitivity of fibre composite materials to compressive loading in fatigue which shows also with notched specimens is likely to be in close relation to the development of delamination damage. But the exact mechanisms covering the whole range of load conditions are still subject to research.

Deformation Behaviour

However, it was shown that increasing damage correlates with an increase in deformation at constant load level (Fig. 10) which would correspond to a decrease in load at strain controlled cycling. The deformation during cyclic loading may be measured for example by a strain gaged extensometer placed on the specimen. The registered deformation during constant amplitude loading with R = -1,0 plotted vs. fraction of life at fracture is presented by the scatter band in Fig. 13. The larger scatter at the end of life is due to test results of specimens with failures not exactly developing within the gauge length. Correspondingly for notched specimens where the failure develops always within the gauge length covering the notch, no such increase in scatter was recognized.

The observed deformation behaviour of fibre composites may cause failure of a component when its deformation at loading has grown to a critical value. For this failure criterion the S-N-curves presenting life to various levels of increase in deformation can be determined from the recorded deformation data. An analysis of the data for lives to 5 and 10 percent increase in deformation resulted in the S-N-curves shown in Fig. 14. Included is the S-N-curve for life to fracture at which the deformation has increased by an average of 18 percent, see Fig. 14. All three S-N-curves are fitted to the results of 26 tests by a non-linear regression analysis. At typical results of such an analysis is shown in Fig. 15. The S-N-curve described by the mathematical equation represents average fatigue strength. The analysis includes static strength data as well as run-out data. The similarity of damage observed during monotonic and cyclic loading is thought to justify the incorporation of static strength data in the fatigue data analysis.

The Effect of Anti-Buckling Measures

A problem the test engineer is faced with is the buckling of thin fibre composite specimens. For example, the tickness of the 17-ply laminate of the unnotched specimen in Fig. 1 is only 2.1 mm. This problem can be overcome by several measures. Rosenfeld and Huang [9] have cut down on effective specimen length and increased the thickness by extending the bonded-on tabs close to the notch in the center of the specimen. The author has used anti-buckling guides of two configurations, one covering the specimen completely and the other leaving the specimen's edges uncovered. Results of comparative fatigue testing, see Fig. 16, showed that with unsupported edges fatigue life to fracture was shortened at least by a factor of 5 at lives N > 10^4. During the whole life to fracture specimens with the edges not supported suffered less increase in deformation than *specimens* with the edges supported by the anti-buckling guide, see Fig. 16.

The analysis results of deformation increase represented by the 5 percent deformation curves in the S-N-diagram *Fig. 16* revealed that specimens with the edges not covered by anti-buckling guide plates fractured when about 5 percent of deformation increase was reached. This amount of deformation increase distinctly preceded facture of those specimens which were completely covered by the anti-buckling guide. To a large degree, this guide configuration apparently has the effect of delaying the growth of fatigue damage initiated here at the specimen edges. Similar findings were reported by Phillips [10] for cfrp. For specimens with holes and anti-buckling guides with and without a window around the hole, where delamination occured, differences in life to fracture up to a factor of 30 were found.

As demonstrated before the delamination at the specimen edges is responsible for the deformation increase. Therefore, it is the feeling that crack opening and local buckling associated with edge delamination is restrained by those anti-buckling plates, which provide support by completely covering the specimen surface. Generally the results indicate that the influence of anti-buckling procedures must be accounted for to make meaningful comparisons. In this respect it is important to note that in actual structure buckling of compression loaded skin areas is prevented by distinct reinforcements. Consequently, support provided by an anti-buckling guide covering only a small portion of the specimen surface just to avoid general section buckling is considered to be close to reality.

III   NOTCHED FIBRE COMPOSITE BEHAVIOUR

Failure Mechanisms at the Notch (Open Hole)

The prevailing failure mechanisms observed at open holes in fibre composite materials vary to a certain degree with fibre diameter and matrix material, see Fig. 17. In composite laminates with small fibres (cfrp) delamination cracks together with matrix cracks running parallel to fibres and being arrested by adjacent plies prevail [11]. With larger fibres debonding, fiber breakage and growth of matrix cracks (parallel to fibres) into adjacent layers are effective damage processes besides delamination cracking [12]. Generally in metal matrix composites fibre breakage prevails and compared to polymer matrix composites less matrix damage is observed but plastic flow of the metal matrix does occur at notch roots [3].

In contrast to metals it has been observed many times that damage in polymer matrix, starting at hole edges, grows parallel to the load axis in form of ply cracks in the 0 °-plies and in form of delaminations following the ply-cracks, as demonstrated by the C-scan pictures in Fig. 18. Associated with the damage growing longitudinally is an effective notch blunting with a pertinent increase in residual strength. In terms of local stressing this indicates, that with the occurence of longitudinal cracks the stresses at the hole were redistributed to a less damaging state. On the other hand, when damage is restrained to local regions around the hole, especially when those regions are predominantly in the net section, residual strength and life is reduced (behaviour of metal matrix composites). The direction in which damage will extend from a notch

in polymeric matrix composites seems to depend on laminate structure and especially on the constraint adjacent layers place on layers with matrix cracks along fibres [14].

Delamination is always observed at a notch and under cyclic loading it is here also more extensive than during static loading. It increases near the end of life, thereby enlarging the deformation or strain of the laminate at the peak loads of the cycle, see Fig. 18.

The sequence of failure events is generally similar to that one observed in unnotched specimens. However, transverse and fibre-direction matrix cracking may increase again following seperation of plies through extensive delamination. At the end of life all damage components begin to accelerate.The spreading fibre breakage may lead directly to fracture or be arrested. In the latter case a mechanistic cycle is repeated starting with extension of delamination [15].

It also appears that laminates with a large portion of 0°-layers and consequently higher strength also have more resistance to growth of effective damage (in contrast to common behaviour in metals).

A wide variety of damage components and mechanisms is observed to occur at a notch in fibre composites. The stress situation at the notch is extremely complex and very difficult to describe. The complexity of modelling the governing interactions and combinations of damage components is demonstrated by the investigations of Kulkarni et. al [16]. Presently no mechanistic model available is able to accurately model the fatigue failure process in fibre composites. However, empirical models are in use which require some testing.

Effect of Structural Notches on Fatigue Behaviour

One of the most striking difference observed between metals and fibre composites is the way they respond to a notch under fatigue loading. In contrast to metals fibre composite materials show a large detrimental influence of a notch on static strength and low cycle fatigue strength, and only a small influence on the high cycle fatigue strength. This notch effect is most pronounced if the fibre composite material is loaded parallel to the fibres and it is observed to be universal for fibre reinforced polymer matrix composites. Fig. 19 demonstrates the notch effect found for a cfrp laminate. The SN-curves of notched specimens representing various structural details exhibit a drastically increasing drop in static strength and fatigue strength with increasing stress concentration. It is also clear from the S-N-diagram that the position of the S-N-curves are greatly determined by the static strength of the specimens. Besides experimental determination, static strength may be estimated by empirical models as for example those developed by Whitney and Nuismer [17]. To apply these models the stress distribution in the laminate around the hole is needed. Stress analysis methods to determine the stresses as well as analysis results are available in the literature [18].

Furthermore it was found that improvement measures like local reinforcement of the hole region and high bolt clamping for instance, have their largest effect on the static strength. One exception being the interference fit in combination with high clamping as long as installation damage can be avoided or can be kept ineffective. These measure have their largest effect on high cycle fatigue strength [2].

Other measures which are known to increase the joint efficiency at static loading is the so-called tailoring or softening as reported in Ref. [19] and the load transfer per bondline instead of fasteners. However, it must be emphasized that the effectivenes of such measures may be less at fatigue loading. The step-bonded joint in Fig. 1, for example, had a joint efficiency of 0.7 at static loading but in the high cycle fatigue range ($N > 10^5$) the joint efficiency was down to 0.35, being less than the value for bolted joints.

It is interesting for designer to note that by a fastener just neatly filling the hole the compressive strength was significantly increased, see Fig. 19. Apparently the constraint offered by the fastener to the hole and by the clamping action of the bolt head and nut are beneficial at compression. These constraints also shift the failure location away from the hole to the gross section ahead of the hole to the edge of the head or nut. This failure mode, bearing failure, and net section failure together with longitudinal cracks were the prevailing modes (see Fig. 20) observed in joints with load transferred by a fastener. Moving along the S-N-curves of these joints the failure mode generally changes from that prevailing at N = 1 (static strength), which is failure of net section at tension and failure "ahead of hole" at compression, to that prevailing in the high cycle fatigue region which is bearing failure. Depending on design details, bearing failure mode or a frequently observed combination of the failure "ahead of hole" mode and the bearing failure mode may already occur at static loading. Then bearing failure is the universal mode for the S-N-curve as it was the case for the two lower S-N-curves in Fig. 19. However, a fundamental difference exists not only in the mode of final failure but also in the preceding failure mechanism when comparing results presented by the three upper S-N-curves in Fig. 19 with those presented by the three lower S-N-curves. Post-fracture analyses show delaminations in the filled hole specimens and definitely in plain and open hole specimens, but there is no evidence of delaminations in the jointed specimens.

Deformation Behaviour

Further difference in damage processes is indicated by the deformation behaviour illustrated in Fig. 21 for unnotched, open hole, and filled hole specimens as well as for single and double shear joints. Increase in deformation is again plotted vs. percentage of number of load cycles to final failure. By far the largest increase in deformation during cyclic loading is observed for the joints. Based on the method used, the deformation measured in the case of single and double shear joints is the relative movement of the parts connected by fasteners. Thus lengthening of the holes due to bearing damage has a great effect on the continuously measured value. Whereas deformation in single-shear joint of fibre composite laminate grows to large values early in life the deformation of double-shear joints increases sharply only towards the end of life. In comparison to the unnotched specimen deformation increase is larger for the open hole and smaller for the filled hole specimens as expected.

Heating at Notches, Acceleration of Testing

Economical reasons will force the investigator to cut down the testing time by increasing the loading frequency in the high life range, as executed with the unnotched specimens, see Fig. 15. Then the problem of self-heating of the specimen arises. Cooling by blowing room temperature air over the unnotched specimens subjected to high speed loading has proved to be effective and admissable. Specimen surface temperatures remained below 50 °C and there was no difference between the fatigue life of the low speed loaded specimens and that of the high speed loaded and cooled specimens [20].

The situation with notched specimens is different. Likely due to the very localized high deformations at the hole edge or near the fastener much heating does occur at these places. This forces the test engineer to keep loading frequencies for constant amplitude loading low. For example, the constant amplitude testing for the S-N-curves in Fig. 15 mentioned before were carried out with realistic loading frequencies [21] not larger than 5 Hz. Otherwise heating up to temperatures above 100 °C may occur at the notch with loading speed of 20 Hz, for example, [20]. Even at 5 Hz a large temperature rise was measured during the last 10 percent of life.

Fortunately heating was not observed during variable amplitude loading with frequencies up to 20 Hz. Here the problems are with the realization of the environmental conditions simulating the in-service conditions. The testing time in combined mechanical and environmental loading is governed by the forced heating and cooling rates, and by moisturizing- and constant temperature-periods. Drastic acceleration of the actual temperature/moisture/loading history is required to get a practicable test programme. Thereby the criterion must be met that a critical structural detail subjected to an accelerated test programme will develop the same damage growth and residual strength as under actual service conditions. Acceleration examples obeying this criterion are given in the literature [22, 23].

IV   COMPOSITE LAMINATE BEHAVIOUR UNDER REALISTIC FATIGUE LOADING

The evaluation of the ability of a composite structure or component to withstand the expected service life conditions requires testing by a programme that incorporates all the conditions essential to damage development, so that during testing damage in a critical structural detail develops the same way it does during actual service.

Comparative testing used with realistic variable amplitude loading test programmes is needed to define those conditions. In this respect a contribution was made by exploring (1) the effects of modifications of load spectra and (2) the effects of different ways of accounting for the environmental conditions. Aircraft wing composite structure was considered which under service conditions is subjected to repeated loading from take-off and landing, flight-manoeuvres and atmospheric gusts and simultaneously to cyclic changes in temperature as well as absorption and loss of moisture. For the mechanical loading the standardized programmes: "Transport Wing Standard Test" (TWIST) and "FAtigue Loading STAndard For Fighter Aircraft" (FALSTAFF) were used. Details of these programmes are given in [24] and [25]. Since cyclic compressive loading is generally more detrimental to fibre composites than cyclic tension, the pertinent load spectra for the wing upper surface conditions were applied, see Fig. 22.

Effect of Spectrum Modification

The effect of modifications of these load spectra on the fatigue life were investigated with respect to allowable simplifications and demands directed to service load recording and simulation. Regarding simplifications the largest pay-off will, of course, result from omission of low loads with high frequency of occurrence, whereas modifications at the high load end of the spectrum will be of more importance to demands with respect to flight load recording and simulation. The modification, shown on Fig. 23 and 24 with the test results, comprise overloading, truncation of high loads and omission of low and high loads. Omission of either high- or low-load produced lives longer than those obtained in complete spectrum tests (baseline). Thereby life was more sensitive to omission of high loads. The increase of the maximum loads in the FALSTAFF spectrum by only a factor of 1.1 reduced life significantly to 80 percent of that achieved in baseline tests, whereas a truncation of the high loads by the same factor (see Fig. 24) showed no effect on life. Of course the effect of overload will depend on the factor the maximum spectrum load is increased. For example overload factors of about 1.25 reduced the lives of the unnotched specimen in Fig. 1 by a factor of 2.0. These results stem from variable amplitude fatigue testing with the load programme TWIST and one similar to FALSTAFF. Generally the test results suggest that in defining test spectra for composite airfoil structure it might be advisable to include loads with lower frequencies as once per 4 000 or 100 flights in the TWIST or FALSTAFF spectrum, respectively, which was found being satisfactory for aluminium structure. More investigation in this direction is needed. Fortunately omission of the lowest load levels of the spectrum shows promise for achieving large reductions in test time without significantly changing test results.

The results of life predictions by the linear damage accumulation theory of Palmgreen Miner, shown in Fig. 23 and 24, indicate a general trend to overestimate the fatigue performance of details of fibre composite structure. More details on this subject will be presented in the following lecture of this series.

Effect of Environment in Realistic Fatigue Loading

As has been demonstrated in the preceding lecture, the environment in which a composite structure operates has considerable influence on damage caused by mechanical loading. The mechanisms causing the effects of the environment are two-fold. On the one hand the polymer matrix softens at high temperature and high moisture content. On the other hand due to hygrothermal anisotropy thermal stress- and humidity stress-cycling (swelling induced stresses) occur in the laminate corresponding to changing temperature and humidity content. The effect of the environmental history expected in service must therefore be accounted for in the fatigue evaluation of a fibre composite structures. At the present state of knowledge

this requires quasi-realtime testing with simultaneous environmental and mechanical loading of the specimen. Of course, this is a very expensive and time-consuming testing procedure. To minimize cost and time allowable simplifications are looked for. The simplification criteria must be met and the acceptability of simplified test programmes may be checked by comparison of their results with those of quasi-realtime testing. This procedure has been applied to the fatigue loading and environmental conditions of the upper surface structure of a fighter aircraft wing. The complex simultaneous environmental and mechanical loading realized in the quasi-realtime testing is explained in detail in [23]. Fig. 25 represents results of the unnotched specimen in Fig. 1 from the still on-going investigation. In baseline testing the specimens were dry and subjected to mechanical loading at room-temperature. In quasi-realtime testing the specimens were wet and subjected to simultaneous environmental and mechanical loading; in simplified testing the specimens were also wet, but environmental loading was preceding mechanical loading at room-temperature. Beside the large detrimental effect of the simulated wing upper surface environment on the life to fracture, the results confirm that environmental conditions and mechanical loading interact in their influence on the damage growth in fibre composites. Thus, the attempt to cut down costs by separating environmental loading from mechanical loading proved to be without success.

Residual Strength Degradation

Degradation of strength was shown in Figures 10 and 18 to occur at constant amplitude loading. The designer is confronted with the requirement that the structure, despite the deterioration accompanying exposure to environment and repeated loading in service, is able to withstand ultimate design loads at all times during one lifetime. Therefore, he needs information on how deterioration develops during exposure to loading and environment occuring in one lifetime. This information may be provided in form of a residual strength curve which includes static and residual strength as well as fatigue life data, see figures 26 and 27. In this illustration the fatigue life at fracture is interpreted as the life at which the remaining strength of a fibre composite has dropped to the value corresponding to the maximum stress of the load programme. Test results are represented by the scatter beams stretching from 90 to 10 percent probability of survival. In this manner the static strength results are plotted above $N = 1$, the residual strength results above the number of cycles the specimens were preloaded with and the lives to fracture are plotted versus the stress level of the fatigue loading; straight lines connect the average test results.

A characteristic difference in strength degradation is seen in Fig. 26 between the unnotched specimen and the double shear joint both shown in Fig. 1. Whereas the unnotched specimen has suffered a significant strength degradation before it fails in fatigue, the strength of double shear joints remained, even close to the end of their lives, on the level of the static strength. Recalling the failure criteria and the failure mechanism preceding final failure of these specimen types the difference in strength degradation could have been expected. For the unnotched specimen the failure criteria is total fracture preceded by ply cracking and delamination and for the jointed specimen rapidly increasing hole lengthening was the failure criteria, see Fig. 21.

Also to the fatigue life data in Fig. 25 resulting from realistic variable amplitude testing, the results of residual strength and static strength tests were added to form the corresponding residual strength curves in Fig. 27. The curves so far indicate equal strength degradation behaviour at wing upper surface loading with and without superimposed environmental conditions.

V   CONCLUDING REMARKS

Most of the data and information presented are related to cfrp-lamintes applied in air-frame structure. More or less significant differences in fatigue response may exist when other composite laminate materials are considered. Some of these difference were pointed out. Bearing this in mind the results and trends reported are:

- In Composite materials, there are a number of fatigue failures, such as delamination, cracking of the matrix, debonding and fibre breaking. They do not combine to form a single self-similar crack normally found in metals. Instead they form a very complex damage state in the laminate.

- The damage mechanisms acting in tension are different from those acting in compression during fatigue loading.

- Compared to static loading more delamination and transverse matrix cracks develop under cyclic fatigue loading. Static strength seems to be controlled by the fibres and the fatigue limit to be dominated by the matrix.

- Growing damage causes deformation increase (stiffness reduction) at cyclic loading and loss of static strength. In the case of notched laminates a loss of strength may be preceded by an increase of residual strength.

- Strength- and stiffness-changes due to cyclic loading should be recorded and analyzed for design charts.

- Fatigue loading in tension-compression is more detrimental than fatigue loading in tension-tension.

- Stress concentrations reduce the static strength and fatigue strength in the short life region, in the long life region their effects diminish. Thus the fatigue notch factor decreases with increasing life (in contrast to metal behaviour).

- Measures improving static strength may not be successful at high cycle fatigue.

- In the analysis of service conditions special attention should be payed to high load occurence and environment because of their large influence found in realistic fatigue testing of composite/laminates.

- Measures to avoid buckling at compression should not restrain realistic damage development. To avoid severe heat generation at notches testing speed should be in the realistic range.

Generally, many questions on fatigue response of composite laminate structure have not yet been answered. To a major part these are related to the understanding of the fatigue mechanisms and of the exact processes by which the damage state controls strength, stiffness, and life-time.

LIST OF REFERENCES

[1]   Schütz, D.; Gerharz, J. J.; Alschweig, E.:
Fatigue Properties of Unnotched, Notched and Jointed Specimens of a Graphite/Epoxy Composite,
ASTM, STP 723, 1981, pp. 31 - 47.

[2]   Gerharz, J. J.; Schütz, D.:
Schwingfestigkeit von lösbaren Krafteinleitungen in Faserverbundkonstruktionen,
to be published: Forschungsbericht aus der Wehrtechnik, Manuscript delivered: June 1982.

[3]   Stinchcomb, W. W.; Reifsnider, K. L.:
Fatigue Damage Mechanisms in Composite Materials,
ASTM STP 675, 1979, pp. 762 - 787.

[4]   Kim, R. Y.:
Experimental Assessment of Static and Fatigue Damage of Graphite Epoxy Laminates,
ICCM 3, Vol. 2; 1980, pp. 1015 - 1028.

[5]   Raju, I. S.; Whitcomb, J. D.; Goree, J. G.:
A New Look at Numerical Analyses of Free-Edge Stresses in Composite Laminates,
NASA TP-1751, December 1980.

[6]   Wang, A. S. D.; Law, G. E.; Warren, W. J.:
An Energy Method for Multiple Transverse Cracks in Graphite Epoxy Laminates,
in: Modern Development in Composite Materials and Structures,
Ed. J. R. Vinson, (1979), p. 17.

[7]   Ratwani, M. M.; Kan, H. O.:
Compression Fatigue Analysis of Fibre Composites,
AIAA Paper 80-0707, 1980, pp. 279 - 284.

[8]   Broutman, L. J.; Salin, S.:
Progressive Damage of a Glass Reinforced Plastic During Fatigue,
in: Proceedings of the 24th Technical Conference,
The Society of Plastic Industry, 1969, p. 11-D.

[9]   Rosenfeld, M. S.; Huang, S. L.:
Fatigue Characteristics of Graphite/Epoxy Laminates Under Compression Loading,
Journal of Aircraft, Vol. 15, No. 5, May 1978, pp. 264 - 268.

[10]   Phillips, E. P.:
Effects of Truncation of a Predominantly Compression Load Spectrum on the Life of a Notched Graphite/
Epoxy Laminate,
ASTM, STP 723, 1981, pp. 197 - 212.

[11]   Whitcomb, J. D.:
Experimental and Analytical Study of Fatigue Damage in Notched Graphite/Epoxy Laminates,
ASTM, STP 723, 1981, pp. 48 - 63.

[12]   Roderick, G. L.; Whitcomb, J. D.:
Fatigue Damage of Notched Boron/Epoxy Laminates Under Constant-Amplitude Loading,
ASTM STP 636, 1977, pp. 73 - 88.

[13]   Huth, H.; Schütz, D.:
Schadensausbreitungs- und Restfestigkeitsuntersuchungen an CFK-Laminaten,
to be published: Forschungsbericht aus der Wehrtechnik, Manuscript delivered May 1982.

[14]   Stinchcomb, W. W.; Reifsnider, K. L.; Yeung, P.; Masters, J.:
Effect of Ply Constraint on Fatigue Damage Development in Composite Material Laminates,
ASTM, STP 723, 1981, pp. 64 - 84.

[15]   Chang, F. H.; Gordon, D. E.; Rodini, B. T.; Mc Daniel, R. H.:
Real-Time Characterization of Damage Growth in Graphite/Epoxy Laminates,
Journal of Composite Materials, Vol. 10, July 1976, pp. 182 - 192.

[16]   Kulkarni, S. V.; Mc Laughlin, P. V. (Jr.); Pipes, R. B.; Rosen, B. W.:
Fatigue of Notched Fiber Composite Laminates,
Analytical and Experimental Evaluation, ASTM, STP 617, 1977 pp. 70 - 92.

[17] Whitney, J. M.; Nuismer, R. J.:
Stress Fracture Criteria for Laminated Composites Containing Stress Concentrations,
J. Composite Materials, Vol. 8 (1974), p. 253.

[18] Crews, J. H. (Jr.); Hong, C. S.; Raju, I. S.:
Stress-Concentration Factors for Finite Orthotropic Laminates With a Pin-Loaded Hole,
NASA-TP 1862, May 1981.

[19] Eisenmann, J. R.; Leonhardt, J. L.:
Improving Composite Bolted Joint Efficiency by Laminate Tailoring,
ASTM, STP 749, 1981, pp. 117 - 130.

[20] Gerharz, J. J.; Schütz, D.:
Schwingfestigkeitsuntersuchungen an Fügungen in Faserbauweise,
Forschungsbericht aus der Wehrtechnik, BMVg-FBWT 79-23, 1979.

[21] Cardrick, A. W.; Smith, M. A.:
An Approach to the Development of Meaningful Design Rules for Fatigue-Loaded CFRP-Components,
Composites, May 1974.

[22] Konish, D. Y.; Johnston, W. R.:
Fatigue Effects on Delaminations and Strength Degradation in Graphite/Epoxy Laminates,
ASTM, STP 674, 1979, pp. 597 - 619.

[23] Gerharz, J. J.; Schütz, D.:
Fatigue Strength of CFRP Under Combined Flight-by-Flight Loading and Flight-by-Flight Temperature
Changes,
AGARD-CP-288, April 1980.

[24] de Jonge, J. B.; Schütz, D.; Lowak, H.; Schijve, J.:
A Standardized Load Sequence for Flight Simulation Tests on Transport Aircraft Wing Structures,
LBF-Bericht FB-106, NLR Report TR 73, Febr. 1973,
Fraunhofer-Institut für Betriebsfestigkeit (LBF), Darmstadt; National Aerospace Laboratory NLR, Amsterdam.

[25] Autorenkollektiv:
Description of a Fighter Aircraft Loading Standard For Fatigue Evaluation FALSTAFF (März 1976),
Flugzeugwerke Emmen (F + W), Switzerland,
Fraunhofer-Institut für Betriebsfestigkeit (LBF), Darmstadt,
National Aerospace Laboratory (NLR), Amsterdam,
Industrie-Anlagen-Betriebsgesellschaft mbH (IABG), Ottobrunn.

[26] Lucas, J. J.; Sainsbury-Carter, J. B.:
Effects of Specimen Geometry on Fatigue Strength of Boron and Glass Epoxy Composites,
Journal of Materials, JMLSA, Vol. 7, No. 4, Dec. 1972, pp. 586 - 589

[27] Schütz, D.; Gerharz, J. J.:
Fatigue strength of a Fibre-Reinforced Material,
Composites, October 1977, pp. 245 - 250.

[28] Gerharz, J. J.; Schütz, D.:
Schwingfestigkeitsuntersuchungen an ungekerbten und gekerbten Faserverbundwerkstoffproben aus
multidirektionalem Laminat,
Forschungsbericht aus der Wehrtechnik, BMVg-FBWT 79-25, 1979.

[29] Matondang, T. H.; Schütz, D.:
The Influence of Anti-Buckling Guides on the Compression-Fatigue Behaviour of Carbon-Fiber
Reinforced Laminates,
Fraunhofer-Institut für Betriebsfestigkeit (LBF), Darmstadt, 1980.
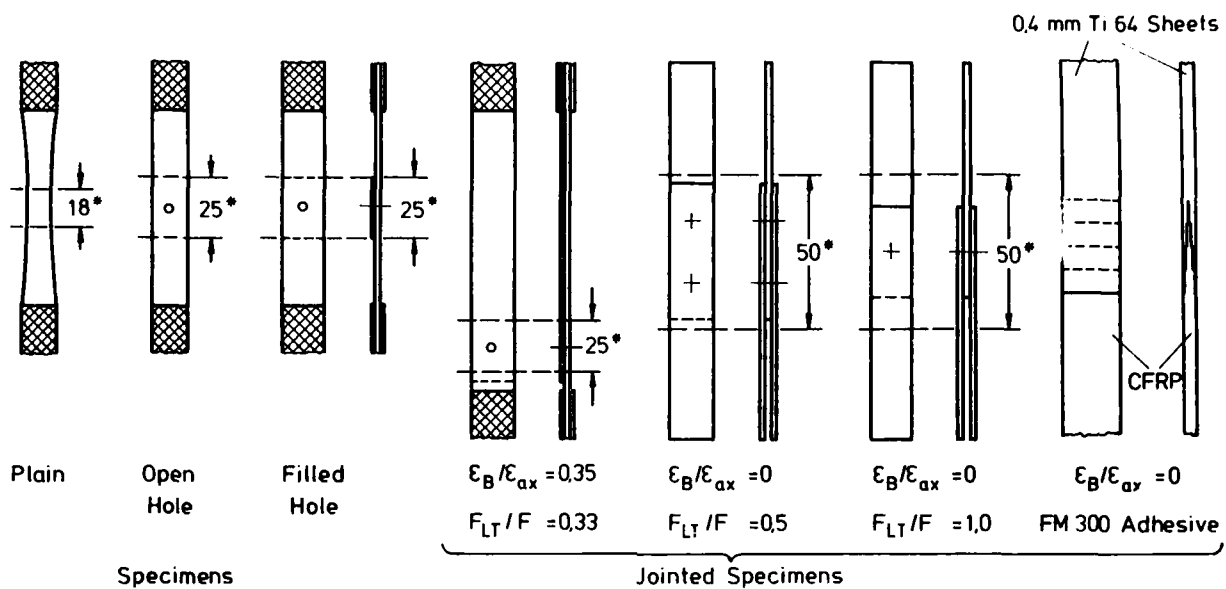
Figure 1: Forms of Specimens, Laminate Structure:
47 p.c. $0°$-; 47 p.c. $45°$-; and 6 p.c. $90°$-Layers [1, 2]

Fatigue Damage in Fibre Composite Materials:

— Matrix Cracking

— Fibre - Matrix Debonding

— Delamination

— Void Growth

— Local Fibre Breakage

— Out-of-Plane Buckling (of Delaminated Plies)

Figure 2: Failures Preceding Final Fracture of Laminates

	GFRP	CFRP	Metal-Matrix
Unidirectional		— Debonding	— Debonding
	— Fibre Breakage		— Brocken Fibres (on as-Machined Surface)
	— Matrix Micro Cracks	— Longitudinal Matrix Cracks	
Multidirectional	— Transverse Matrix Cracks	— Transverse Matrix Cracks	
		— Delamination	
		-- Out-of-Plane Buckling of Delaminated Plies	

Figure 3:   Observed Failures in Unnotched Specimens [3]

Transverse Crack   Delamination
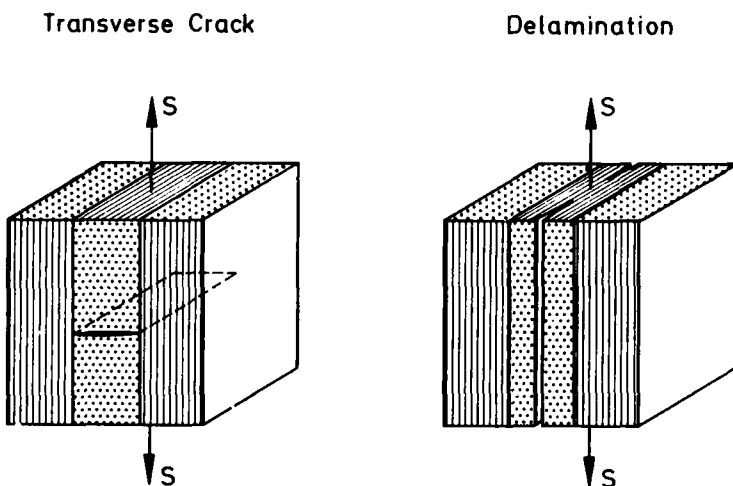
Figure 4:   Prevailing Failures in Multidirectional Laminates

Laminate Damage Experiments Show,

For Ply Transverse Cracks (in 90 and 45°- Layers)

— a Stress Threshold

— a Fatigue Cycle Threshold 〉 for Onset of Transverse Cracking

— a Stable Crack Density State (Maximum Number of Cracks)

— an Influence of Thickness of 90° - Layer,

Increasing Thickness: 〈 Decreasing Stress Threshold / Decreasing Number of Cracks in the Stuble Crack Density State

— Cracks Start in 90°-Layer and May Initiate Cracks in Neighbouring 45°- Layers, but are Restrained by Adjacent 0°- Layers

— in Most Cases Transverse Cracking Precedes Delamination Cracking

— Fatigue Loading Introduces More Cracks than Static Loading (in the Stable Crack Density State)

Figure 5:   Observed Particularities of Ply Transverse Cracks

Laminate Damage Experiments Show

For Delamination Cracking

— Association With Interlaminar Stresses at or Near Edges in Multidirectional Laminates

— no Restraint

— it Follows Transverse Matrix Cracking Along Fiber

— Precede the Bulk of Fibre Breakage

— Increases as Fracture is Approached

— it is More Extensive Under Cyclic Loading than During Static Loading

— it Reduces in Plane Stiffness, Leading to Buckling (or Micro Buckling)

— it Changes Internal Stress State

Figure 6: Observed Particularities of Delaminations
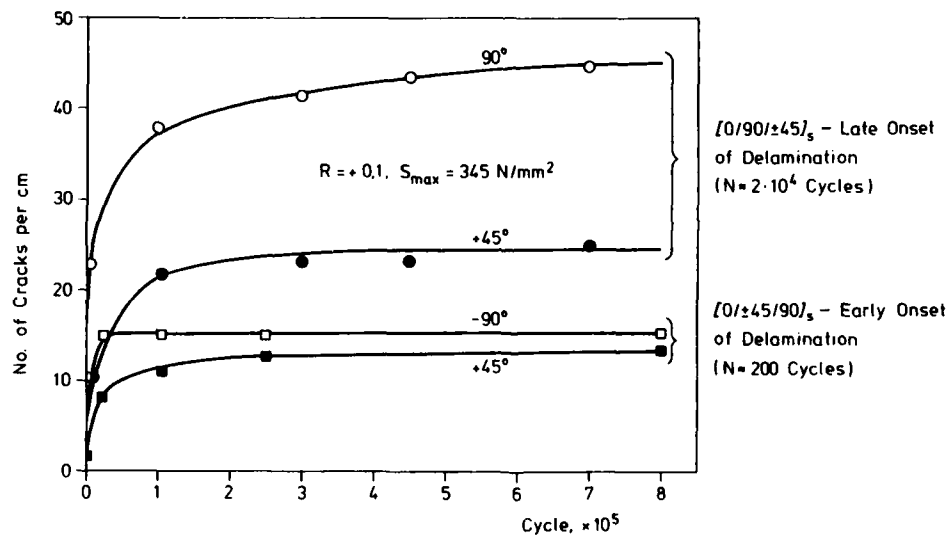
Figure 7: Transverse Crack Density During Fatigue Loading [4]

Delamination at Static and Fatigue Loading

	Static	Fatigue	
Interlaminar Stress at Tensile Load	Tension	Tension-Tension	Tension- Compression
Tension ($[0/\pm45/90]_s$)	— Delamination at — Critical Stress	Delamination at Stress — Ditto Level Below crit Stress	
Compression — ($[0/90/\pm45]_s$)	no Delamination —	Delamination due to Interlaminar Shear	— Delamination due to Local Compression- Tension Interlaminar Stress Cycle

Figure 8: Delamination at Static and Fatigue Loading
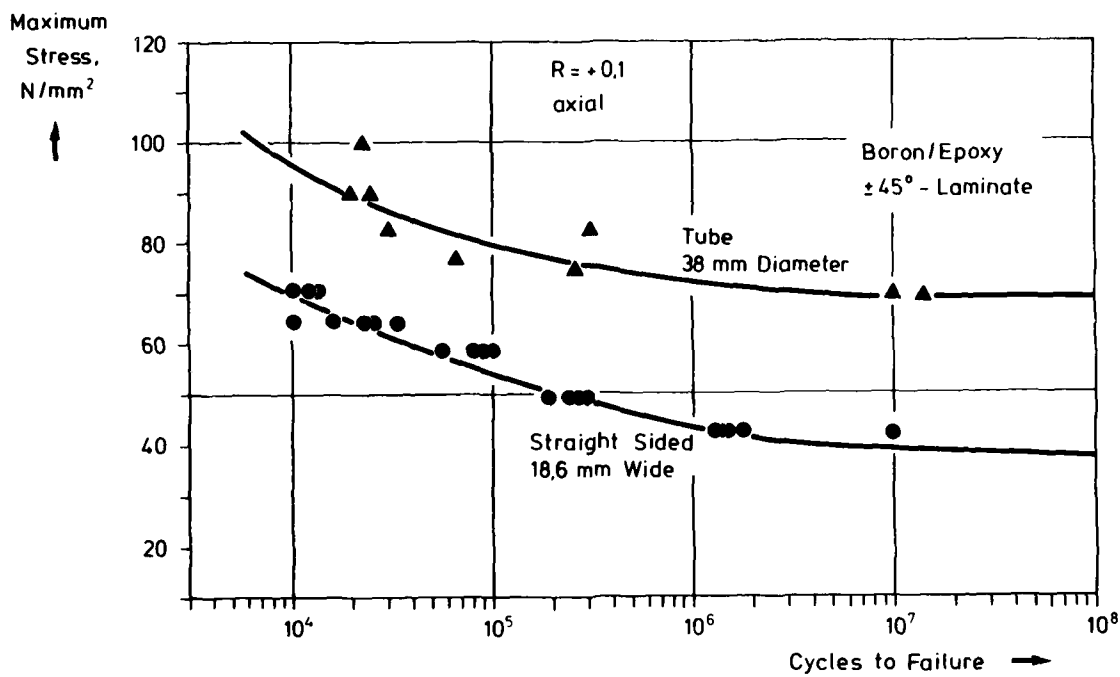
Figure 9: Effect of Specimen Shape Due to Interlaminar Stresses [26]
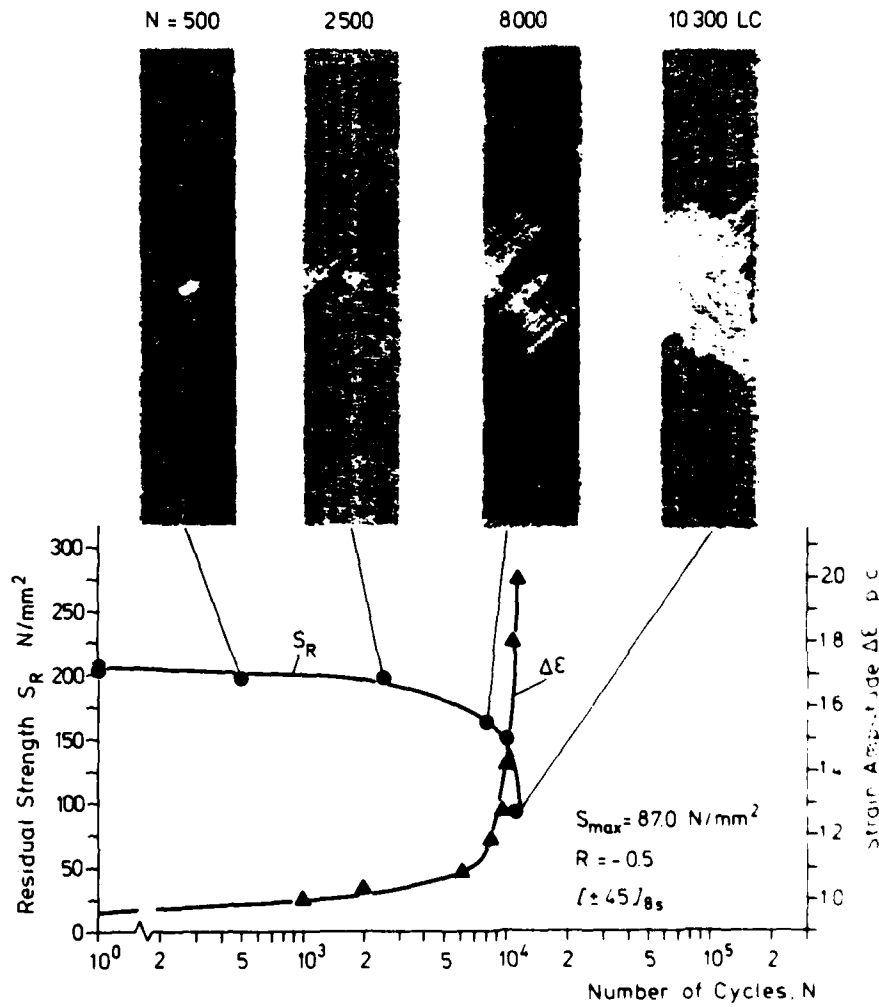
Figure 10: Damage Development, Residual Strength- and Deformation Behaviour [13]
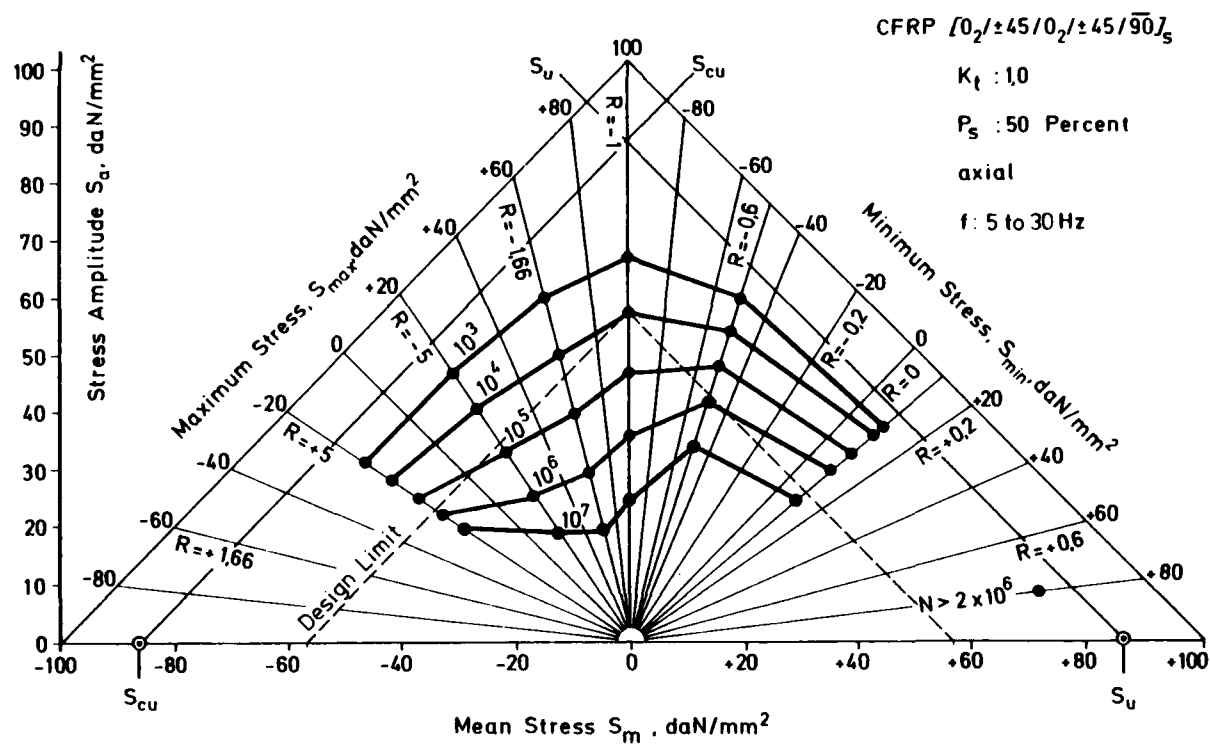
Figure 11: Constant Life Diagram of Unnotched Carbon Epoxy Laminate (Axial Loading) [27]
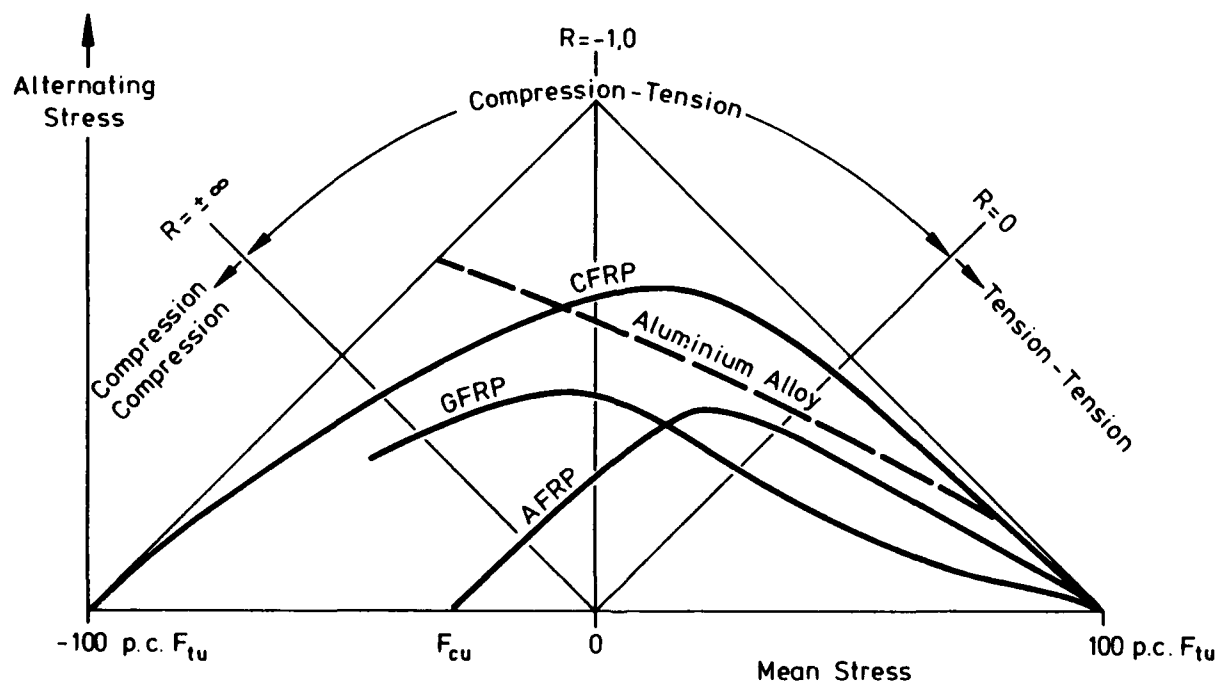

Figure 12: Effect of Compressive Loading

7-14
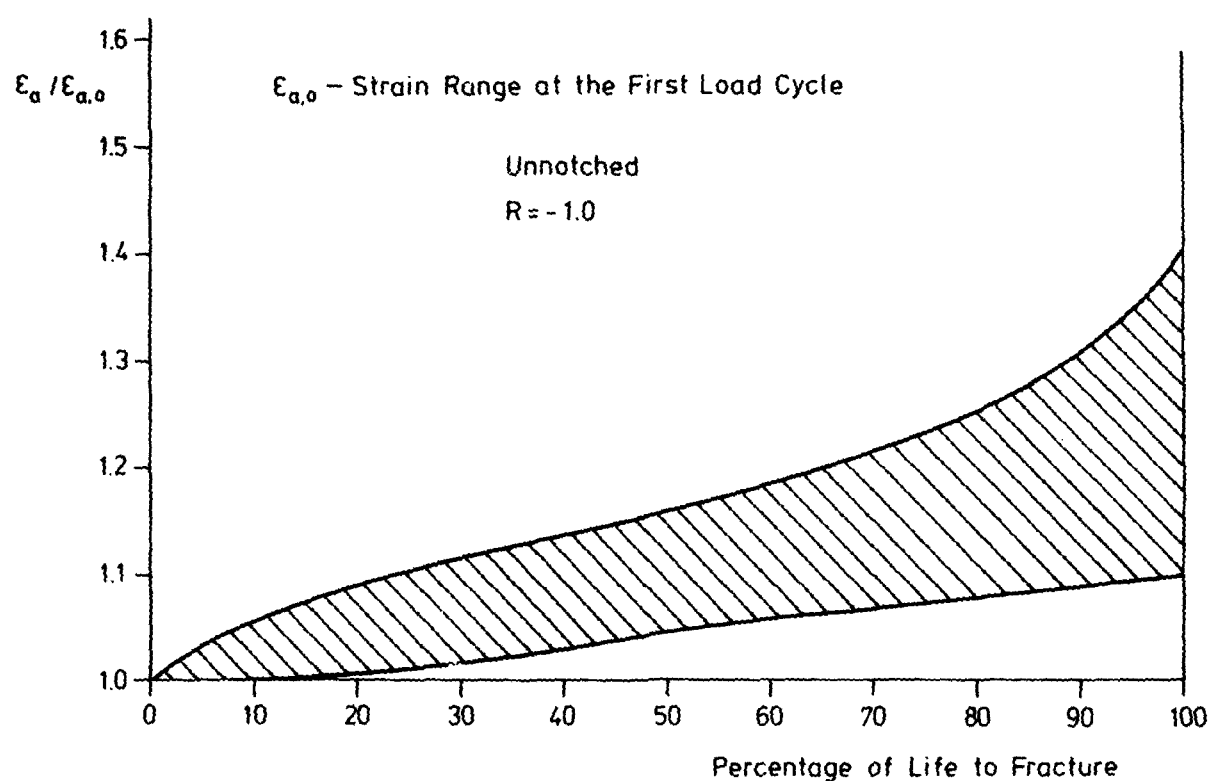
Figure 13: Deformation Behaviour During Cyclic Loading [28]
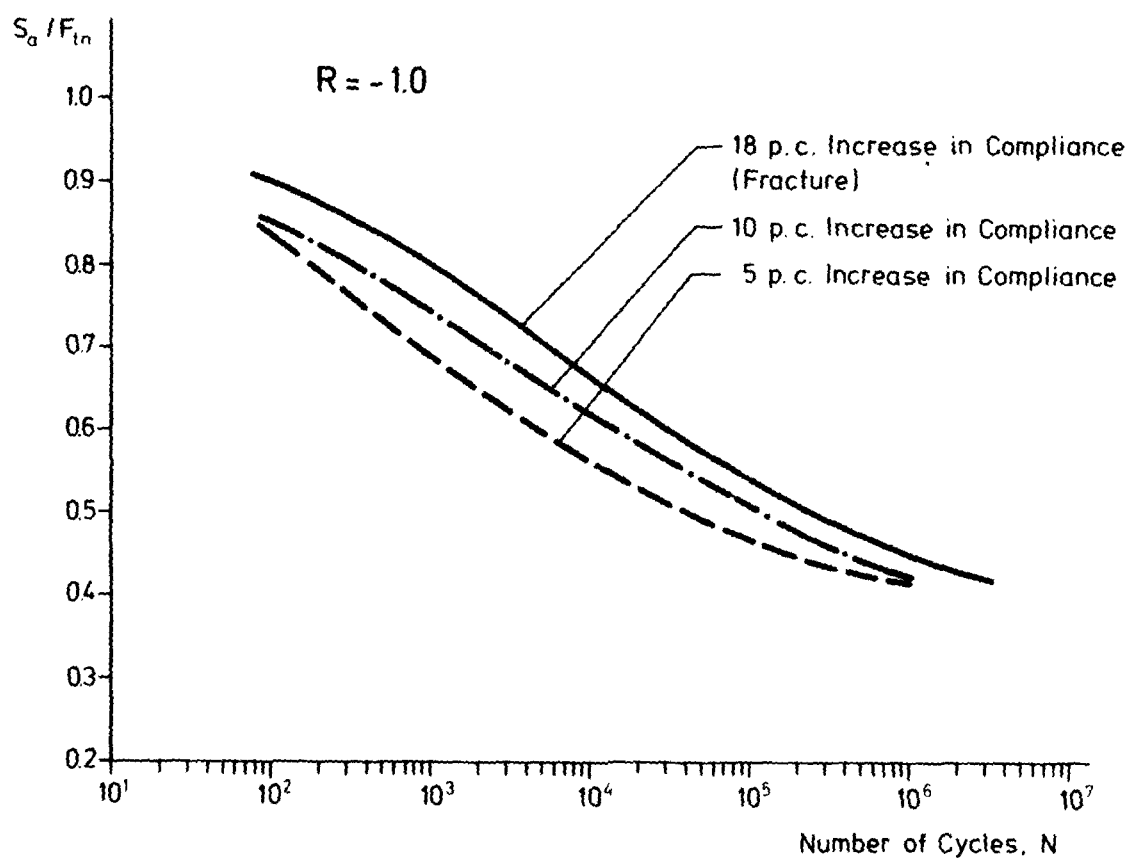
Figure 14: SN-Curves at Constant Increase in Compliance [28]
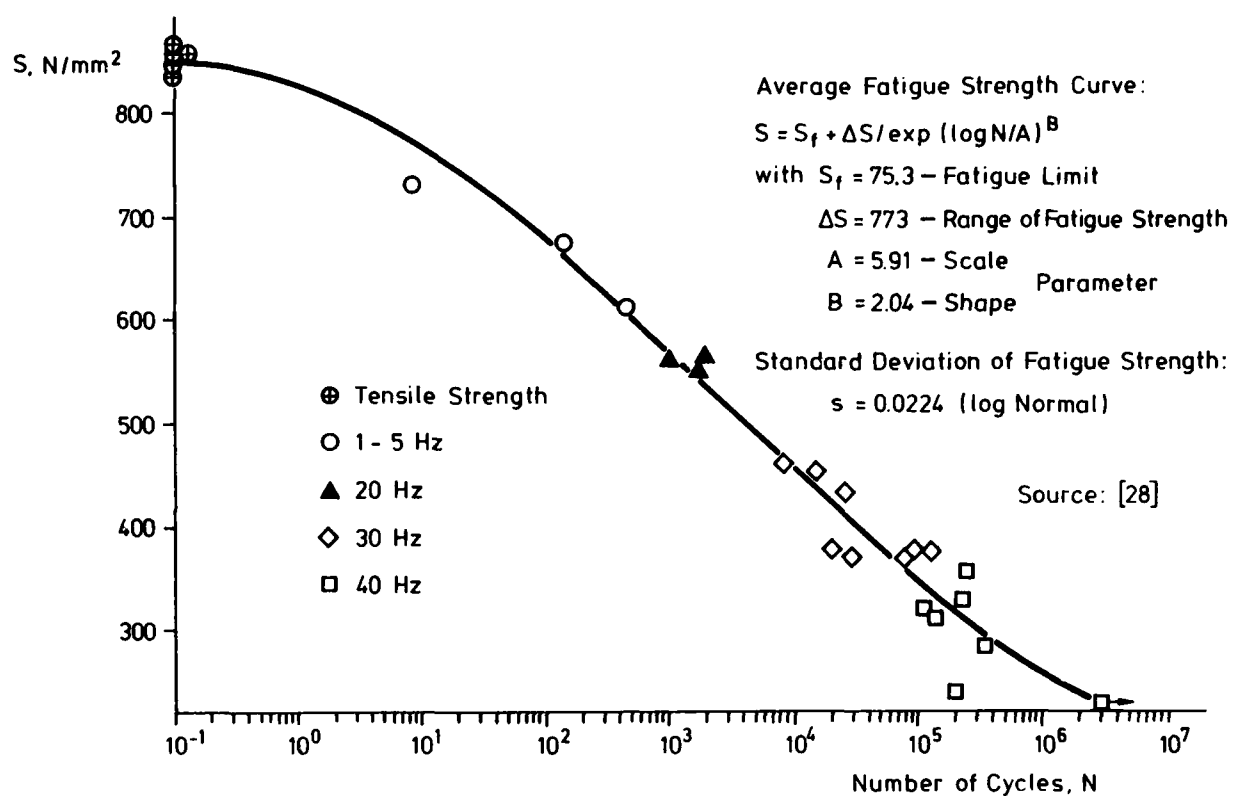
Figure 15: Fatigue Test Data and Results of Regression Analysis:
Plarn Specimens from CFRP Laminate $[(0_2/\pm45)_2\,90]_s$, R = -1.0 [28]
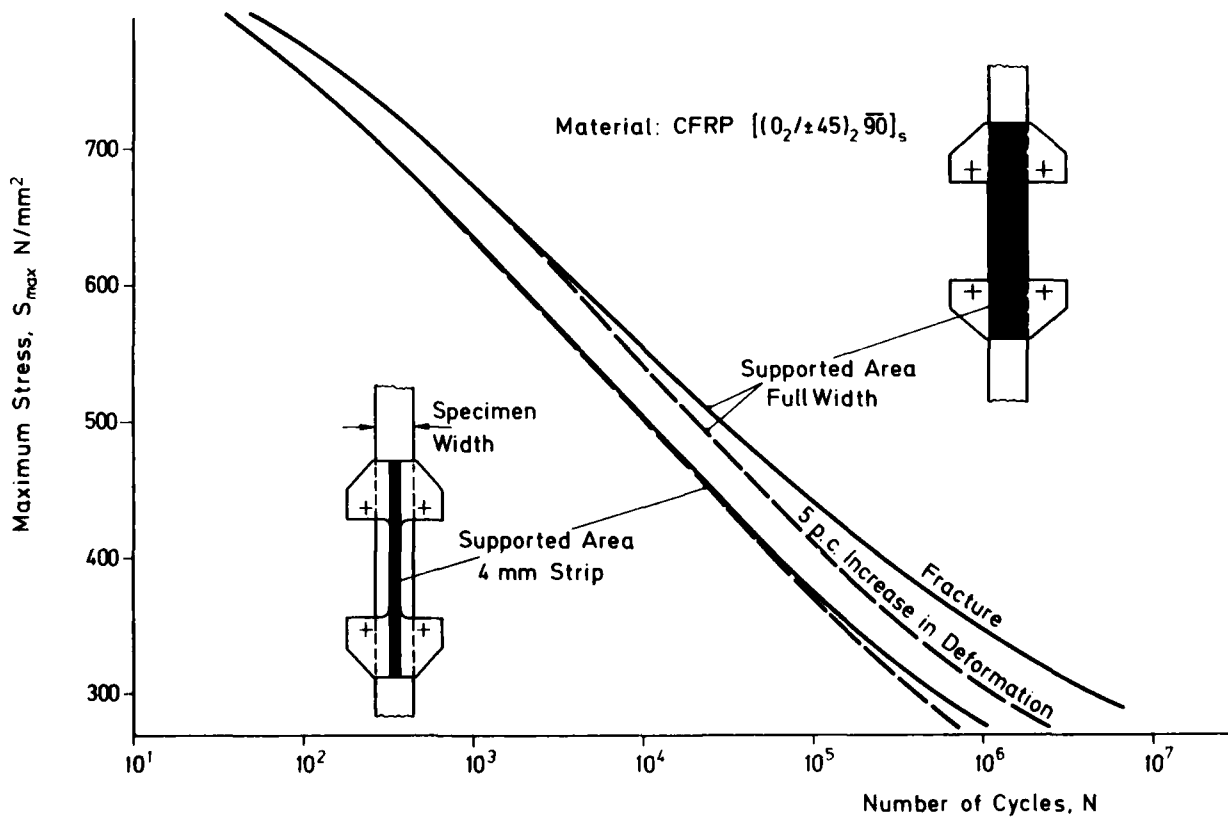
Figure 16: Effect of Antibuckling Guides at Tension-Compression Fatig. Loading [29]

Damage Around Open Hole

Polymeric Matrix		Metal Matrix
Large Fibre *	**Small Fibre** * (CFRP)	

— Debonding		— Plastic Flow
— Matrix Cracking Growing Into Adjacent Plies	— Matrix Cracking Arrested by Adjacent Plies	— Matrix Cracking
— Delamination	— Delamination	— Delamination
— Fibre Breakage		— Fibre Breakage
	— Damage Along 0°-ply Direction Notch Blunting	— Damage Perpendicular to Load Axis
	— More Matrix Damage	— Less Matrix Damage
	— Micro Buckling (Compression)	*Diameter

Figure 17:   Failures Observed at a Hole Preceding Fracture, Influence of Fibre Diameter and Matrix Material [3, 11]

S_R

$\Delta\varepsilon$

$S_{max} = 495$ N/mm^2
$R = -0.5$
$[0/\pm45/0]_s$

Residual Strength, S_R N/mm^2

Strain Amplitude, $\Delta\varepsilon$, p.c.

Number of Cycles, N
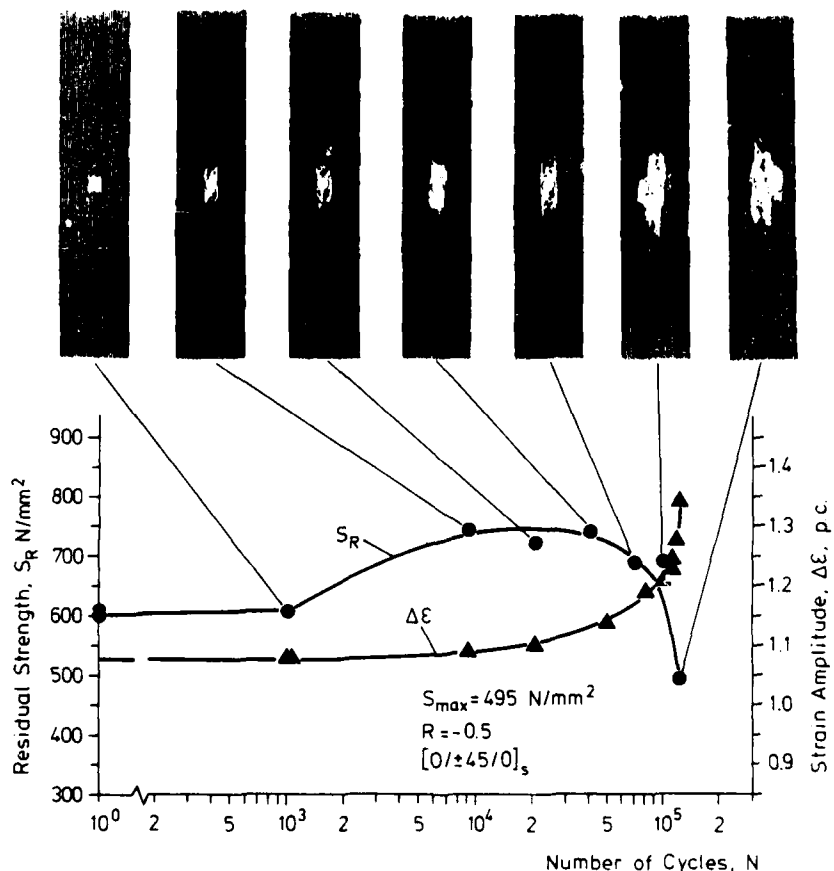
Figure 18:   Damage Development, Residual Strength- and Deformation Behaviour [13]

S, N/mm²

Plain

Increasing
Stress Concentration

R = -1.66

Filled Hole

Material: Graphite/Epoxy
914 C / T300
47 p.c. 0°
47 p.c. 45°
6 p.c. 90°

Open Hole

Interference fit

Clearance

With Delamination

Clearance

Without Delamination

Number of Cycles, N
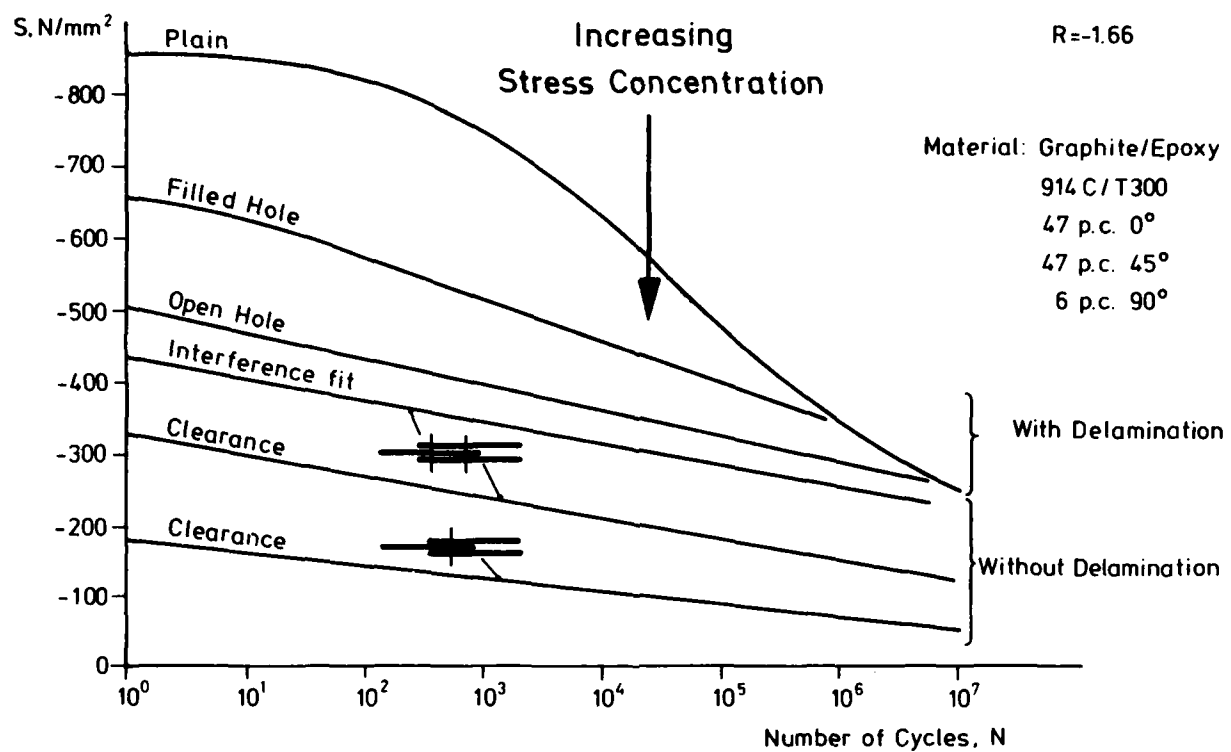
Figure 19:   Effect of Notches on Fatigue Behaviour of a CFRP Composite Laminate [1, 2]

Prevailing at Static Loading (N = 1):
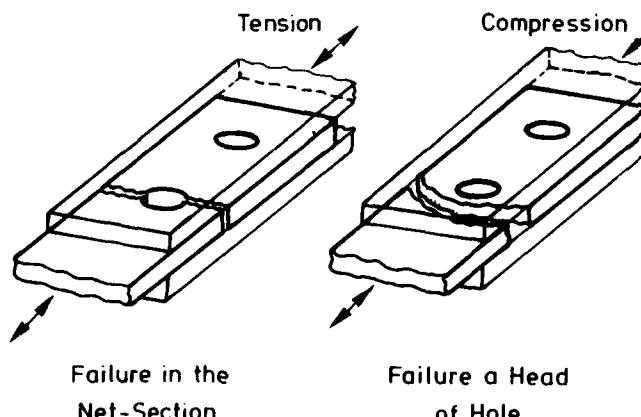
Prevailing at High Cycle Fatigue:

Tension   Compression

Failure in the
Net-Section

Failure a Head
of Hole
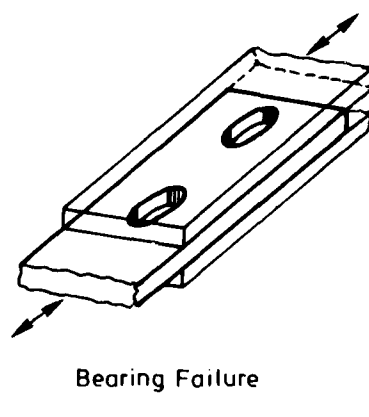
Bearing Failure

w/d = 5.0 ; e/d = 4.0

Figure 20:   Failure Modes in Bolted Joint of CFRP Laminate [2]
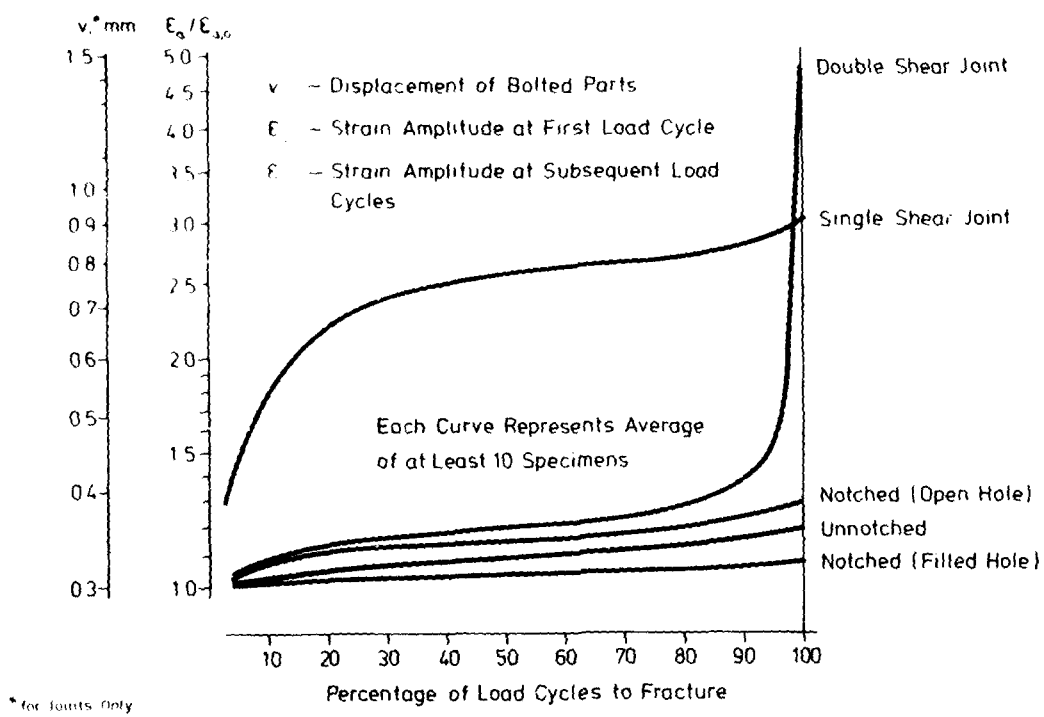
Figure 21: Increase in Deformation During Fatigue Loading, $R = -1.66$ [1]
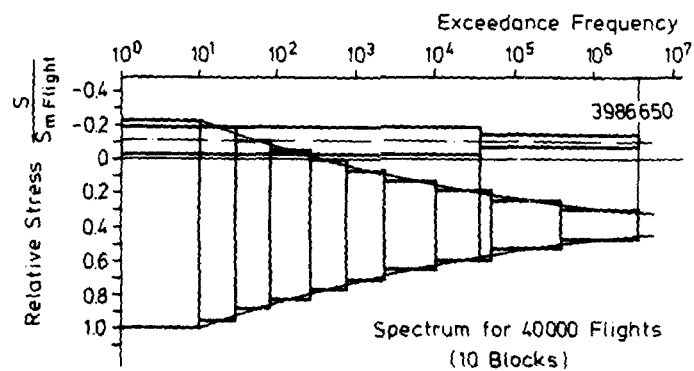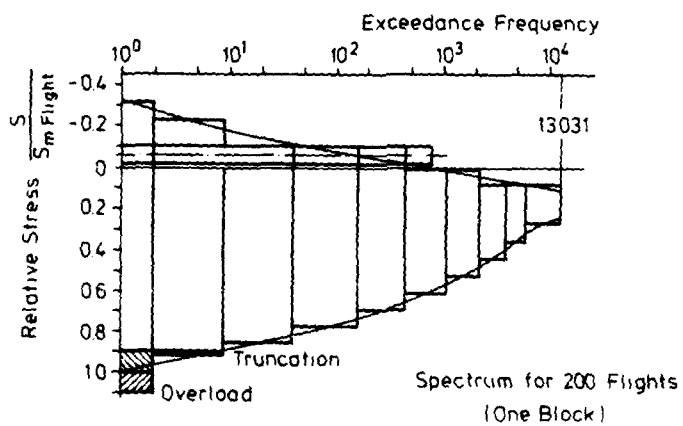
Figure 22: Test Load Spectra for Wing Lower Surface [24, 25]

Notched (Open Hole), TWIST

SPECTRUM TRUNCATIONS		LIFE BASELINE LIFE	PREDICTED LIFE * TEST LIFE
NONE (BASELINE SPECTRUM)		1.00	17.3
LOWEST LOAD LEVEL OMITTED		.87	19.8
TWO LOWEST LOAD LEVELS OMITTED		1.62	10.7
FOUR LOWEST LOAD LEVELS OMITTED		2.14	8.1
TWO HIGHEST LOAD LEVELS OMITTED		3.13	12.6
FOUR HIGHEST LOAD LEVELS AND THE LOWEST LOAD LEVEL OMITTED		11.17	6.6

MEDIAN FATIGUE LIFE, FLIGHTS

*Miner's Rule
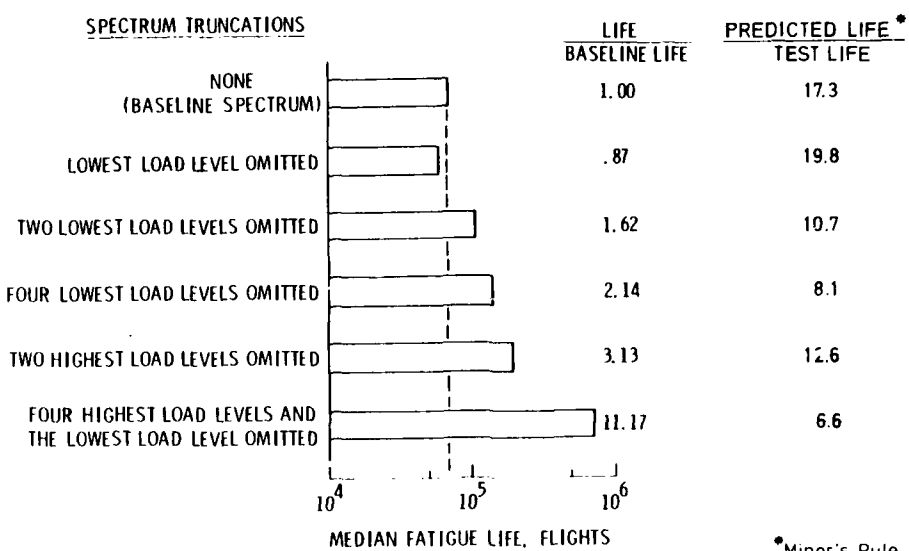
Figure 23: Effect of Spectrum Load Changes [10]

Unnotched, FALSTAFF

		Life Baseline Life	Predicted Life * Test Life
Baseline Spectrum		1 00	3 1
Increase of Maximum Load to 110 Percent		82	2 3
Spectrum Truncation at 90 Percent of Maximum Load		1 02	3 3
Three Lowest Load Levels Omitted		1 71	1 7

Average Fatigue Life, Flights

*Miner's Rule
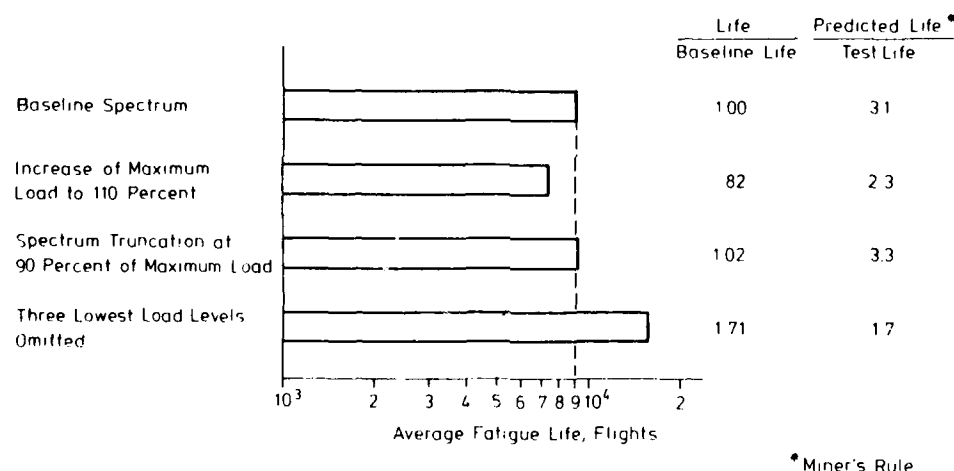
Figure 24: Effect of Spectrum Load Changes [27]

	Material CFRP; 914 C/ T 300
Room Temperature, Dry s = 0.12	Laminate $[(0_2/\pm 45)_2\ \overline{90}]_s$
	Specimen Unnotched
Content of Humidity 10 p.c. Simultaneous Environmental and Mechanical Loading s = 0.64	Load Programme FALSTAFF
1 91	Length of Beams Average Life Data
Content of Humidity 10 p.c. Consecutive Environmental and Mechanical Loading s = 0.26	s = Standard Deviation(log L)
1 24	

Life, Number of Flights, L

Figure 25: Effect of Environment on Life to Fracture, Wing Upper Surface Conditions
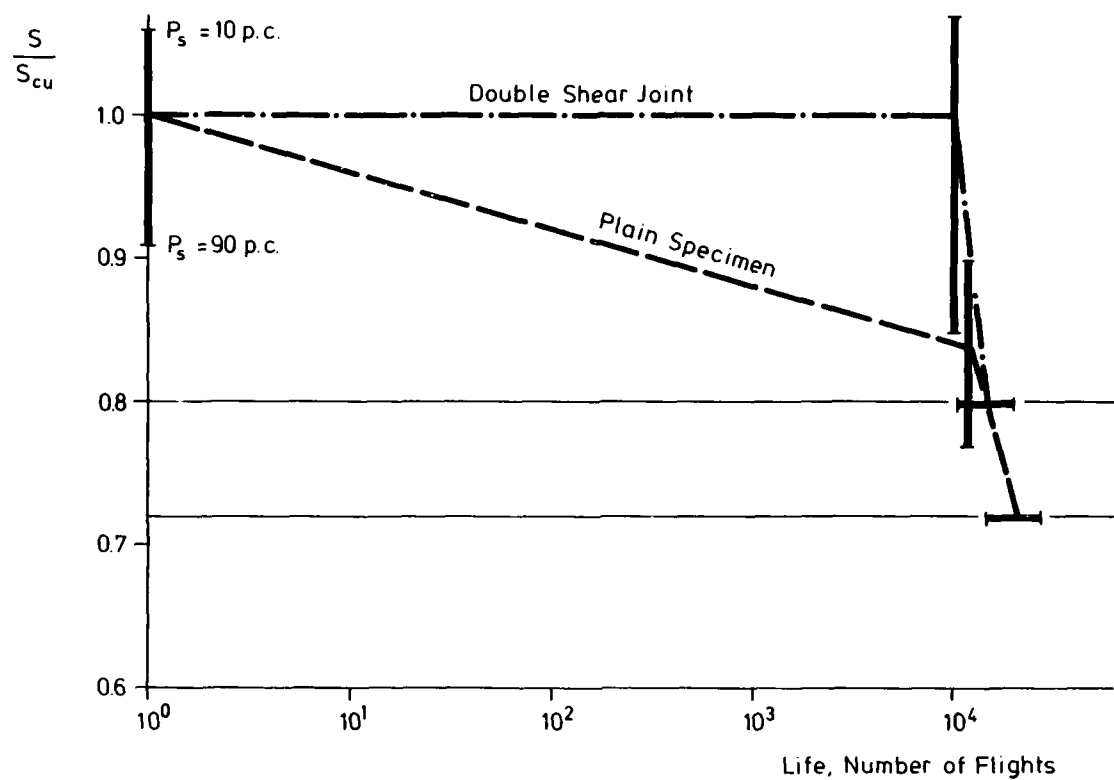
Figure 26: Strength Degradation of CFRP Plain Specimens and Joints
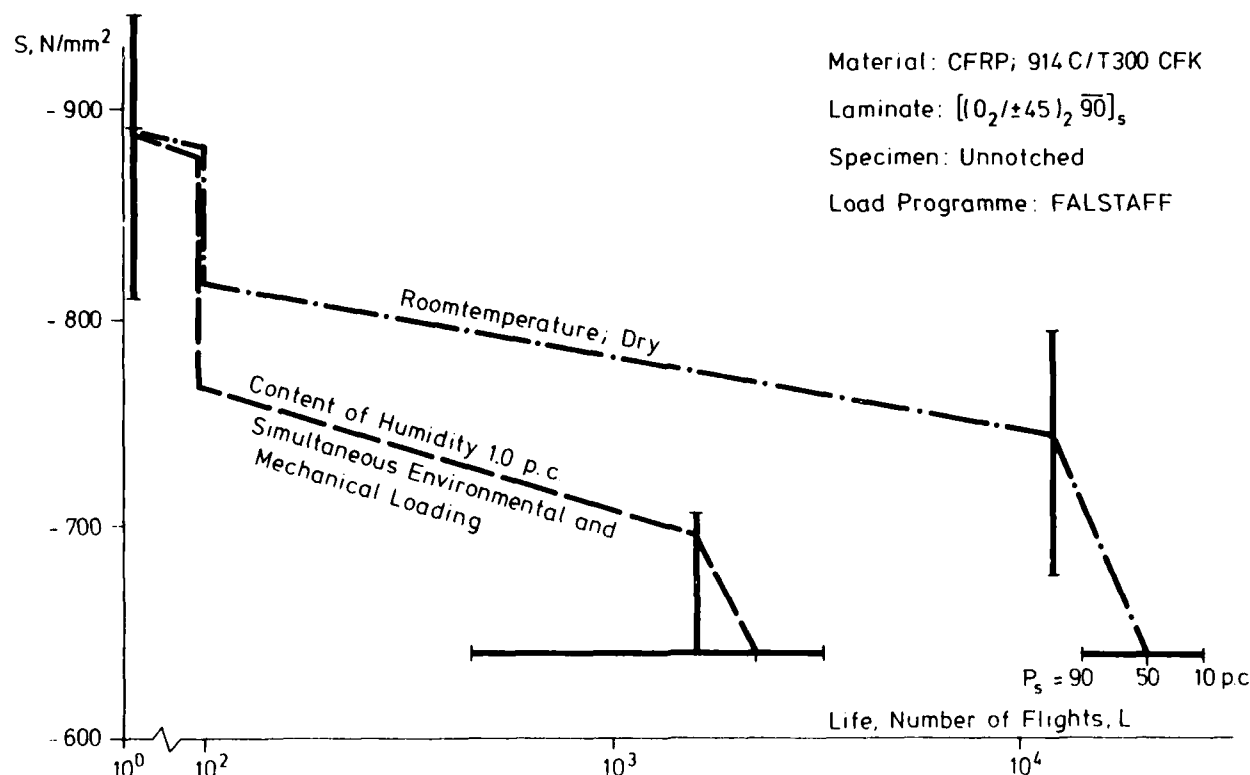
Figure 27: Strength Degradation With and Without Environment

PREDICTION OF FATIGUE FAILURE

J. J. Gerharz

Fraunhofer-Institut für Betriebsfestigkeit (LBF), Darmstadt, Germany W.

I   INTRODUCTION

Determination of ultimate life and residual strength is most important in the design of economical and reliable air frames. Besides the parameters: expected loads, expected environment, failure criteria and material behaviour, reliable prediction methods should be available. For metal airframe structures Miner's cumulative damage rule is pre-dominantly applied to predict ultimate life. The linear elastic fracture mechanics analysis provides the instantaneous residual strength of a damaged structural element, when inspection reveals the crack length. By periodic inspections those structural elements with cracks larger than a critical length are rejected. The maximum possible crack length remaining is therefore known and the corresponding residual strength and the remaining life can be calculated (deterministic approach). An equivalent method to calculate residual strength and total life of an element is required for composite structures. No inexpensive and simple inspection methods presently exist for composites whereat the weakest structural members can be screened out. Therefore one needs to determine the residual strength distribution. The interest is in the lower end of the frequency distribution and therefore the Weibull extreme value distribution is used to describe the weakest element data (statistical approach).

Life prediction models offered in the literature are summarized in Fig. 1. The new models can be grouped into those with general applicability, as for example:

- the mechanistic model by Pipes et. al I 26 I,
- the fatigue fracture model by Hashin and Rotem I 28 I and
- the purely empirical model (statistical approach) by Hahn and Kim I 1 I and Awerbuch and Hahn 1 2 1

and into models with restricted application, as for example:
- the wear-out model by Halpin et al. 1 6 1 (statistical approach) for unnotched laminates,
- the strength degradation model by Hahn and Kim 1 1 1 and Yang and Liu I 3 I (statistical approach) for unnotched laminates; and
- the delamination propagation model by Ratwani and Kan   I 11 I and Prinz I 12 I for tension-compression and   compression-compression fatigue loading.

With exception of the Fatigue Fracture Model by Hashin and Rotem all other models are based on power law damage growth equations. Thus these models are able to estimate residual strength and life to final failure assuming a pre-existing flaw. The main differences in the outcome and in data required for their practical applications are summarized in Fig. 3 and 4. The Fatigue Fracture Models of Hashin & Rotem predicts laminate fatigue behaviour from ply fatigue behaviour via failure functions which differentiate the failure modes: fibre failure, matrix failure, and interlaminar failure. As basic material static strength data for static failure, fatigue strength data (SN-curves) of the lamina and of simple angle-ply laminates are needed here with the fatigue failure functions. The authors claim good agreement of test results with the predicted fatigue failure mode relevant to the specific laminate. This is not a damage growth model like the others. It was included to mention the possibility of deriving laminate SN-curves from lamina fatigue data.

This presentation comprises the following:
- the damage growth models will be briefly commented on
- the applicability of Miner's rule to fibre composite life prediction is evaluated and
- a practical application of the strength degradation concept is demonstrated.

II   LIFE PREDICTION WITH MINER'S RULE

The Miner Rule is the most applied method to determine fatigue life of metallic aircraft structures. Nevertheless, experience has shown that calculated damage sums at actual fracture of typical structural metallic elements and materials may vary between 0.3 and 5. It seems to be useful to evaluate the applicability of Miner's rule to composites, since it is easy to apply and empirical modifications may be found with increasing number of tests. Therefore results of life prediction with Miner's rule are compared with results from variable amplitude loading of fibre composite structural features.

The test results and the calculated life of unnotched cfrp-laminate specimens subjected to FALSTAFF upper surface loading (predominantly compressive) are shown in Fig 5. For this standardized loading (predominantly compressive) are shown in Fig 5. For this standardized load programme as well as for the modifications reported in the preceding lecture the results of the Miner calculation are on the unsafe side. The ratios predicted life/test life were between 2 and 3. With the same specimens damage calculation and tests were carried out by Hahn and Weisgerber,I 17 I, using 5 different flight-by-flight loading programmes. All load programmes had most of their loads in compression. Comparison of test and calculation results showed that the Miner Rule, with

at the endurance limit and varying the counting methods applied to the test load history did not change the results.

Ref. I 15 I reports some results of flight-by-flight testing (FALSTAFF upper surface) with <u>bolted double-shear joints</u> of the cfrp laminate. The tests were run with different loading speeds. At low speed testing (5 Hz) the predicted life was on the unsafe side and for the high speed testing (25 Hz) the calculated life was on the safe side. Because there were only a few jointed specimens tested, this outcome presents just a tendency.

There is higher significance to the following results received with <u>bonded cfrp-titanium step joints</u>, I 14 I. Test lives and calculated lives are plotted in Fig. 6. The testing programme was again FALSTAFF for wing upper surface. The comparison of the results shows that the Miner calculation overpredicts the test lives by a factor 2.0 in the average. In Ref. I 18 I, Waddoups reports similar results for bonded titanium-cfrp joints. He found overestimates of test lives in the range 2.2 to 2.8.

<u>Open hole specimens</u> were used by Whitehead, I 19 I, Rosenfeld und Huang, I 20 I, and by Phillips I 21 I, in flight-by-flight testing with typical airplane wing load programmes for the upper surface. The Miner Rule again overestimated the lives to fracture resulting from the tests. The ratios of predicted life to test life were 4 to 31 in the invest-igations by Whitehead and 2 to 170 in the investigations by Rosenfeld and Huang. Phillips examined the influence of load omissions in the standardized programme TWIST (see preceding lecture) and found predicted lives being larger than corresponding test lives by factors ranging from 7 to 20.

Test lives and predicted lives using Miner's Rule are summarized in Fig. 7. The data points represent average values. It is clearly illustrated that Miner's Rule does not predict the test lives with satisfying accuracy and it's results are generally non-conservative. Nevertheless it is believed that it may become a useful tool in fatigue design of composite structure since:

- with increasing amount of flight-by-flight test data an empirical adjustment of the damage sum ($\sum n/N$) will become possible
- it can be expected that empirical damage values emerge being associated with classes of structural elements. The data summary in Fig.7 does not so far reveal such a correlation
- Miner's Rule is easy to apply in an early design stage.

III   FATIGUE FAILURE PREDICTION MODELS FOR FIBRE COMPOSITE LAMINATES

T h e   W e a r - o u t - M o d e l   I 6 I

The wear-out-model applies functions of the linear elastic fracture mechanic, accordingly it is assumed that damage grows perpendicular to load direction. Thus, longitudinal matrix cracks frequently observed at open holes can not be described by this model. It is the feeling that this method still relates strongly to the crack propagation of in-homogeneous materials. But, compared to the initiation and propagation of a single dominant crack occuring in metals, the onset and growth of many different failures characterize the fatigue behaviour of composite laminates. Due to the inherent hetero-geneity of these materials cracks in composites do not have the same implication as in metals. Typical failures as:

> broken fibres,
> matrix cracks,
> debonded fibres, and
> delaminated plies

do not occur separately but interconnected. It is therefore difficult, if not impossible to identify growth directions at all.

T h e   S t r e n g t h   D e g r a d a t i o n   M o d e l

Because of this rather statistical nature of composite fatigue behaviour the strength degradation model takes a phenomenological approach starting directly with the mathe-matical description of the strength degradation rate, accounting for the appropriate relation between ultimate strength and fatigue life. Therefore, physical events have not to be specified within this model. The strength degradation model has been developed by Yang et al. I 3, 7 I to universal applicability for unnotched composite laminates. For example, the deterministic fatigue model proposed by Broutman and Sahu, I 26 I, and the wear-out model by Halpin and Waddoups can be derived by some approximations of the strength degradation model. Verification testing shows that predictions are close to experimental results. One drawback of this model is that it can not consider increase of residual tensile strength observed in preloaded open hole specimens.

The basic assumptions of this model are:

- strength of the laminate is reduced somewhat by every load cycle
- fatigue failure occures, when residual strength has dropped to the maximum stress of the fatigue loading
- the rate of degradation at the nth load cycle is a power function of the current residual strength, S (N), and the current maximum cycle stress S

- strength and life data of a single specimen are statistically interconnected.

This implies the following: Could the same specimens be loaded to static and fatigue fracture, then one specimen out of the sample would, for instance, take the third rank of the ordered results from both, the static strength and fatigue testing. The strongest specimen in static strength would also be the strongest in fatigue. This assumption is therefore called the "strength-life equal rank" assumption. If this holds, then it is felt that damage under static loading should develop the same way it does under cyclic loading. This preferably seems to be the case for unnotched specimens, I 2 I. Fatigue loaded open hole specimens frequently broke in the gross section I 4, 5 I, whereas statically loaded they fractured in the net section. Thus there is a controversy whether or not the strength-life equal rank assumption is valid in notched laminates. Nevertheless, this assumption eases not only the predictions of residual strength and life but also provides the base for the so-called proof load method. By periodic proof loading of a composite structure the weakest structural members are screened out. For the remaining members a minimum life is guaranteed which corresponds statistically to the static strength being equal to the proof load stress. Proof loading and it's applicability have received some discussion in the literature as for example I 27 I.

It has also been observed that the composite residual strength drops sharply within a very short period at the end of life. This is called "sudden death" behaviour, I 24 I. It is assumed:
- the strength does not change with every load cycle
- cyclic loading causes laminate "damage" which does not lead to strength degradation.
In case of this behaviour no life predictions are possible by a "strength degradation" model.

A comparison of the Miner concept with the statistical concept such as the strength degradation Model reveals a fundamental difference:
- the damage calculation by Miner's Rule applies average data,
- within the strength degradation model life and strength data are treated as random variables.
The residual strength distributions and the distribution of the ultimate life is derived from the distribution of the static strength. This should be remembered when speaking of life and residual strength predicted by the strength degradation model. There is, of course, a distribution function needed. As already mentioned, the Weibull extreme value distribution was chosen. The characteristics and the applicability of the Weibull distribution to fibre composites data have received extensive discussion in the literature, as for example I 6 I and I 25 I. In the following some differences and correlations between the Weibull and the familar normal distribution are briefly pointed out.

The normal distribution is applied to the logarithm of life to failure because life to failure cannot be negative, but a normally distributed variate can take on negative values. Thus the log-normal distribution is fitted to the life to failure data. The curves corresponding to the probability density functions of the Weibull ($\alpha > 1.0$) and log-normal distribution reach zero probability of failure at zero life time. But, Weibull and log-normal distribution differ in their hazard functions of their practical domain. Whereas, the harzard functions of the Weibull distribution increase with life time, the hazard functions of the log-normal distribution decrease after an initial sharp increase. Thus, the Weibull distribution implies that with increasing life time the number of specimens that survice a certain life time decreases relative to the number of specimens that broke exactly at this life whereas, the log-normal distribution implies the contrary. Therefore, the Weibull distribution seems to be more appropiate to the situation considered here. However, statistical analyses of test results have sofar not revealed that the Weibull distribution fits the data significantly better than the normal distribution.

The application of the Weibull distribution is preferred because it is more easy to work with. It's cumulative function for the fraction of population failed at x is:

$$F(x) = 1 - exp\left[-\left(\frac{x}{\beta}\right)^{\alpha}\right]$$

where β is the "scale" parameter or the characteristic value of the random variable x occurring at the 63.2 percent failure point and α is the "shape" parameters. The estimation of the parameters can either be done graphically using so-called probability paper, or by the maximum likelihood method as recommended in I 16 I. The Weibull parameters correlate with the parameters of the normal distribution through the mean or expected value and the coefficient of variation:

- expected value: $E(x) = \mu = \beta \cdot \Gamma\left(\frac{1}{\alpha} + 1\right)$

- coefficient of variation: $\sigma/\mu = \left[\Gamma(2/\alpha - 1) - \Gamma^2(1/\alpha - 1)\right]^{1/2} / \Gamma\left(\frac{1}{\alpha} + 1\right)$

where Γ = standard Gamma function.
Thus the scatter is proportional to $1/\alpha$ and the relations indicate a sharp increase in scatter (σ/μ) when α becomes smaller than 4.0. The mean and the median (F(x) = 0.5) do not generally coincide as for the normal distribution. At α = 3.75, when the mean and the median are equal the Weibull distribution is a good approximation of the normal distribution.

Delamination Propagation Model

As shown in the preceding lecture, compression is more critical in fatigue loading than tension. During tension-compression loading extensive delamination cracking occurs. The delamination governs the damage development preceding the final fracture. The observed mechanisms I 11, 29 I are:
- out of plane buckling and frequent instability cracks of delaminated plies, which finally result in the collapse of the laminate plate. The location of the delamination can be obtained by the analysis of interlaminar stresses.
- Ryder and Walker, I 30 I, have observed a threshold stress at which delamination does not propagate during tension-compression loading.
- They also observed that the size of the delamination at failure was small for large compression loads, and vice versa. Thus load dependent critical delamination sizes exist, which can be determined by the Euler formula.

Based on these observations and assumptions Ratwani and Kan, I 11 I, developed a delamination propagation model to calculate ultimate life. Within the verification procedure the authors found that fatigue data from various sources fell in one scatterband when plotted as function of interlaminar shear stress range. The correlation found might be improved by introducing an equivalent interlaminar stress considering shear as well as normal stresses. Ratwani and Kan verified the model with fatigue data comprising results of various laminate-struct res and of unnotched and notched specimens. Prinz, I 12 I, has expanded the model to residual strength prediction of unnotched laminates. In both applications the delamination propagation model was claimed to give good correlations between predicted and observed data.

Mechanistic Model

A completely different approach to the problem of life prediction in composites has been considered by Pipes et al. I 26, 5 I. They specifically consider the problem of fatigue in notched laminates, although the philosophy can be applied to all laminates. In notched boron epoxy I $0_2/ \pm 45$ I$_s$-laminates they noted that the fatigue failure mode was often different to the static failure mode. Statically the notched specimens broke in the net section, whereas fatigue loading caused severe delamination and fracture in the gross section. The strength-life equal rank assumption is probably not valid in notched laminates. The mechanistic model does not involve this assumption and can accommodate the increase in residual strength found in notched composites.

The basic assumptions of the model are:
- repeated load applications cause a degradation of the basic material properties, viz tension, compression and shear strengths and the corresponding elastic moduli. It is assumed that the material around the notch will be degraded faster than elsewhere due to the high shear stresses which exist in this region and that the rest of the laminate will experience little deterioration, see Fig. 8.
- The fatigue degraded properties are then used in a static failure function to predict the residual static strength, fatigue failure occurring when the strength falls below the fatigue load.
- The static failure model can incorporate different failure modes and the re-distribution of stresses due to changes in the elastic moduli can cause failure to occur in a different mode to that observed statically.

This model relies on the mechanical behaviour of the single ply. This has the advantage that once these basic (material) properties have been established, their values can be used for all lay-ups, given a general strength model. Of course, also the mechanistic model requires empirical derivation of some constants. Generally, however, the experimental effort is less compared to the statistical models. The development of this model to design applicability has not been completed yet. A critical link in this model seems to be the failure function, which should also handle the interlaminar stresses causing delamination. One should also be aware that much of the fatigue damage in composite laminates occurs long before ultimate failure and, hence, there can be many types of subcritical failures. Much more details to this model are presented in Ref. I 31 I and, of course, in the publications of the research workers developing this model.

IV   APPLICATION OF THE STRENGTH DEGRADATION MODEL

For a safe life design of a composite structure it is required that:
- the "A" values of residual strength do not drop below the design ultimate stress during the total design life and
- the specified life is less than the actual life at a required probability of survival.

This situation is illustrated in Fig. 9. Considering for example the upper surface wing structure of a fighter aircraft the relevant data needed for the proof may either directly derived through flight-by-flight testing with FALSTAFF load programme or by life prediction using constant amplitude fatigue data. The experimental way may go without residual strength testing when the exponents of the residual strength curve are known. In the following the strength degradation model is applied

- to the presentation of the results from flight-by-flight-, residual strength-, and static strength testing (the corresponding distribution parameters are determined)
- to derive the exponents of the residual strength curve for future application of the model without residual strength testing being necessary and finally,

- to determine residual strength and life to failure from SN-data, using the distribution parameters derived by data analysis.

Unnotched feature and double shear joints, see Fig. 10, of the wing upper surface structure are evaluated. For all three cases the analysis results are plotted in form of constant reliability curves in diagrammes which show the instantaneous strength as a function of number flights (residual strength curves). The test data points from Fig. 11 are included in the diagrammes for comparison. The static strength data S(o) are plotted vs. $N = 10^o$, the residual strength data S(N) vs. number of flights (N) of preloading, and life to failure data at the stress level (maximum spectrum load) S.

In SN-diagrammes life data on several stress levels are connected with static strength data by constant probability curves. Likewise in residual strength diagrammes the static- and residual strength data are connected with the life data. But within the statistical analysis for the determination of the percentile residual strength data (as for example, 90 percent and 10 percent probability data) it must be considered that the residual strength results stem from surviving specimens. Those which did not survive cyclic preloading because their residual strength had already dropped below the preload stress level before the preloading had ended must be incorporated in the analysis. This is made possible by the strength-life equal rank assumption which is part of both the empirical and analytical strength degradation model.

Analysis and Presentation of Test Results by the Empirical Strength Degradation Model

The cumulative distribution functions by which the values of static and residual strength as well as of the life to failure for a given probability of survival are calculated, are listed in Fig. 12. The equations for the static strength and the life to failure are both the two-parametric Weibull distribution function. Estimates of the scale and shape parameters β_S, β_L and o_S, o_L, respectively, were determined from the test results (Fig. 11) using MLE method for censored samples I 16 I.

Because the residual strength data stem from surviving specimens the corresponding distribution function must resemble conditional probability, see Fig. 12. For the parameters of the conditional distribution function no equations for a maximum likelihood estimation (MLE) are available. Therefore the graphical method is used to determine o_r and β_r. The median rank estimates are applied for the data plotting on probability paper and linear regression analysis provide the estimates of the parameters. In the course of the analysis it was recognized that the second term in the conditional distribution function (Fig 12) would have a very small value and could therefore be deleted. Thus, in the present situation, the simplified distribution function $(S_r \ S)$ exp I-(S_r/β_r) I could be fit to the residual strength data by maximum likelihood estimation of β_r and o_r.

The parameter estimates used for the data presentations are summarized in Fig. 13. The shape parameters put in parentheses are weighted average values which include MLE's from former test series with unnotched I 4 I and jointed specimens I 15 I of the same configuration, material and laminate. Because the weighted average values are more representative than those from one sample only, they are used in the calculations that follow. The static strength-, residual strength-, and life values for given levels of probability of survival can be easily calculated using the equations shown in Fig. 11. The results are called percentiles. The percentiles corresponding to the reliabilities 0.1, 0.25, 0.75, and 0.9 are listed in Fig. 14 together with the averages of the test results. The tenth and ninetieth percentiles as well as the averages (expected values) are plotted for the unnotched specimen in Fig. 15, and for the jointed specimen in Fig. 16. The data points of the averages and the points of equal probability of survival are connected by straight lines. These are the residual strength degradation model. Of course further test results are needed to increase the statistical significance of the outcome. Comparing the residual strength curves in Fig. 15 with those in Fig. 16 a difference in fatigue behaviour is revealed, which was already presented in the preceding lecture.

Presentation of the Test Results by the Analytical Strength Degradation
The Determination of the Exponent of the Residual Strength Curves

Residual strength curves are now fitted to the results of the static strength-residual strength-, and fatigue-testing (Fig. 11) using the analytical strength degradation model of Yang and Jones, I 7 I. As mentioned already a power function describes the degradation of the residual strength. The relation between the strength, S(N), and the life, N, is of the same form as that one developed in the "wear-out" model I 6 I, that is:

$$\bar{S}^v (N) = \bar{S}^v(0) - f(\bar{S}, \bar{S}_{cu}) \cdot N$$

$$\text{where} \quad \bar{S}(\ldots) = S(\ldots)/\beta_S$$

The last term of this equation is a linear function of the load time with the linearity factor $f(\bar{S}, \bar{S}_{cu})$. Most of the crack propagation formulas for homogeneous materials also have this linear relationship.

With the assumptions already listed in the appendix and by substitions and transformations Yang and Jones, I 7 I, obtained the following mathematical description of the residual strength - life time relation:

$$\bar{S}^v(N) = \bar{S}^v(0) - \frac{\bar{S}^v(0) - \bar{S}^v}{\bar{S}^c(0) - \bar{S}^c} \cdot \frac{N}{\beta_L} \tag{2}$$

The exponent c is the ratio of the Weibull shape parameters, $c = \alpha_S/\alpha_L$, and the exponent v is the slope parameter of the residual strength curves. The effect of this parameter on the strength degradation curves is schematically illustrated in Fig. 17. The value of v is determined by fitting the curves to the test results. In doing this one has to recall that S(N) and S(o) are random variables, consequently their values are given by their adherent distribution functions. With S_γ(o) being the static strength at the probability of survival γ and based on the strength-life equal rank assumption the equation of the constant probability curves S_γ(N) = f(N) is obtained; with the substitution of S_γ(o) = $(-\ln\gamma)^{1/\alpha_s}$ (see Fig. 12) into equation (2), that is:

$$S_\gamma(N) = \beta_S \left[(-\ln\gamma)^{v/\alpha_s} - \frac{N}{\beta_L} \cdot \frac{(-\ln\gamma)^{v/\alpha_s} - \bar{S}^v}{(-\ln\gamma)^{c/\alpha_s} - \bar{S}^c} \right] \tag{3}$$

With v = 8, found by curve fitting, the residual strength curves fit the test results of the unnotched specimens best.

Fig. 18 shows the corresponding strength degradation curves of 10 and 90 percent probability of survival and of the average values. The distribution parameters used in equation (3) to calculate the percentiles are those derived from the statistical data analysis, see Fig. 13. The same values had already been used in the data presentation by the empirical strength degradation model shown in Fig. 15.

Comparing the outcomes of the empirical model with those of the analytical model one notes that the constant probability curves, as for example the 90 percent curves, do not end at the same ultimate life values (at S(N) = $\bar{S}$). This discrepancy exists because for the ultimate life different distribution functions are applied. That is for the analytical model:

$$\gamma(L) = \exp\left[-\left(\frac{L}{\beta_L} + \bar{S}^c \right)^{\alpha_L} \right]$$

and for the empirical model:

$$\gamma(L) = \exp\left[-\left(\frac{L}{\beta_L} \right)^{\alpha_L} \right]$$

The additional term in the first equation decreases the ultimate life at 90 percent probability of survival indicating larger scatter as in the empirical model.

For the test result of the double shear joint no exponent was found that could make the strength degradation curve fit reasonably well to the test results. The presentation of the test results with the empirical model, Fig. 16, demonstrated that the strength of the double shear joint remained on the initial level up to 70 percent of the ultimate life. The displacement measurements revealed that at the preload level of N = 10^4 flights the majority of the joints had not experienced an increase in displacement larger or equal 0.3 mm which is the fracture criteria. However, with continued load cycling a rapidly increasing displacement, already observed under constant amplitude loading, occurs. It is therefore concluded that the sudden death model should rather be assigned to the residual strength behaviour of cfrp double shear joints.

Prediction of Life and Residual Strength with Strength Degradation Model

Like Miner's Rule the prediction by the strength degradation model applies constant amplitude SN-data. However, for each load level of the load spectrum not only the number of cycles to fracture but also the strength degradation curves for the constant amplitude loading are needed, that means the exponents of equation (3) must be known. They are assumed to be constant in the life cycle range $10^3 \leq N \leq 10^7$.

On the other hand, the strength degradation predicts not only life to failure but also the residual strength in relation to the fatigue loading period. Furthermore not only the average values but also the statistical distributions of residual strength and life to fracture are obtained by the model.

In the following constant probability residual strength curves are determined for the unnotched specimens subjected to FALSTAFF upper surface loading. The constant amplitude SN-data presented by the constant life diagramme in Fig. 11 of the preceding lecture were used. In a residual strength diagramme the predicted residual strength is compared with the test data. Also a comparison is made between the life to failure predicted by the strength degradation model with the one predicted by Miner's rule.

Prediction of Residual Strength

If the degradation of the residual stress by each single load cycle or by each cycle block of the load programme is considered,

- the residual strength after k-load cycles is

$$\bar{S}^v(k) = \bar{S}^v(0) - \sum_{i=1}^{k} \frac{1}{\beta_{L,i}} \cdot J_i \qquad (4)$$

- the residual strength after j-blocks is

$$\bar{S}^v(j) = \bar{S}^v(0) - j \sum_{i=1}^{m} \frac{n_i}{\beta_{L,i}} \cdot J_i \qquad (5)$$

where $\sum_{i=1}^{m} n_i$ is the number of load cycles in one block,

and

$$J_i = \frac{\bar{S}^v(0) - \bar{S}_i^v}{\bar{S}^c(0) - \bar{S}_i^c}$$

These equations were derived from equation (3).

Fig. 19 illustrates how the strength degradation model and Miner's Rule accumulate damage during a simple 3-step loading sequence. From this illustration it is clear that opposite to Miner's Rule, the damage sum depends on the load level at final failure. The damage sum also correlates with the shape of the residual strength curves, that means with the values of the exponents c and v.

For constant amplitude loading of the unnotched specimen residual strength curves were not established for the established; instead it was assumed, as recomended by Yang and Jones, I 7 I, that v = c. With J_i = 1.0 and $\bar{S}^c(o) = (-\ln\gamma)^{1/\alpha_L}$ the equation (5) becomes

$$S_\gamma(j) = \beta_S \left[(-\ln\gamma)^{1/\alpha_L} - j \sum_{i=1}^{m} \frac{n_i}{\beta_{L,i}} \right]^{1/c} \qquad (6)$$

This is the equation needed for the prediction of residual strength at given levels of reliability γ. Here, $\beta_{L,i}$ are the lives to fracture from the SN-curves and γ is the reliability or the probability of survival. Scale and shape parameter β_S and α_S were taken from Fig. 13. The shape parameters α_L were determined by the statistical analyses (pooling) of the constant amplitude fatigue test results I 4 I. On the load levels of the FALSTAFF upper surface programme shape parameters between 0.7 and 2.0 evolved. For the prediction α_L = 2.0 was chosen. This value adheres to the load levels with the larger sums of n/N. With these distribution parameters the residual strength after 3 to 150 blocks (j = 3,..., 150) were calculated for 10, 50 and 90 percent probability of survival. The results of the calculation are shown in Fig. 20 in form of the familiar strength degradation curves. The test results fall between the 90- and 10-percent curve. But compared to the residual strength curves fitted to the available FALSTAFF test results shown in Fig. 15, a larger scatter is predicted. The predicted residual strength at 90 percent probability of survival is less than that resulting from test data analysis. This is related to the difference of shape parameters. The cycles to failure at constant amplitude loading showed larger scatter (α_L = 2.0) than the flights to failure at flight-by-flight loading (α_L = 4.0) which is a well known fact in metal structure behaviour.

Prediction of Life

By substitution of the fatigue failure criteria:

$$S_\gamma(j) = \bar{S} \quad \text{and}$$
$$j = L/200 \quad \text{(the FALSTAFF load programme has 200 flights per block)}$$

into equation (6) and by some transformation the equation of life prediction is obtained:

$$L_\gamma = \frac{(-\ln\gamma)^{1/\alpha_L} - (\bar{S}/\beta_S)^c}{\sum_{i=1}^{m} \frac{n_i}{\beta_{L,i}}} \cdot 200$$

Thereby, it was assumed that the specimens fail when the maximum stress ($\bar{S}$) of the load spectrum occurs. The corresponding equation of life prediction by Miner's Rule is:

$$L_{Miner} = \frac{1}{\sum_{i=1}^{m} \frac{n_i}{N_i}} \cdot 200$$

where L and N_i respectively are the average values of life and load cycles to failure. To compare the life prediction from the strength degradation model with that from Miner's Rule the ratio of the predicted lives is considered on the base of average values. With S(o) being the average static strength this ratio is:

$$\frac{L_{St.Deg.}}{L_{Miner}} = \left(\frac{S(0)}{\beta_S}\right)^c - \left(\frac{\bar{S}}{\beta_S}\right)^c$$

Because of $0 < S(0)/\beta_S < 1$ and $\bar{S} < S(0)$ the ratio of predicted lives is:

$$\frac{L_{St.Deg.}}{L_{Miner}} < 1.0$$

Principally the strength degradation model provides smaller lives to failure than the life prediction by Miner. In view of the fact that life prediction by Miner's Rule overpredicts the actual life to fracture the predictions by the strength degradation model are closer to reality. This is demonstrated by some examples in the following table:

Specimen	Load Level	Predicted Life/Test Life	
		Miner	Strength Degradation
unnotched	- 640 N/mm^2	3.6	2.5
	- 710 N/mm^2	3.1	1.9
bolted joints	- 380 N/mm^2	3.0	1.7
bonded joints (titanium-cfrp)	- 240 N/mm^2	2.0	1.1
	- 260 N/mm^2	2.2	1.5
	- 315 N/mm^2	1.9	1.4

V   CONCLUDING REMARKS

Methods of failure predictions for fatigue loaded fibre composite laminates were reviewed exhibiting their most important characteristica. For unnotched cfrp-specimens subjected to FALSTAFF upper surface loading life to failure was predicted by Miner's Rule and by the strength degradation concept. The predicted life was compared to the test life. Finally, it is to say that it was not intended to verify the strength degradation model, but to demonstrate it's applicability.

In summary it was found:

regarding the published fatigue failure prediction models
- besides Miner and Relative Miner further universal models and methods are:
  · the mechanistic model by Pipes et. al, I 5 I, and
  · the method of Hashin and Rotem, I 9 I
- other important models and their field of application are:
  · the wear-out model of Halpin, I 6 I, for unnotched specimens
  · the strength degradation concept I 1, 3, 7, 25 I for unnotched specimens
  · the delamination propagation model I 11, 12 I at fatigue loading largely in compression,
  · the percent failure (Miner-)rule I 25 I for life data with large scatter
- the strength degradation concept used here is the best verified model
- the models predicting laminate failure from ply failure are the mechanistic model and the method by Hashin and Rotem; for these models would require only a small amount of testing; the other models need SN data for each laminate stack-up.
- with all statistical analyses the Weibull distribution functions are used

regarding the presentation of test results in residual strength diagrammes:
- static strength, residual strength and life to fracture data could be correlated through curves of constant probability of survival; this was made possible by a purely statistical analysis procedure by Awerbuch and Hahn, I 2 I, as well as by the method of Yang and Jones, I 7 I, through the statistical analysis of the static strength and ultimate life data and the fitting of the strength degradation curves of constant survival probability to the results of the residual strength testing
- the two methods did not give equal results:
  · the test results of double shear bolted cfrp joints could only be analyzed by the method of Awerbuch and Hahn, I 2 I; because of non-existing strength degradation the method of Yang which is based on strength degradation could not fit the data; the test result of the bolted joints rather follow the "sudden death" model, I 24 I,
  · the analysis by Yang and Jones resulted lower averages and larger scatter of ultimate life as the method of Awerbuch and Hahn;
- the analysis method of Awerbuch and Hahn is only useful if at a given number of preload cycles more than one residual strength test is carried out; the model of Yang and Jones does not have this restriction

- the criterion for a reasonable application of both models was met: unnotched and double shear joint specimens show the same mode of fracture after monotonic and cyclic loading

regarding the evaluation of Miner's Rule application:
- Miner's Rule strongly overestimates the safe life of composite structures; an improvement will probably be reached by empirical fitting

and finally regarding the application of the strength degradation (st. deg.) model
- life to failure as well as residual strength was predicted by the st. deg. model
- the prediction includes not only average values but also statistical distribution of the the residual strength and of the ultimate life; the distribution of the static strength must be given
- the application of the st. deg. model therefore requires determination of the Weibull parameters for the distribution of the load cycles to fracture and of the static strength
- the st. deg. method principally predicts shorter lives to failure than Miner's Rule
- the predicted ultimate life and residual strength at 90 percent probability of survival were smaller than those of the test results (prediction and analysis with the st. deg. model)

LIST OF SYMBOLS

c	–	parameter (exponent) of strength degradation, $c = o_S/o_L$
$E(...)$	–	expected value of ..., average value of ...
j	–	number of cycle blocks of a load programme; one block in the FALSTAFF programme comprises 200 flights
J	–	parameter of the damage sum; $J = (\bar{S}^v(0) - \bar{S}^v)/(\bar{S}^c(0) - \bar{S}^c)$
L	–	ultimate life at programme loading
L_γ	–	ultimate life, reached or exceeded by γ-percent of all specimens; the value of ultimate life for reliability γ
N	–	number of flights
n_i	–	number of load cycles at programme load level i
N_i	–	number of cycles to failure (from SN-curve) at programme load level i
$S; S(0)$	–	static strength
S_r	–	residual strength
$S(...)$	–	residual strength at life ...
$\bar{S}$	–	highest stress in load spectrum, the variable amplitude test load level
$\bar{S}(...)$	–	$S(...)/\beta_S$
$\bar{\bar{S}}$	–	$\bar{S}/\beta_S$
$S_\gamma(0)$	–	the value of static strength for reliablity γ
$S_\gamma(...)$	–	the value of residual strength at life ... for reliablity γ
S_i	–	stress at load level i, the constant amplitude test load level
v	–	parameter (exponent) of the residual strength degradation; determined by curve fitting
α	–	shape parameter of the Weibull distribution function
β	–	scale parameter of the Weibull distribution function
γ	–	probability of survival; for instance: $\gamma(L) = P[L > L_\gamma]$

Indices:

L	–	life
r	–	residual strength
s	–	static strength

Definition:

$\gamma(S_r|S)$ -   probability of the residual strength being larger than a value S under the condition that the residual strength is above the preload level $\bar{S}$;
$\gamma(S_r|S) = P \left[(S_r > S)|(S_r > \bar{S}) \right]$

APPENDIX

Assumptions used in the strength degradation model (analytical)

- fatigue fracture occurs, when the residual strength $\bar{S}(N)$ has dropped to the load level stress of the preloading $\bar{S}$ and this happens at the load time N = L, then:

$$f(\bar{S}, \bar{S}_{cu}) = \left[\bar{S}^v(0) - \bar{S}^v \right]/L$$

where L is a random variable,

- the static strength data follow the two-parametric Weibull distribution function

$$\gamma(S) = exp\left[-\bar{S}^{\alpha_s}(0) \right]$$

- the ultimate life data (N = L) follow the truncated distribution function:

$$\gamma(L) = exp\left[-\left(\frac{L}{\beta_L} + \bar{S}^c \right)^{\alpha_L} \right] \qquad for \quad L \geq 0$$

$$\gamma(L) = 0 \qquad\qquad\qquad for \quad L < 0$$

where $c = \alpha_s/\alpha_L$

- static strength and ultimate life are statistically correlated, strength-life equal rank assumption:

$$\gamma(S) = \gamma(L)$$

thus with the equation given above

$$L = \beta_L \left(\bar{S}^c - \bar{\bar{S}}^c \right)$$

LIST OF REFERENCES

[1] Hahn, H. T.; Kim, R. Y.:
Proof Testing of Composite Materials,
J. Composite Materials 9, July 1975, p. 297 - 311.

[2] Awerbuch, J.; Hahn, H. T.:
Fatigue and Proof Testing of Unidirectional Graphite/Epoxy Composites,
ASTM STP 636, 1977, p. 248 - 266.

[3] Yang, J. N.; Liu, M. D.:
Residual Strength Degradation Model and Theory of Periodic Proof Tests for Graphite/Epoxy Laminates,
J. Composite Materials 11, April 1977, p. 176 - 204.

[4] Gerharz, J. J.; Rott, D.; Schütz, D.:
Schwingfestigkeitsuntersuchungen an ungekerbten und gekerbten Faserverbundwerkstoffproben aus multi-direktionalem Laminat,
BMVg-FBWT 79-25.

[5] Kulkarni, S. V.; Mc Laughlin, P. V. (Jr.); Pipes, R. B.; Rosen, B. W.:
Fatigue of Notched Fiber Composite Laminates: Analytical and Experimental Evaluation,
Composite Materials: Testing and Design (Fourth Conference),
ASTM STP 617, 1977, pp. 70 - 92.

[6] Halpin, J. C.; Jerina, K. L.; Johnson, T. A.:
Characterization of Composite for the Purpose of Reliability Evaluation,
in: ASTM STP 521, 1973, pp. 5 - 64.

[7] Yang, J. N.; Jones, D. L.:
Load Sequence Effects on the Fatigue of Unnotched Composite Materials,
ASTM, STP 723, 1981, pp. 213 - 232.

[8] Hahn, H. T.:
Fatigue Behavior and Life Prediction of Composite Laminates,
ASTM, STP 674, 1979, pp. 383 - 417.

[9] Rotem, A.:
Fatigue Failure of Multidirectional Laminate,
AIAA Journal, Vol. 17, No. 3, March 1979.

[10] Huth, H.; Peter, O.; Schütz, D.:
Schadensausbreitungs- und Restfestigkeitsuntersuchungen an CFK-Laminaten,
LBF-Bericht Nr. 3976/2, 1981.

[11] Ratwani, M. M.; Kan, H. P.:
Compression Fatigue Analysis of Fiber Composites,
AIAA-Paper No. 80-0707, 1980.

[12] Prinz, R.:
Schadensfortschritt in CFK bei Schwingbelastung,
Strukturmechanik Kolloquium, 25. Juni 1981,
DFVLR, Forschungszentrum Braunschweig, Institut für Strukturmechanik.

[13] Schütz, D.; Gerharz, J. J.:
Fatigue Strength of a Fibre-Reinforced Material,
Composites, October 1977, pp. 245 - 250.

[14] Gerharz, J. J.; Rott, D.; Schütz, D.:
Schwingfestigkeit von lösbaren Krafteinleitungen in Faserverbundkonstruktionen,
LBF-Bericht Nr. 3978, Juni 1981.

[15] Gerharz, J. J.; Rott, D.; Schütz, D.:
Schwingfestigkeitsuntersuchungen an Fügungen in Faserbauweise,
BMVg-FBWT 79-23.

[16] ASTM Committee E-09.03:
Recommended Practice for Statistical Analysis and Interpretation of Data for Composite Materials.

[17] Weisgerber, D.; Hahn, P.:
Lebensdauervorhersage mittels Schadensakkumulations-Hypothesen für KFK-Strukturen,
MBB-Bericht Nr. UFE 1461, Dez. 1978.

[18]   Waddoups, M. E.:
unpublished fatigue data of General Dynamics,
in: ASTM, STP 521, p. 62.

[19]   Whitehead, R. S.:
unpublished fatigue data of BAe Warton, 1979,
in: BAe Report No. SON(P) 179, Febr. 1979, p. 3.

[20]   Rosenfeld, M. S.; Huang, S. L.:
Fatigue Characteristics of Graphite-Epoxy Laminates Under Compression Loading,
AIAA/ASME 18th Structures, Structural Dynamics and Materials Conference, March 1977, Paper No. 473.

[21]   Phillips, E. P.:
Effects of Truncation of a Predominantly Compression Load Spectrum on the Life of a Notched
Graphite/Epoxy Laminate,
ASTM, STP 723, 1981, pp. 197 - 212.

[22]   Yang, J. N.:
Fatigue and Residual Strength Degradation for Graphite/Epoxy Composites Under Tension-Compression
Cyclic Loadings,
in: J. of Composite Materials, Vol. 12 (Jan. 1978), p. 19.

[23]   Ramani, S. V.; Williams, D. P.:
Notched and Unnotched Fatigue Behaviour of Angle-ply Graphite/Epoxy Composites,
ASTM STP 636, 1977, pp. 27 - 46.

[24]   Chou, P. C.; Croman, R.:
Degradation and Sudden-Death Models of Fatigue of Graphite/Epoxy Composites,
in: ASTM STP 674, 1979, pp. 431 - 454.

[25]   Chou, P. C.; Wang, A. S. D.; Croman, R.; Miller, Harry; Alper, J.:
Statistical Analysis of Strength and Life of Composite Materials,
AFWAL-TR-80-4049, April 1980.

[26]   Pipes, R. B.; Kulkarni, S. V.; Mc Laughlin, P. V :
Fatigue Damage in Notched Composite Laminates,
Material Science and Engineering 30 (1977), pp. 113 - 120.

[27]   Wang, A. S. D.; Chou, P. C.; Alper, J.:
Effects of Proof Test on the Strength and Fatigue Life of a Unidirectional Composite,
ASTM STP 723, 1981, pp. 116 - 132.

[28]   Hashin, Z.; Rotem, A.:
A Fatigue Failure Criterion for Fiber Reinforced Materials,
in: Glass Reinforced Epoxy Systems,
Materials Technology Series, Vol. 2, Editor: C. J. Hilado, 1974.

[29]   Konishi, D. Y.; Johnston, W. R.:
Fatigue Effects on Delaminations and Strength Degradation in Graphite/Epoxy Laminates,
ASTM, STP 647, pp. 597 - 619.

[30]   Ryder, J T.; Walker, E. K.:
Effect of Compression on Fatigue Properties of a Quasi-Isotropic Graphite/Epoxy Composite,
ASTM, STP 636, pp. 3 - 26.

[31]   Gordon, B.; Whitehead, R. S.:
A Critical Review of Life Prediction Methods for Composite Structures,
British Aerospace, Aircraft Group, Report No. SON(P) 179, Feb. 1979.
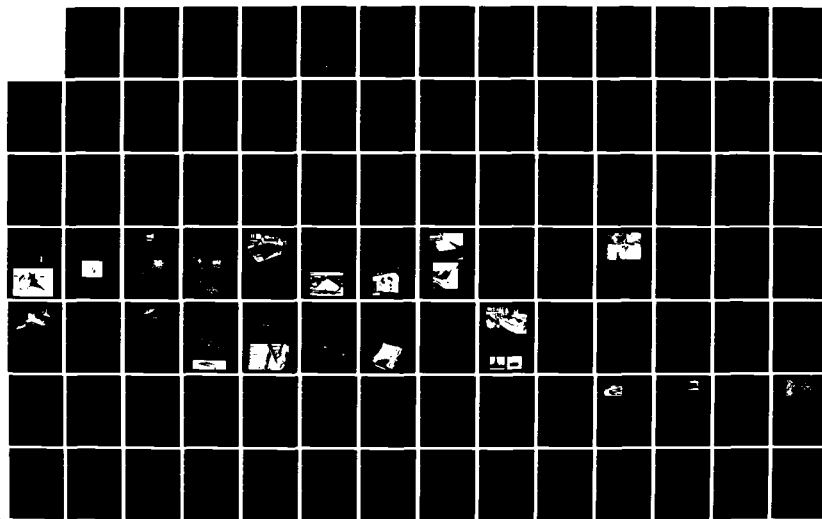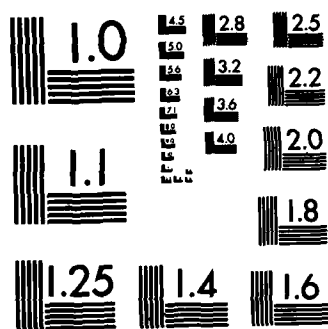
MICROCOPY RESOLUTION TEST CHART
NATIONAL BUREAU OF STANDARDS-1963-A

Life Prediction Models

— Miner's Linear Damage Accumulation

— Strength Degradation, Analytical Model [3, 7, 22]

— Mechanistic Model of Pipes, Kulkarni et al.[5]

— Wear-out Model of Halpin et al. [6]

— Fatigue Fracture Model of Hashin & Rotem [9]

— Delamination Propagation Model by Ratwani & Kan [11]

— Strength Degradation, Empirical Model [1, 2]

Figure 1: Fatigue Failure Prediction Models for Fibre Composite Laminates

Source	Method	Result of Calculation	Application	Input	Assumptions and Relations
	Miner Rule (Percent Life Rule [25])	average life (deterministic)	unnotched and notched specimens	constant life curves for the laminate	linear damage accumulation damage sum $\sum \frac{n}{N} \triangleq$ Life used up
Cou, Alper 1977, in: [25]	Percent Failure Rule (Miner)	statistical distribution of life	at large scatter of cycles to failure	– const. life curves – distribution of life (laminate data)	– linear damage accumulation – Weibull distribution – sum of failure probability $\sum_i \Delta F_i (n_i)$
Hahn, Kim, 1975 [1] Awerbuch, Hahn, 1977 [2]	Residual Strength Degradation (Empirical Model)	strength and life in relation to probability of survival	generally for analysis and presentation of test results	– static strength data – residual strength data – life to failure (laminate data)	– strength-life equal rank – Weibull distribution
Halpin et. al. 1973 [6]	Wear-out	– residual strength curves of constant probability – distribution of residual strength and life at failure	not for notched specimens (residual strength increase is not accounted for)	– distribution parameters – fracture mechanics properties – static strength data	– strength life equal rank – crack propagation power function (LEFM) – Weibull distribution
Yang, Liu, 1977 [3] Yang, 1978 [22] Yang and Jones 1978, [7]	Residual Strength Degradation (Analytical Model)	– residual strength curves of constant probability – distribution of residual strength and life at failure	not for notched specimens (residual strength increase is not considered)	– distribution parameter – const. life curves or SN-parameters (laminate data)	– strength-life equal rank – degradation rate power function – Weibull distribution
Chou and Croman, 1978 [24]	Sudden Death	distribution of life to failure	no decrease or increase of residual strength	– distribution of static strength	– strength-life equal rank
Kulkarni, Pipes, 1977 [5]	Mechanistic Model (in development stage)	characteristic (or average) residual strength and life at failure	notched and unnotched specimens (increase in residual strength will be predicted	– mechanical properties of the ply – parameter of the change in stress-strain behaviour (stiffness reduction)	– fracture function – degradation of strength and stiffness – stress analysis at the notch in each layer
Ratwani and Kan, 1980 [11] Prinz, 1981, [12]	Delamination Propagation	average residual strength and life at delamination	fatigue loading in compression (T-C and C-C)	– thickness of delaminated plies – interlaminar stresses – compressive strength	– delamination governs damage development – Euler critical buckling – interlaminar stresses at the delamination crack tip
Rotem, 1977 [9]	Fatigue Fracture Function	average of life at critical failure mode	fatigue loading in tension	– mechanical ply properties – SN-curves of lamino and simple angle-ply laminate	– critical stresses are included

Figure 2: Brief Summary of the Methods Applied in Fatigue Failure Prediction Model for Fibre Composite Laminates

Models:	Outcome:
Strength Degradation Model and Wear-out Model:	— Constant Probability Curves of Residual Strength and Life to Failure

Needs:
"Strength-Life Equal Rank"
Assumption
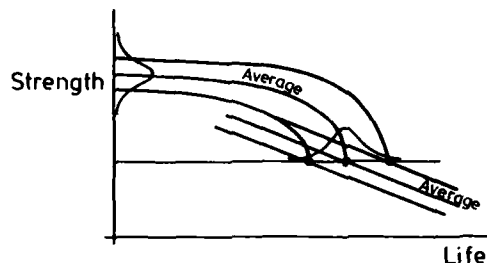
Delamination Model and Mechanistic Model:	— Average Residual Strength and Life to Failure

Figure 3: The Main Difference in the Outcome of the Fatigue Fature Prediction Models

Required Data:

Strength Degradation:	— <u>Distribution Parameters</u>* — Static Strength — Laminate SN-Curves
Wear-out Model:	— <u>Distribution Parameters</u>* — Static Strength — Fracture Mechanics Properties
Delamination Model:	— Lamina Properties — Delamination Threshold — Compressive Strength
Mechanistic Model:	— Lamina Properties — Stiffness Reduction Data (Change in Local Stress Strain Behaviour)

*Strength and Life Data

Figure 4: Required Input Data for the Fatigue Failure Prediction Models
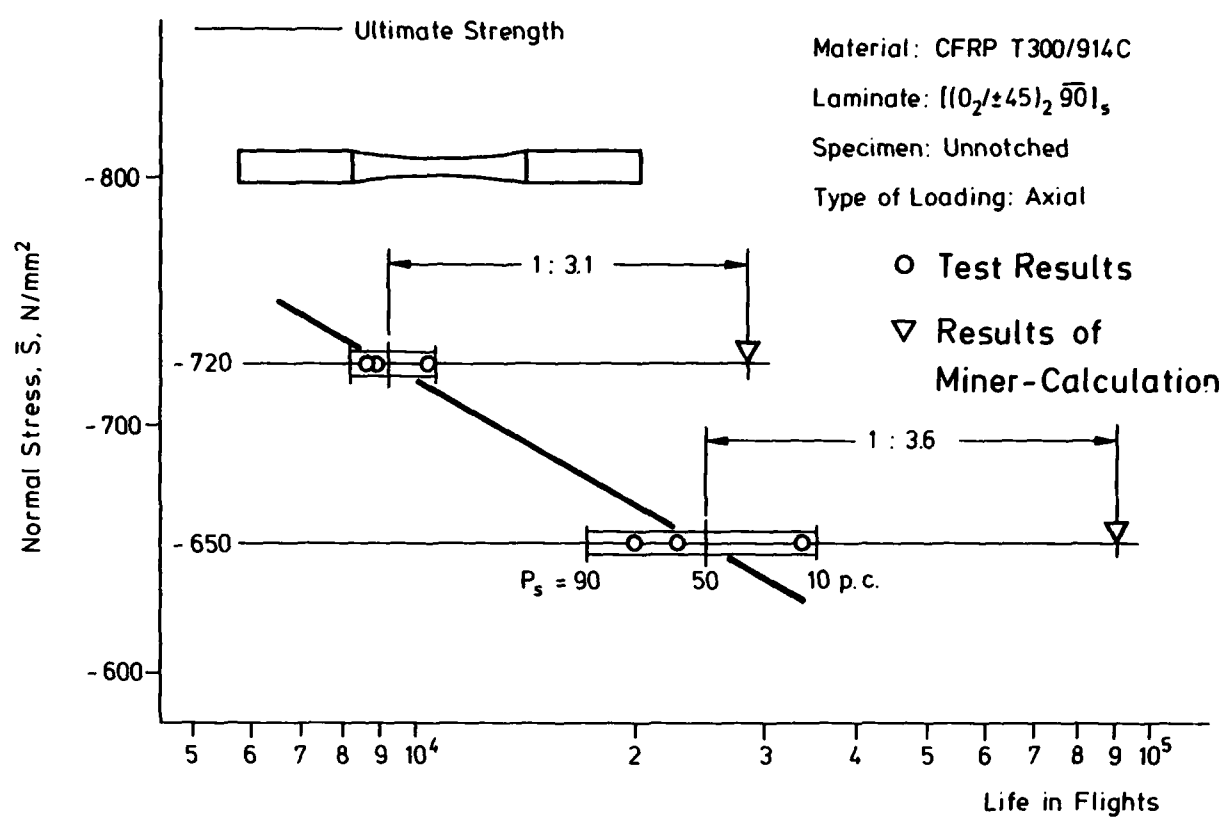
Figure 5: Life of an Unnotched CFRP Laminate, Derived Experimentally and by Calculation for FALSTAFF Loading (Wing Upper Surfache) [13]
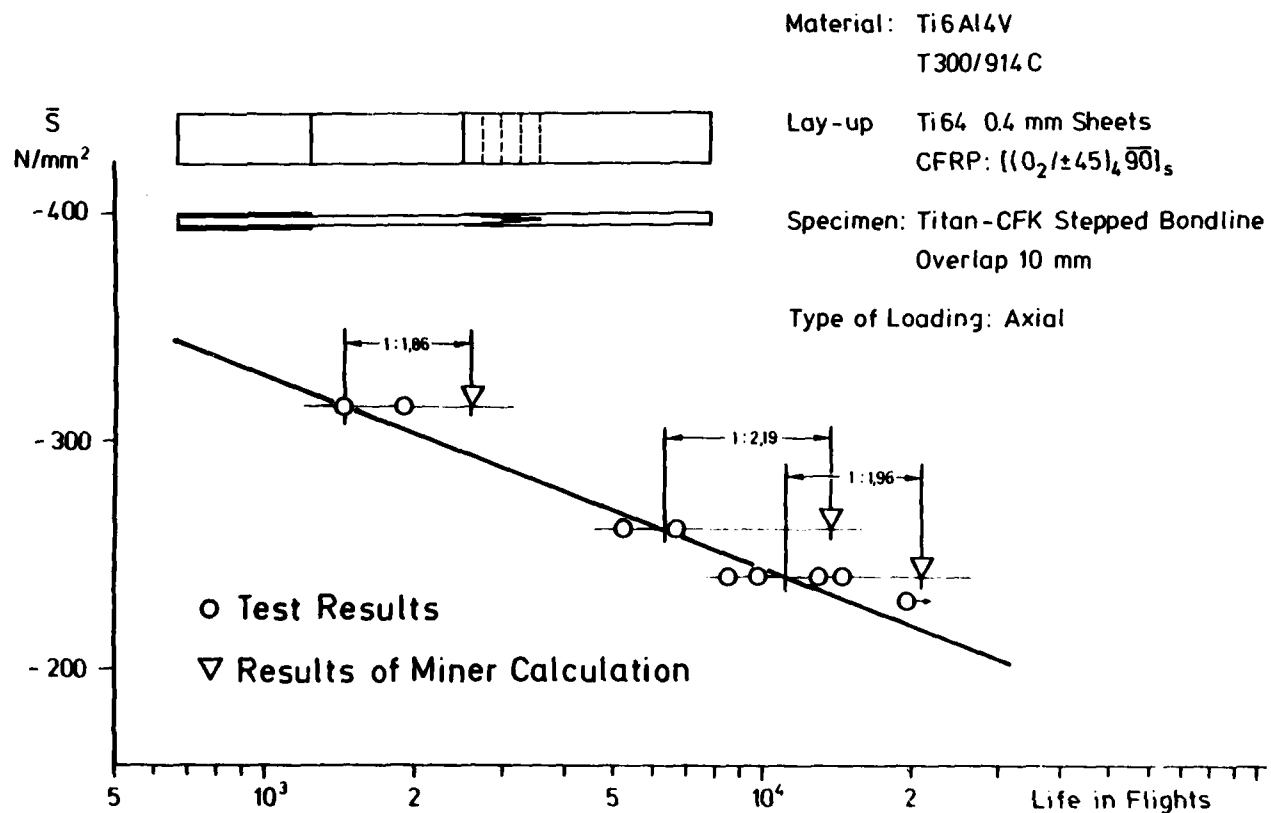
Figure 6: Life of Bonded Joints, CFRP/Ti 64 Sheets [14], Derived Experimentally and by Calculation for FALSTAFF Loading (Wing Upper Surface)

	FALSTAFF	TWIST	Other Spectra	Relative Miner's Rule
	Upper Surface			
Unnotched	○		●	⊕
1/4" Hole	□ ⊡*	◘		
Bolted Joint	◇			
Bonded Joint	△			

*Lower Surface

Test Life, Flights

Calculated Life, Flights
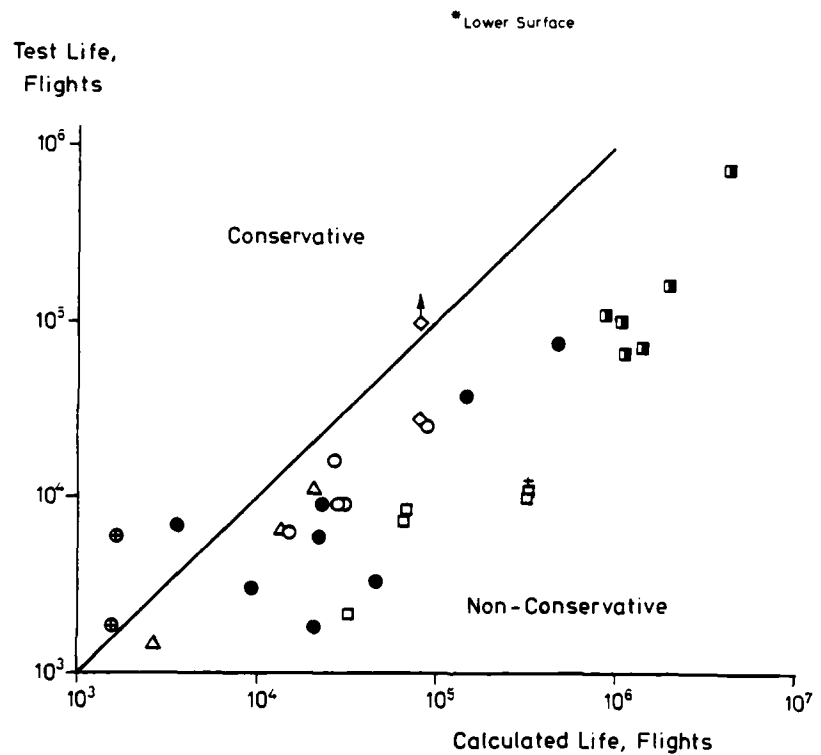
Figure 7:   Comparison of Calculated Life, Using Miner's Rule, with Results from Flight-by-Flight Testing
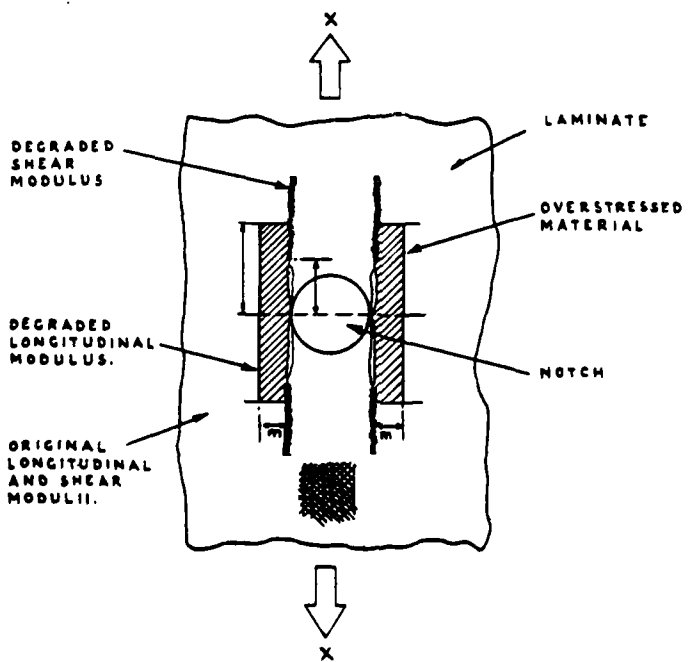
Figure 8:   Degraded Modulus and Strength Regions in a Notched Laminate after Fatigue Cycling in Mechanistic Model [5]
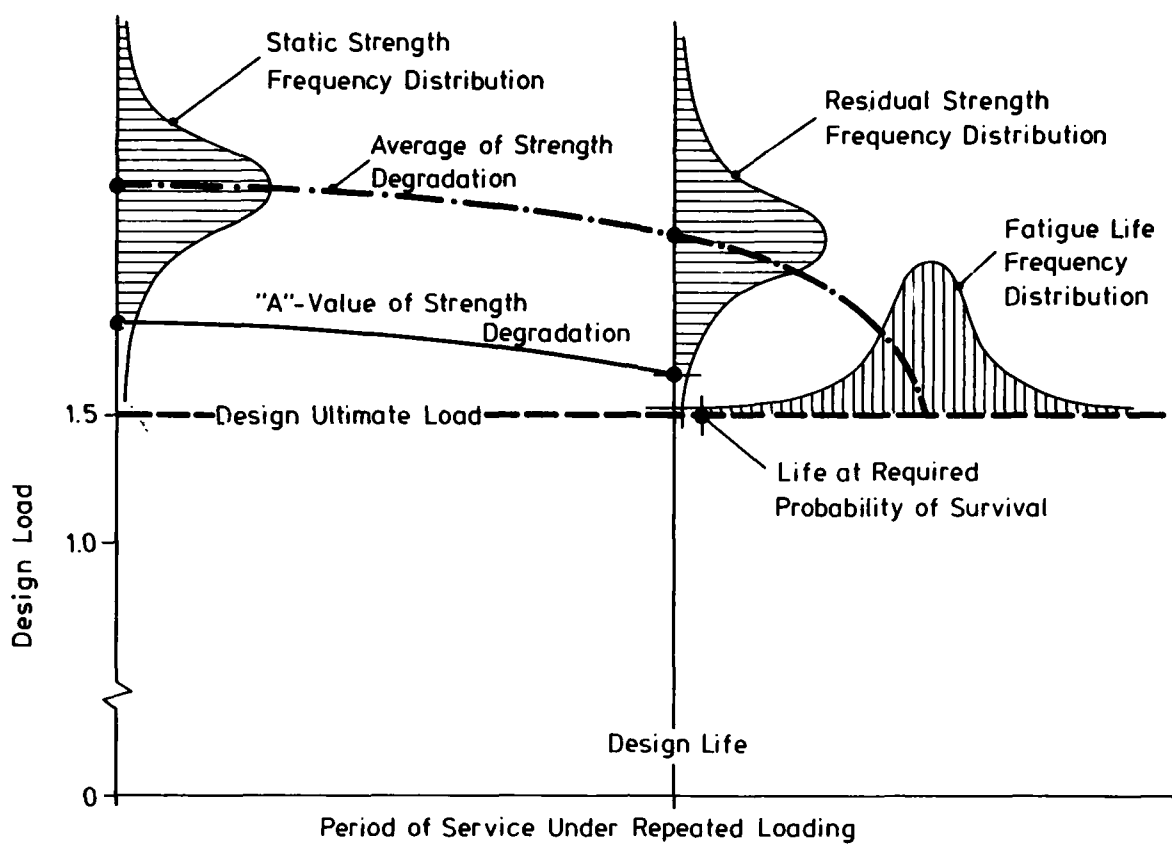
Figure 9: Residual Strength During Lifetime

Material:
CFRP T300/914 C

Laminate:

$[0_2/+45/0/-45/\overline{90}]_s$

$[0_2/\pm45/0_2/\pm45/\overline{90}]_s$

Fibre Content:
60 p.c. vol.

e/d = 3.75
w/d = 5.0
d/t = 1.9

Fit:
Low Clearance

Clamping:
2 Nm Torque
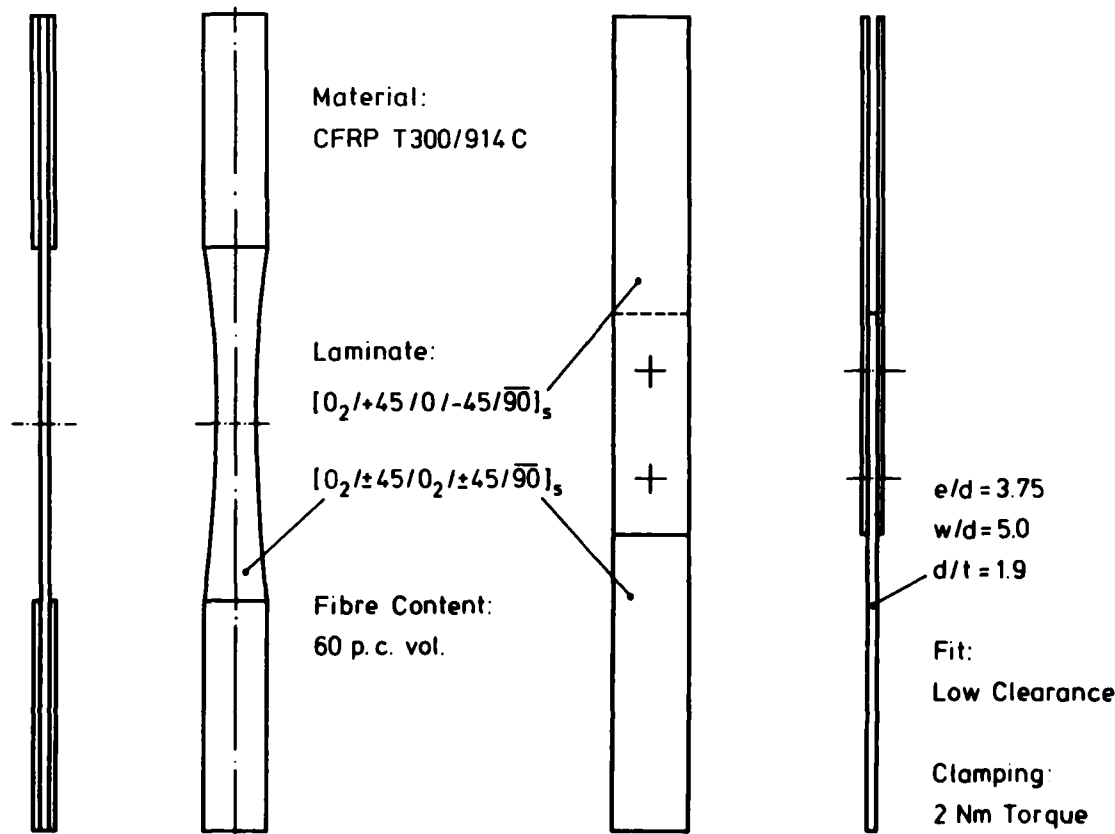
Figure 10: Unnotched Specimen and Double Shear Joint Specimen

	Unnotched Specimens	Double Shear Joint
Static Strength N/mm^2	- 840 - 862 - 872 < - 758 < - 787 < - 798 < - 860 < - 891 - 896 - 934	- 441 - 412 < - 314 < - 295
Residual Strength N/mm^2	- 641 - 742 - 774 $N = 12\,000^{a}$ - 792 5x < - 640 - 800 $N = 17\,690^{a}$ - 686 $N = 23\,490^{a}$	- 393 - 420 - 433 $N = 10^{4}$ ^{a} - 459 4x < - 340 - 318 $N = 14\,550^{a}$
Life to Failure ^{a} **Flights**	15 000 15 700 17 680 18 380 20 350 > 26 770 > 23 490 > 17 690 5x > 12 000	6 450 12 200 13 100 15 200 > 14 650 > 17 200 4x > 10 000

^{a} FALSTAFF (upper surface),   Stress Level:
Unnotched $\bar{S} = - 640 \; N/mm^2$
Joints $\bar{S} = - 340 \; N/mm^2$

Figure 11:   Test Results

	Comulative Distribution Functions, $1-F_\gamma(...) = \gamma(...)$	Percentiles for Constant Probability Curves
Static Strength: at $L = 10^{0}$	$\gamma(S) = \exp\left[-\left(\frac{S}{\beta_S}\right)^{\alpha_S}\right]$	$S_\gamma(0) = \beta_S\left[-\ln\gamma\right]^{1/\alpha_S}$
Residual Strength Test Data: (Surviving Specimens)	$\gamma(S_r\vert\bar{S}) = \exp\left[-\left(\frac{S_r}{\beta_r}\right)^{\alpha_r} + \left(\frac{\bar{S}}{\beta_r}\right)^{\alpha_r}\right]$	———
Const. Probab. Curves: (All Specimens) at $L=N$	$\gamma(S_r) = \gamma(S_r\vert\bar{S}) \cdot \exp\left[-\left(\frac{N}{\beta_L}\right)^{\alpha_L}\right]$	$S_\gamma(N) = \beta_r\left[-\ln\gamma + \left(\frac{\bar{S}}{\beta_r}\right)^{\alpha_r} - \left(\frac{N}{\beta_L}\right)^{\alpha_L}\right]^{\frac{1}{\alpha_r}}$ $S = \bar{S}$
Life to Failure: at $S = \bar{S}$	$\gamma(L) = \exp\left[-\left(\frac{L}{\beta_L}\right)^{\alpha_L}\right]$	$L_\gamma = \beta_L\left[-\ln\gamma\right]^{\frac{1}{\alpha_L}}$

Figure 12:   Cumulative Distribution Functions Applied in the Empirical Strength Degradation Model

Estimated Weibull Parameters Applied in the Residual Strength and Life Prediction by the Strength Degradation Model

	Unnotched Specimen[b]		Double Shear Joint[b]	
	"Shape"	"Scale"	"Shape"	"Scale"
Static Strength S, N/mm^2	$\alpha_s = (20),37$[c]	$\beta_s = 904$	$\alpha_s = (20),35$	$\beta_s = 433$
Residual Strength[a] S_r, N/mm^2	$\alpha_r = 20$	$\beta_r = 766$	$\alpha_r = 20$	$\beta_r = 438$
Life to Failure L, Flights	$\alpha_L = (4)\,4.6$	$\beta_L = 23000$	$\alpha_L = 4$	$\beta_L = 16\,400$

[a] Preloading: FALSTAFF-Upper Surface

	N = 12 000 Flights	N = 10000 Flights
	$\bar{S} = -640$ N/mm^2	$\bar{S} = -340$ N/mm^2

[b] Failure Criterion: Fracture   Displacement $v - v_o = 0.3$ mm

[c] Weighted Average

Figure 13:   Estimated Weibull Parameters Applied in the Residual Strength and Life Prediction by the Strength Degradation Model

Percentiles and Average of Static Strength, S, Residual Strength, S$_r$, and Life to Failure, L.

Probability of Survival γ	A = $-\,\mathrm{Ln}\,\gamma$	Static Strength, N/mm^2 $S\gamma\,(0) = \beta_s\,A^{1/\alpha_s}$		Life, Flights $L\gamma = \beta_L\,A^{1/\alpha_L}$		Residual Strength, N/mm^2 $S\gamma\,(N) = \beta_r\,(A + A_r - A_L)^{1/\alpha_r}$	
		Unnotched	Jointed	Unnotched	Jointed	Unnotched	Jointed
0.1	2.3026	- 942	- 451	27 175	19 380	- 798	- 456
0.25	1.3863	- 919	- 440	24 550	17 510	- 778	- 444
0.75	0.2877	- 849	- 407	17 930	12 780	- 718	- 405
0.9	0.1054	- 808	- 387	14 660	10 460	- 681	- 362
Average Values $E(...) = \beta... (\frac{1}{\alpha...} + 1)$		- 889	- 427	21 000	14 700	- 746	- 427

				$A_r = (\bar{S}/\beta_r)^{\alpha_r}$	$A_L = (N/\beta_L)^{\alpha_L}$
Unnotched Specimen:				0.0275	0.0387
Jointed Specimen:				0.0063	0.0891

Figure 14:   Percentiles and Average of Static Strength, S, Residual Strength, S$_r$, and Life to Failure, L
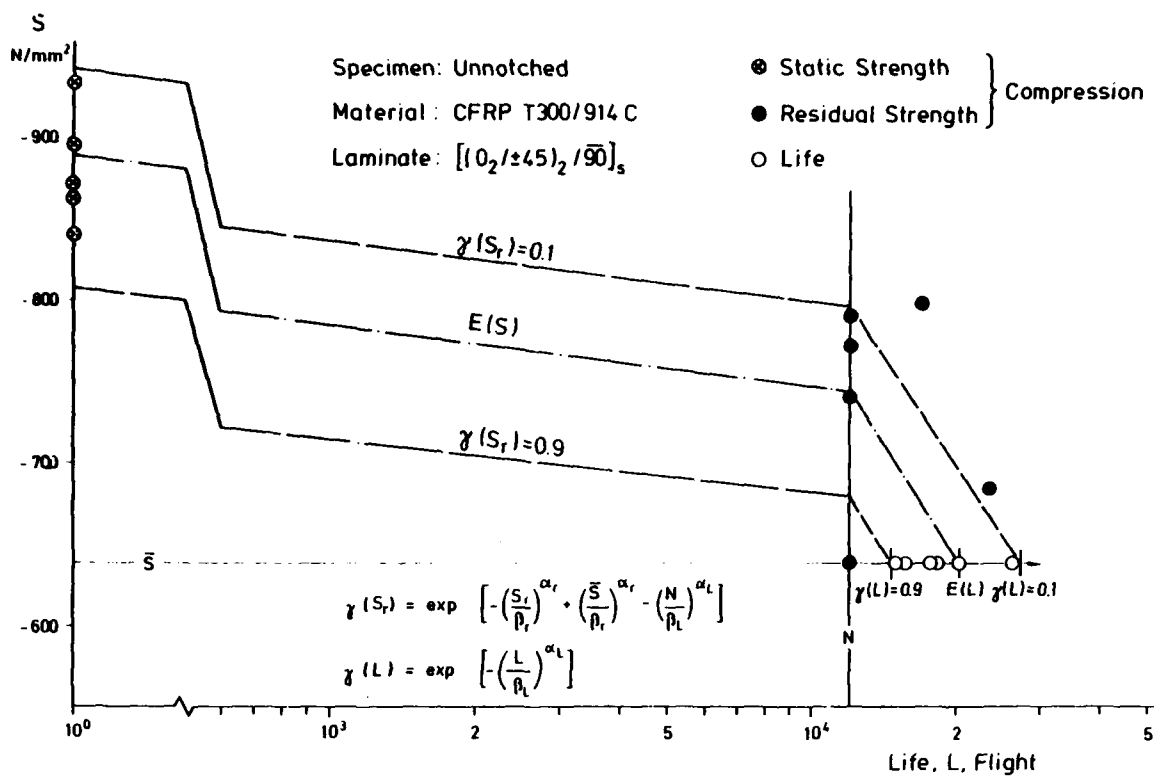
Figure 15: Residual Strength Degradation, Result of Statistical Data Analysis (Empirical Strength Degradation Model)

Within the figure:

Specimen: Unnotched
Material: CFRP T300/914 C
Laminate: $[(0_2/\pm45)_2/\overline{90}]_s$

Static Strength ⊗ } Compression
Residual Strength ● }
Life ○

$\gamma(S_r) = 0.1$
$E(S)$
$\gamma(S_r) = 0.9$

$$\gamma(S_r) = \exp\left[-\left(\frac{S_r}{\beta_r}\right)^{\alpha_r} + \left(\frac{\overline{S}}{\beta_r}\right)^{\alpha_r} - \left(\frac{N}{\beta_L}\right)^{\alpha_L}\right]$$

$$\gamma(L) = \exp\left[-\left(\frac{L}{\beta_L}\right)^{\alpha_L}\right]$$

$\gamma(L)=0.9$ $E(L)$ $\gamma(L)=0.1$

Axes: S, N/mm² (vertical); Life, L, Flight (horizontal)
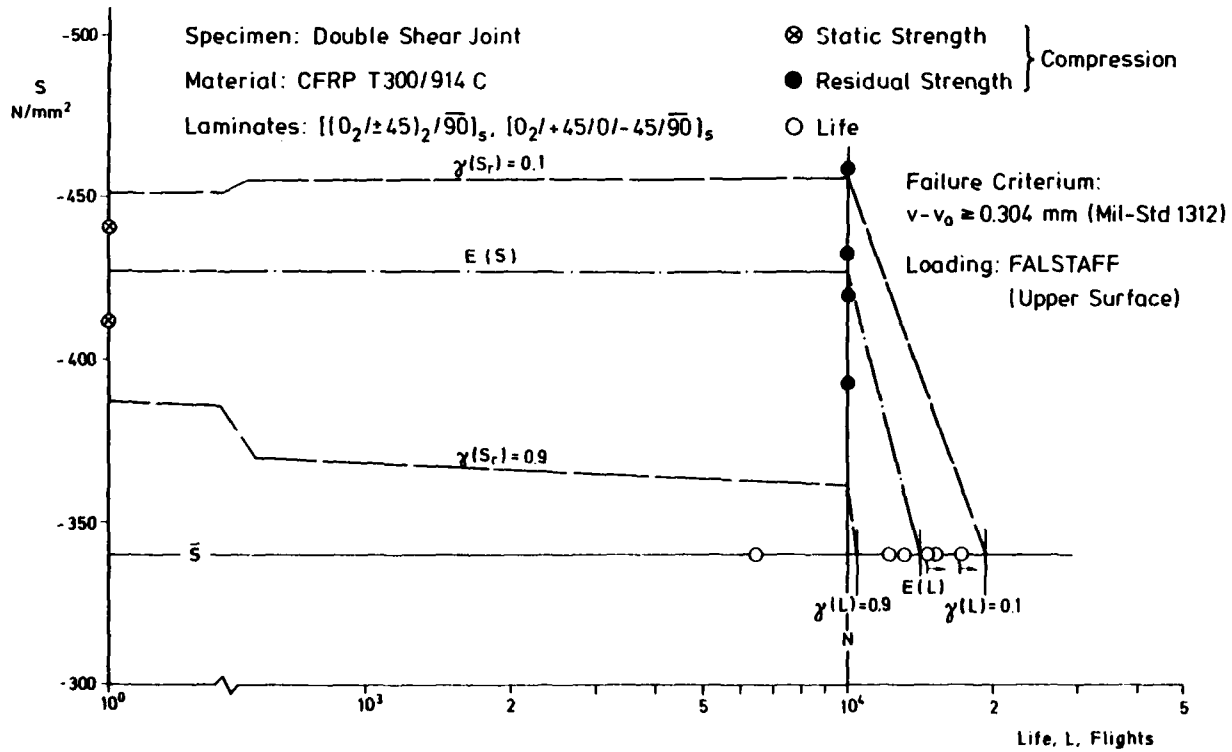
Figure 16: Residual Strength Degradation, Result of Statistical Data Analysis (Empirical Strength Degradation Model)

Within the figure:

Specimen: Double Shear Joint
Material: CFRP T300/914 C
Laminates: $[(0_2/\pm45)_2/\overline{90}]_s$, $[0_2/+45/0/-45/\overline{90}]_s$

Static Strength ⊗ } Compression
Residual Strength ● }
Life ○

Failure Criterium:
$v-v_0 \geq 0.304$ mm (Mil-Std 1312)

Loading: FALSTAFF
(Upper Surface)

$\gamma(S_r) = 0.1$
$E(S)$
$\gamma(S_r) = 0.9$

$\gamma(L)=0.9$ $E(L)$ $\gamma(L)=0.1$

Axes: S, N/mm² (vertical); Life, L, Flights (horizontal)
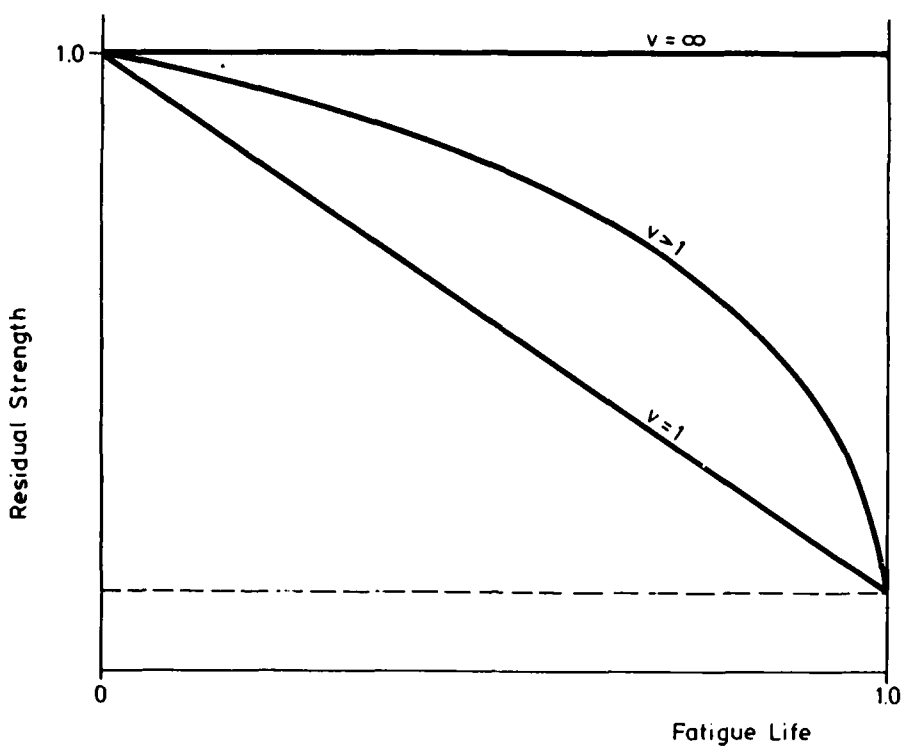
Figure 17: Illustration of the Effect of v on the Strength Degradation
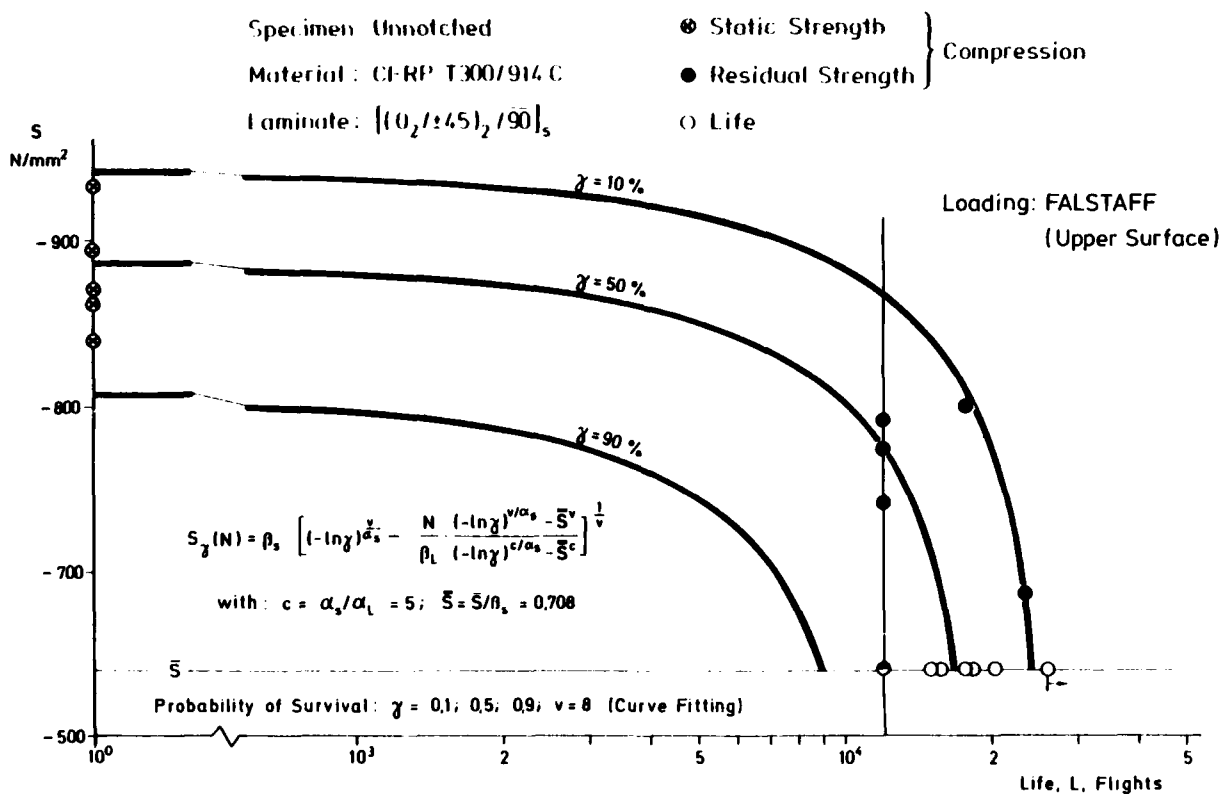
Figure 18: Residual Strength Degradation. Curve Fitting to Test Data by the "Strength Degradation Model" (Analytical)
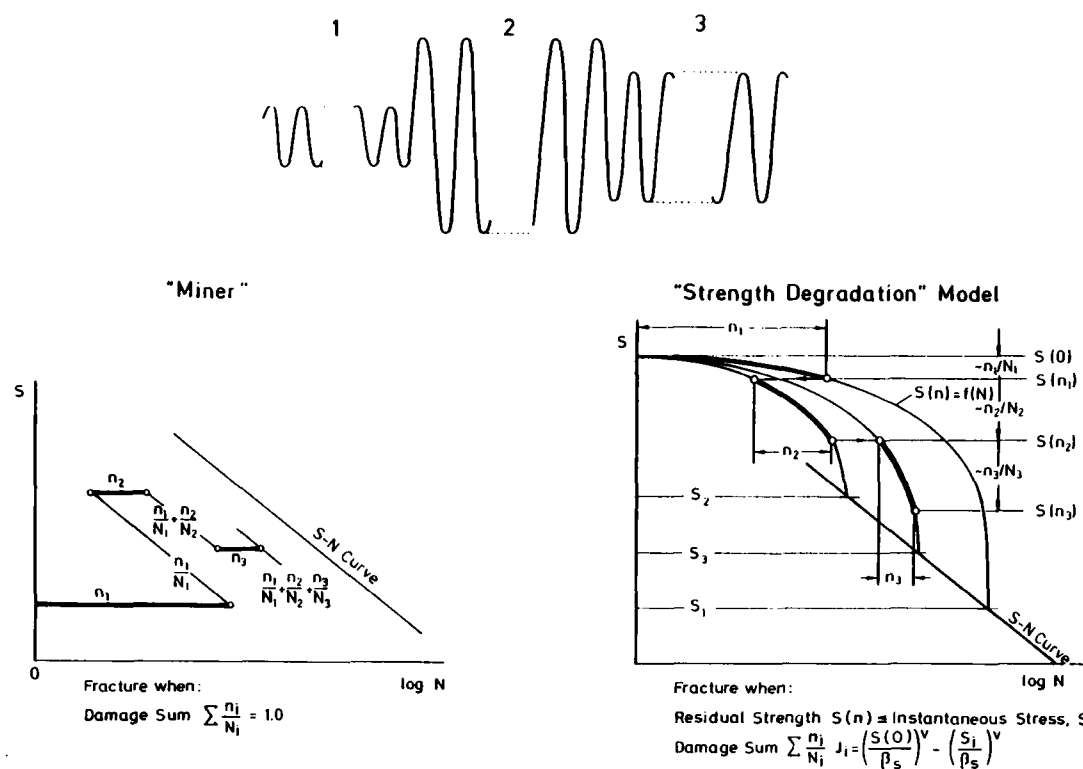
Figure 19: Damage Accumulation by Miner and by the "Strength Degradation" Model (Schematically)
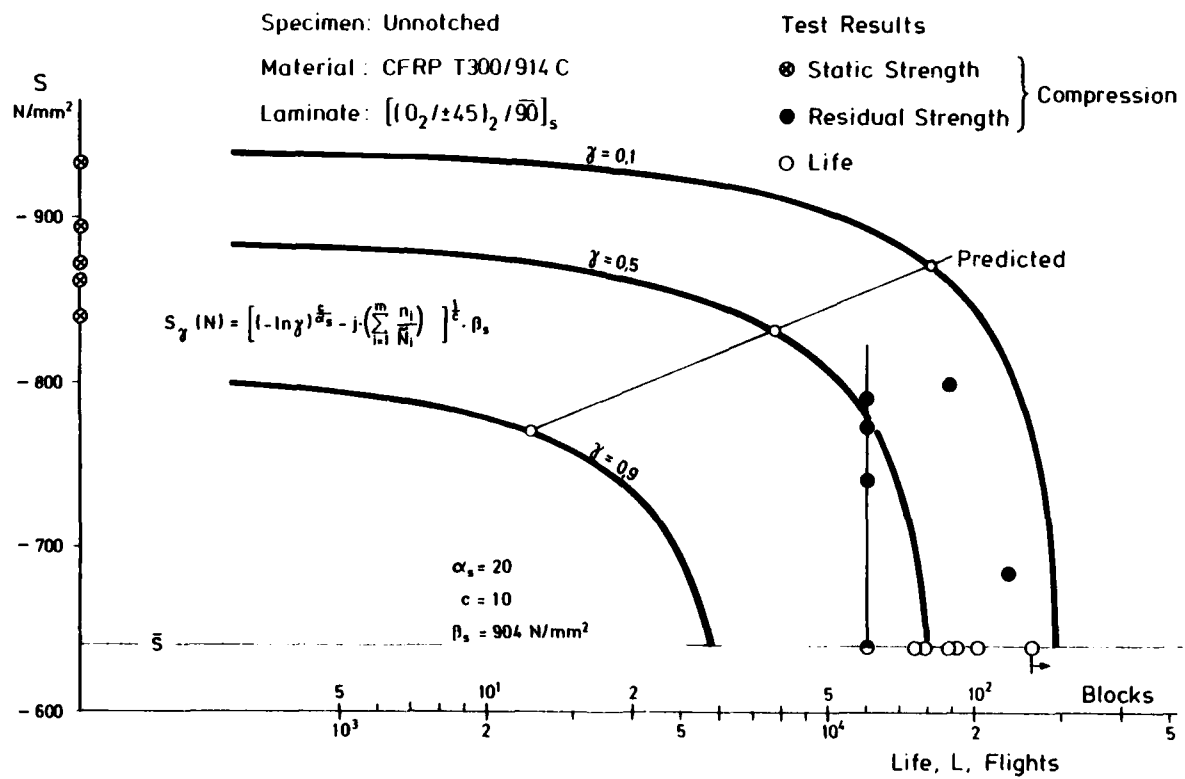
Figure 20: Residual Strength Degradation, Prediction and Test Results. FALSTAFF (Wing Upper Surface) Loading

THE ELECTRICAL PROPERTIES OF CARBON FIBRE COMPOSITES

by

J. M. Thomson
Ministry of Defence (Procurement Executive)
Royal Aircraft Establishment
Farnborough, Hants, UK

SUMMARY

The essential electrical difference between a carbon fibre composite and conventional metal alloys is that its resistivity is about three orders higher. This fact affects the electromagnetic compatibility (EMC) of the airframe, its performance as an antenna ground plane, the provision of power and of earth returns and radar cross-section.

Research on the electrical properties of carbon fibre composites under these headings is reviewed and the importance of good bonding and jointing emphasized. The major problem areas (which tend to occur at frequencies less than 30 MHz) are outlined, as are those areas where problems are likely to be minor.

Although electrical research lags structures and materials research by some 10 to 15 years, nonetheless sufficient work has been due for some interim design recommendations to be formulated, and these are discussed in the paper.

1   INTRODUCTION

The essential electrical difference between composite materials and metals conventionally used for airframe construction is resistivity: carbon fibre composites, for example, have resistivities of about 25-150 $\mu\Omega$ m, whereas a typical aluminium alloy has a resistivity of about 0.052 $\mu\Omega$ m.

What is the significance of this difference? Structural and design engineers are well aware that a carbon fibre composite (CFC) is not simply a 'black metal' and to treat it structurally as such is to invite disaster. This is true, too, of its electrical aspects, and it is not possible to assume that carbon fibre composites will automatically fulfil the electrical requirements of the structure in the same way as a metal would. In essence this means that the electrical requirements of the structure have to be defined, a design approach formulated, and, where necessary, a research programme initiated to acquire necessary basic data.

It is not always appreciated that essentially structural components also have an electrical aspect to their performance, usually because the metal structure, with its ease of electrical bonding, satisfies these requirements without any special precautions being needed. There is a surprisingly wide variety of electrical requirements, some of which were outlined to the AGARD Structures and Materials Panel[1] long before composites were receiving the wide attention they do now.

The higher resistivity of CFC is significant in the use of the airframe as a power return, its electromagnetic shielding capability and its usefulness as an antenna ground plane, its radar cross-section, its vulnerability to the direct and indirect effects of a lightning strike, and its capability to dissipate static electricity safely.

The implication, therefore, is that it is necessary to understand the basic behaviour of the material and then to use this information to develop adequate construction techniques. There has always been some interest in its electrical properties by materials scientists - firstly, because electrical resistivity measurements, for example, can give an indication of the quality of fibre alignment, and secondly, because the possible damage from a lightning strike was always self-evident. Serious interest by electrical and radio engineers, however, did not develop until about 1976 or 1977 when it became evident that structural engineers were seriously intending to use the material for aircraft projects. Suddenly, the prospect of losing the friendly, protective metallic shell with all its inbuilt useful attributes stimulated intensive effort in both government and industrial laboratories in the USA, UK, Germany, France and elsewhere. The task essentially was twofold - to catch up on the 10 or 15 years' lead structural designers have over their electrical counterparts, and, having done that, to ensure that electrical aspects are adequately considered. To some extent, this has been successful, and the subject has matured enough for some interim guidance to be available.

This paper therefore covers the following ground:

(a)   an explanation of EMC and the electrical requirements of the airframe;

(b)   a brief description of research on the electrical properties of CFC, and

(c)   an indication of how the results of (b) can aid in meeting (a) - an outline of the fundamentals of electrical design in CFC.

2   EMC AND THE ELECTRICAL REQUIREMENTS OF THE AIRFRAME

2.1   Electromagnetic compatibility (EMC)

Consider Fig 1. This shows the 'electrical aircraft' and the factors which influence electromagnetic compatibility (EMC). Gone are the days when aircraft could be flown with mechanical controls only. Now electrical signalling is dominating - often in flight-safety critical areas with no manual reversion. Flight controls and fuel controls are examples of such systems; others are marked on Fig 1. In essence, such systems may be thought of as a wire terminated at either end in an impedance and with the return circuit being made through either the airframe or a dedicated wire.

The EMC problem is the pick up of interference on this wire and its transmission into the load where it can adversely affect the performance of the equipment, often by a process of detection and demodulation in nonlinear circuit elements.

Sources of interference can be both internal and external to the aircraft. Inside the aircraft, interference can be transmitted through common power supplies or inductively couple from one cable to another. Often it arises as generator noise, as switching transients, or as harmonics generated by the steeply-rising waveforms of digital signals. It may thus be broadband noise or narrowband signals or spikes and surges[2].

External sources are many and varied. Ground-based radio and radar transmitters, especially those operating at high powers or with high gain antennas, can generate signals large enough to be picked up by and affect electronic circuits. Operationally, this means that HIRTAs ('High Intensity Radio Transmission Areas') have to be established within which aircraft should not approach transmitter sites. Similarly, aircraft and helicopters operating close to ships may be at risk; the same also applies to aircraft operating in formation. In all these cases the interference is caused by a wanted signal *which cannot be removed*. The only protection possibilities are circuit design - not to respond to frequencies other than those strictly necessary for signalling purposes - or shielding.

Lightning may also cause interference to avionics and electrical systems. Physical damage caused by heating and mechanical shock ('direct effects') is obvious, but more insidious and not so apparent is that the passage of a large current pulse of tens of kiloamps down the fuselage creates a magnetic induction field which can couple energy in the form of a spike into electrical and electronic circuits ('indirect effects'). Such spikes have been known to trip out generator protection circuits and to corrupt information in navigation computer memories.

In military applications, the effects of the nuclear electromagnetic pulse (EMP) are also important. The detonation of a nuclear weapon has as one of its secondary effects the generation of a short-term electromagnetic field whose amplitude and duration are functions of the weapon yield, burst altitude and distance from ground zero. The case usually considered is an exoatmospheric burst at altitudes higher than 35 km as the effects of this can be continent-wide. The effects of such a detonation are similar to the indirect effects of a lightning strike, but the rise times of the pulse are much shorter - of the order of nanoseconds - with the fall time being of the order of microseconds. Hence the frequency content of the pulse extends to hundreds of megahertz compared with less than 10 MHz for lightning.

But the greatest source of EMC problems on aircraft is generally the radio transmitters it carries. These are intentional radiators - radio frequency energy is purposely generated but, because of inefficiencies in the transmitting systems, not all of it is radiated. That which remains may find its way - by conduction or radiation - into the variety of susceptible circuits. The problem is severe at frequencies up to 400 MHz and is particularly acute in the HF band (2-30 MHz). In the VHF and UHF bands (118-136 MHz and 225-400 MHz respectively) the transmitting element is usually a separate aerial - one of the short stubs or fins seen on the airframe. This acts in association with a ground plane which is the local area of airframe and hence any undesirable effects are somewhat, though not totally, localized. This is not the case with HF transmitters, as whatever the design of antenna (long wires and notches being the two most common) the essential principle is that the whole aircraft is part of the radiating element. The physical reason for this is that the wavelengths (150 m at 2 MHz and 10 m at 30 MHz) are comparable with the length of the aircraft. In fact it is the *half-wavelengths* (5 m at 30 MHz) which are important in representing the aircraft as a dipole. Thus electric currents are developed over the full length of the outside of the aircraft and if any seams or apertures are present they will penetrate into its interior. It is surprising to note that down at 2 MHz, where the half-wavelength is 75 m, HF systems on strike aircraft can have efficiencies as low as 0.1%: thus of the 400 W of transmitter power available, only 0.4 W will be radiated, the rest being absorbed in the aircraft. This is generally acknowledged to be the greatest source of EMC problems.

The corollary to the transmitter problem is, of course, that when the aircraft is acting as a receiver to the external environment, to lightning or to EMP it will pick up most energy somewhere in the HF band, depending on its physical dimensions. Unfortunately, this is where the highest power transmitters are used - 250 or 500 kW are common - and where lightning and EMP have their greatest spectral energy contents. Thus the problem is compounded.

Fig 2 summarises in diagrammatic form the possible coupling paths for electromagnetic interference (EMI) both from inside and outside the airframe.

What is the impact of composites on the EMC problem? Fig 2 shows the aircraft skin with energy propagating through it in an undefined manner. In fact three mechanisms are possible: (i) down antenna leads, (ii) by penetration or leakage through apertures and seams, and (iii) by direct diffusion through the skin material. Mechanism (iii), direct diffusion, is obviously affected by a change of material from aluminium alloy or other metals to CFC, but so, perhaps surprisingly, are the other two. For antenna leads the effect is indirect, but the use of CFC may require a different antenna installation and hence generate an easier coupling path; similarly, the constructional methods for seams, hatches, etc, may change and also affect the ease of penetration. The impact of these mechanisms is discussed in section 3 under the broad headings of 'Shielding' (for (iii)) and 'Bonding' (for (i) and (ii)). But essentially, the impact is that the use of composites potentially has the capability of changing the gross levels of EMI present in aircraft.

2.2   Airframe electrical requirements

Aside from EMC protection, the airframe also fulfils a variety of disparate electrical functions. These include its use as the second wire in a 2-wire dc power system, as the neutral wire in a 3-phase 4-wire ac power system, as the return path for electrical equipment signal currents, and as a ground plane for antennas. For these purposes the structures will be carrying currents ranging from microamperes as an antenna ground plane, to hundreds of thousands of amperes in ac or dc system return paths. A low electrical resistance is an evident structural requirement for these electrical needs, and the measurement of a low resistance path between structure extremities is at present taken as sufficient evidence of an electrically satisfactory airframe. This measurement does not, however, necessarily indicate the presence of unwanted high resistance structure joints because of parallel paths and so further experimental work has been done on mapping airframe impedance patterns; this work has yet to be incorporated in aircraft procurement requirements.

The trade-off that has to be made, therefore, is between the reduction in mass achieved by using composite materials in the airframe and the corresponding mass penalty incurred by the need for a dedicated earth return system. The design of a separate earth return system is a function of the distribution, location and power consumption of the aircraft's electrical equipment and will, of necessity, vary from aircraft to aircraft.

Antenna installations have been mentioned in the previous section, in the context of EMC. There it was noted that usually the airframe forms part of the antenna counterpoise: accordingly, the prime requirement is to allow the desired RF currents to flow in the installation, and hence adequate bonding and jointing techniques must be available. As antennas - *eg* fins and blades - are usually supplied ready for direct fitting to the aircraft the question to be answered is whether the mechanical techniques, fasteners, etc, developed for metal aircraft are also suitable for composite aircraft.

Radar cross-section may also be affected by the use of composites. The concept here is that when illuminated by a radar the aircraft reflects energy back and hence becomes 'visible'. The amount and type of reflection is obviously a function of the aircraft's shape and the radar frequency but also of its surface conductance: the higher this is, in general, the more energy is reflected. The design of (military) aircraft to minimise radar reflections is a major, and to a large extent empirical, art but a simple way of visualizing the problem is to imagine the aircraft as a mirror reflecting light - large smooth areas will reflect in a reasonably stable manner whereas sharp edges will 'glint'. These properties are a function of the *shape* of the aircraft: its *material* may also affect the radar returns. Two effects are possible: the first is that if the material has such a low conductance that it appears transparent, then the radar reflections will be from the structures underneath, and hence the internal design becomes critical; the second is that if the material has some conductivity a portion of the energy may be absorbed and dissipated in the structure and not reflected: the aircraft may tend to become 'invisible'. Both these effects have been postulated for CFC.

Static electrification problems are a result of the aircraft acquiring charge as it moves through dust or precipitation. The problems occur when this charge discharges either locally on the aircraft or to ground giving rise to electromagnetic interference or to shock hazards. This type of problem is well-known on conventional aircraft and is usually alleviated by the fitting of static discharge wicks at suitable points. Any problems remaining are essentially local and can be dealt with on an *ad hoc* basis. As far as composites are concerned the major problems are likely to arise when they are in contact with moving liquids - *eg* fuels - where a discharge may cause sparking followed by a fire or explosion. This may be in fuel tanks forming part of the structure in wings, etc, or in pipes of composite material.

It has probably become apparent that the essence of many of these problems - of EMC and airframe electrical requirements - is the potential difficulty of achieving satisfactory bonding between composite structural materials or between composites and metals. If 'good' bonding can be achieved then many of the other problems start to disappear.

Allied with bonding is the question of corrosion control. Carbon itself is an inert material and does not corrode under ambient conditions. However, it does act as if it were a noble metal, and so promotes the corrosion of other, less noble, metals. Consequently, corrosion control methods are usually employed where CFC is in contact with other metals to prevent this enhanced corrosion. These methods often involve the isolation of the carbon in an attempt to stop the formation of the corrosion cell. The isolation of the carbon, whilst rarely good enough to prevent the ultimate corrosion of the less noble

metal, is usually good enough to prevent the achievement of good electrical properties for the composite joint. Whilst some corrosion control is undoubtedly necessary the need for compromise to achieve good electrical properties means that some reappraisal of protection methods is called for in areas where the two requirements conflict. If these requirements are considered early in the design process, then the cost of this compromise will be minimal. If the electrical requirements are not considered or left until late in the process, then the result will be an expensive redesign or poor electrical joints - or both.

3 RESEARCH ON THE ELECTRICAL PROPERTIES OF COMPOSITES

3.1 General

In countries which have embarked upon research and measurement programmes on the electrical properties of composites events have followed in much the same order. First of all, electrical properties have been measured as an aid to understanding mechanical aspects of the material - the fact that the measurements were electrical is incidental. Then, measurements have been made as part of debates on particular aspects of performance, usually lightning vulnerability and adequacy as an antenna ground plane. Finally, when the full potential of the material to cause a fundamental rethink of EMC and electrical systems aspects of aircraft was realised, full-scale programmes starting with investigation of the basic electrical characteristics of composites have been initiated.

This paper does not follow this chronological sequence. Rather it presents the results of the research programmes in a series of discrete, but interlinked, areas, viz:

> Basic electrical properties - conductivity, etc
> Shielding
> Antenna performance
> Lightning vulnerability
> Nonlinear effects
> Bonding and jointing.

The design recommendations of section 5 are based on the distillation of research on these topics.

3.2 Basic electrical properties

Fig 3 is a diagram of two typical CFC lay-ups: $(0^\circ, 90^\circ)$ and $(0^\circ, \pm45^\circ)$, as representing the most common practices. The precise lay-up used for any particular application is a function of structural requirements.

Electrically, because CFC consists of fine, graphitised carbon fibres in an insulating resin matrix, it is anisotropic. Conduction is much easier in the fibre direction than in directions perpendicular to it, where conduction must take place by chance contacts between adjacent fibres. In the special case of unidirectional fibres with volume fractions of structural interest (0.60 to 0.65) this results in resistivities some 200 times higher perpendicular to the fibres compared to those in the fibre direction. In multi-directional lay-ups the leakage between adjacent plies tends to reduce this difference in resistivity until a four-directional quasi-isotropic lay-up can be regarded on a macro scale as electrically isotropic within the plane of the composite (ie in the x and y directions in Fig 3). Because of the excess resin between adjacent plies, the through thickness resistivity (in the z direction) is always higher than that in the plane of the lay-up. In chopped fibre filled composites, the number of fibre-to-fibre contacts, and hence the resistivity, is governed by the volume fraction of carbon and the fibre length.

Theories of the mechanism of conduction in CFC are somewhat limited especially at frequencies higher than dc; indeed, as far as it is known it has not been possible to make a theoretical prediction of the high frequency behaviour of CFC. Probably the best available work can be found in Refs 3, 4 and 5. Smithers[4] attempted, with some success, to develop a theory of conductivity based on earlier work which he cites and including consideration of skin effect and coupling between fibres within a tow.

Some calculations are possible, at dc and low frequencies, on conductors of various regular cross-sections - circular, rectangular - but as frequency rises the accuracy of such a transmission line approach decreases.

However, despite this lack of a cohesive theoretical framework there does exist a substantial body of measurements of the resistivities of a variety of samples. A typical set of results is shown in Fig 4. These are for two sizes of samples: 25 mm × 10 mm and 25 mm × 5.5 mm, both having a thickness of 1.98 mm. It can be seen that the resistivity is lower for the narrower sample. This is consistent with the existence of a skin effect for current flow, since in the narrower sample the loss in effective cross-sectional area will be proportionately less than in the wider sample as current retreats to the surfaces and edges as the frequency rises.

This change in distribution of current over the cross-section (skin effect) occurs because those parts of the cross-section which are circled by the largest number of magnetic flux lines have a greater inductance than other parts and hence a greater reactance. These parts thus carry least current. With the flat strip used in these measurements - and which represents typical sheets used in aircraft construction - the current

density is greatest at the edges, reduced at the flat surfaces and least in the centre. Hence, skin depth of current flow controls the resistance for alternating (including RF) currents. It can be shown that in a conductor of circular cross-section current penetration depth is proportional to $f^{-\frac{1}{2}}$ and high frequency resistance is proportional to $f^{\frac{1}{2}}$. Fig 5, where the data of Fig 4 is replotted against $f^{\frac{1}{2}}$, shows a substantially linear relationship.

Table 1 below shows the range of resistivities of CFC at a number of frequencies. These ranges are characteristic of samples where good contact is maintained at the current entry and exit points.

Table 1

Ranges of resistivity of CFC (after Smithers, Ref 4)

Frequency fMHz	Resistivity ranges (all except unidirectional samples) $10^{-5}\,\Omega\,m$	Resistivity of unidirectional samples $10^{-5}\,\Omega\,m$	
		Parallel to lay	Perpendicular to lay
1	3 to 15	2	1100
10	5 to 15	6	1100
50	12 to 35	12	1300
100	17 to 60	16	*
300	32 to 150	30	*

* Measurement not possible

Of the other basic properties of the material, particularly permittivity, ε, and permeability, μ, permittivity cannot be measured as it can for normal dielectrics because conductivity is too high and permeability, of course, has the free-space value of unity appropriate to non-metallic materials.

3.3 Shielding

'Shielding' is a qualitative term used to describe the capability of material to attenuate an electromagnetic field impinging upon it. Intuitively, it should be possible to ascribe a number to shielding effectiveness such that the higher the number the less the energy penetrating the shield. In practice, it is difficult, probably impossible, to define or measure an *absolute* quantitative value of shielding effectiveness.

Consider Fig 6 which perhaps will give some clue as to the measurement and definition of shielding. Fig 6a represents an infinite plane sheet upon which an electromagnetic wave impinges. This wave travels from left to right and has a certain value at A. This value is defined by the power density, $\underline{P}$, electric field strength, $\underline{E}$, and magnetic field strength, $\underline{H}$: further $\underline{P} = \underline{E} \times \underline{H}$. If it is a plane wave then $\underline{P}$, $\underline{E}$ and $\underline{H}$ are mutually perpendicular and the scalar product $P = E \times H$ applies. On the far side, at B, the wave has values $\underline{P}'$, $\underline{E}'$ and $\underline{H}'$. Shielding effectiveness, in this case, can be defined as the ratio of the values of the wave *at B only* with and without the shield present – whether $\underline{P}$ is chosen, or $\underline{E}$ or $\underline{H}$ alone, depends on the application. If, and only if, the values at A are the same whether or not the shield is present (and they may in fact change if energy is reflected by the shield), then shielding effectiveness can also be defined in terms of the values at A and B.

Infinite sheets, though convenient, are not truly representative of practice. Aircraft more closely approximate to the solid shell of Fig 6b. Here A and B are inside and outside the shell, respectively. The problem that arises is that the values of $\underline{P}'$, $\underline{E}'$ and $\underline{H}'$ at B are a function of the shape and dimensions of the shell: this holds true even if $\underline{P}$, $\underline{E}$ and $\underline{H}$ at A are forced to be constant.

A full discussion of the problems of defining and measuring shielding effectiveness is well beyond the scope of this paper but, nonetheless, for practical purposes the problem is not intractable. There are two ways out:

(i) to measure the shielding effectiveness of the material when it is incorporated in a *defined* (and fixed) solid shell.

(ii) to consider the effect which the shielding is presumably guarding against – *eg* the current on the wire into the 'black box' of Fig 1 – and to define shielding effectiveness as a function of changes in this quantity.

Approach (ii) has the advantage of being directly relatable to problems of interest, but needs a secondary effect (*eg* current) to be measured; approach (i) is pragmatic, not absolute, but is independent of the final effect, and has the advantage of allowing, in isolation, comparison between different materials of the same shape. This, in fact, is its principal virtue.

Most workers, in fact, initially adopt approach (i) for their measurements, often having the CFC samples as one face of a cube; sometimes, subsequent progress is made with approach (ii), measuring interference effects in aircraft or aircraft-like structures.

Typical results are reported by Bull *et al*[3]. Here separate measurements were made of the electric field shielding effectiveness and magnetic field shielding effectiveness. The enclosure used was a 1m cube, five of whose sides were copper and the sixth the CFC material being tested. Fig 7a&b show sample results for magnetic and electric field shielding respectively. Measurements were made both with the edges plated and unplated: the former approximates to desirable aircraft practice whilst the latter essentially means the CFC sheet is insulated from the enclosure. The loss of shielding (20-40 dB in the regions of prime interest) with unplated sheets emphasises the care that must be taken when joints are fabricated in CFC or metal/CFC aircraft structures.

For samples with plated edges the magnetic field shielding increases with frequency up to 30 MHz; at the lower frequencies it is quite low (~ 20 dB) compared to a metal sheet. This is believed to be because the material thickness is less than the penetration depth and the surface impedance is high: hence absorption loss is low, as is reflection loss; at higher frequencies both increase. Above 30 MHz measurements were not possible as instrumentation sensitivity was not high enough; it may be possible to extend the frequency range to about 100 MHz.

Electric field attenuation with plated edges is high (~ 90-105 dB) over the frequency range 50 MHz to 1 GHz; this probably approaches the results obtainable with typical aluminium alloys.

The essence of this and other work on shielding is that at frequencies above 100 MHz there is very little difference between CFC and conventional aircraft materials. Below 100 MHz, and particularly in the HF band, 2-30 MHz, the magnetic field shielding offered by CFC is substantially smaller. Unfortunately, as noted earlier in section 2.1, this is where the greatest EMC threats lie.

3.4   Antenna performance

There is little published on the performance of antennas on CFC structures. However it is generally accepted (*eg* Refs 6 and 7) that for antennas, especially monopoles, operating at frequencies above 100 MHz radiations patterns and efficiencies are little different whether the ground plane is metal or CFC, and that CFC is acceptable.

However, as noted in sections 2.1 and 2.2, in radiating systems where the radiating current flows through the structure, such as in HF notch aerials, it is likely that some loss in efficiency will result due to CFC's higher resistance at these frequencies. This would be particularly true when electrically small high current loop excitations are employed, in which the radiation resistance is low compared with the loss resistances in the radiating structure.

Sidford and Owen[7] have reported some work to quantify this loss of efficiency. Ideally, a complete CFC aircraft should have been used, together with an aluminium replica, but as this was not practicable, a tail fin mock-up in CFC containing an HF notch was compared with its aluminium equivalent. (In fact, the CFC fin was internally stiffened with aluminium honeycomb which may have affected the results.) Measurements were made with each mounted in turn on a section of fuselage 12 m long and 3 m in diameter. As the bulk of the currents responsible for radiation at low HF frequencies flows in the immediate vicinity of the notch, this should be sufficient to determine the practicability of using this type of antenna in CFC airframes. In fact three notches were examined - CFC, aluminium and aluminium-lined CFC.

Fig 8 shows the radiation efficiencies of each of these notches. As can be seen the CFC notch was approximately 10 dB less efficient at 3 MHz than either the aluminium or the aluminium/CFC notches. Small differences were observed between the latter two at frequencies under 12 MHz. Above 12 MHz there were no significant differences between any of the notches.

For radio communications there will be no difference between the performances of all aluminium and CFC/aluminium notches. Use of the completely CFC notch would result in differences on reception, but since signals are usually external noise limited, these may not be as large as the relative efficiency measurements suggest. Difficulties may, however, arise on transmission. Transmissions between 2 and 4 MHz, using ground wave propagation, would be badly affected and some reduction would also occur in the range 5-9 MHz where the sky wave begins to predominate. The conclusion drawn from the work is that provided well-bonded local metallisation is incorporated, notch antennas in CFC fins may be expected to radiate with similar efficiency to comparable antennas in metallic fins.

3.5   Lightning vulnerability

As noted in section 1, lightning vulnerability was amongst the first of the electrical aspects of CFC to be considered. Consequently, a considerable amount of research and development has been done and a large literature has built up. The paper by Little[8] is an excellent introduction to the subject.

In a severe lightning strike the current flowing in the aircraft may have an initial component, of duration a few tens of microseconds, of peak amplitude as high as 200 kA, usually followed by components of longer duration but lower amplitude; the total charge

transfer would be up to 200 coulombs and the total action integral (which is the measure of the energy dissipated in a given resistance) up to 2×10^6 A^2 s (or joules/ohm). The behaviour has been investigated of CFC and mixed CFC/metal structures when subjected to such short but intense current pulses. Such investigations have covered both damage ('direct') effects and induced voltage ('indirect') effects.

As a preliminary to investigation of damage effects consideration of the behaviour of CFC panels under pulsed current conditions is of interest. Experiments have been conducted (Burrows, Luther and Pownall[9]) with pulses designed to reproduce the peak currents of lightning currents and covering a wide range of current densities (540 A/m^2 – 1.3×10^8 A/m^2) but with the action integral kept low so that bulk heating was held well below the damage level and thermal effects could be ignored. The results indicated that in the bulk CFC Ohm's Law was obeyed over the entire range of current density tested (five orders of magnitude) but that in the region of CFC/metal interfaces nonlinearity was apparent in the voltage/current relationship, the law being approximately $V \propto I^{0.85}$.

If the current density is such that the temperature does rise considerably then it is found that nonlinearities arise. Two effects are observed (Scruggs and Gajda[10]): at 65°C the longitudinal resistance drops, with the mechanism being unknown but postulated to be some change within the fibres themselves, and at 110°C the transverse resistance increases, due to the resin softening at this temperature and hence relaxing fibre-to-fibre contacts. The fall in resistance at 65°C can create local hot-spots, as current concentrates in hot fibres. Further, as this temperature is much lower than the temperature to which aluminium can be safely heated, and as the thermal conductivity of CFC is much lower than that of aluminium, then dangerous hot-spots in fuel systems, for example, are more likely in CFC.

These considerations lead into the special factors affecting direct, thermal, lightning damage to CFC at an arc attachment point. These are the higher burning voltage of the arc with CFC which increases the heat produced at the arc root, the high bulk resistivity of CFC which generates greater ohmic heat in the surrounding area, and, as mentioned, the lower thermal conductivity of CFC. Lightning damage is always due to local heating, for example at the lightning attachment point on the surface or where current is forced to flow through structures of restricted cross-section; the latter has been experienced particularly at adhesively-bonded joints. Severe surface damage is likely to be confined to the top few laminae and provided there is sufficient material to carry the current without excessive temperature rise there is unlikely to be significant concealed damage or loss of strength. A thin (6-20 μm) aluminium foil on the surface provides efficient protection, as does an embedded aluminium mesh. Such protection would also improve its general electromagnetic shielding properties but it raises questions of durability (in surface films), repairability and complication in manufacture and so its use is likely to be confined to particularly vulnerable areas.

Indirect, induced voltage, effects arise because lightning currents produce high intensity transient magnetic fields which may link with electrical cables to induce hazardous voltage transients. This is especially significant for electronic flying and engine controls whose continued operation is vital to flight safety. In metal aircraft, penetration of lightning fields is mainly through electromagnetic apertures, such as canopies and radomes, but because of the high resistance of CFC the time-constant for current and flux penetration through the material is much shorter than for aluminium (the ratio is estimated to be 1000) and in fact is much shorter than the duration of the initial 'fast' component of the lightning current. It is to be expected therefore that significant penetration of lightning fields will occur through CFC panels. Experimentally, it has been shown that a CFC panel insulated from the surrounding metal fuselage behaves substantially as an aperture, in contrast to a metal panel which provides substantial shielding even in these circumstances. Wires under well-bonded composite panels will experience induced voltages of waveform similar to that of the lightning current and amplitude proportional to the product of the current and the resistance of the panel; in contrast, wires beneath metal panels experience negligible voltages while those near apertures have induced voltages proportional to the rate of change of current.

3.6 Nonlinear effects

The 'rusty bolt effect' has long been known in metal structures: it is that a nonlinear junction will generate or re-radiate harmonics and intermodulation products from nearby communications and radar transmitters. Because CFC materials consist of strands of conductors laid in light contact with each other it was postulated that they could form a potential source of nonlinear junctions.

Work by Watson[11] has shown that this is not the case. He observed no harmonic generation for plain or jointed CFC samples even when stressed. The same remarks apply to bonded, bolted, plated and reinforced samples. This is because the internal contacts between the carbon fibre strands are probably self-shielded. Significant harmonics were only generated by lightly touching panels and for badly damaged samples (when CFC fractures, large (10-100 mm) jagged splinters of carbon fibre strands project from the material providing many lightly touching unshielded joints). In general, though, the 'rusty bolt effect' is not likely to be of importance.

3.7 Bonding and jointing

Throughout the work described in this paper the importance and influence of adequate bonding and jointing keeps arising. Possible design measures are discussed later, in

section 5; this section reviews some of the aspects that influence the electrical aspects of bonding and jointing.

The essential difference between metal and CFC is that if metallic components are jointed together with no special attention paid to electrical bonding the joint is still likely to be satisfactory. In CFC, however, this will not be so, as to be good electrically all the individual fibres in one component must be electrically connected to all the individual fibres in the other component. This is not easy, either for mechanical or adhesive joints, as Lodge et al[12] have shown.

Mechanical joints. Surprisingly, it has been found that the shank of a bolt does *not* play a large part in making contact between a bolt (or rivet) and CFC. Several factors contribute: firstly, incorrect drilling can leave oversize holes; secondly, wrong speed drilling or feed rate can smear epoxy resin over the ends of the fibres thus insulating them, or it can break off the ends of the fibres completely, thus leading to erratic characteristics; and thirdly, titanium bolts generally used in aircraft applications tend to have a tenacious non-conducting oxide film.

Most contact, in fact, takes place between the composite and the bolt head, as the pressure under the bolt head is sufficient to break down the epoxy-rich layer on the surface. Furthermore, conduction is better with hexagonal head than with countersunk bolts: this is because the area of contact under the bolt head is greater for hexagonal head bolts. At the other end of the bolt, the current re-enters the composite via the nut in a similar manner. There is very little direct panel-to-panel conduction, again due to the epoxy rich surface layer. Thus sealants, etc, have very little effect on electrical performance.

Typical measurements of bolted joints are shown in Fig 9. (At higher frequencies, measuring 'Effective series resistance (ESR)' removes the effects of the surrounding material.)

Adhesive joints. With the high cost of titanium bolts and the tight tolerances required of their bolt holes adhesive bonding is sometimes considered as a means of assembly, either by co-curing or by using film adhesives.

As its name implies, co-curing involves one component being assembled or laid up with a second. As the first is cured, it simultaneously bonds with the second into one structure and the joint becomes part of the bulk material. It thus becomes electrically 'invisible' and the structure appears as if it had no joint in it. This bonding method is electrically very good.

Film adhesives on the other hand are very poor. Cold setting adhesives have bulk conductivities of 10^{-13} to 10^{-15} S/m and are effectively open circuit. Film adhesives which are heat curing often have metal powder incorporated for hot strength and these impart a little conductivity to the joint. Joints with a similar overlap to bolted and rivetted joints have joint admittances of 8×10^{-4} S/m of joint and 12 to 20×10^{-4} S/m if the mating surfaces are initially abraded.

This slight conduction is something of a disadvantage. It arises where chance strings of conducting fibres join two sides of a joint. The resulting localised small current flow causes local hot-spots and these can free fibres from the matrix allowing more current to flow across the joint. This is undesirable, both electrically and from a structural point of view.

This type of damage is not confined to adhesive joints and can occur at current densities as low as 0.1 A/m^2. The best preventive measure is to improve the electrical conductivity of the joint to prevent large potential differences from developing across it.

Fig 10 shows a typical measurement of a basic adhesive joint (plotted as impedance or effective series resistance - not conductance).

4   PRELIMINARY ASSESSMENT OF THE ELECTRICAL IMPACT OF COMPOSITES

Table 2

Preliminary assessment of the electrical impact of composites

Minor problem areas	Major problem areas
1 Direct damage lightning effects	1 CFC properties at HF and below lead to penetration through the material of energy from on-board and external sources, EMP and lightning; they also affect HF antenna installation.
2 Nonlinear effects (harmonics and intermodulation product generation)	
3 Antenna installation at VHF and above	2 Bonding and jointing: without adequate electrical design there can be penetration of energy through joints and difficulties with antenna installations
4 Power supply earth returns	
5 Shielding at VHF and above	3 Fuel system safety

Table 2 presents a preliminary assessment of the electrical impact of CFC. The essential message is that the major problem areas arise because of the characteristics of the material at HF and below; above this frequency range there is little difference between CFC and aluminium alloys. These findings are true for more or less all the lay-ups examined.

It appears that direct damage lightning effects are not serious, though attention should be paid to structures containing a metal honeycomb and to adhesive joints. Electrical nonlinearities have not been found in the material itself or in joints; in any event the effects of the generation of harmonics or intermodulation products by such a source would be restricted to the possible degradation of radio receiver performance. Antenna installation at VHF and above is not seen as a problem: the performance of the material as a ground plane at these frequencies is virtually indistinguishable from aluminium alloy. Although it will not be possible to use CFC for a power earth return, with careful design even with extensive use of composites the associated weight penalty may only be a few tons of kilograms, particularly if certain longitudinal structural elements are retained in aluminium alloy. The shielding properties of the material itself may be *different* at VHF and above - not necessarily *worse* - but this will be because the pattern of surface current distribution, and hence penetration, is changed. Work on aircraft incorporating composite panels confirms this opinion. In any case, even in metal aircraft it is not wise to rely on the shielding offered by the fuselage for the protection of sensitive electrical and electronic systems.

The characteristics of the material, and its differences from aluminium alloys, at HF and below are that its impedance is much higher and that it offers much less shielding to magnetic fields. These differences are important for several reasons. Firstly, in the EMC of aircraft systems, on-board HF installations cause considerable problems in conventional metal aircraft, and it is likely there will be even more penetration of HF energy through CFC skins. This also applies when the aircraft is exposed to an external transmitter. Similarly, induced voltage lightning effects will be more severe, as the typical lightning current has significant content at these frequencies. The frequency spectrum of EMP includes these frequencies, though it also extends higher into the VHF and UHF regions. Accordingly, it is possible that electromagnetic interference susceptibility specifications will need to be more severe in the HF band. Furthermore, when an aircraft HF transmitter uses a notch aerial the whole structure acts as a radiating element. To be adequately efficient for this task requires careful design for CFC or CFC/metal aircraft. In total, the deficiencies of the material in the HF band may be serious enough to affect the requirements and specification (airframe and equipment) of the aircraft as a complete weapon system. As a palliative, the RF interference problem may be reduced by the judicious siting of cables to take maximum advantage of the shielding offered by the metal part of the airframe, but in addition it may be necessary to metallise the structure in particularly critical areas. This also applies to lightning protection.

The second major problem area uncovered by the research programme is that of bonding and jointing. Time and again the report has been that the limiting factor in electrical performance is not the material itself but the joint. This obviously applies to use of the airframe to carry current from power (dc and RF) and lightning sources, to its use as a ground plane, particularly at HF, and to the limitation of nonlinear effects. More insidiously, an imperfect joint allows electromagnetic energy to penetrate the airframe and hence increases the likelihood of EMI susceptibility problems. This is a highly important area where materials and structural engineers must be made aware of the design measures needed to achieve electrically invisible joints.

The third problem area is that of fuel system safety arising from the generation of local hot-spots, as mentioned in sections 3.5 (lightning) and 3.7 (bonding).

5   ELECTRICAL ASPECTS OF DESIGN IN CFC

5.1   General

As noted in the Introduction, section 1, R&D on the electrical aspects of CFC was initiated in order to catch up on the 10 or 15 years' lead held by structural designers. As such, basic information is still being generated and the subject is not sufficiently mature for detailed design recommendations to be formulated or generally agreed without reservation.

Nonetheless, some ideas have been forthcoming in various sectors of the programme, notably lightning protection and bonding. These are detailed below. These, in fact, are the areas of most general application, as opposed to the specific requirements of antenna installation, earth return structures, and radar cross-section. At the moment these latter demand consideration based on their individual requirements and are outside the scope of this paper.

5.2   Lightning protection

With regard to the 'direct' damage effects of lightning it has been observed[8] that the properties of CFC combine to make some damage at the arc root more likely than with aluminium alloy. On the other hand, this is usually limited to vaporization of the matrix resin and tufting of fibres at the arc root, and delamination of the top two or three layers for up to approximately 200 mm around the attachment point. Mechanical tests have shown no measurable deterioration outside the area of visible damage, and hence this type of effect is categorized in Table 2 as a minor problem area.

Protection against surface damage is possible, depending on the 'zone' of the aircraft (the various zones of aircraft are categorized from 1 to 3 depending on their attractiveness to lightning - see Philpotts[13]. In zone 1A and 2A areas protection can be obtained with a metallic coating over all or part of the CFC. In zones 1B or 2B solid metal is preferable, but if arc 'hang-on' does not occur it is possible to use, for example, thin aluminium foil of 20 μm to 100 μm, the heavier foil being necessary in zone 1A. Another method is for the thin aluminium layer to be produced by applying aluminised glass fabric on the outer surface.

The foil operates as a sacrificial layer. The arc attaches preferentially to the foil because the burning voltage is lower on metal than CFC, and pursues the retreating metal edge as the foil evaporates. Bigger areas are eroded on thinner foils. Also, because of the high conductivity of the foil, the technique offers protection against both arc root damage and resistive heating. The foil can be painted without affecting the protection it affords, so risk of corrosion is reduced.

Other alternatives include flame-sprayed aluminium, a mesh of stainless steel wire or an aluminium mesh, on the surface, or aluminium wires woven in the outermost layer of the CFC fabric. Protection need not cover the whole of the aircraft surface, only those zones at risk. Repairs, however, are troublesome. As noted, in section 3.7, co-cured adhesive bonds can be electrically 'invisible' and can be made safe to lightning, but other types of bond (both CFC/CFC and CFC/metal) need more attention. The most difficult problems are those associated with hatches, bay doors, inspection covers, etc, where frequent opening is required. Finger contacts and spring-loaded gaskets are liable to fatigue, and conductive rubber is not conductive enough to bond well.

With regard to 'indirect' induced voltage effects, it can be shown that the coupling can be reduced if cables (and also fuel pipes to reduce ignition risk) are positioned away from thin CFC panels and close to metal structures or CFC spars. If done at the design stage this incurs no weight penalty.

5.3 Bonding and jointing

Mechanical joints. As discussed in section 3.7 conduction through a mechanical joint is not by the shank of the bolt or rivet but through the bolt head. Thus, if the surface of the CFC is insulating then the joint conductivity will be low. Thus glass-cloth and other non-conducting materials should be removed locally from around the fasteners. If required, the surface could be resealed once the fasteners are installed.

Conductivity will be improved by increasing the contact area. Use of a larger diameter fastener or of larger head and tail fittings does this but with weight and cost penalties. It can also be improved by tighter tolerances on hole drilling, but this is expensive and the surfaces of such holes are very delicate. High closing pressures give an electrical improvement but are likely to cause structural damage to the composite.

With composite/metal interfaces the biggest influence is the state of the oxide film on the metal. Removing this from titanium bolts, for example, increased the joint admittance from 15 to 120 S/m. Of particular interest is the poor performance of aluminium rivets where the particularly tenacious oxide film prevents good contact between the carbon and aluminium.

Coating the inside of the fastener hole with a conductive deposit improves joints (this can also be used to repair damaged holes). In this way, all the carbon fibres which touch the fastener hole are connected together and contact to one of them is equivalent to contact to all. Possibilities include electrodepositing, flame spraying and electroless plating with such metals as copper, or to use conducted particles suspended in a carrier.

Adhesive joints. Apart from the electrically invisible co-cured joint, adhesive joints are generally much worse than mechanical joints. Their behaviour depends essentially on the properties of the adhesive. Cold curing resins are generally insulators, having bulk conductivities of about 10^{-13} S/m. Some types of hot curing adhesives, however, have metal particles incorporated to improve their hot strength. The adhesive becomes partly conducting, with an admittance of about 0.01 S/m. This small conductivity can be a disadvantage, though, leading to the problems of localised hot-spots discussed earlier.

It is not easy to improve the electrical properties of adhesive joints. Increasing the metal loading in the adhesive can increase the conductivity, but not enough. With such levels of loading (eg 75% silver flakes) the adhesive properties suffer, of course, and they are no longer usable.

A possibility for improving adhesive joints without detriment to their strength involves using a film adhesive spacing scrim. This nylon mesh, used to control the glue line thickness, can be removed from the film adhesive and replaced with a metal gauze of the same thickness. This method is still under development[14].

6 CONCLUDING REMARKS

Considering the relatively short time in which the electrical properties of composites have been investigated - particularly when compared to the effort put into structural and materials aspects - it is remarkable how much useful information has been generated. This is because, in those countries where it is seriously intended to use composites in

airframes, the need for such information has been recognised and concerted, national, programmes initiated.

Taking the long view, the basic research programmes are, perhaps, half-way through their lives. What is more important is that design guides for electrical aspects of composites are now being formulated. Not only will these outline the penalties of using CFC but they will also indicate positive steps to achieve good electrical performance.

The essence of the message is the need to take a positive attitude to the electrical properties of a composite structure, rather than letting them take care of themselves as is usually the case with metals. This means more work for the designer, *in the short term*, but the potential is for CFC aircraft whose EMC and electrical performance is even better than for their metallic rivals!

GENERAL REFERENCES

1.   AGARD Conference Proceedings 283: Electromagnetic effects of (carbon) composite materials upon avionics systems; Lisbon, Portugal, 16-19 June 1980

2.   Digest of Meeting: The electrical properties of carbon fibre composites; Culham Laboratory, Abingdon, UK, 15-16 December 1981

REFERENCES

1.   P.A. Shaw, Some comments on the use of aircraft structures as electrical conductors; presented at the 34th Meeting of the AGARD Structures and Materials Panel, Lyngby, Denmark, 9-14 April 1972 (republished as Royal Aircraft Establishment Technical Memorandum EP 510, June 1972)

2.   D.A. Bull and G.A. Jackson, Interference survey in military transport aircraft; First Symposium on Electromagnetic Compatibility, Montreux, Switzerland, 20-22 May 1975

3.   D.A. Bull, G.A. Jackson and B.W. Smithers, RF resistivity and screening characteristics of CFC materials, General Reference 1, Paper 6

4.   B.W. Smithers, RF resistivity of carbon fibre composite materials, IERE EMC Conference, Southampton University, UK, 16-18 September 1980

5.   D.C. Brewster, Theoretical calculation of RF properties of carbon fibre laminates, General Reference 1, Paper 5

6.   G.L. Weinstock, Electromagnetic integration of composite structure in aircraft, General Reference 1, Paper 15

7.   M.J. Sidford and J.I.R. Owen, HF notch aerials in carbon fibre composite structures, General Reference 2, Paper 13

8.   P.F. Little, Lightning hazards due to composite materials in aircraft, IEEE EMC Symposium, Santa Clara, Ca, USA, 8-10 September 1982

9.   B.J.C. Burrows, C.A. Luther and P. Pownall, Resistance measurements on bulk CFRP and metal/CFRP joints, Culham Laboratory Lightning Studies Unit, (CLSU), UK, Memo No.56, October 1977

10.   L.A. Scruggs and W.J. Gajda, Low frequency conductivity of unidirectional graphite/epoxy samples, IEEE EMC Symposium, Seattle, Wa, USA, 2-4 August 1977

11.   A.W.D. Watson, Nonlinear effects in carbon fibre composites, General Reference 2, Paper 9

12.   K.J. Lodge, J. Brettle and N.J. Leggre, The design of carbon fibre composite joints for electromagnetic compatibility, IERE EMC Conference, Surrey University, UK, 21-23 September 1982

13.   J. Phillpott, Recommended practice for lightning simulation and testing techniques for aircraft, CLSO Report CLM-R-163, May 1977

14.   K.J. Lodge, The electrical properties of joints in carbon fibre composites, Symposium on Jointing in Fibre Reinforced Plastics, Imperial College, London, 13-14 July 1982

7   ACKNOWLEDGMENTS

In preparing a review paper such as this I have inevitably culled information from a variety of sources. These sources include the literature and personal contacts.

In the UK, I have been fortunate in being involved with the Composites Electrical Properties Advisory Group from its inception in 1978. The advice, contacts and, most

importantly, the stimulation this 30-strong Government/Industry group has given me is priceless.

I am also deeply indebted to all the workers from UK, Europe and the USA that I met at two major meetings: the 39th Technical Meeting of the AGARD Avionics Panel in Lisbon, June 1980, and the 2-day Technical Meeting at Culham Laboratory, December 1981.

I must specifically mention the following for the volume of their freely-given advice and information: John Birken, US Naval Air Systems Command; David Bull, ERA Technology Ltd; Philip Little, Culham Laboratory Lightning Studies Unit; Kevin Lodge, Plessey Research (Caswell) Ltd; Brian Smithers, ERA Technology Ltd; Roy Stratton, Rome Air Development Center, USA. To these and everyone else I am very grateful.
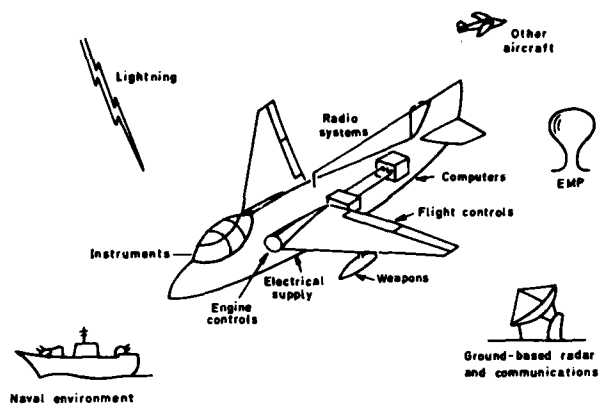
Fig 1 The electrical aircraft
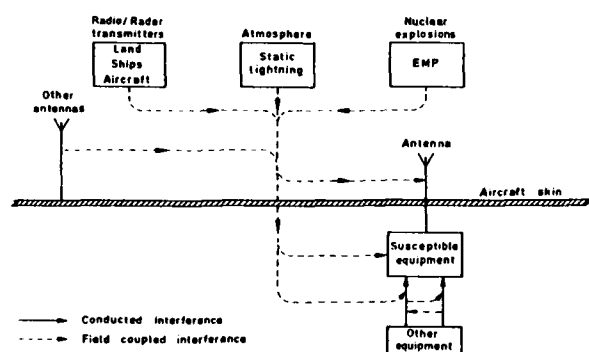
Fig 2 Interference coupling paths into aircraft
equipment

(a) 0°, 90°

(b) 0°, ±45°
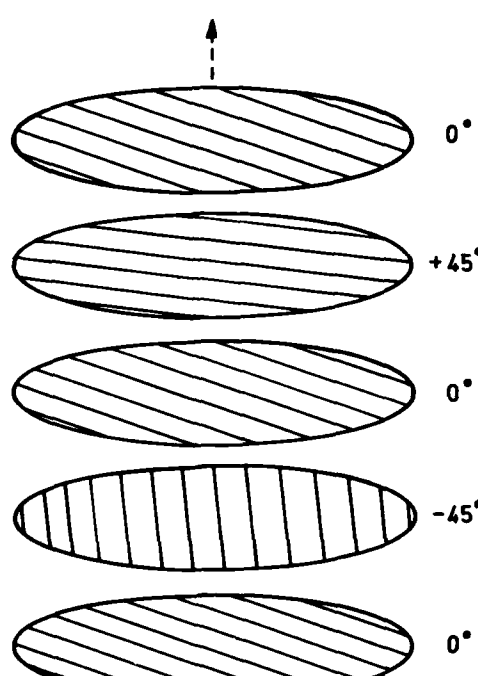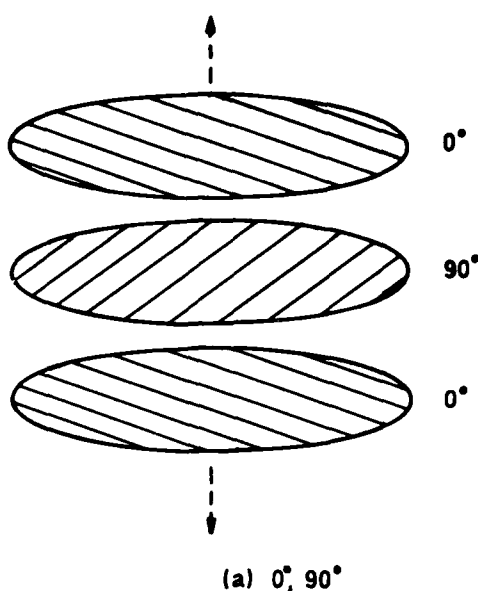
Fig 3a&b Typical CFC lay-ups
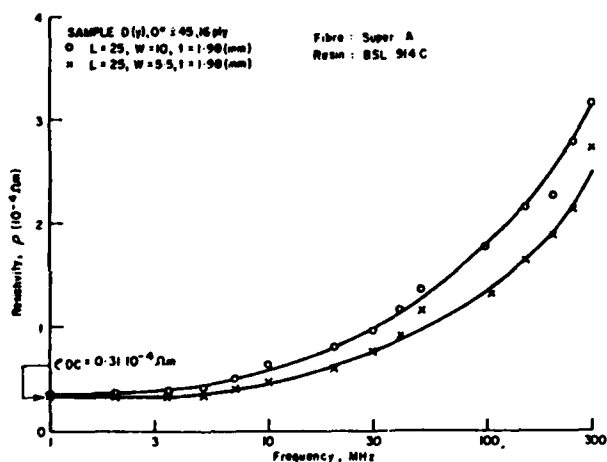
Fig 4 Typical resistivity - frequency
characteristics (plotted on a linear scale)
(after Smithers, Ref 4)
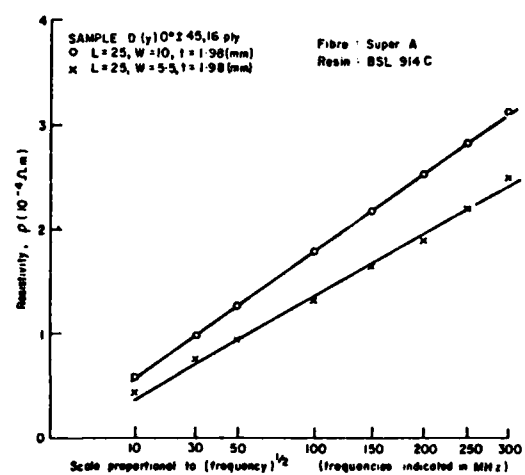
Fig 5 Typical resistivity - frequency characteristics (plotted on an $f^{\frac{1}{2}}$ scale)

a   Magnetic field attenuation

b   Electric field attenuation

Fig 7a&b   Shielding properties of CFC (after Bull *et al*, Ref 3)
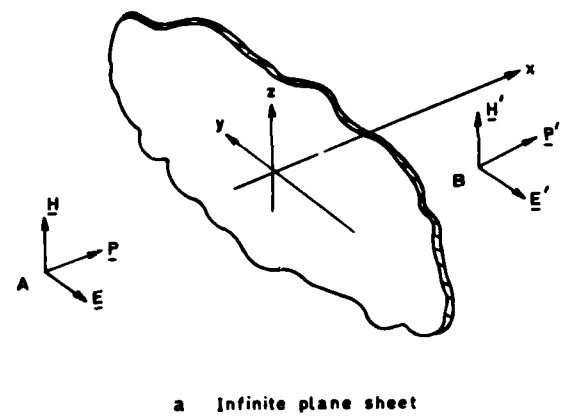
a   Infinite plane sheet
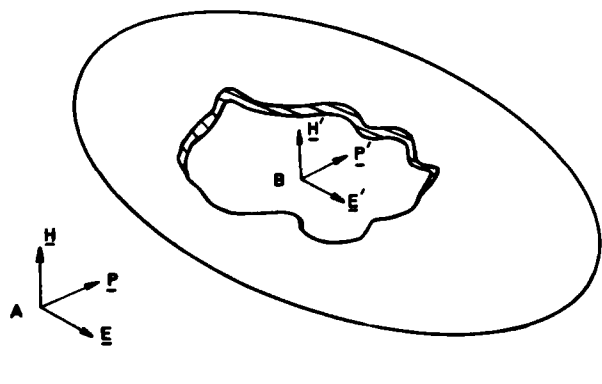
b   Solid shell

Fig 6a&b   Meaning of shielding
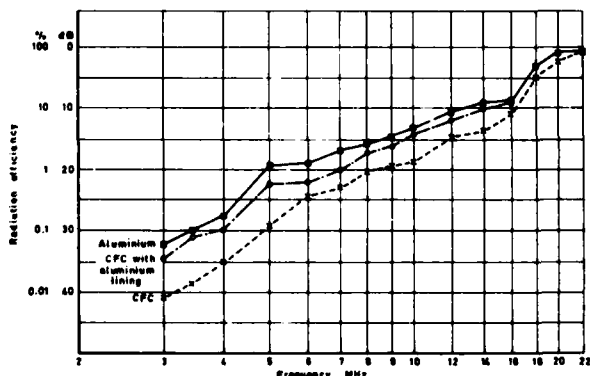
Fig 8   Radiation efficiencies of notch aerials (after Sidford and Owen, Ref 7)
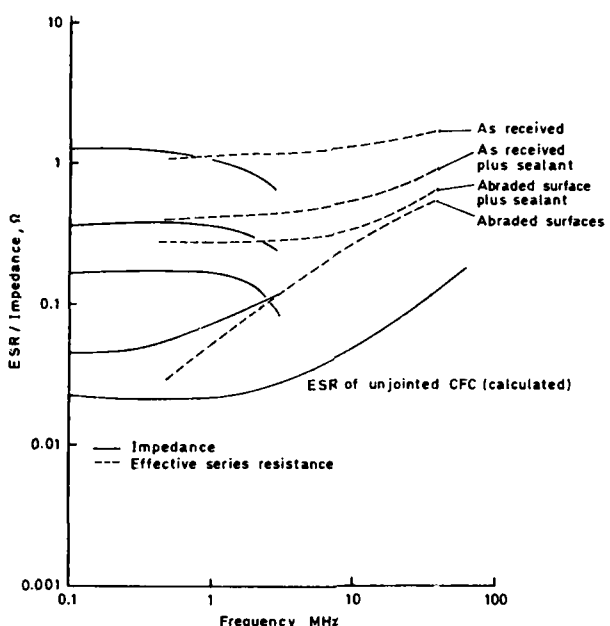
Fig 9   High frequency properties of bolted
joints with various pretreatments
(after Lodge *et al*, Ref 13)
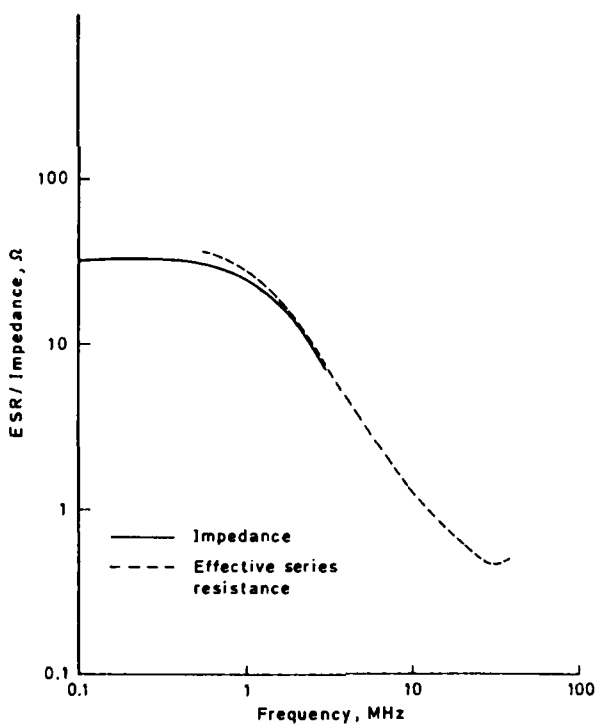
Fig 10   High frequency properties of a typical
adhesive joint
(after Lodge *et al*, Ref 13)

ENVIRONMENTAL DEGRADATION OF COMPOSITES

GRAHAM DOREY

Materials Department,
Royal Aircraft Establishment,
Farnborough,
Hampshire, UK.

SUMMARY

Advanced composite materials comprise well ordered high strength fibres in a matrix of organic polymer, metal or ceramic material. Carbon fibres are inert to most environments except high temperature oxidizing atmospheres. Ceramic fibres such as glass are sensitive to surface microcracks and can lose strength in corrosive media. Most organic polymers, including aramid fibres and epoxy resins absorb moisture which can affect their chemical structure and typically reduce their high temperature performance. Composites may, in addition, be affected at the fibre/matrix interface, which plays an important part in composite behaviour. Certain combinations of moisture and temperature can cause irreversible damage which degrades the composite properties, especially matrix or interface dominated properties such as shear strength or compressive strength, particularly at elevated temperatures.

It is important therefore to have sufficient information about the absorption and desorption kinetics to be able to predict the moisture content of composite components in their service environment, and to know what effect that moisture will have on their properties. It may, however, take many years for a composite component to reach an equilibrium moisture content, so there is a need for accelerated test techniques that can be accurately correlated with any real time degradation. This has important implications for airworthiness clearance procedures for composite structures.

As well as the effects of moisture, natural weathering hazards may include ultra-violet radiation from sunlight, erosion from liquid and solid particles, lightning strike and galvanic corrosion. Each hazard needs to be adequately assessed, and, where necessary, protection schemes developed. Advanced composite materials have been in service for a number of years, yielding valuable information on their environmental performance.

1. INTRODUCTION

Advanced composite materials are being used in increasing numbers of applications in aerospace primary and secondary structures. They offer potential savings in weight, they offer the ability to tailor the material more closely to the design requirements and they offer manufacturing advantages in being able to mould complex shapes and hence reduce the numbers of parts and the numbers of joining operations. High strength and/or high stiffness are required for fixed wing applications and hence carbon fibres or aramid fibres are used. For helicopters some applications require more compliance (hub) or more damage tolerance (blades) and glass fibres are useful, although for some rotor blades, where more efficient complex shapes require increased stiffness, carbon fibres are being incorporated into hybrid carbon fibre/glass fibre designs. Most of these applications use the fibres in a polymeric matrix, usually an epoxy resin.

These components have to survive in a range of different environments of moisture, temperature and loading in different parts of the world, at different altitudes and for different performance envelopes. Moisture can vary from relative humidities of 0 to 100%. Temperatures for helicopters and civil aircraft are typically in the range $-40^\circ C$ to $70^\circ C$ in flight and up to $90^\circ C$ on the runway. Supersonic fighters require skin materials to survive temperatures of up to about $130^\circ C$, and even higher temperatures for the application of composites to areas near to the engines.

On the microscopic scale, the internal stresses in fibre composites are complex and the constituent materials have to perform acceptably under the possible combinations of applied stress, residual internal stresses and adverse environmental conditions. As damage tolerant design philosophies become more prevalent, the effect of the environment on damage growth and on its associated critical residual strength will need to be known in more detail.

Resin matrices have to have adequate properties at high temperatures and, for thermosets, this normally means having a high cross link density and it necessitates moulding at a relatively high temperature (about $170^\circ C$ for supersonic aircraft and $120^\circ C$ for helicopters and civil aircraft). However, there are important considerations of manufacturing technology in deciding the final formulation. In order to extend the shelf life of the partially cured preimpregnated material, recourse is sometimes

made to solid hardeners such as dicyandiamide that do not dissolve in the resin below temperatures of about 120°C, or to accelerators such as a boron trifluoride complex that are not activated until the temperature is raised in the mould. These compounds can be susceptible to hydrolysis from absorbed moisture and alter the curing characteristics of the material. The viscosity of the resin during moulding can have significant effects on the tolerances needed to control the temperature and pressure during the curing process, and so mixes of resins are used to increase viscosity and aid the manufacturer. Some of these additions cause increased moisture uptake in the final cured composite material.

Thermoplastics have advantages of fast processing times and infinite shelf lives, and they are therefore being considered for aircraft applications. The amorphous high temperature thermoplastics such as polyethersulphone (PES) are susceptible to solvent attack but crystalline thermoplastics such as polyetheretherketone (PEEK) have a low moisture uptake (about 0.2%) and a greater chemical stability.

There are thus conflicting requirements of manufacture and performance for advanced composites. Aircraft structures have to be designed to last at least 20 years in service and because of the possible susceptibility of the resin matrices to absorbed moisture, designs usually aim to take maximum advantage of the fibre controlled properties. However some critical properties, such as compression strength under hot/wet conditions where microbuckling of the fibres dominates the failure, are determined by environmental effects and can restrict the design limit of the material (to about 0.4% strain for hot/wet compression for CFRP). It is important therefore to allow for the effects of absorbed moisture in deciding design allowable properties. There are continual developments and improvements in resin matrices and standard procedures need to be established to assess environmental performance. These would also be useful in monitoring the variation in resin batches.

2   MOISTURE ABSORPTION

Most composite materials absorb moisture from humid atmospheres. This is usually confined to moisture uptake by the resin matrix, though for reinforcement by aramid fibres they too absorb moisture. Epoxy resins absorb a maximum of between 1% and 10% by weight of moisture[1] (depending on chemical composition), so in composites with 60% by volume of fibres the moisture uptake is between 0.3% and 3% by weight. For most composites used for aerospace applications the maximum moisture uptake is between 1% and 2% by weight.

The absorption of moisture is by a diffusion controlled process[2,3,4]. In most applications, where the thickness of the sheet is small compared with the other dimensions, the diffusion can be described by a one-dimensional analysis. Most of the moisture uptake follows Fick's law of diffusion

$$\partial c/\partial t = D\partial^2 c/\partial x^2 \qquad (1)$$

where c is the concentration of the diffusing species, t is time, D is the diffusion coefficient and x is distance. For a flat plate absorbing moisture through both surfaces the initial moisture uptake is

$$M/M_m = (4/h)(Dt/\pi)^{\frac{1}{2}} \qquad (2)$$

where M is the moisture uptake at time t, M_m is the maximum moisture uptake under the appropriate environmental conditions and h is the plate thickness. As the moisture content increases, the rate of uptake decreases and approaches its maximum or equilibrium value assymptotically; this can be described[3] by an empirical modification of equation (2).

$$M/M_m = \tanh[(4/h)(Dt/\pi)^{\frac{1}{2}}] \qquad (3)$$

Typical moisture uptake curves are shown in Fig 1 for environments of different relative humidity (RH). The initial slopes show that moisture uptake is proportional to the square root of time, in agreement with equation (2). The equilibrium moisture content depends on the relative humidity of the environment (see Fig 2) and over most of the RH range the relationship is linear[1,3,4]. Sometimes there is a departure from linearity as 100% RH is approached, but the exact nature of this depends on the detailed chemistry of the resin. The initial rate of moisture uptake depends on the temperature (see Fig 3) because the diffusion coefficient is temperature dependent according to an Arrhenius relationship,

$$D = D_o \exp(-E/RT) \qquad (4)$$

where E is the activation energy for diffusion, R is the universal gas constant and T is the absolute temperature (K). This is shown in Fig 4.

Thus we have the well-known approximate statements (eg ref 2):

i   The equilibrium moisture content is insensitive to the temperature but depends on the moisture content of the environment;

ii   The time required to reach the equilibrium moisture content is insensitive to the moisture content of the environment but depends on the temperature.

The moisture uptake described by equation (2) indicates that the initial rate of uptake depends on the thickness of the laminate. Typical curves for moisture uptake for laminates with different thickness are shown in Fig 5. If moisture can diffuse through the edges of the laminate as well as through the surfaces, then for thicker laminates a three dimensional analysis is needed to describe the moisture uptake; Whitney[5] was able to demonstrate this for test pieces 25 mm x 25 mm x 2.5 mm where the three dimensional analysis gave a better agreement with the experimental data than either the one dimensional approximation or the one dimensional exact solution. However for most applications this would result in only minor deviations from the one dimensional case.

Since the diffusion of moisture is usually only through the resin the diffusion coefficient will clearly depend on the volume fraction V_f of the fibres in the composite (see Fig 6). For diffusion parallel to the fibres, the resin cross section is $(1-V_f)$ and the diffusion coefficient is given by

$$D_{11} = Dr(1-V_f) \qquad (5)$$

where Dr is the diffusion coefficient for the resin alone. For diffusion perpendicular to the fibres, the diffusion coefficient will be reduced to zero when all the fibres are touching, which for cylindrical fibres in a square array is for a V_f of $\pi/4$; and Shen and Springer[2] give

$$D_{22} = Dr(1-2(V_f/\pi)^{\frac{1}{2}}) \qquad (6)$$

For other angle α to the fibres[2].

$$D_\alpha = D_{11} \cos^2\alpha + D_{22} \sin^2\alpha \qquad (7)$$

Augl[6] has done a more exact numerical analysis of diffusion parallel to and perpendicular to the fibres and obtained good agreement with experimental data (his numerical analysis agreed with an analytical solution for electrical conductivity produced by Lord Rayleigh in 1893!).

There is concern, not only with total moisture contnt in a composite, but also with the distribution of moisture since moisture gradients could cause internal stresses. The diffusion analysis given above can be used to generate moisture profiles through the thickness of the laminate for various times, temperatures, and humidities[7] (see for example Fig 7). It should be noted that the surface plies of a laminate quickly reach the equilibrium moisture content but for thick laminates it may take many years for the inner plies to reach equilibrium under normal service conditions. For example[8] a 10 mm thick CFRP laminate at 65% RH and 23°C will still be effectively dry over the middle 2 mm after 100 days and it will take over 10 years to absorb 95% of the equilibrium moisture content for those conditions.

Desorption can also be described by the one dimensional diffusion analysis and examples are given in ref 3 for theoretical and experimental moisture contents for changing environments assuming complete reversibility (the analysis is simple if the laminate reaches equilibrium in each environment before it is changed, but allowances have to be made for moisture distribution if equilibrium has not been reached). There are suggestions that the diffusion kinetics for absorption, desorption and re-absorption are not all simple Fickian diffusion kinetics. Tajima[7] found for a particular CFRP that the first absorption was a simple Fickian process with a constant value of D, the first desorption was Fickian but with a D that depended on water concentration, and further absorption was anomalous leading to non-standard moisture profiles through the thickness. This suggests that cycling the laminate (hygrothermal cycling) produces some irreversible changes and the kinetics indicate the existence of sites for water molecules with different binding energies. If laminates are being dried for experimental purposes great care must be taken not to alter the internal structure, and the temperature should be kept as low as possible.

Some laminates (resins) do not obey simple Fickian diffusion kinetics, even on the first absorption, and models have been developed using sources and sinks of diffusing water molecules, similar to Langmuir's theory of adsorption. Moisture uptake curves for an epoxy resin exposed to several different humidities for up to two years agreed well with the model, suggesting that the anomalies in the diffusion kinetics were not related to water concentration effects. The departure form simple Fickian diffusion usually manifests itself as a further slow uptake of moisture after the main part of the absorption (see Fig 8). Bonniau and Bunsell found that the hardener used to cure the epoxy resin had an effect on the diffusion kinetics for cured glass fibre reinforced laminates; a diamine hardener resulted in classical diffusion, a dicyandiamide hardener gave a Langmuir two phase diffusion behaviour and an anhydride hardener resulted in such damage above 40°C that it was not possible to describe the diffusion.

The diffusion of moisture can be affected by the stress in the resin[10] and significant increases occur in D above certain combinations of stress and moisture content (for a typical CFRP this was 45% UTS and 1% moisture). The increase in D was attributed to the early formation of splits through the thickness of the plies parallel to the fibres.

In some applications, composite laminates are used for the skins of sandwich panels. Moisture can diffuse through the skins and humidify the air in the pores of the core material. Subsequent increases in temperature, such as for re-entry vehicles for space or supersonic aircraft, can cause significant increases in internal pressure in the panel[11,12] and this must be considered in the design.

There is still controversy about the reversibility of these diffusion processes. For high concentrations of moisture and high temperatures the absorbed moisture can cause damage and produce irreversible effects. For very low concentrations it is difficult to remove all the water molecules. But for most practical purposes simple, reversible, classical diffusion can be used to predict moisture contents.

4. EFFECTS OF MOISTURE ON RESINS

Water molecules diffuse into organic polymer materials and become attached by hydrogen bonding to polar groups such as hydroxyl and amine groups. This causes an expansion of the molecular network, depending on the cross-link density, and a swelling of the resin[1,13] as in Fig 9. In some cases voids are produced in the resin.

The water causes a plasticization of the resin and reduces the transition temperature Tg between the glassy state and the rubbery state. The exact definition of Tg and its correlation with structural changes in the resin is complex and the glass transition can occur over a range of temperatures. But the effect of moisture in reducing the transition temperature can be seen in torsional damping experiments (Fig 10) and in creep tests under constant load and a constant heating rate (Fig 11). The reduction in Tg is approximately linear with moisture uptake (Fig 12) and for epoxy resins there is a 100°C decrease in Tg for about 5% moisture uptake.

This reduction in Tg can be modelled by a free volume theory of mixtures of two components[14,15]. For a diluent such as water in a polymer this gives[15]

$$Tg = [\alpha_p V_p Tg_p + \alpha_d(1-V_p)Tgd]/[\alpha_p V + \alpha_d(1-V)] \tag{8}$$

where α is the thermal coefficient of volume expansion, V_p is the volume fraction of polymer, the suffix p stands for polymer and the suffix d stands for diluent. A value for the Tg for water has to be used and this is usually taken as about 273K. One problem with non polymeric diluents is determining the partial thermal expansion coefficient which determines the temperature dependent contribution of the diluent to the total free volume. An alternative theory by Carter and Kibler[16] is based on configurational entropy and applies to water absorption primarily by localization at strongly polar molecular groups. Water molecules are frozen at the sites in the glassy state by hydrogen bonds but are free to jump sites in the rubbery state. This predicts

$$Tgf = Tgo[1-(R/M_s \Delta C_p)y(r)] \tag{9}$$

where

$$y(r) = rl_n(1/r) + (1-r)l_n(1/(1-r)) \tag{10}$$

and

$$r = (M_s/M_w)f \tag{11}$$

Tgf is the Tg for the material with f = mass moisture/mass dry resin, M_s is the effective formula weight of a hydrogen bond site, ΔC_p is the jump in specific heat due to the glass transition in the dry resin, and M_w is the molecular weight of water. This was tested[16] for an epoxy resin with moisture contents up to 7% and good agreement was obtained with experimental data. However it is difficult to differentiate between the two models over the normal range of moisture in epoxy resins and more data will be needed to determine the mechanism of Tg reduction.

The primary effect in composites of this reduction in Tg is to reduce matrix dominated strengths and stiffnesses at high temperatures as discussed below.

5. ENVIRONMENTAL DAMAGE IN COMPOSITES

Carbon fibres are chemically inert except in high temperature oxidising atmospheres. High modulus fibres are more resistant to air oxidation than the lower modulus high strength carbon fibres[17]. The oxidation rate is also markedly dependent on impurities, and small quantities of residual sodium in PAN-based carbon fibres can significantly increase the oxidation rate. However, the temperatures at which carbon fibres are appreciably oxidized is above the operating range of epoxy resins (up to about 170°C), although fibre oxidation could become important with polyimide resin matrices with operating temperatures up to 370°C.

Aramid fibres are susceptible to degradation by ultra-violet radiation including the "near UV" wavelengths in sunlight. Fig 13 shows the loss in strength, when exposed to sunlight, of bare 1500 denier aramid yarn of intermediate modulus. In service, aramid fibre composites must always be protected by a layer opaque to UV and great care should be taken of aramid fibres when stored and during manufacture of structural components.

Glass fibres are susceptible to stress corrosion cracking. In humid atmospheres the strength of glass fibres is not significantly affected but the presence of liquid water allows leaching of alkali salts from the glass which accelerates the stress corrosion process. The protective finishes applied to glass fibres immediately after drawing help to minimise surface attack, make the fibres more handleable during manufacture and increase the adhesion between the glass fibres and resin matrices, especially under wet conditions[18]. The glass finishes are usually organic silanes, one end of the molecule being polar to give adhesion to the glass surface and the other end being organic to bond to the resin matrix. The molecules are best kept monofunctional because polymerization of the protective finish can lead to bridging of the surface leaving parts of it unprotected.

Even with these protective finishes there is evidence of attack at the fibre/resin interface. Sodium salts can be leached from the glass and, in extreme cases, osmosis can lead to small pockets of high pressure at the interface and resin cracking[19]. There is some controversy about the reversibility of moisture absorption and desorption in GRP at room temperature, partly because of the different systems studied. In hot water it is generally considered that irreversible damage is done; in one E glass/epoxy system, 168 hours in boiling water reduced the interlaminar shear strength by 70%, only half of which was recovered on drying. The water attacks the interface and coupling agent by hydrolysis.

Acidic environments too can cause rapid deterioration of GRP. Applied stresses cause debonding of the fibres and allow the acid to wick along the interface. There are changes of concentration of the acid and of the leached salts along the interface and at some stage the conditions are ideal for stress corrosion cracking in the glass filaments. This leads to local stress raisers, increased local stresses and accelerated attack. This whole process seems to be worse in epoxy resins than in polyester resins (Fig 14) because of the detailed differences in the debonding processes in the two systems[20]. To reduce the environmental damage to GRP, the stress should be kept low, the glass should be adequately protected, water soluble impurities should be minimized, the resin should have the minimum of hydrolysable groups, the coupling agent or surface finish should be carefully chosen for the application and a high crosslink density resin will limit the rate of diffusion of moisture to the interface.

Carbon fibre reinforced plastics are much less susceptible to attack by moisture at the fibre/resin interface, partly because of the chemical inertness of the carbon and partly because of the stronger fibre/resin bond. Impurities, such as sodium left from the manufacturing process, can cause problems but with

suitable washing precautions these can be avoided. Experiments on CFRP, made from carbon fibres with different levels of surface treatment[21], showed that for systems with high bond strengths immersion in boiling water for 168 hours reduced the ILSS by 25% with a partial recovery to about 90% of the original value on drying. For untreated fibres, with a weaker fibre/matrix bond, boiling water had no effect on ILSS; this suggests that the reduction in ILSS for CFRP with the stronger bond strengths was caused by changes in the resin rather than by degradation of the interface.

When composites are cooled from the moulding temperature, differential contractions between the fibres and the resins causes internal strains in the resin. The contraction perpendicular to the fibres is greater than that parallel to the fibres which is almost zero. Thus in multidirectional laminates, where contractions are constrained by the fibres in adjoining layers, transverse tensile strains perpendicular to the fibres are produced. These internal strains can be calculated by measuring the curvature in asymmetric strips[22]. In several carbon fibre/epoxy laminates after curing at 170°C and cooling to room temperature, these internal tensile strains were found[22] to be between 0.4% and 0.5%, which is almost sufficient to cause transverse splitting in the plies. Absorbed moisture causes swelling of the resin which reduces the internal strains; to approximately 0.2% in a 65% RH environment and to 0 in a 95% RH environment. On redrying, the internal strains will again increase. This drying occurs most rapidly at the surfaces and edges and can lead to sufficiently high tensile stresses to cause surface splitting or edge delamination[23].

As already discussed some solid hardeners, such as dicyandiamide, do not always completely dissolve and residual particles in the curved resin can lead to hydrolysis and localized cracking when moisture is absorbed. But for most carbon fibre/epoxy systems currently used or contemplated for aerospace applications there should be no significant environmental degradation from absorbed moisture, for subsonic service.

However, for supersonic flight in which skin temperatures can reach about 140°C, there could be significant damage[24] if the moisture content had previously been sufficient to reduce the Tg to about 140°C. There is evident that these "thermal spikes" cause irreversible damage which on subsequent exposure to moisture produces increased moisture uptake[25] (Fig 15) and increased swelling[1] which is not the usual linear increase with moisture content. At temperatures near Tg the polymer molecular network relaxes, allowing more room for water molecules and a more rapid diffusion. On cooling below Tg, moisture may become trapped at certain sites in the resin or at the fibre/resin interface causing high local stresses and microcracking[26]. This is supported by anomalous increases in the thermal coefficient of expansion on cooling moist epoxies, and microcracking would explain the subsequent increased moisture uptake. Thermal spiking needs to be investigated in more detail and carefully related to the material and flight envelope for each aircraft.

6. EFFECTS OF MOISTURE ON COMPOSITE PROPERTIES

Absorption of moisture from humid environments at room temperature is in general a reversible process and with most advanced composites there is no degradation in room temperature mechanical properties[1]. Because moist resins soften at elevated temperatures, resin dominated strengths and stiffnesses are significantly less at these temperatures, than are those for dry composites. Certain combinations of temperature and moisture (and stress) can produce microcracking in the resin or at the fibre/matrix interface which will degrade the mechanical properties even at room temperature but more particularly on further hygrothermal cycling. For instance 15% to 60% loss of interlaminar shear strength can be expected at temperatures and moisture contents expected in service.

Fig 16 shows the effect of moisture and temperature on the tensile stress-strain curve of a $[(+45)_2]_s$ CFRP laminate. For 1.5% moisture and 130°C the failure stress was only reduced by about 10% compared with the room temperature/dry case, but the strain to failure was almost doubled, from 4.5% to 7.0%. Similar results for in-plane shear stress-strain curves for unidirectional CFRP showed that moisture alone increased the strain to failure, but combinations of moisture and temperature (1% moisture and 150°C) reduced the failure stress by about 40%. This was due almost entirely to reductions in the flow stress of the resin. Much greater reductions were obtained in the transverse tensile stress, where moisture alone reduced the strength while not reducing the modulus, whereas combined moisture and temperature reduced both strength and modulus. For multidirectional laminates tested in tension, temperature and moisture have little effect on the failure strain of the 0° plies.[27] If there are sufficient plies to carry load after the 0° ply failure substantial effects can be produced[27] by temperature and moisture (Fig 17). In compression, the fibres rely on the matrix to provide the support necessary to prevent fibre buckling; under hot/wet conditions the resin softens and the compression strength is reduced (Fig 18). In flexure, failure can in general be either on the tensile surface or on the compression surface. Since the compressive strength is reduced under hot/wet conditions, the flexural strength shows a similar trend[27] (Fig 19) and exhibits compression face failures. The effects of moisture and temperature on resin properties and resin dominated composite properties have been generalized[28] into a simple algebraic expression for incorporation into available composite micromechanics equations:

$$\frac{\text{wet resin mechanical property at test temperature}}{\text{dry resin mechanical property at room temperature}} \simeq \left[\frac{T_s - T}{T_s - T_o}\right]^{\frac{1}{2}} \tag{12}$$

where T_s is the Tg of the wet resin, T is the test temperature and T_o is 273K. This kind of relationship is shown in Fig 20 for unidirectional flexural strength, in-plane shear strength, in-plane shear modulus, transverse modulus and matrix tensile strength.

The bahaviour of composite materials when notched depends on the complex processes involved in creating damage zones at the notch tip. It is not obvious how these will be affected by the environment. Experiments with GRP have shown[29] that moisture can increase crack growth rate for cyclic loading but decrease the rate for static loading. Work with CFRP[30] indicated that plain unnotched laminates could be degraded by combinations of moisture and temperature, but that notched laminates tested in tension (a more design critical condition) was relatively insensitive to moisture contents and temperatures expected in service (including thermal spikes), and insensitive to preloads similar to what might be applied in a proof test. Similar conclusions were reached[31] after over 200 tests on various bolted joints (another possible critical design feature) after hygrothermal conditioning with and without thermal spikes - the maximum reduction from room temperature,dry performance to hot, wet performance was 18%.

7. ACCELERATED CONDITIONING

It has already been stated that under service conditions a component may take many years to reach its equilibrium moisture content. To test composite materials in a moist state they have to be conditioned at an elevated temperature in order to reduce the time. Boiling water has often been used as a quick method to condition specimens but it is not satisfactory because it tends to leach soluble components from the resin and fibre/resin interface. Conditioning is better done in warm, humid air and the most convenient way to control humidity is by the use of saturated salt solutions[4] such as NaCl (75% RH), NaNo3 (60% RH), MgCl2 (32% RH) and LiCl (12% RH).

In order to decide on the conditions for accelerated conditioning one needs to know the equilibrium moisture content and diffusion coefficient for various values of RH and temperature. These can be determined reasonably quickly[32] from a series of moisture uptake tests, and the moisture distribution through the thickness can be measured by a slicing technique. Laminates approach their equilibrium moisture contents assymptotically which means that in a constant environment the final stages can take a considerable time. However, using knowledge of diffusion kinetics and moisture distributions, faster conditioning procedures can be employed and in one example[33] a CFRP laminate was conditioned to a uniform moisture content of 1% in 60 days, instead of over 200 days, by using a three stage procedure (see Fig 21). Care has to be taken in accelerated conditioning that the moisture contents and temperatures used do not produce effects that are not representative of effects expected in service[25]. Tg forms an effective upper bound to the service envelope and accelerated ageing must also be realistic.

If relationships are known between time and temperature effects in tests such as creep tests, master curves of temperature and moisture-compensated creep strains (or moduli) versus time can be obtained. By performing short term (15 minutes) creep tests at different temperatures and by using transfer functions to shift the data parallel to the time axis, long time creep behaviour can be predicted[34,35,36]. These procedures are particularly useful for predicting visco-elastic behaviour such as in-plane shear behaviour under hot/wet conditions (Fig 22).

Some environmental changes occur during specific stages in the flight envelope of aircraft. If environmental changes influence fatigue performance it is difficult to accelerate the testing because of the diffusion processes involved. Simplified simulation of environmental changes allow higher loading frequencies to be used but the results need to be checked against "quasi real time" flight-by-flight tests incorporating temperature and humidity cycles[37]. These are tedious tests and on full scale structural components they are prohibitively expensive. For airworthiness clearance therefore simplified "standard" tests are required[38], or environmental test reduction factors[39]. Further information on environmental effects and accelerated ageing is required before such simplifications can be made with confidence.

8. NATURAL WEATHERING AND IN-SERVICE EXPERIENCE

The real test for advanced composites comes when they are used in-service, where they are subjected to all the natural hazards of service life. First there is sunlight, and it has been shown[40] that solar radiation has a significant effect on the moisture content of naturally weathered composites (Fig 23). Ultra-violet radiation can severely degrade epoxy resins but in composite materials this seems to be limited to the surface epoxy layer leaving the carbon, boron or glass fibre filaments unaffected[38]. Effective UV protection is readily achieved using the standard aircraft paints and no UV degradation has been observed in service.

Lightning strike is another hazard of the natural environment, with discharge currents of up to 200,000 amperes. Unprotected panels can be seriously degraded by lightning discharges[38]. However, surface protection can be provided by flame sprayed aluminium, aluminium wire mesh or co-cured aluminium foil. One problem with aluminium foil is that it is impervious to moisture; if moisture does get in at pinholes or where there has been surface damage and the temperature is subsequently increased, the moisture cannot get out and the foil can become blistered[12].

Erosion by rain or sand can be a serious hazard with both CFRP and GRP[41,42,43]; 500 hours of helicopter flight in a desert without repainting damaged paintwork resulted in 60% loss in thickness of the surface skin of a main rotor blade[41]. Sand erosion is by very small particles (<100μm) thrown up by the wind or the downdraught from the rotor blades. The airflow sweeps the particles to either side of the leading edge and causes erosion some distance from the leading edge depending on particle size and rotor blade speed; protection is needed for 40% of the chordwise distance[41]. Rain, being larger particles, causes erosion at the leading edge; the high pressures generated at the edges of the impinging drops cause pits, cracks and weight loss. Rain erosion is a fatigue process and there is a characteristic incubation period followed by a period of constant rate of weight loss[42]. For protection against erosion it is found that metal is more effective against rain whereas polyurethane thermoplastic coatings are more effective against sand[43]. Metal leading edge erosion strips are stainless steel or hot formed titanium and very careful surface preparation has to be used to avoid erosion strip delamination in service. Polyurethane coatings for sand erosion protection do not last indefinitely; with the BO-105 in Northern Europe repainting is necessary after 1000 hours service whereas in the Gulf of Mexico the coating has to be redone after only 300 hours. Coatings must be chosen with care - PTFE coatings on GRP were found to decrease the incubation period and to cause increased weight loss, because of stress waves set up in the coating[42]. Testing for erosion rates and protection schemes is done using a whirling arm in the appropriate environment; but more fundamental understanding is being learned by analysis of the erosion processes.

Galvanic corrosion can be a problem for metal matrix composites[44] or when carbon fibre or boron fibre composites are used in conjunction with metals in a structure. When two conductors are immersed in an electrolyte a voltage can be set up between them. If there is an electrically conducting path between them, a current will flow causing corrosion of one or both materials. The table gives the standard electrode potentials against a standard hydrogen electrode for a series of elements, and the galvanic series in a salt solution.

Standard electrode potential (Volts)		Galvanic series in salt solution (Volts)	
Gold	+1.5	Gold	+0.3
Carbon	>1.0	Carbon	?
Copper	+0.3	Titanium	+0.2
Iron	-0.4	Copper	0
Titanium	-1.6	Iron	-0.4
Aluminium	-1.7	Aluminium	-0.6
Magnesium	-2.3	Magnesium	-1.3

The galvanic series gives a truer idea of the potential difference in a corrosive environment, but the actual voltages will depend on the electrolyte. It can be seen that there is a serious problem if carbon fibre composites are used in conjunction with aluminium resulting in corrosion of the aluminium. A typical protection scheme would require all aluminium parts to be clad or anodized, all aluminium parts to be painted before assembly, and bondlines between the CFRP and aluminium to contain GRP, with overlap at the edges, to prevent electrical contact. Even so, problems can arise at fasteners and wet assembly would be recommended wherever possible to keep moisture out.

Carbon fibre reinforced aluminium suffers rapid corrosion at the interface in aqueous environments and adequate protection must be used. Boron fibres coupled to aluminium in a salt solution do not produce a galvanic current, but during high temperature fabrication intermetallic compounds are produced and boron/aluminium (B/Al) composites suffer preferential attack at the fibre/matrix interface. B/Al also suffers stress corrosion and delayed time fractures can result when the composite is loaded to over 80% of the fracture toughness; for loads corresponding to less than 80% of the fracture toughness no fractures are observed up to 1000 hours of sustained load.

Practical experience with advanced composite components has so far been uneventful. One report[45] states that up to 1980, over 200 composite components had given excellent service for 2.5 million total component hours and no significant degradation had been observed in residual strength of composite components or environmental exposure specimens after 5 years service or exposure. But the potential hazards need to be recognized and related to the details of each new design.

9. CONCLUDING REMARKS

Practical experience with advanced composite materials in service over the past decade has increased confidence in their use in the real environment. There are still some unresolved problems with thermal spikes during sypersonic flight.

However present designs use conservatively low values of design strain, partly to allow for environmental effects. More efficient use of composite components will result in increased strains and increased temperatures. There will be a need to know more about the behaviour of individual fibre/matrix system and the development of resins that absorb less moisture might offer advantages.

Clearance procedures to allow for environmental effects on structural components should concentrate on those critical features of the design which might be affected by the environment.

REFERENCES

1   W.W. Wright.   The effect of diffusion of water into epoxy resins and their carbon-fibre reinforced
    composites.   Composites 201-205 (1981).

2   C. Shen, G.S. Springer.   Moisture absorption and desorption of composite materials.   J. Composite
    Materials, 10, 2-20 (1976).

3   E.L. McKague, J.D. Reynolds, J.E. Halkias.   Moisture diffusion in fiber reinforced plastics.
    Trans. ASME Journal of Engineering Materials and Technology, 92-95, January (1976).

4   P. Bonniau, A.R. Bunsell.   A comparative study of water absorption theories applied to glass epoxy
    composites.   J. Composite Materials, 15, 272-293 (1981).

5   J.M. Whitney.   Three-dimensional moisture diffusion in laminated composites.   AIAA Journal 15,
    1356-1358 (1977).

6   J.M. Augl.   Private communication.

7   Y.A. Tajima.   The diffusion of moisture in graphite fiber reinforced epoxy laminates.   SAMPE Quarterly
    11, 1-9 (1980).

8   P.T. Curtis.   A BASIC computer program to calculate moisture content in resins and fibre reinforced
    resin composites.   RAE Unpublished Memorandum (1981).

9   H.G. Carter, K.G. Kibler.   Langmuir-type model for anomalous moisture diffusion in composite resins.
    J. Composite Materials 12, 118-131 (1978).

10 O. Gillat, L.J. Broutman.   Effect of an external stress on moisture diffusion and degradation in a
    graphite-reinforced epoxy laminate, in Advanced Composite Materials - environmental effects.   ASTM
    STP 658 (1978).

11 R.A. Garrett, R.E. Bohlmann, E.A. Derby.   Analysis and test of graphite/epoxy sandwich panels subjected
    to internal premises resulting from absorbed moisture, in Advanced Composite Materials - environmental
    effects.   ASTM STP 658 (1978).

12 H.W. Bergmann, P. Nitsch.   Predictability of moisture absorption in graphite/epoxy sandwich panels.
    AGARD Conference proceedings No 288, Athens (1980).

13 H.T. Hahn, R.Y. Kim.   Swelling of composite laminates, in Advanced Composite Materials - environmental
    effects.   ASTM STP 658 (1978).

14 M.L. Williams, R.F. Landel, J.D. Ferry.   The temperature dependence of relaxation mechanisms in
    amorphous polymers and other glass-forming liquids.   J. Am. Chem. Soc., 77, 3701 (1955).

15 F. Bueche.   Physical properties of polymers.   Interscience Publishers, London (1962).

16 H.G. Carter, K.G. Kibler.   Entropy model for glass transition in wet resins and composites.
    J. Composite Materials, 11, 265-275 (1977).

17 P.E. McMahon.   Oxidative resistance of carbon fibres and their composites, in Advanced Composite
    Materials - environmental effects.   ASTM STP 658 (1978).

18 H. Ishida, J.L. Koenig.   The reinforcement mechanism of fibre-glass reinforced plastics under wet
    conditions.   Polym. Eng. Sci. 18, 128 (1978).

19 N.R. Farrar, K.H.G. Ashbee.   Destruction of epoxy resins and of glass-fibre-reinforced epoxy resins
    by diffused water.   J. Phys. D. Appl. Phys., 11, 1009 (1978).

20 F.R. Jones.   Stress corrosion in GRP laminates.   University of Surrey Course on The technology of
    fibre-reinforced plastics composites: processing and quality assurance, Guildford (1982).

21 D.V. Dunford, J. Harvey, J. Hutchings, C.H. Judge.   The effect of surface treatment of type 2 carbon
    fibre on CFRP properties.   RAE TR 81096 (1981).

22 P.T. Curtis.   Residual strains and the effects of moisture in fibre reinforced laminates.   RAE TR 80045
    (1980).

23 C.D. Shirrell, J. Halpin.   Moisture absorption and desorption in epoxy composite laminates, in
    Composite Materials: testing and design.   ASTM STP 617 (1977).

24 E.L. McKague, J.E. Halkias, J.D. Reynolds.   Moisture in composites: the effect of supersonic service
    on diffusion.   J. Composite Materials 9, 2-9 (1975).

25 E.L. McKague.   Environmental synergism and simulation in resin matrix composites, in Advanced
    Composites - environmental effects.   ASTM STP 658 (1978).

26 R. DeIasi, J.B. Whiteside.   Effect of moisture on epoxy resins and composites, in Advanced Composite
    Materials - environmental effects.   ASTM STP 658 (1978).

27 C.E. Browning, G.E. Husman, J.M. Whitney.   Moisture effects in epoxy matrix composites, in Composite
    Materials: testing and design.   ASTM, STP 617 (1977).

28 C.C. Chamis, R.F. Lark, J.H. Sinclair. Integrated theory for predicting the hygrothermomechanical response of advanced composite structural components, in Advanced Composite Materials - *environmental effects*. ASTM, STP 658 (1978).

29 J.F. Mandell, F.J. McGarry, D.S. Barton, R.P. Demchick. Effect of water on the crack prapagation rate in fiberglass laminates under static and dynamic loading. Report MITSG-75-18 (1975).

30 T.R. Porter. Environmental effects on composite fracture behaviour, in Test methods and design allowables for fibrous composites. ASTM, STP 734 (1981).

31 D.J. Wilkins. Environmental sensitivity tests of graphite-epoxy bolt bearing properties, in Composite materials: testing and design. ASTM, STP 617 (1977).

32 S.M. Copley, T.A. Collings. The determination of through-thickness moisture distribution and diffusion coefficients in fibre reinforced plastic laimnates. RAE TR 81105 (1981).

33 S.M. Copley. A computer program to model moisture diffusion and its application to accelerated ageing of composites. RAE TR 82010 (1982).

34 F.W. Crossman, R.E. Mauri, W.J. Warren. Moisture-altered viscoelastic response of graphite/epoxy composites, in Advanced Composite Materials - environmental effects. ASTM, STP 658 (1978).

35 H.F. Brinson, D.H. Morris, Y.T. Yeow. A new experimental method for accelerated characterization of composite materials. VDI Berichte 313 (1978).

36 K.G. Kibler. Effects of temperature and moisture on the creep compliance of graphite-epoxy composites. AGARD Conference proceedings No. 288, Athens (1980).

37 J.J. Gerharz, D. Schutz. Fatigue strength of CFRP under combined flight-by-flight loading and flight-by-flight temperature changes. AGARD Conference proceedings No. 288, Athens (1980).

38 I.G. Hedrick, J.B. Whiteside. Effects of environment on advanced composite structures, AIAA conference on aircraft composites: the emerging methodology for structural assurance, San Diego (1977).

39 J.C. Ekvall, C.F. Griffin. Design allowables for T300/5208 graphite/epoxy composite materials. AIAA 416-422 (1981).

40 E.C. Edge. The implications of laboratory accelerated conditioning of carbon fibre composites. AGARD Conference proceedings No. 288, Athens, (1980).

41 K. Brunsch. Service experience with GRC helicopter blades (BO-105), AGARD Conference proceedings No. 288, Athens (1980).

42 G.S. Springer. Erosion of composite materials. AGARD Conference proceedings No. 288, Athens (1980).

43 M. Torres. Erosion et impacts sur les pales d'helicopteres en composites. AGARD Conference proceedings No. 288, Athens (1980).

44 B. Harris. The promise and realities of fibre composites. The Metallurgist and Materials Technologist 77-81, February (1981).

45 H.B. Dexter. Composite components on commercial aircraft. AGARD Conference proceedings No 288, Athens (1980).
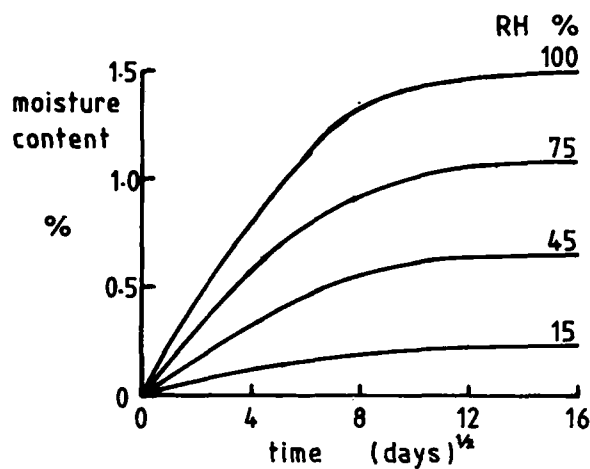
Fig 1 Moisture uptake by CFRP laminate
2 mm thick in environments with
different relative humidities - 25°C
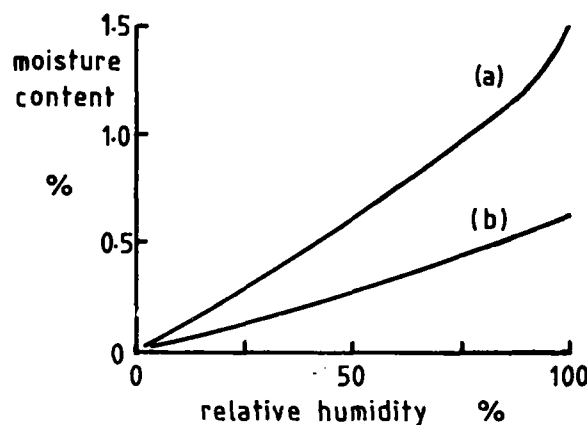
Fig 2 Effect of relative humidity on
equilibrium moisture content of CFRP
(a) MY 720 based resin matrix
(b) MY 750 based resin matrix

$D = D_o \exp(-E/RT)$

$E = 11$ kcal/mole
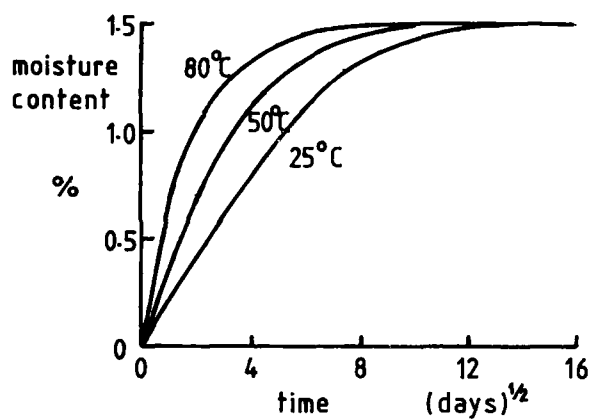
Fig 3 Moisture uptake by CFRP laminate
2 mm thick at different temperatures -
100% RH
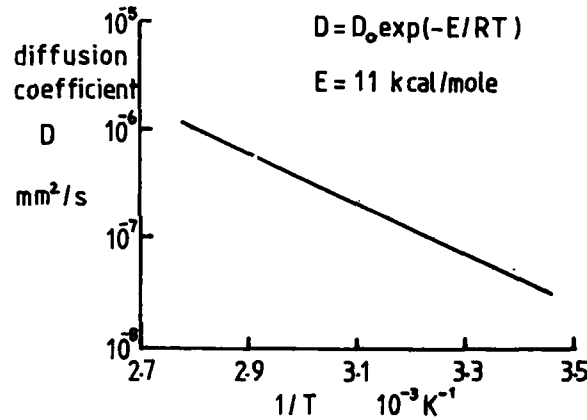
Fig 4 Relationship between diffusion
coefficient and temperature for CFRP
laminates
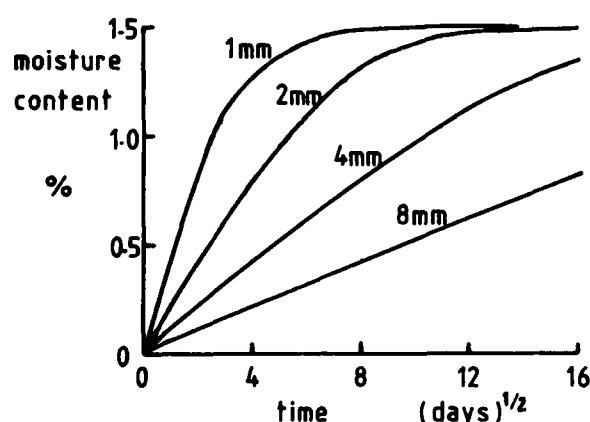
Fig 5 Moisture uptake by CFRP laminates
of different thicknesses -
25°C 100% RH
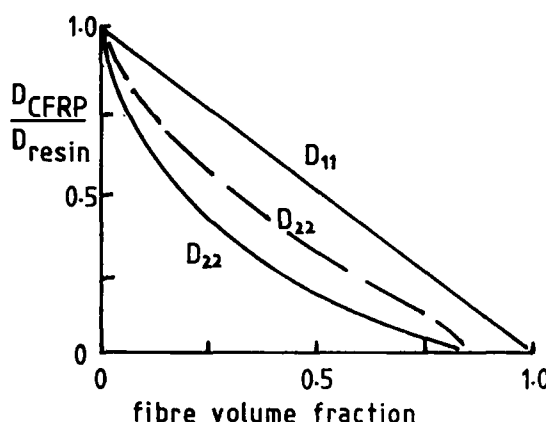
Fig 6 Diffusion coefficients in CFRP
———— after Shen and Springer
— — after Augl
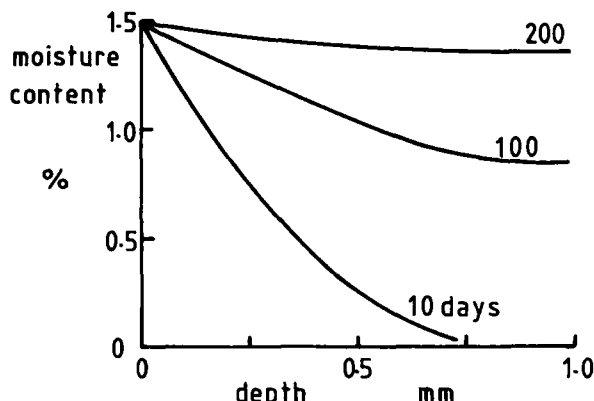
Fig 7 Distribution of moisture through thickness of CFRP laminate 2 mm thick 25°C, 100 % RH
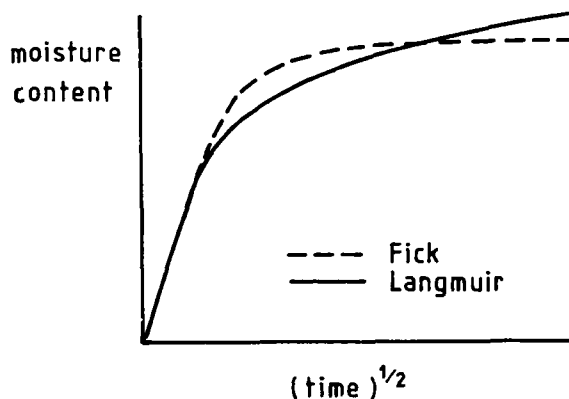
Fig 8 Comparison of moisture uptake for classical Fickian diffusion and anomalous Langmuir diffusion
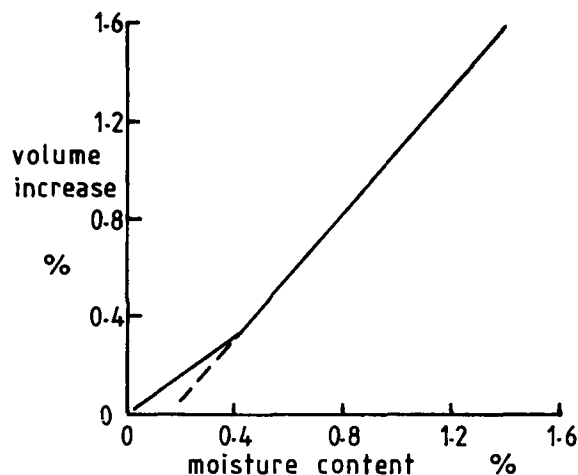
Fig 9 Swelling of CFRP composite with moisture uptake
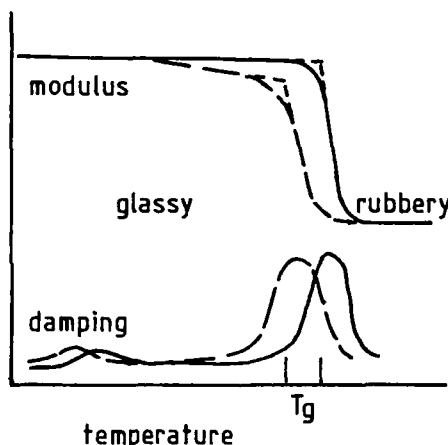
Fig 10 Effect of moisture on torsional damping of epoxy resins
——— dry ——— wet
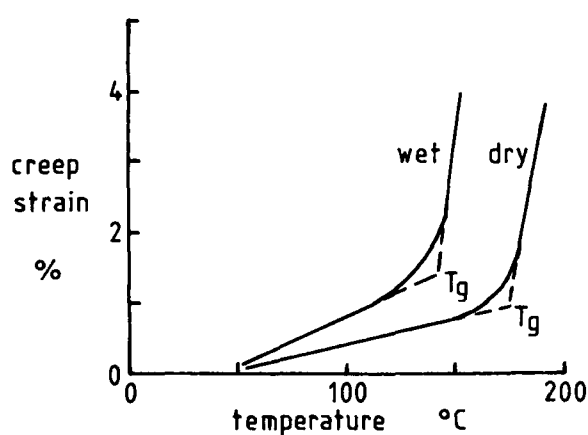
Fig 11 Effect of moisture on creep strain of $[(\pm45)_2]_s$ CFRP laminate under constant heating rate
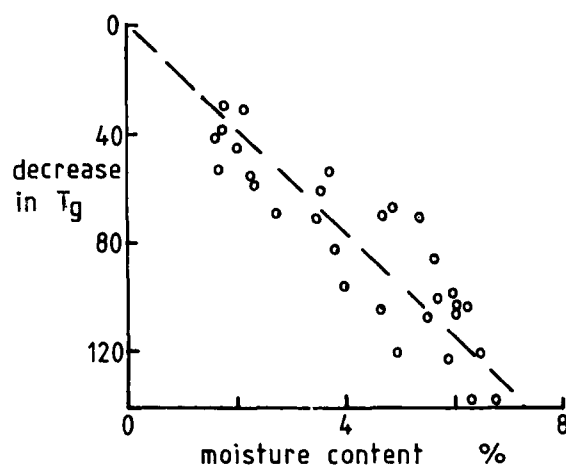
Fig 12 Decrease in Tg with moisture uptake for different epoxy resins
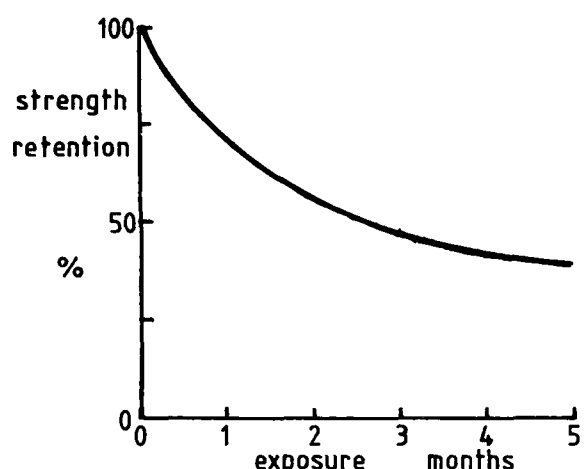
Fig 13 Effect of outdoor weathering on the tensile strength of aramid fibre yarn
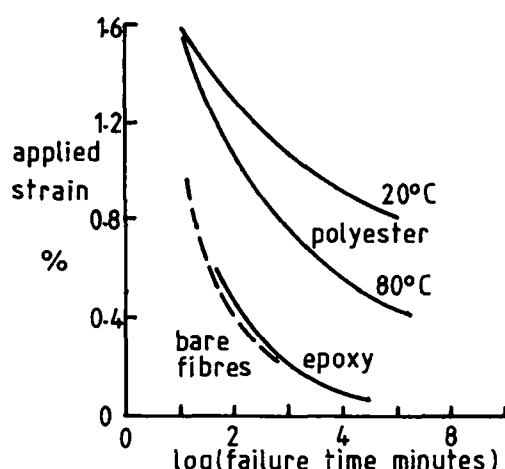
Fig 14 Stress corrosion of glass fibres and GRP in an acid environment
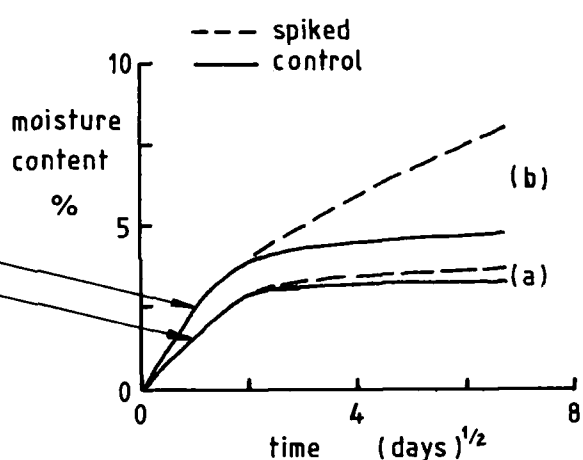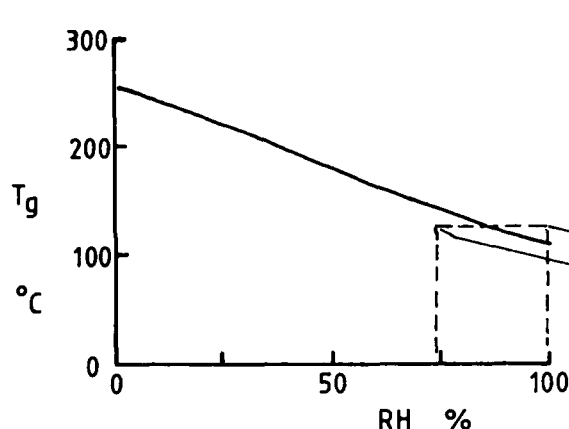
Fig 15 Effect of thermal spikes on moisture uptake in an epoxy resin. Specimens conditioned at 65°C and spiked twice weekly to 125°C (a) 74 % RH (below Tg) (b) 100 % RH (above Tg) (after McKague)
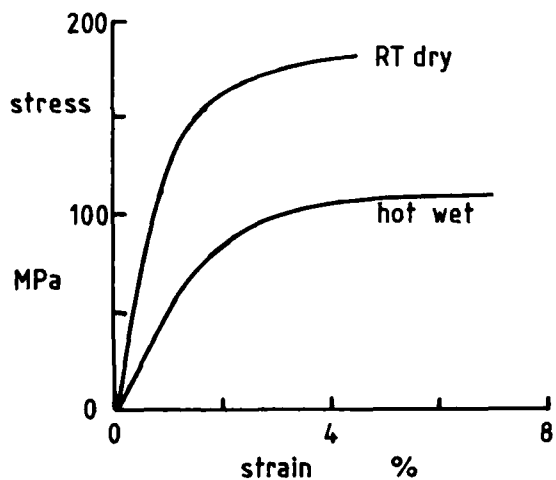
Fig 16 Stress-strain curves for [(±45)$_2$]$_s$ CFRP laminate (hot - 130°C) (wet - 1.5 % moisture)
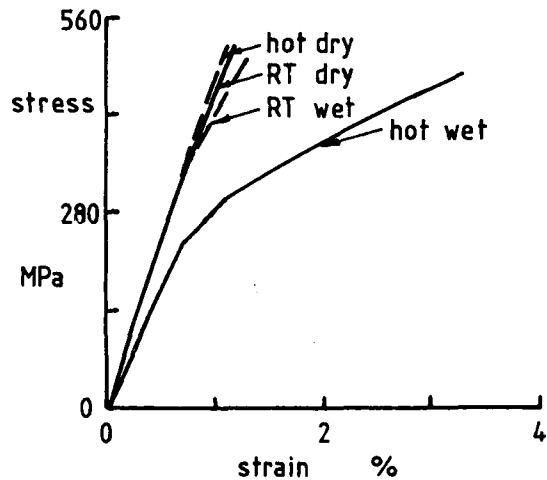
Fig 17 Stress-strain curves for [0 ±45 90]$_s$ CFRP laminate (hot - 120°C) (wet - 1.05 % moisture)
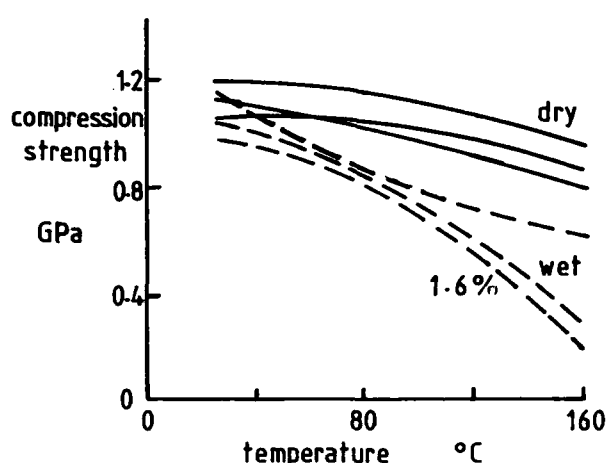
Fig 18 High temperature compression strength of dry and wet unidirectional CFRP laminates
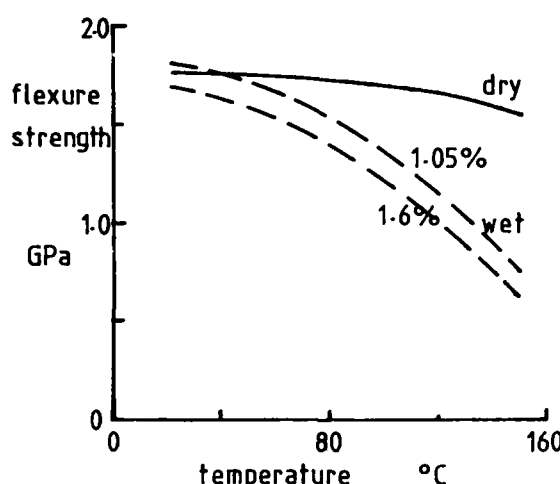
Fig 19 High temperature flexural strength of dry and wet unidirectional CFRP laminates
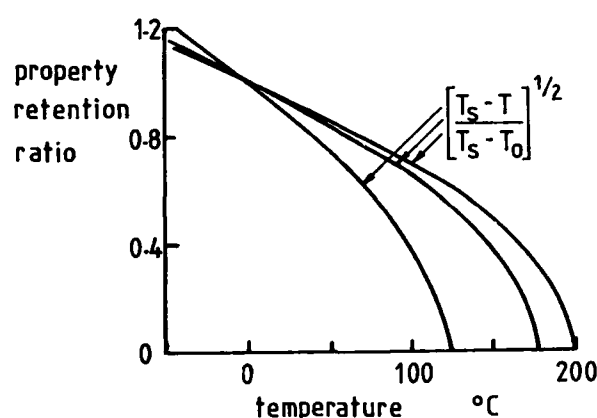
Fig 20 Generalized effect of temperature and Tg on matrix-dominated properties of composites (after Chamis et al)
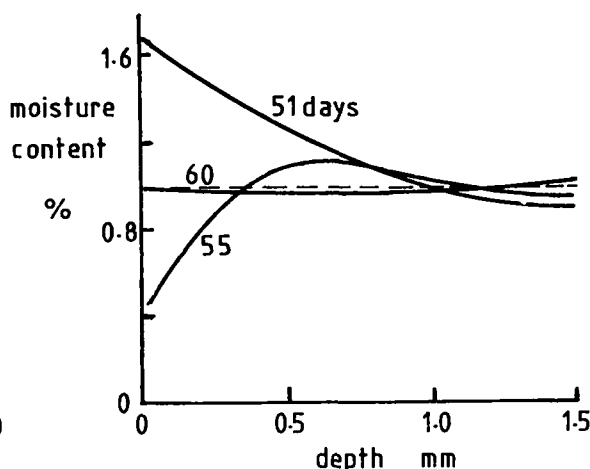
Fig 21 Accelerated conditioning to get uniform 1 % moisture content (60°C 51 days 95 % RH, 4 days 26 % RH and 5 days 56 % RH)
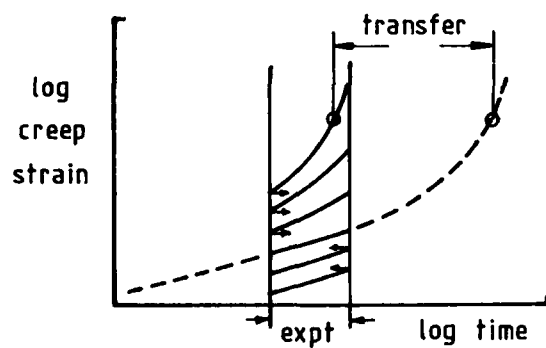
Fig 22 Generation of master curve from short term experiments
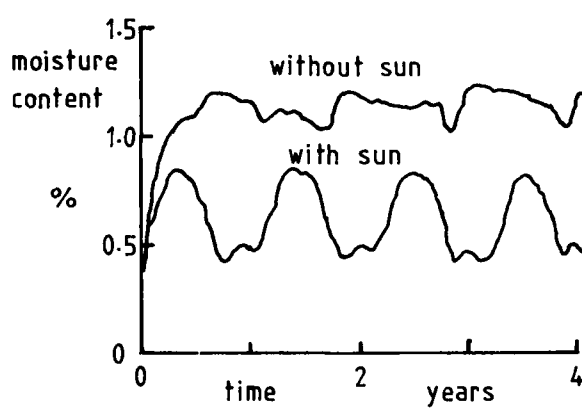
Fig 23 Effect of sunlight on moisture content during outdoor weathering

MANUFACTURING PROCESSES FOR
AERONAUTICAL STRUCTURES*

Richard Hadcock, Director
Advanced Development
John Huber, Section Head
Automated Manufacturing Systems Development
Grumman Aerospace Corporation
Bethpage, New York 11714, U.S.A.

SUMMARY

Current manufacturing processes for fabricating composite aeronautical structures are reviewed. Laminating, autoclave curing, hot press molding, injection molding, pultrusion, drilling and trimming are discussed for three principal composite materials - boron/epoxy, graphite/epoxy and Kevlar/epoxy. Emphasis is placed on the unique manufacturing operations associated with each type of material up to and including the curing process. The effect of various tooling concepts and materials on production rates and costs is discussed. Unique processing equipment developed for the several composite materials forms available is described.

Manufacturing sequences for composite structures are compared to those for conventional metal structures. The effect of prepreg "out-time" and relatively slow curing cycles is identified for such typical production plant operations as shop loading, part storage and material tracking.

Tooling needed to produce quality composite structures is discussed. Major layup and curing tools for large aerospace components such as skins and wing covers are emphasized. The advantages and disadvantages of alternative tooling materials with respect to part configuration, curing temperature and production rate are presented.

The effect of various material forms (e.g., unidirectional tape and woven broadgoods) on production methods and facilities is discussed. Particular emphasis is placed on mechanized equipment to lay tape, dispense broadgoods and trim the laid-up prepreg plies. Laser, high-pressure water-jet and reciprocating-cutter trimming methods are analyzed with respect to the equipment, feed rates and potential benefits unique to each process. Special controls and/or programming needs are highlighted, where applicable, for each trimming operation.

Curing processes for both autoclave- and press-fabricated composite parts are described. Preparatory operations, such as vacuum bagging and bleeder application, as well as process cycle times, temperatures and pressures, are discussed for various types of curing methods. The specialized machining requirements for cured composite parts are also discussed, especially with respect to drilling and trimming operations.

Key cost elements associated with the individual composite manufacturing operations, such as laminating/dispensing, contour forming, trimming, handling and curing, are analyzed. Special emphasis is placed on the effects of automation on the various processing costs for several selected applications.

INTRODUCTION

The application of composites to aerospace structures has been one of the most significant technology developments during the past twenty years. Composite technology has reached a level of maturity which has led to the use of composite stabilizers on all United States fighter aircraft since 1970 (F-14A, F-15, F-16, YF-17, F-18). F-18 wing covers and the covers and substructure of a V/STOL attack aircraft (AV-8B) are being made from graphite/epoxy composite material. The next generation of commercial aircraft (Boeing 757 and 767) will use composites for such secondary structural parts as ailerons, elevators, rudders and spoilers.

The manufacturing processes needed to fabricate these structures have begun change the traditional aircraft production factory. The fabrication of composite structure has moved from a minor function to produce secondary components to a key element in fabricating new high-performance aircraft. Future projections indicate that composite manufacturing will become a principal factor in the cost of these new structures.

A typical composite manufacturing flow with associated key features is shown in Fig. 1. The principal difference between the production flow for composite structure and that for traditional metal structure is the need to perform the composite prepreg operations within a predetermined time to ensure proper curing of the organic-matrix material (Fig. 2) in a controlled environment. This requires a more disciplined approach to the manufacturing cycle than is used with metal structures.

- - - - -

*The referenced background information presented in this paper is in the public domain.

```
┌─────────┐
│ PREPREG │        NESTED BROADGOODS, TAPE LAYING,
│ LAYUP   │
└────┬────┘
     │
┌────▼────┐
│ PREPREG │        MANUAL, RECIPRO KNIFE, WATER JET, LASER, BLANKING
│ TRIM    │
└────┬────┘
     │
┌────▼────┐
│ STACK   │        MANUAL, ROBOTIC, VACUUM LIFT
│ PLIES   │
└────┬────┘
     │
┌────▼────┐
│  CURE   │        AUTOCLAVE, PRESS
│         │
└────┬────┘
     │
┌────▼────┐
│  TRIM   │        SAW, ROUTER, WATER JET
│         │
└────┬────┘
     │
┌────▼────┐
│ASSEMBLE │        DRILL, SHIM, BOND
│         │
└─────────┘
```
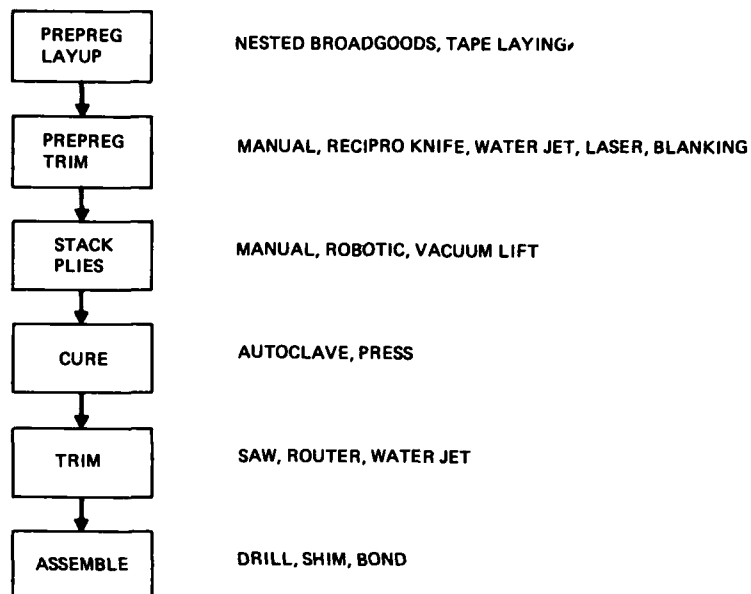
Fig. 1 Composites Manufacturing Flow

METALS   SCHEDULE FLEXIBILITY

```
        STORE    STORE    STORE    STORE    STORE

SHEAR   ROUTE    DRILL    FORM    PAINT    ASSEMBLE
```

COMPOSITES

SCHEDULE CONSTRAINED TO PROCESS REQUIREMENTS

```
LAYUP    TRIM    STACK    FORM    BAG    CURE
```
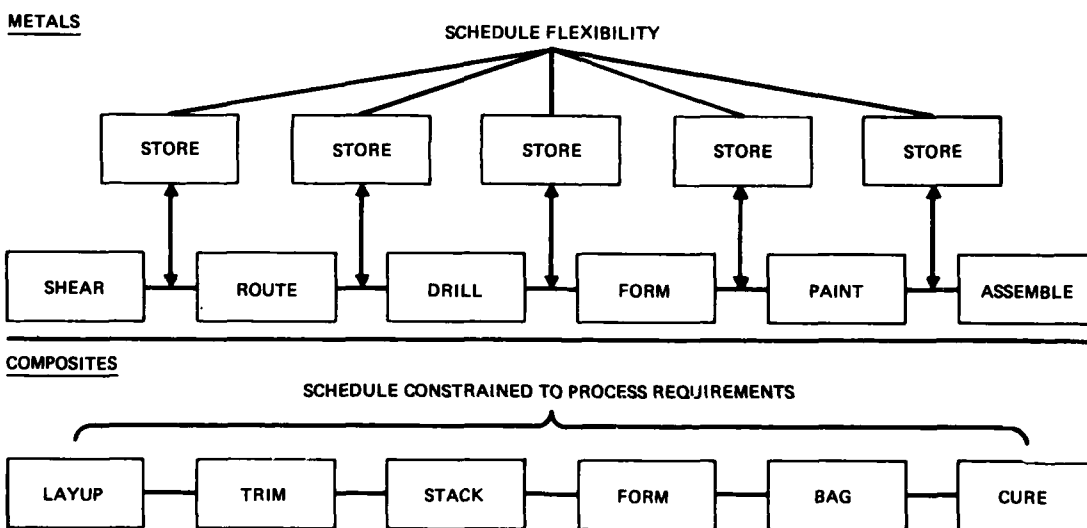
Fig. 2 Comparison of Metals and Composites Scheduling

BASIC MANUFACTURING PROCESSES

The basic manufacturing processes used to fabricate aircraft structures for the purpose of this presentation will be divided into the following three elements:

- **Bulk Processing** – general-purpose commercial processes used for high volume production that do not control fiber orientation as is generally required in typical aircraft composite layups. The two bulk processing methods considered most applicable to aircraft structures are injection molding and compression molding

- **Laminate Buildup** – those processes associated with controlled orientation of fibers. The three most applicable processing approaches are filament winding, pultrusion and layup of tape/broadgoods prepreg

- **Post-Cure Operations** – those processes utilized after a component is cured, such as trimming and drilling.

Bulk Processing

The two primary, bulk processing methods used in the manufacture of aircraft components are injection molding and compression molding. Injection molding, illustrated

schematically in Fig. 3, involves the heating of a measured charge of thermosetting plastic or thermoplastic molding compound in a chamber to a plastic or viscous state followed by flow, under high pressure, through a nozzle into the sprues, runners, gates and cavities of a mold. After rapid solidification of the material, the mold is opened and the part or parts are ejected. The main advantages of injection molding are high production rates, low per-part cost, little or no post-molded finishing, good dimensional accuracy, capability to produce complex shapes and good surface finish. The primary limitations of this process are high initial tooling costs and high per-part cost on short production runs. The most commonly used materials for aircraft applications are acrylic, polycarbonate, polysulfone, nylon, acetal, and filled (glass, graphite) versions of these materials. Typical injection molded aircraft components are shown in Fig. 4. In summary, injection molding involves the use of commercially available equipment to produce finished complex components at high rates. The primary limitation on the use of the process to produce typical, low production-run aircraft components is the high cost of the molds or tooling required.
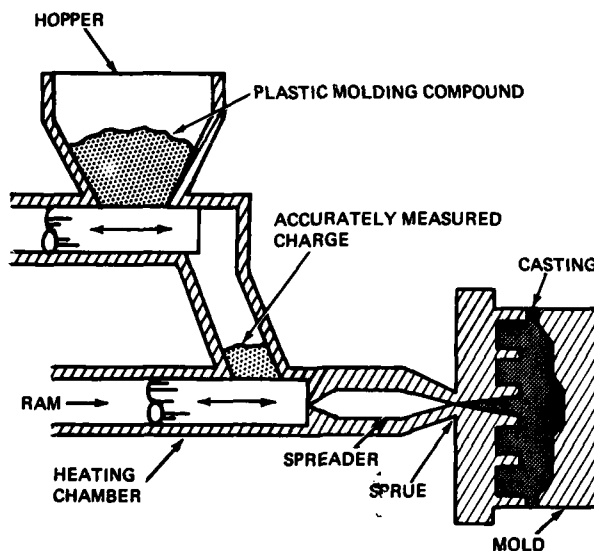
Fig. 3 Schematic Representation of Injection Molding Process

Fig. 4 Typical Injection Molded Aircraft Parts

Compression molding involves the placement of thermoplastic or partially polymerized, thermosetting plastic compounds, often filled with chopped reinforcing fibers, in a heated mold cavity (Fig. 5), followed by closing of the mold and application of heat/ pressure until the molding compound flows to fill the mold cavity and cures to form a rigid, polymerized part. The main advantages of compression molding are minimal material waste, low finishing costs and applicability to large bulky parts. Principal limitations of this process are its impracticality for extremely intricate parts involving undercuts, side draws, small holes or delicate inserts. Commonly used materials for aircraft applications are phenolics, allyl diglycol carbonates, diallyl phthalates, epoxies, and polyesters. Typical compression molded components are shown in Fig. 6. In summary, compression molding provides a cost-effective approach for producing low-production-rate, secondary structural components.
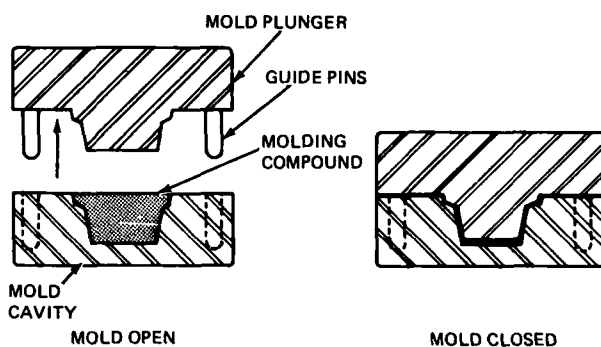
Fig. 5 Schematic Representation of
Compression Molding Process
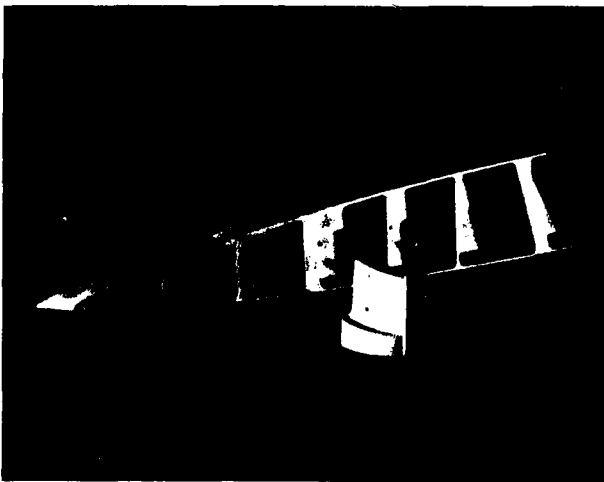
Fig. 6 Typical Compression Molded Aircraft
Parts

Laminate Buildup

There are three principal classes of processing that provide controlled fiber orientation through the buildup of a required laminate. They are:

- Filament winding

- Pultrusion

- Layup of tape/broadgoods prepreg.

Filament winding (Fig. 7) uses a narrow ribbon of filaments or fibers as the material form. The dry fibers are fed through a resin bath and wound at a controlled tension and direction onto a rotating tool or mandrel. The wound component is then bagged and cured in an autoclave. Fiberglass, Kevlar and graphite are applicable fibers. The most successful application to date has been pressure vessels; some development work is being done on helicopter tail booms and rotor blades. The principal advantage of filament winding is that it provides a fully mechanized approach to the fabrication of highly contoured structures. The main disadvantage is that a filament wound structure is most efficient when there is a minimum of cutouts in the structure. As a result, severe weight penalties can be encountered in more complex aircraft structures.
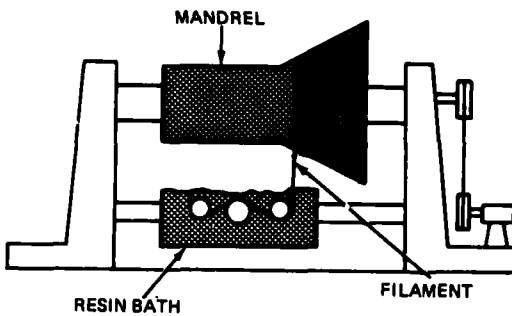
Fig. 7   Schematic Representation of
Filament Winding Process

The pultrusion process (Fig. 8) generally uses unidirectional tape or fibers which are wetted in the matrix resin, wound on the desired mandrel shape, pulled through a die similar to an extrusion die to compact the plies to the desired shape, and rapidly cured with a high-frequency or a microwave energy source. Fiberglass, Kevlar and graphite are applicable fiber materials. Tne principal advantage of pultrusion is that it provides a high-volume, low-cost, continuous, fully mechanized process. The main disadvantage is that the process can be applied only to constant-section and constant-thickness members. It should be noted that most aircraft applications require tapered sections with varying thicknesses along the section for optimum design. Consequently, the general application of pultrusion has been somewhat limited to date. The most promising area of potential application appears to be in large transport aircraft.
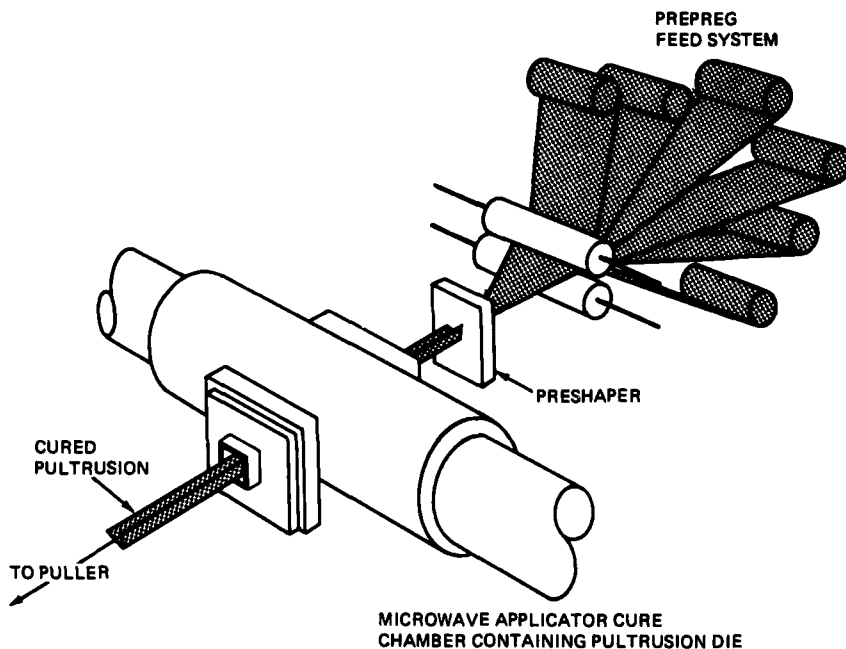
Fig. 8   Schematic Representation of Pultrusion Process

Prepreg layup is the principal manufacturing process used to fabricate compos: components at the present time. The two principal material forms are unidirectional tape and woven broadgoods. The general advantages and disadvantages of each form are shown in Fig. 9. The mechanical property variations are controlled by preimpregnating the fibers with stageable epoxy resins to form prepregs. The materials are molded at temperatures of 250° to 350°F. The principal layup operations are:

- **Ply Layup** - This is accomplished by laying up either unidirectional tape or broadgoods materials in a predetermined orientation to make a ply. The tape laying function can be accomplished manually by laying the material on Mylar templates (Fig. 10) or automatically using a tape laying machine (Fig. 11).

- **Ply Trimming** - This operation involves cutting the prepreg material to the proper geometric configuration. This is accomplished by either manually cutting the prepreg tape or broadgoods with a template or using numerically controlled cutting equipment.

- **Ply Stacking** _ This operation involves the sequential stacking of plies onto a mold form or tool to build up a desired composite laminate. This can be accomplished manually (Fig. 12) or by mechanized methods.

- **Laminate Bagging** - Once the plies are stacked on a mold form, the required number of bleeder plies used to absorb excess resin are added to the laminate and an air-tight nylon film covering is placed over the layup and sealed. Vacuum is then applied to the assembly. For thick sections, intermediate vacuum bagging with heat may be required to assure satisfactory precompaction.

- **Curing** - The mold form and vacuum bagged layup are placed in an autoclave for the necessary pressure/temperature cycle to cure the matrix material being used. Typical cure cycles for the most commonly used prepreg materials are illustrated in Fig. 13. The types of tooling applicable to these operations, together with their advantages and disadvantages, are listed in Fig. 14.

MATERIAL FORM	ADVANTAGES	DISADVANTAGES
UNIDIRECTIONAL TAPE	• LESS MATL WASTE • HIGHER STRENGTH PARTS • GREATER DESIGN FLEXIBILITY	• MORE LABOR-INTENSIVE
WOVEN BROADGOODS	• LESS LABOR • EASIER HANDLING	• LOWER STRENGTH PARTS • MORE MATL WASTE

Fig. 9   Advantages and Disadvantages of Tape and Woven Broadgoods
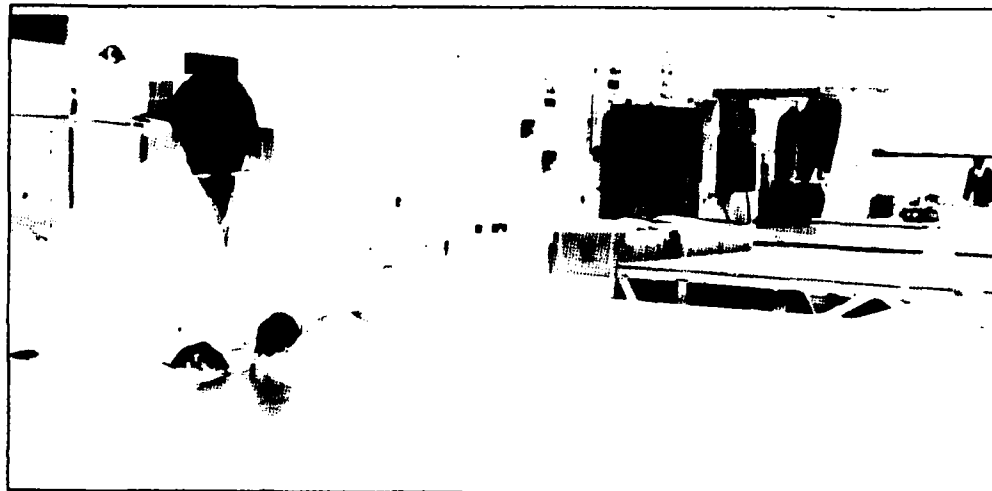

Fig. 10   Manual Ply Layup Operation
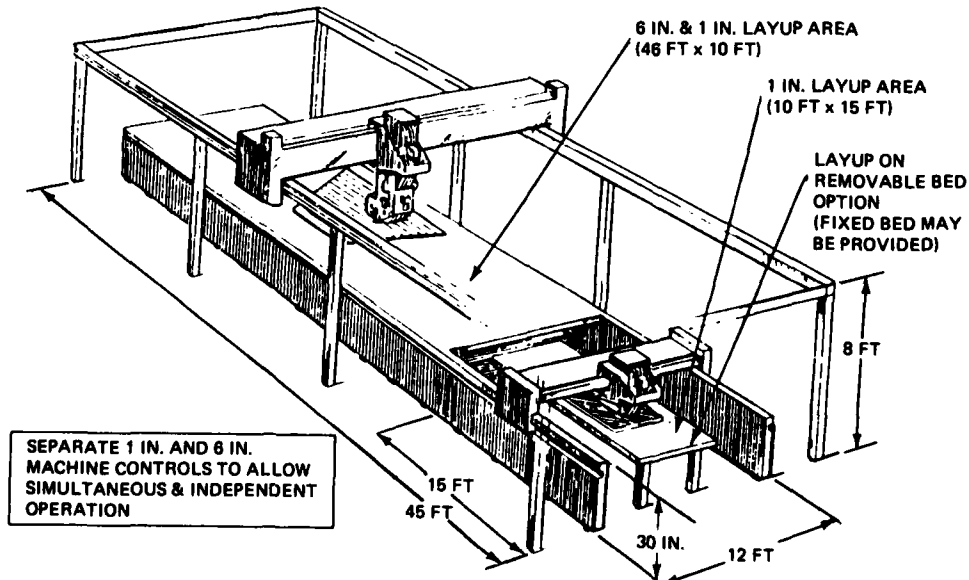

Fig. 11   Automated Tape Laying Machine
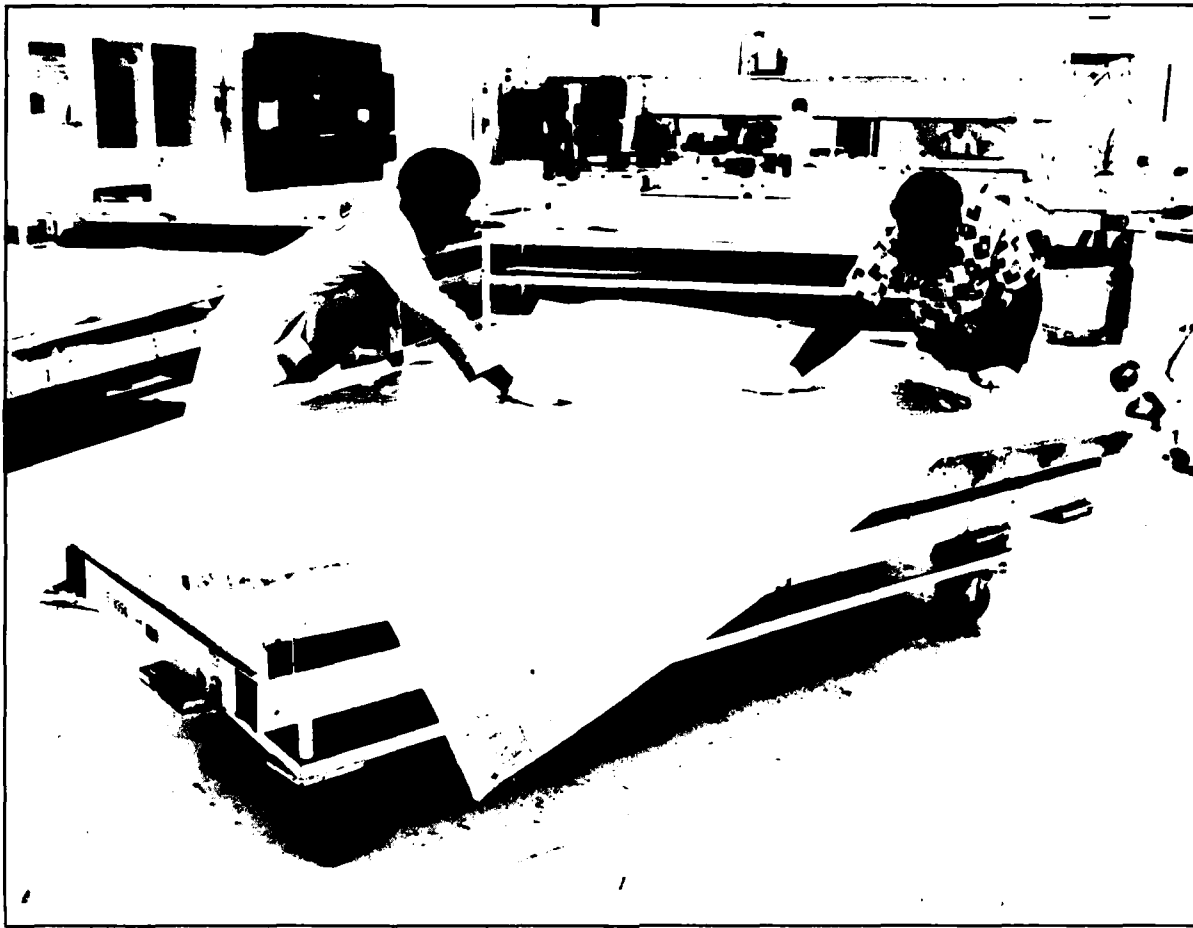
Fig. 12 Manual Ply Stacking
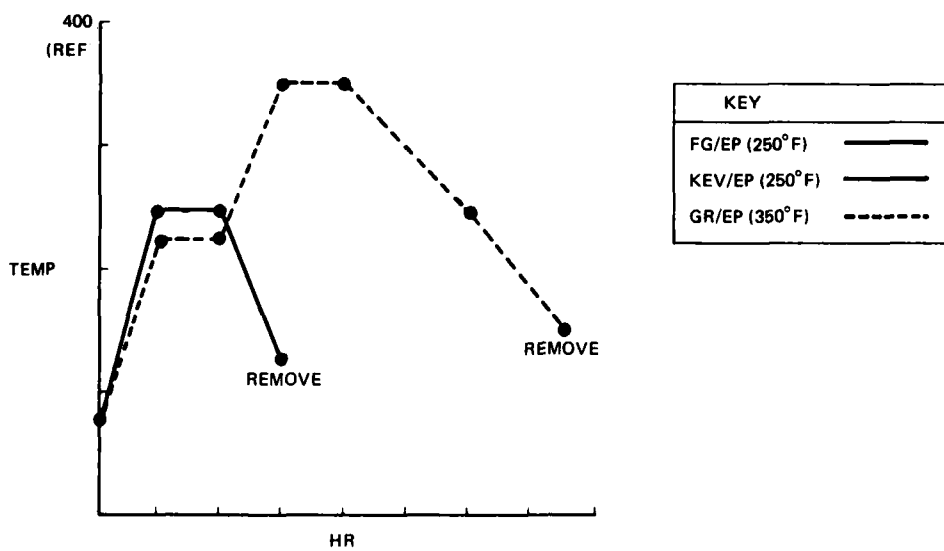
Fig. 13 Typical Cure Cycles for
Composite Prepreg
Materials

MATERIAL	ADVANTAGES	DISADVANTAGES
NICKEL PLATE	• MOLD TO SHAPE • DURABLE	• COST
HIGH-TEMP EPOXY	• MOLD TO SHAPE	• MAINTENANCE • SLOW HEAT-UP
ALUMINUM	• MACHINABLE • RAPID HEAT-UP	• HIGH COEFF EXP
STEEL	• STABLE	• COST • SLOW HEAT-UP

Fig. 14 Comparison of Composite Tooling Materials

Automation of prepreg fabrication operations has been a key goal of most aircraft manufacturers because these operations generally represent over 50% of the labor required to produce these components. Grumman's initial effort was directed at automating the production of the boron/epoxy covers for its F-14A horizontal stabilizer (Fig. 15), the first production application of advanced composites. The approach taken was started in 1974 and was based on cost data accumulated on 150 shipsets in production. The production labor distribution is shown in Fig. 16. This situation together with a projected need to produce a 27-ft-long composite stabilizer for the B-1 bomber led to the development of the Integrated Laminating Center (ILC) (Fig. 17). The ILC is a modular manufacturing system that can be readily expanded to handle a wide variety of aircraft covers or skins. The system functions in the following manner: The transfer gantry, shown in the parked position between the tape layup station and laser trimming station, moves toward the end of the layup table, grasps a tape carrier material (paper) and pulls it over the table. The paper carrier is then cut off with a traveling rotary knife. With the transfer gantry back in its original position, the tape layup gantry (Fig. 18) moves over the tape layup table dispensing 3-in.-wide boron/epoxy (prepreg tape) onto the carrier paper which is held in place with a vacuum. The tape dispensing head is a four-axis controlled machine (X and Y gantry position coordinates, alpha fiber angular orientation and beta tape cutoff shear angle).

When the preprogrammed ply has been completed, the tape laying gantry returns to the park position. The transfer gantry then moves over the tape layup table, grips the next piece of carrier paper, uses its vacuum to pick up the first ply on the tape layup table, pulls out the carrier paper and cuts it off. The transfer gantry releases the carrier paper and moves over the trim table. The first ply is deposited on the trim table, while the tape laying head moves up to lay the second ply on the layup table. The transfer gantry moves back to park while the trim gantry moves up to make a final net trim on the first ply. Trimming is performed using a continuous-wave, CO_2 laser (Fig. 19). Once the preprogrammed trim is accomplished, the excess material is removed manually, the part is inspected and, if acceptable, the trim table is rotated 180 degrees to place the ply on the mold form (Fig. 20). A mechanical bar pushes the ply onto the mold form as the vacuum is released. The table then returns to its normal position and the cycle continues until the preprogrammed laminate has been built.
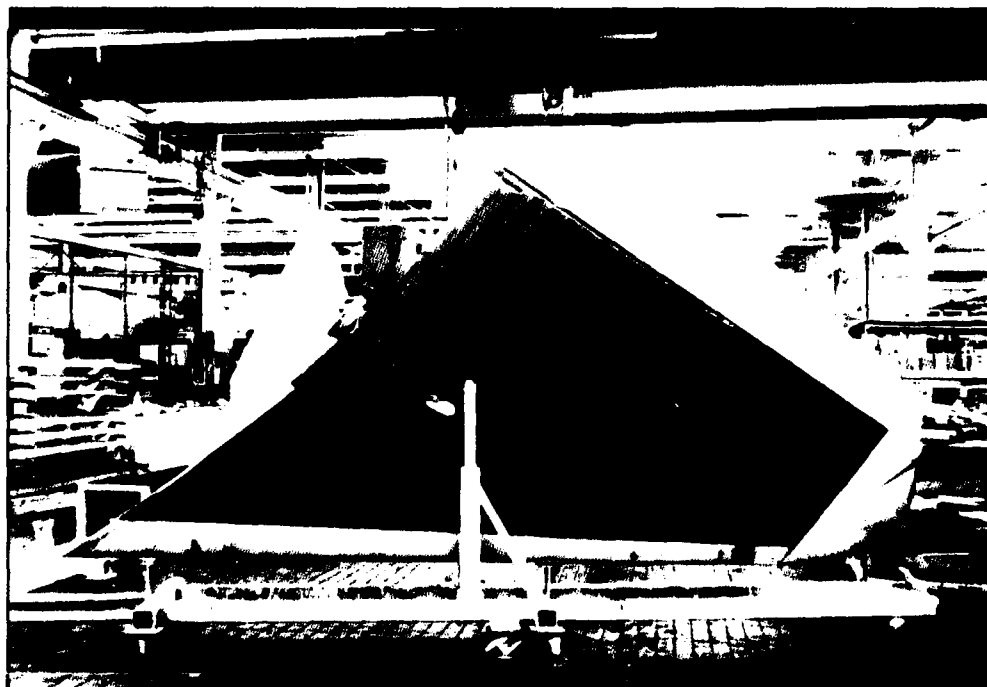

Fig. 15 F-14A Horizontal Stabilizer
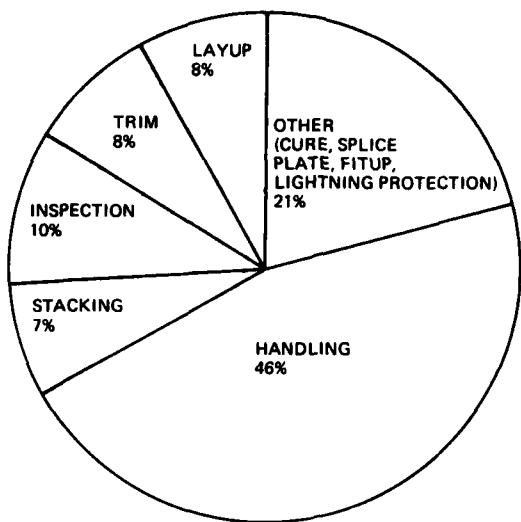
Fig. 16 Breakdown of Manufacturing Operations for
F-14A Horizontal Stabilizer Cover
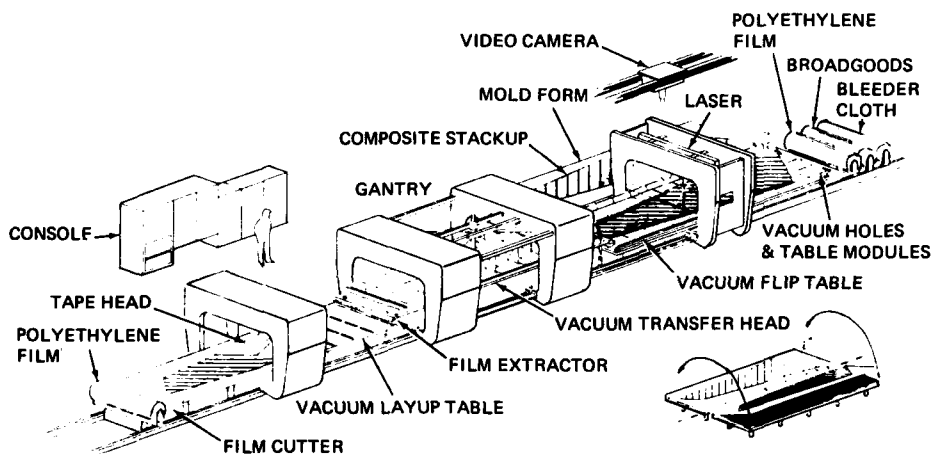
Fig. 17 Integrated Laminating Center (ILC)
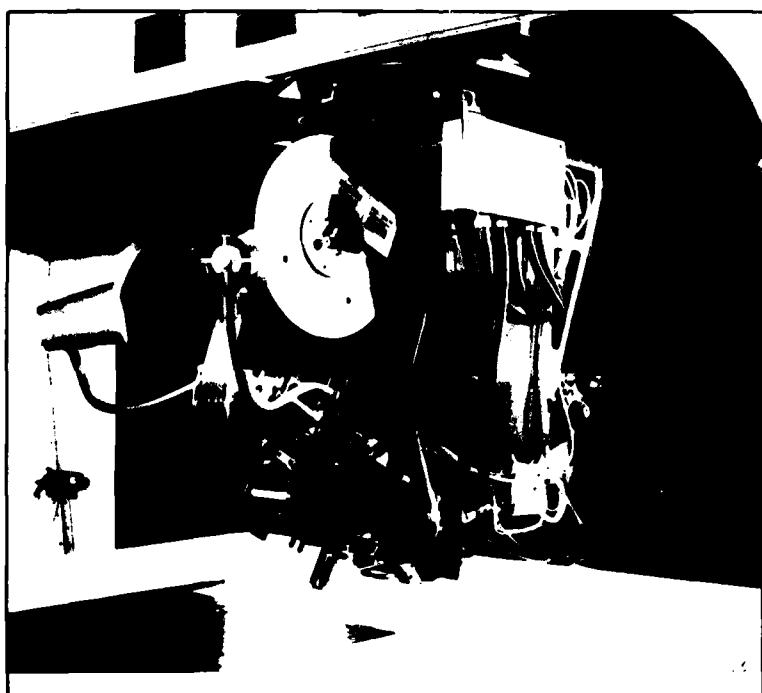

Fig. 18 ILC Tape Laying Head
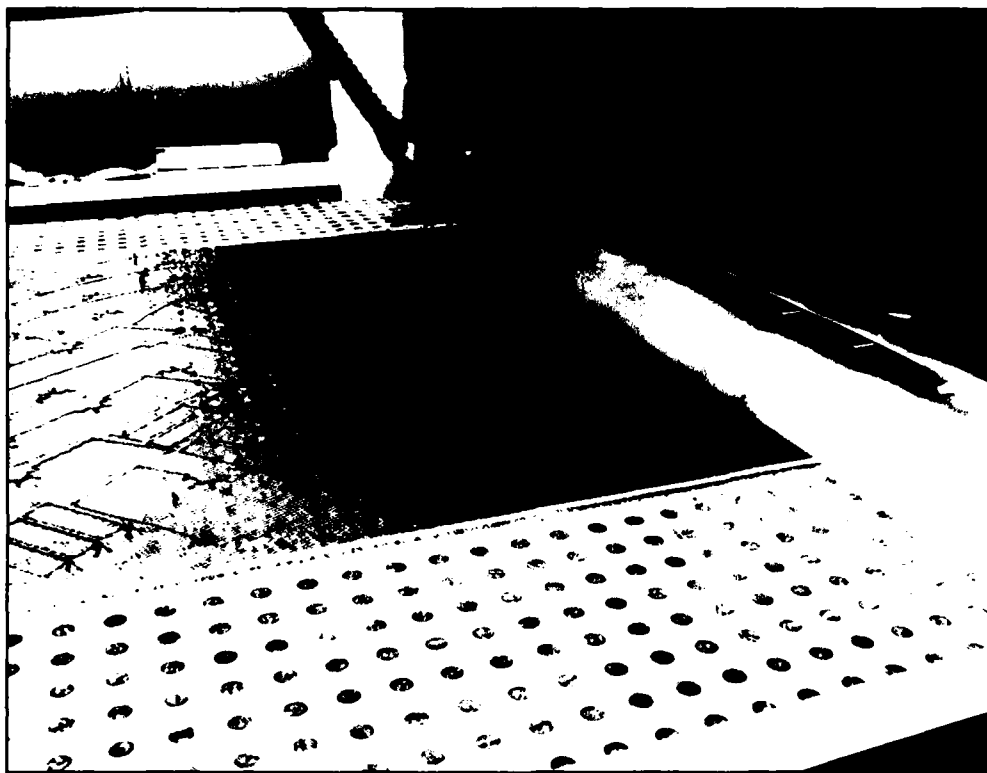
Fig. 19   ILC Laser Trimming Station
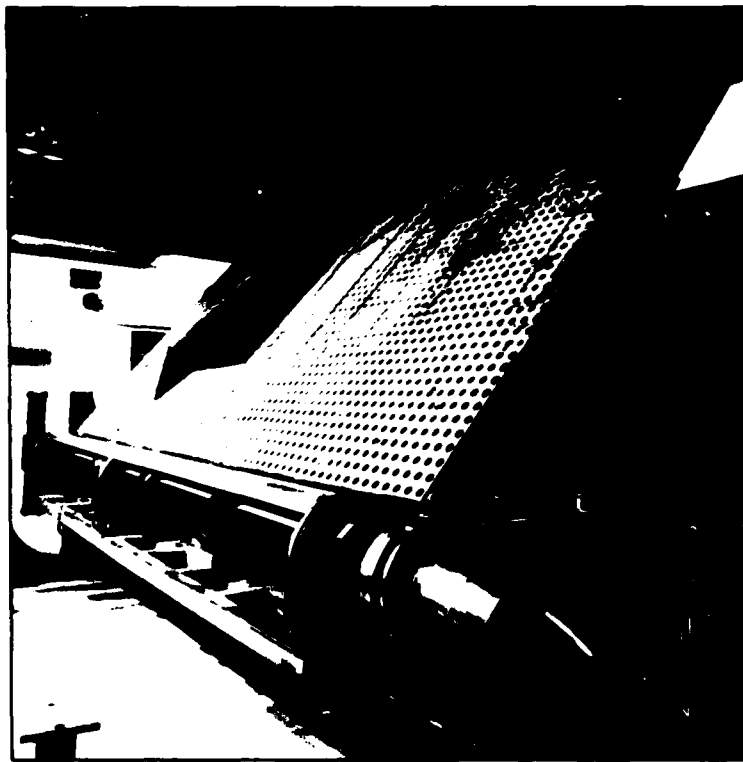
Fig. 20   ILC Trim Table Transferring Ply to Mold Form

Overall system control is provided by two Allen Bradley minicomputers and a supervisory software program. Programmable application logic (PAL) is used to direct the sequence of machine operations. The system uses either N/C tape or floppy discs for program storage.

The ILC has been in production for over three years at Grumman's Composites Production Facility in Milledgeville, Georgia. The ILC has reduced production labor by 50% (from 65 to about 30 hours per cover).

Although there are several approaches to mechanizing prepreg layup operations, the selection of the optimum method for a particular operation depends on the following:

- Available facilities

- Production rate

- Component design

- Material selection

In the case of broadgoods, the general approach is to use a computer-controlled cutting system that will permit mechanized cutting of the prepreg material. The cutting methods that can be used and the characteristics associated with each of the approaches are listed in Fig. 21. A key element in production application is the ability to produce data for a cutting system directly from a corporate CAD/CAM system.

1 – GOOD
2 – FAIR
3 – POOR

	LASER	RECIPRO. KNIFE	CHISEL	WATER-JET	STEEL RULE
CUTTING RATE	2	1	2	1	1
MULTI-LAYER	3	1	1	1	1
TOLERANCE	1	2	2	2	1
HEAT EFFECT	3	1	1	1	1
RAGGED EDGES	1	2	2	1	1
RADIUS LIMITS	1	2	2	1	1
MOISTURE	1	1	1	3	1
PARTIAL CUT	1	1	1	1	2
COMPATIBILITY	1	2	2	2	3
MECH. FORCE	1	2	2	2	2

Fig. 21 Composite Broadgoods Prepreg Trimming Alternatives

Post-Cure Operations

After the prepreg material has been cured, it becomes a product similar to the typical sheet-metal components used in aircraft fabrication. For many applications it has been found that a high-pressure water-jet cutting system (Fig. 22) will provide a clean, low-feed force system for cutting many cured composite components. Typical operating conditions and operating conditions for such a system are identified in Fig. 23.

Drilling of composites is generally an assembly operation (Fig. 24) performed with power-feed portable equipment. The type of tool material used is a function of the composite material (Fig. 25).

CONCLUSIONS

The future of composites is bright. During the past ten years, the aerospace industry has shown that it is capable of reliably building production composite structures. It is no longer a question as to whether composites will hold a major place in aircraft manufacturing - but how long it will take.

REFERENCES

1. Huber, J., "Automated Lamination of Production, Advanced Composite Aircraft Structures," SAE International Congress and Exposition, February 1981

2. Micillo, C., "Advanced Composites Manufacturing - New Techniques and Materials," American Institute of Aeronautics and Astronautics (AIAA), August 1980
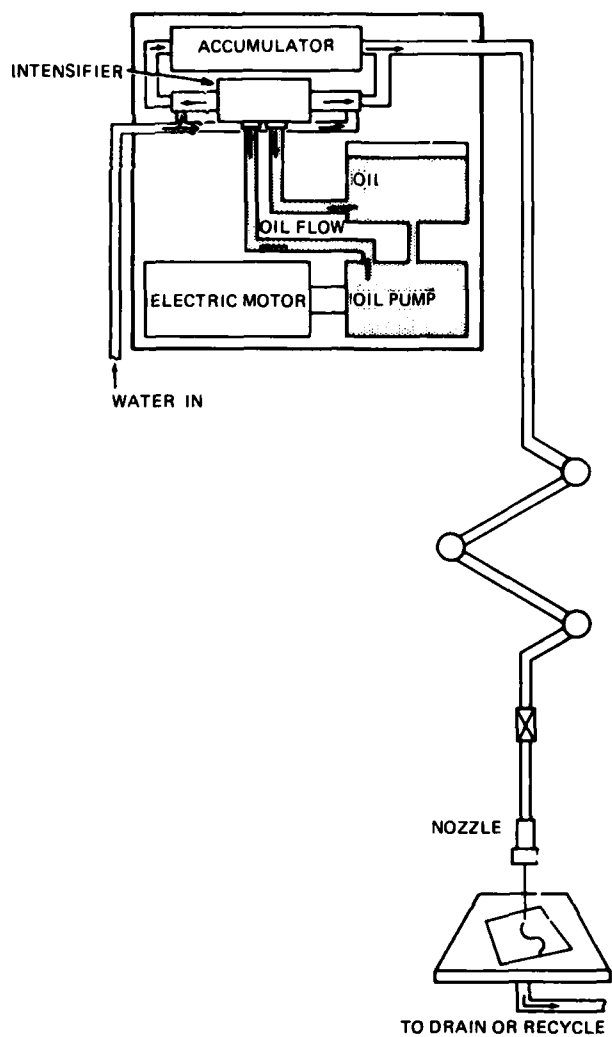
Fig. 22   Schematic Representation of
          High-Pressure Water-Jet
          Cutting System

MATERIAL	THICKNESS, IN.	WATER-JET CUTTING PARAMETER		
		PRESSURE, KSI	DIAMETER, IN	FEEDRATE, IPM
GRAPHITE/EPOXY	1/16	55	0.008	60
	1/8	60	0.010	30
	1/4	60	0.014	7
KEVLAR/EPOXY	1/16	55	0.006	120
	1/8	55	0.010	30
FIBERGLASS/EPOXY	1/8	60	0.010	6

Fig. 23   High-Pressure Water-Jet Operating Conditions

Fig. 24   Assembly Drilling Operation

MATERIAL	HSS	CARBIDE TIPPED	SOLID CARBIDE	DIAMOND IMPREG
GR/EP	HIGH WEAR*	MOD WEAR LOW COST	LOW WEAR LOWEST COST	LOWEST WEAR HIGH COST
B/EP	HIGH WEAR*	HIGH WEAR*	HIGH WEAR	LOW WEAR LOWEST COST
KEV/EP	LOW WEAR LOW COST	LOWEST WEAR HIGH COST	LOWEST WEAR HIGH COST	CLOGGING*

*UNACCEPTABLE

Fig. 25   Cutting Tool Materials for Composite Structures

SPECIFIC EXAMPLES OF AEROSPACE
APPLICATIONS OF COMPOSITES*

Richard Hadcock, Director
Advanced Development
John Huber, Section Head
Automated Manufacturing Systems Development
Grumman Aerospace Corporation
Bethpage, New York 11714, U.S.A.

SUMMARY

The state-of-the-art of the use of composites in both prototype and production, structural and nonstructural aerospace components is reviewed. Historic material usage trends for both commercial and military applications are presented. The applications selected are intended to show the evolution of composite components from relatively simple parts to the current, large and complex structures.

The use of composite materials in the new generation of commercial transport aircraft is presented. Specific areas of application, such as spoilers, flaps and fairings, are discussed in terms of impact on part weight, type of construction, and material selection factors. The effect of these factors on operating costs are projected.

Selected, major composite programs for military aircraft, including the Grumman F-14A fighter, the McDonnell Douglas F-18 fighter and AV-8B V/STOL aircraft, the Rockwell International B-1 bomber and the General Dynamics F-16 fighter, are reviewed. Composite materials used in these aircraft are analyzed with respect to the percent of the structural weight, type of material utilized, areas of application, type of construction and special manufacturing processes used in production.

The test procedures utilized to evaluate composite structures are reviewed. Typical tests performed to assure structural integrity are illustrated.

INTRODUCTION

Since the beginning of the century, many different materials and types of construction have been used for airframe structures. The Wright brothers used wood, wire and fabric for their aircraft in 1903. This was the standard type of construction until the mid-1920's when metal framing began to replace wood. Aluminum stressed-skin had become an accepted form of construction by the early thirties, about 20 years after the first flight of Hans Reissner's all-metal monoplane in 1912. Magnesium airframes came and went, primarily because of major corrosion problems--during the thirties and forties, as did stainless steel, primarily because of weight and manufacturing problems--during the forties and fifties.

Material availability has often driven the design. During World War II, shortages of aluminum led to production of the all-wood de Havilland Mosquito bomber and the use of wooden wings in conjunction with aluminum fuselages on the Messerschmitt Me163. In their time, both the Mosquito Bomber and Me163 fighter had outstanding performance characteristics.

Titanium had become an accepted material for high-temperature applications by the middle fifties. Titanium utilization reached a peak during the 1960's with the all-titanium SR-71/YF-12 and the planned U.S. supersonic transport. Titanium is still extensively used for the wings and carry-through structure of such aircraft as the F-14A and F-15.

By the late sixties, organic-matrix advanced composites became sufficiently developed for production of the covers of the F-14A horizontal stabilizers. Production applications were extended during the seventies to vertical stabilizers and rudders (F-15, F-16), wing covers (F-18) and, finally, to the complete wing, stabilizer and part of the forward fuselage (AV-8B).

Aircraft material applications during the twentieth century are summarized in Fig. 1. Implementation of advanced composites is illustrated in Fig. 2. The material mix in past, present and future fighter aircraft is shown in Fig. 3.

The trend toward increased use of composite materials is driven by three factors:

● Improved performance criteria derived from the greater strength-to-weight and stiffness-to-weight ratios

● Declining manufacturing costs for the fabrication of composite structures due to new mechanized methods

● Energy conservation, which composites make possible by weight reduction, is a major goal of the industry since the quantum jump in aircraft fuel costs in the mid-1970's.

-----
*The referenced background information presented in this paper is in the public domain.
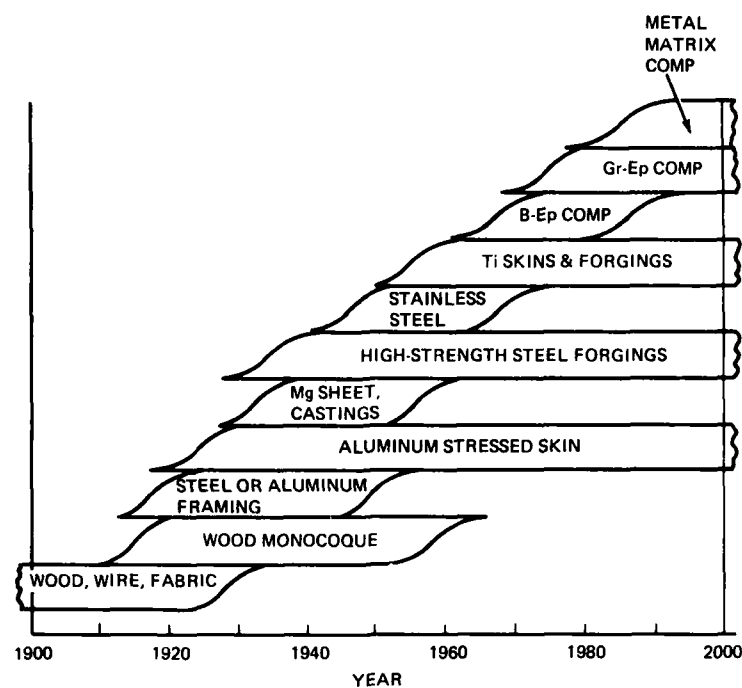
Fig. 1 Aircraft Material Application
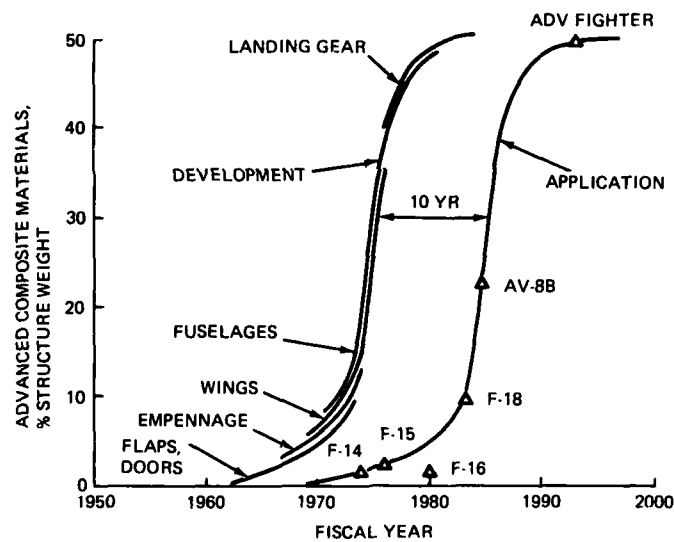
Fig. 2 Advanced Composite Implementation (Aircraft)
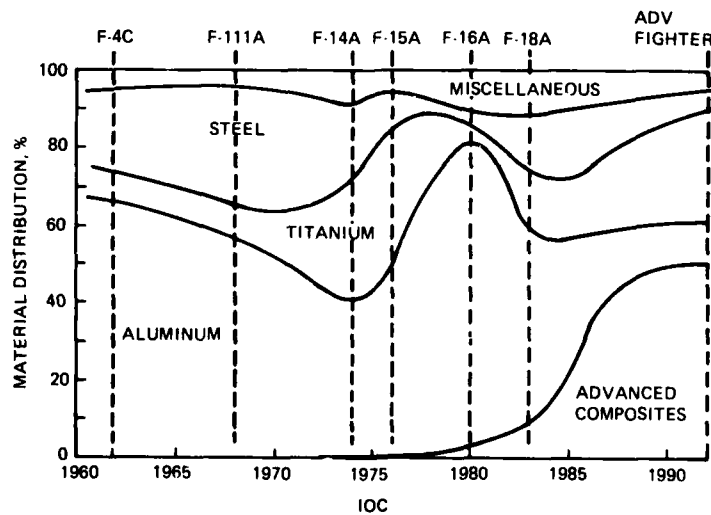
Fig. 3 Material Utilization - Fighter Aircraft

MATERIAL DISTRIBUTION IN PRESENT AND PLANNED STRUCTURES

Each new aircraft structure has involved greater use of advanced composites. This trend began with the Grumman F-14A which, although relying on composite materials for only 0.8% of its primary structure, was the first to use composites for a primary safety-of-flight production component. Grumman's F-14A was followed by McDonnell's F-15 (1.6%), General Dynamics' F-16 (2.5%), and McDonnell's F-18 (9.5%) and AV-8B (26%) as shown in Fig. 4. Military aircraft in the conceptual stage also promise far greater use. The trends toward increased composite use for airframes are summarized in Fig. 5.

APPLICATION	COMPOSITE STRUCTURE %
PRODUCTION	
F-14A	0.8
F-15	1.6
F-16	2.5
F-18	9.5
DEVELOPMENT	
AV-8B ATTACK V/STOL	26.0
CONCEPTUAL	
ATF (ADV. TAC. FIGHTER)	40-50
ADVANCED V/STOL	50-65

Fig. 4 Application of Composite Structures in
Military Aircraft
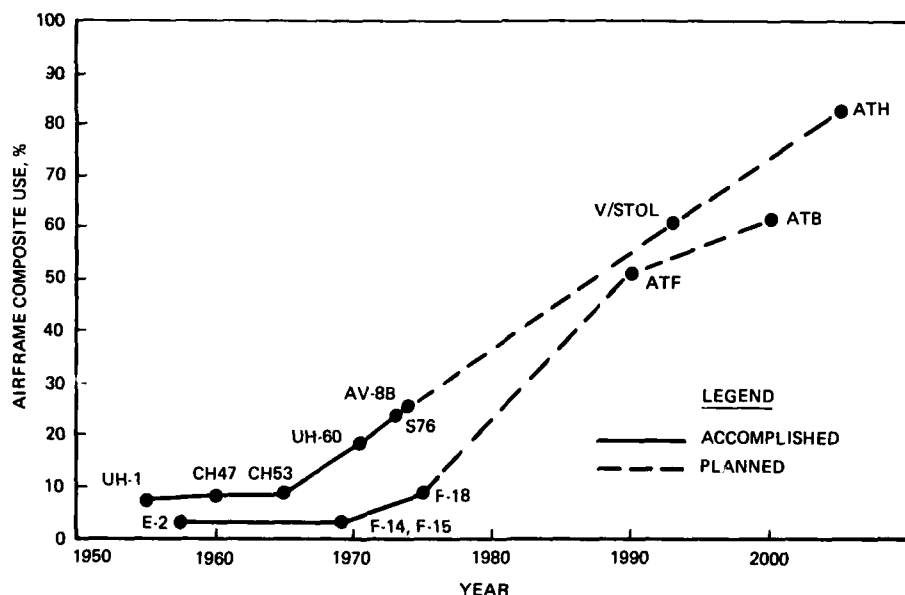
Fig. 5 Projected Composite Applications

At present, the Navy's AV-8B (an attack-type vertical take-off and landing aircraft), incorporates the greatest amount of composites of any production military aircraft. The AV-8B has demonstrated flight suitability with an airframe consisting of 26 percent by weight of composites (1,317 pounds of graphite/epoxy in a 5,006-pound structure). Composites are used in the wings, forward fuselage, stabilizer and rudder (Fig. 6).

Even more extensive use of composites in the future is predicted. An analytical study of an advanced-design composite aircraft (Fig. 7) performed by Grumman under the sponsorship of the Air Force Flight Dynamics Laboratory indicates that using composites for 75-80 percent of the airframe would reduce the overall weapon system weight by 26 percent. Current subsonic and supersonic V/STOL aircraft studies (Fig. 8 and 9) indicate that a 65-percent composite structure would reduce weight by as much as 20 percent. Similarly, an advanced all-composite helicopter airframe (Fig. 10) promises 22 percent weight savings and greater resistance to radar detection than a metal airframe.

STRUCTURAL
WEIGHT
GRAPHITE/EPOXY_____26.3%
ALUMINUM_____47.7%
OTHER_____26.0%

5,006 LB OF STRUCTURE
1,317 LB OF GRAPHITE/EPOXY
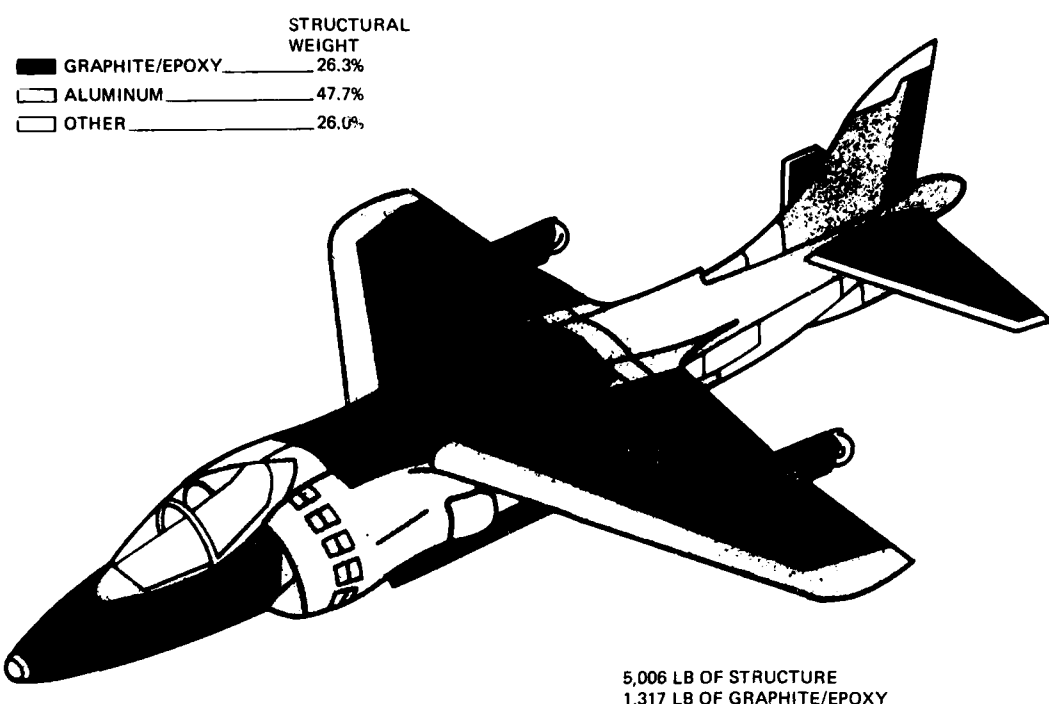
Fig. 6   Material Distribution for Navy AV-8B Attack V/STOL Aircraft

ADVANCED-DESIGN COMPOSITE AIRCRAFT

Gr/Ep
K/Ep OR Gl/Ep
Gr-Gl/Ep
Al
Ti OR STEEL
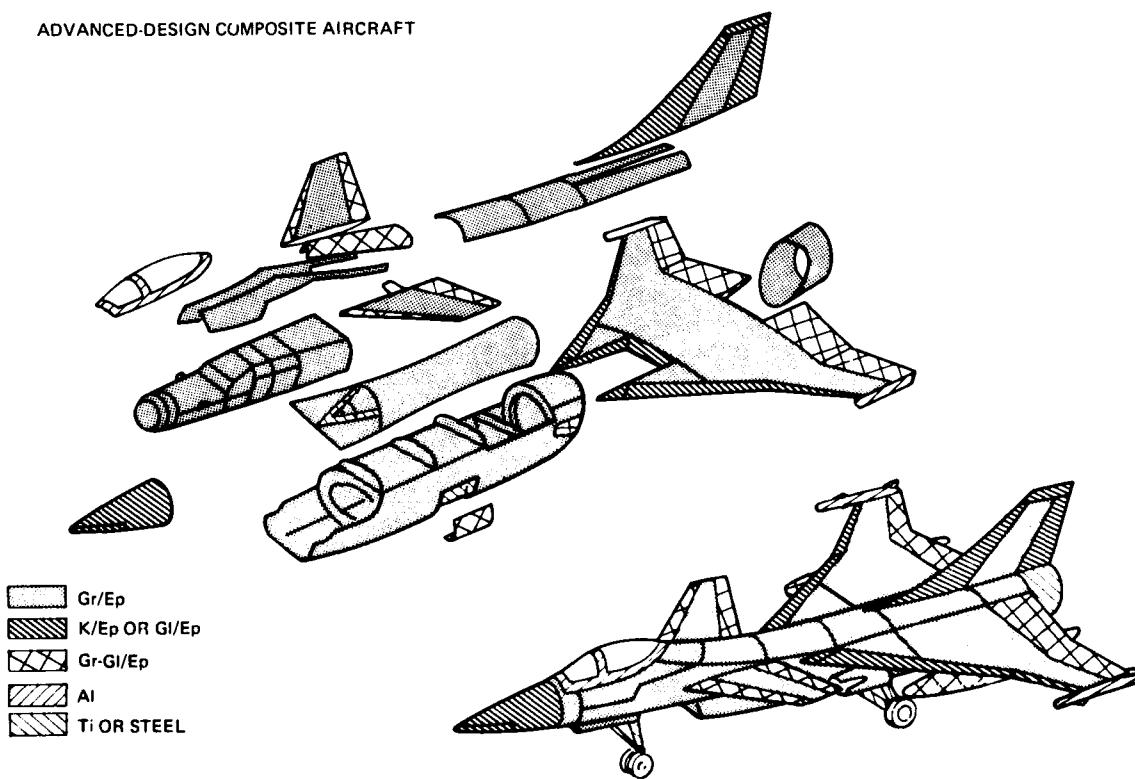
Fig. 7.   Material Distribution for Advanced Design Composite Aircraft

Gr/Ep

K/Ep OR Gl/Ep

Gr/K/Ep

Al

Ti

B/Al OR SiC/Al
OR STEEL
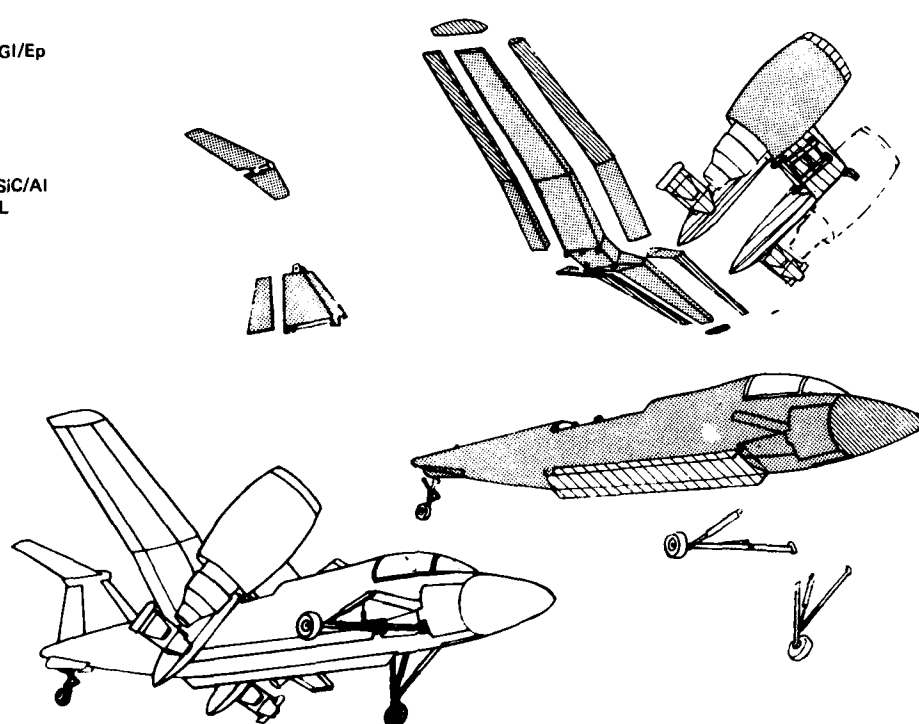
Fig. 8. Material Distribution for Subsonic V/STOL Aircraft

Gr/Ep

Gr/PI OR SPF/DB TITANIUM

K/Ep OR Gl/Ep

Gr-K/Ep

Al

Ti

STEEL OR B/Ti
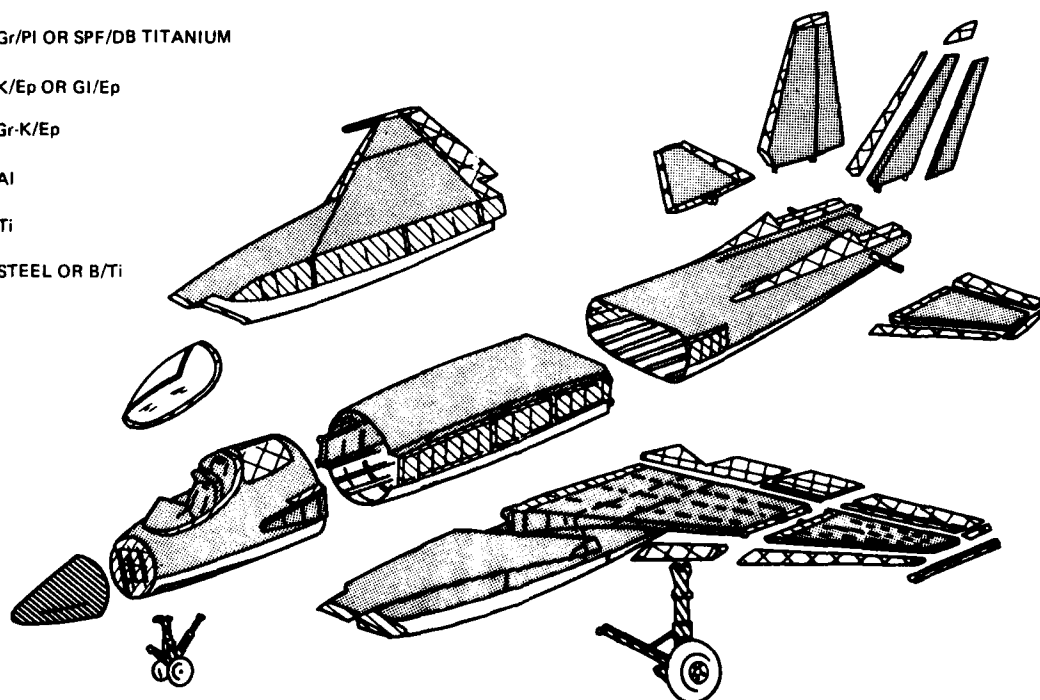
Fig. 9. Material Distribution for Supersonic V/STOL Aircraft

Gr/Ep

Gl/Ep
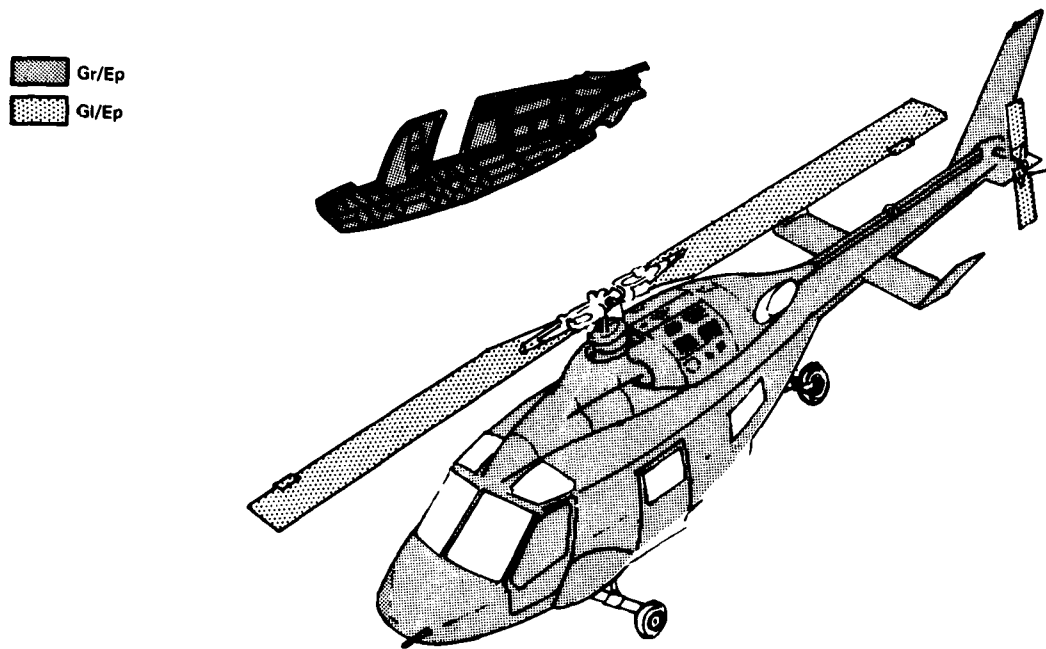
Fig. 10 Material Distribution for Advanced Attack Helicopter

The evolution of the commercial application of composites is illustrated in Fig. 11. Overall material distribution trends for commercial aircraft are shown in Fig. 12. These trends are similar to those predicted for military aircraft. Graphite/epoxy use on the new Boeing 757/767 transports (Fig. 13) reduces the weight of each model by about 1,250 pounds. The confidence to apply this new material was gained as a result of a series of service evaluations, including installation of graphite/epoxy spoilers on 28 Boeing 737 airliners operated by seven major airlines throughout the world. As of March 1980, 1,348,023 flight-hours were accumulated on these spoilers. Visual, ultrasonic and destructive tests have shown no significant evidence of moisture migration into these structures or a reduction in the strength of the composite material.

Probably the most dramatic application of composites is in the LearAvia Lear Fan 2100 executive aircraft (Fig. 14) that was test flown in 1981. The airframe consists of 70 percent by weight of graphite/epoxy and Kevlar/epoxy. The application of this amount of composites has reduced operating costs by over 50 percent.

TYPES OF STRUCTURE

Composite structure can be discussed in terms of three principal types:

● Bonded structure

● Built-up structure

● Single cure or integral structure
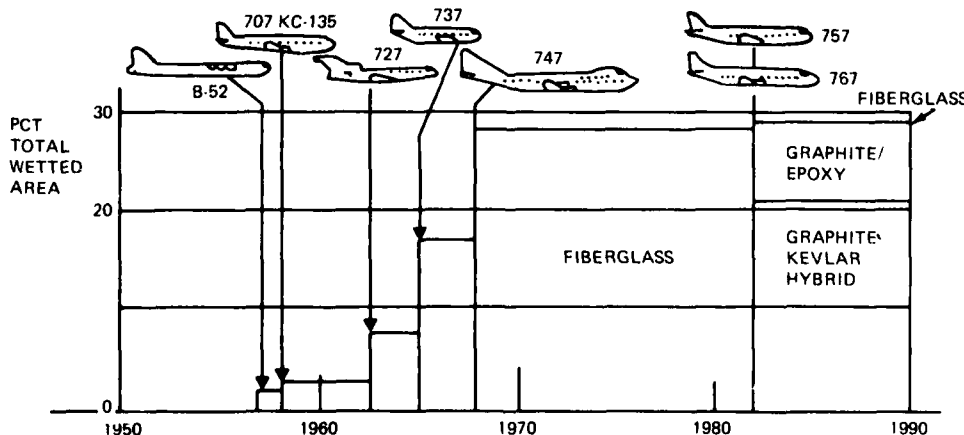
Fig. 11 Evolution of Composite Structures for Large Commercial Aircraft

COMPOSITES POTENTIAL
65 PCT

IMPROVED ALUMINUM
ALLOYS 17 PCT

ALUMINUM
82 PCT

STEEL
13 PCT

TITANIUM
4 PCT

FIBERGLASS
1 PCT

STEEL
14 PCT

TITANIUM
4 PCT

COMPOSITES
3 PCT
(FIBERGLASS
0.5 PCT)

ALUMINUM
79 PCT

STEEL
15 PCT

ALUMINUM
17 PCT

TITANIUM
3 PCT

TYPICAL IN-SERVICE
AIRPLANE

1980 DESIGN
AIRPLANE

1985-1995 SUBSONIC
AIRPLANE
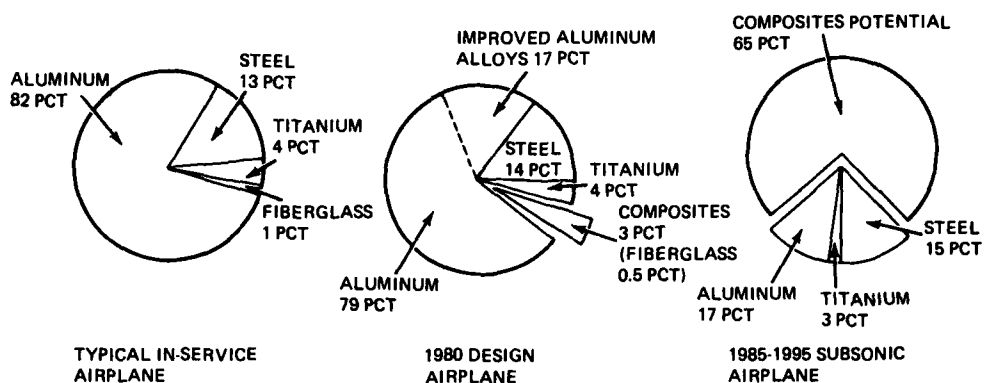
Fig. 12 Material Distribution Design Trends for
Commercial Aircraft

Gr/Ep
K-Gr/Ep

1250 LB WEIGHT SAVED
PER MODEL

LANDING GEAR
DOORS

LOWER L.E.
ACCESS PANELS
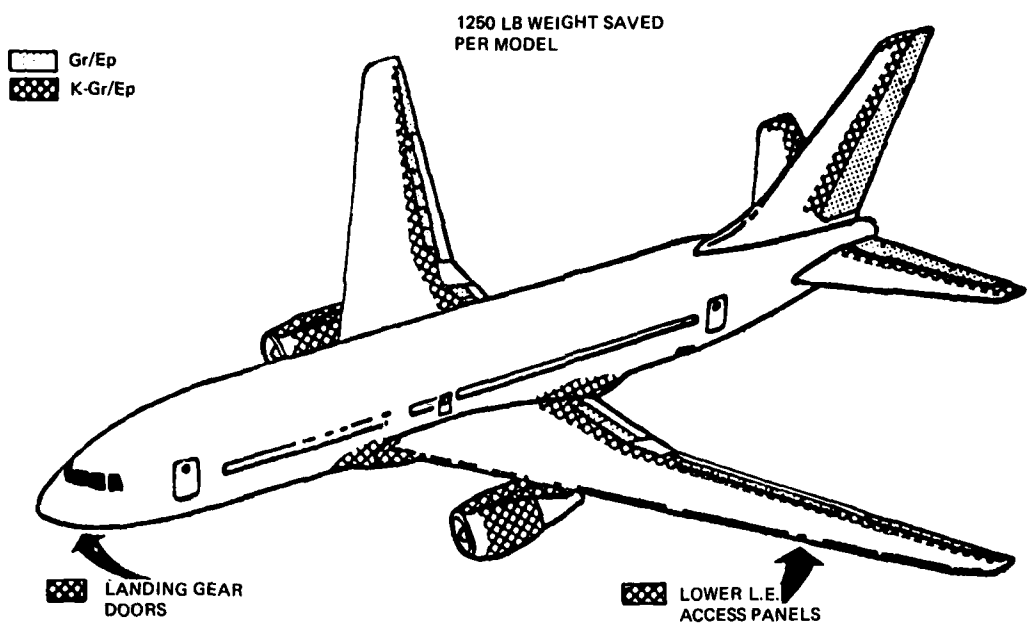
Fig. 13 Boeing 757 Composites Applications
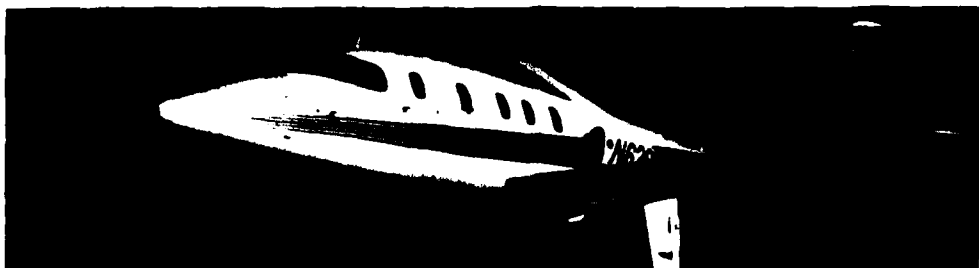
Fig. 14 LearAvia Lear Fan 2100

   Bonded structure, the first generation of composite applications, generally involves bonding a cured composite skin or cover to an aluminum or phenolic honeycomb core substructure. This concept is most applicable to stabilizers, doors and control surfaces. The F-14A horizontal stabilizer (Fig. 15) is typical of this type of structure where the composite skin or cover has replaced the traditionally heavier, bonded aluminum skin. The advantage of this approach is that it presents a minimal impact on the fabrication cycle because similar skills and equipment are used. It does, however, require careful fitup of detail parts and nondestructive testing to assure structural integrity.

   Built-up structure refers to building assemblies in a manner similar to that used for metal structures. The components are aligned in a fixture (Fig. 16), shimmed as required, and then mechanically fastened. The principal concerns are fitup and damage induced by improper drilling or trimming of the cured composite components.

ALUMINUM HONEYCOMB CORE

BOX BEAM SUBSTRUCTURE

BORON/EPOXY COVER(S)

STABILIZER MODULE ASSEMBLY
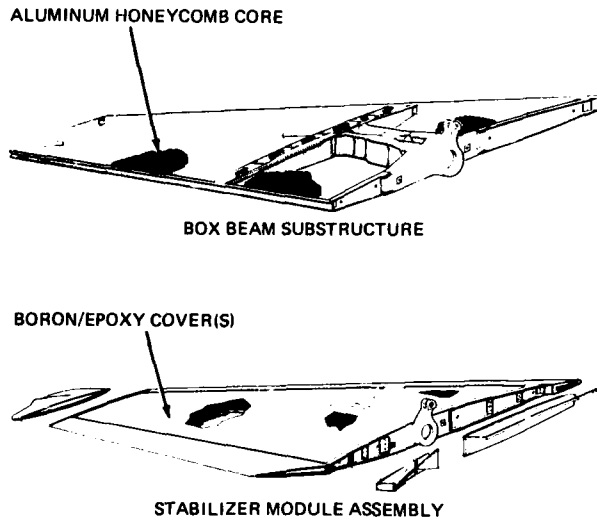
Fig. 15.   F-14A Horizontal Stabilizer
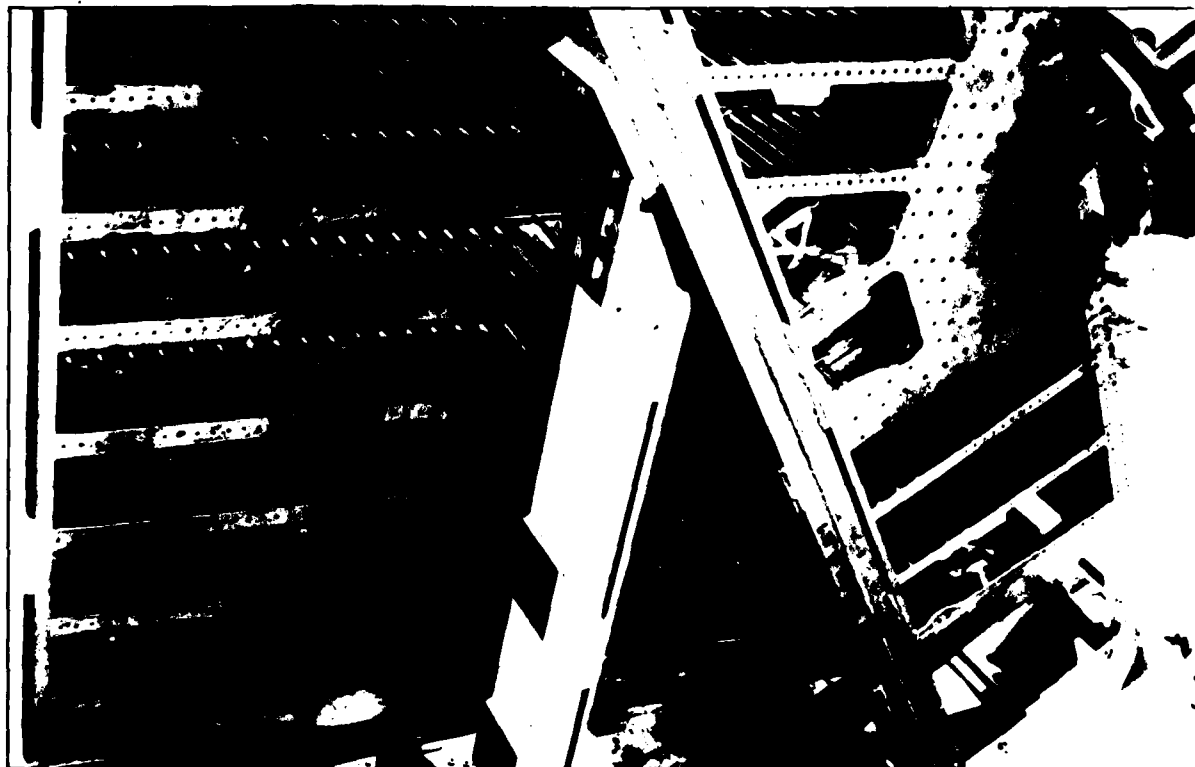
Fig. 16   B-1 Horizontal Stabilizer Graphite/Epoxy Substructure in
Assembly Fixture

Single-cure or integral structure is an approach that permits a somewhat complex assembly to be cured in one step to yield an integrally stiffened structure without a series of bonding operations. Several illustrative examples are given in Fig. 17, 18 and 19. The 757 spoiler assembly (Fig. 17) involves cocuring both air-passage and inner skins with the honeycomb core to eliminate two skin bonding operations. Tailored tooling, processing and prepreg flow conditions are required to perform this operation. The B-1 graphite/epoxy sine-wave spar (Fig. 18) is laid-up and formed from several prepreg laminates that are assembled and cured into a single component. The integrally stiffened developmental structure shown in Fig. 19 is fabricated in a similar manner to provide both hat-shaped stiffeners and transverse frames integral with the skin.

TESTING

Successful application of composites to aircraft structures requires a thorough and disciplined quality assurance system. Fabrication of composite structure literally requires the buildup and placement of thousands of pieces of prepreg. The prepreg fabrication operations required to build a laminate must be completed within a specified time in a controlled environment to assure proper curing of the laminate. Fig. 20 identifies the principal quality control surveillance functions needed to assure part integrity. The major quality/manufacturing functions involved are:

- Material Procurement -- to ensure that the incoming raw materials meet requirements and are stored properly

- Design and Manufacturing Planning -- to ensure that design and manufacturing procedures will permit proper control of product

- Tooling -- to certify that the tools produced will produce the required component

- Detail Part Fabrication -- to monitor production fabrication for proper environment, fabrication sequence, and processing with non-destructive and destructive testing to ensure final detail component integrity

- Assembly -- to monitor bonding, mechanical fastening, fitup, sealing and finishing operations using both nondestructive and destructive testing techniques.

The two principal nondestructive testing approaches used for composite structures are ultrasonics and radiography. Although several ultrasonic techniques are available, the choice of the technique to be used is determined by the allowable defect size and the geometry of the component to be inspected.
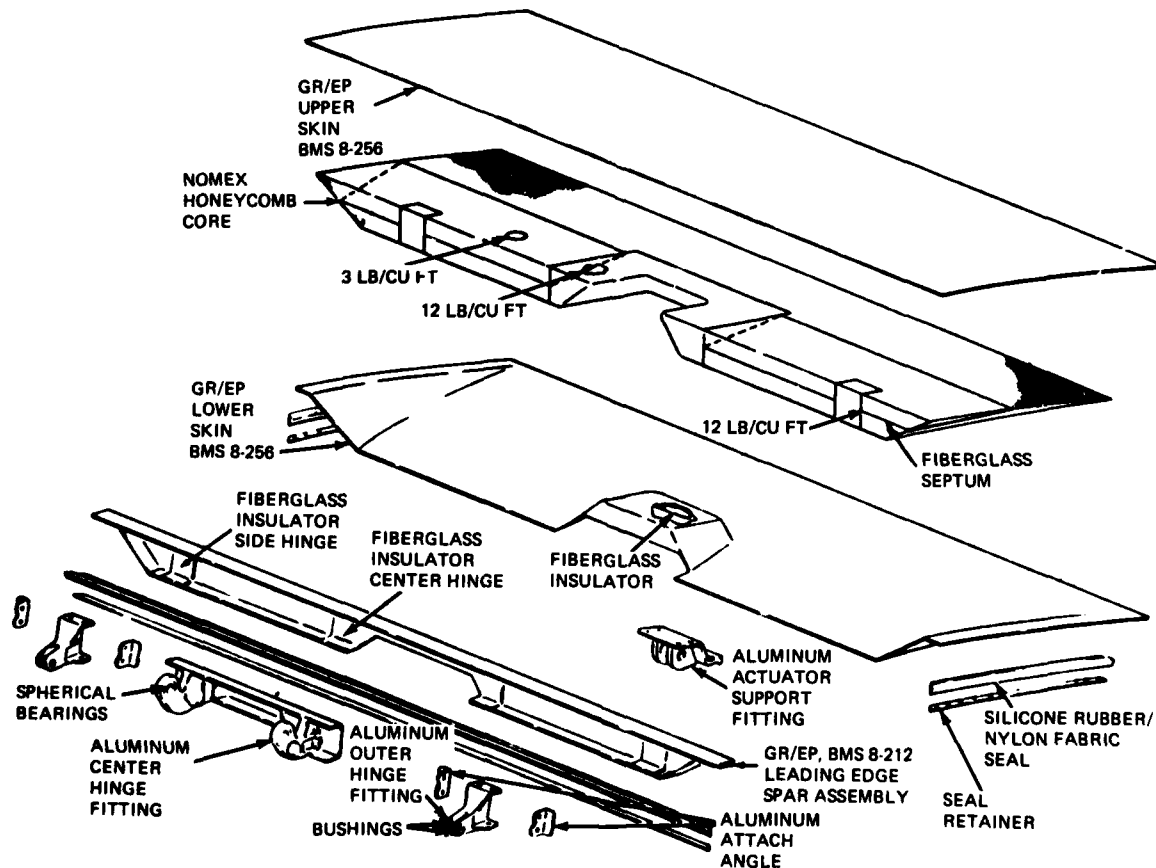

Fig. 17 Boeing 757 Spoiler Assembly
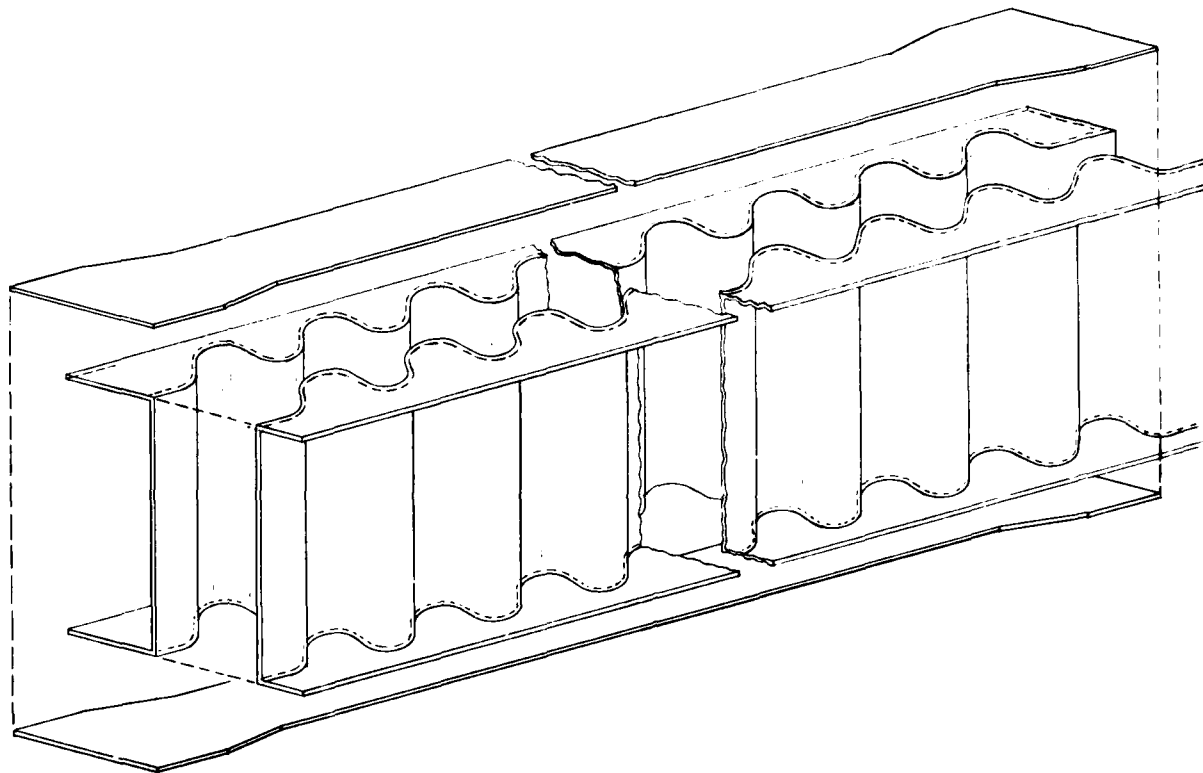
Fig. 18 B-1 Graphite/Epoxy Sine-Wave Spar
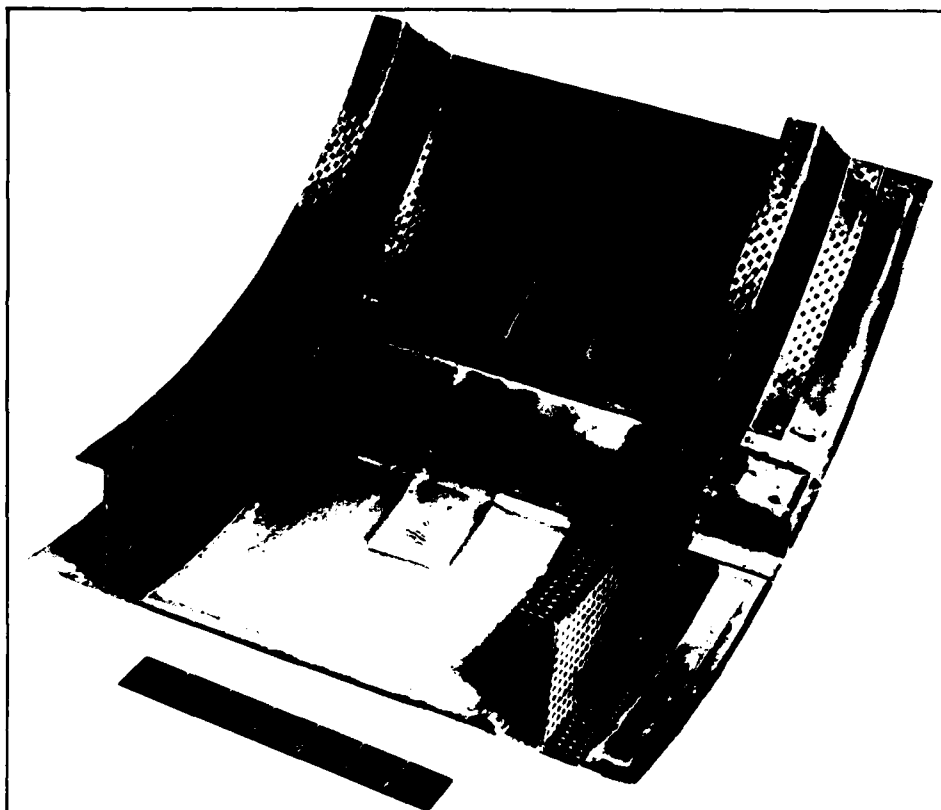
Fig. 19 Integrally Stiffened, Graphite/Epoxy Development Structure
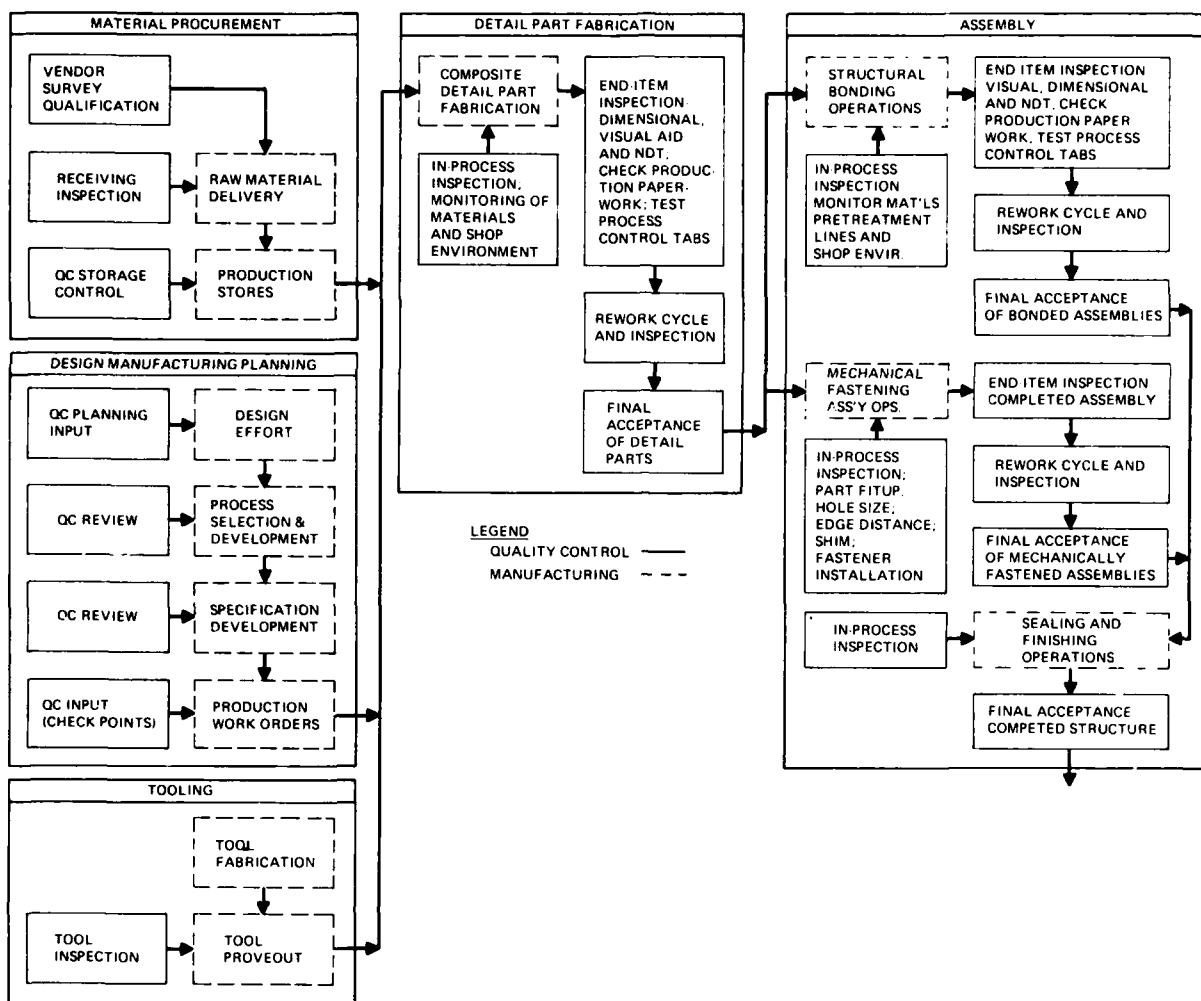
Fig. 20 Quality Control Surveillance Function for Composite Manufacturing

In the ultrasonic immersion through-transmission (reflector plate) technique, which utilizes a single transducer, ultrasonic energy is passed through the component, reflected off a surface through the specimen, and reflected back to the transducer (Fig. 21). In general, resolution is not a problem with this technique. If a defect is present, it presents an interface that blocks a proportional amount of acoustic energy from reaching the reflector. This results in a loss of sound energy reflected to the reducer which attenuates the display signal. The immersion technique utilizes automated scanning and provides a rapid means of 100% inspection, but does not provide depth-of-defect information. For depth-of-defect information, the contact transducer technique and pulse-echo techniques are used. These techniques were successfully used on the B-1 horizontal stabilizer covers and substructure.

In general, non-destructive evaluation of radii in composite structures is performed by radiography because of the defect location and part geometry restrictions imposed by ultrasonic inspection techniques. Low-kilovoltage (35-50 kv) radiography using beryllium-window X-ray tubes and fine-grain, single-coated film have given excellent results. During inspection, the primary beam is directed tangentially to the radius (Fig. 22) to produce the maximum reinforcement of an internal delamination between the plies. Fig. 23 shows a radius delamination and the associated radiograph of this area. Delaminations as tight as 0.002 in. have been detected in graphite/epoxy structures using radiography.

POTENTIAL COST IMPACT OF COMPOSITE STRUCTURES

Composite structures and materials will be sufficiently mature by the late 1980's to seriously consider them for primary usage on the airframes of advanced tactical fighter/attack aircraft. Approximately 70% by weight of these airframes would consist of composite materials, resulting in aircraft that would be significantly smaller, lighter, and more efficient than their current counterparts. Figure 24 shows that takeoff gross weight would increase by 29% if the materials and construction currently used on such aircraft as the F-14A, F-15, and F-16 were to be used in place of the advanced materials. Using all-aluminum 1960 construction, the takeoff gross weight would increase by 46%. It should be noted that these are all iterated weight penalties obtained by resizing the aircraft for the same mission performance.
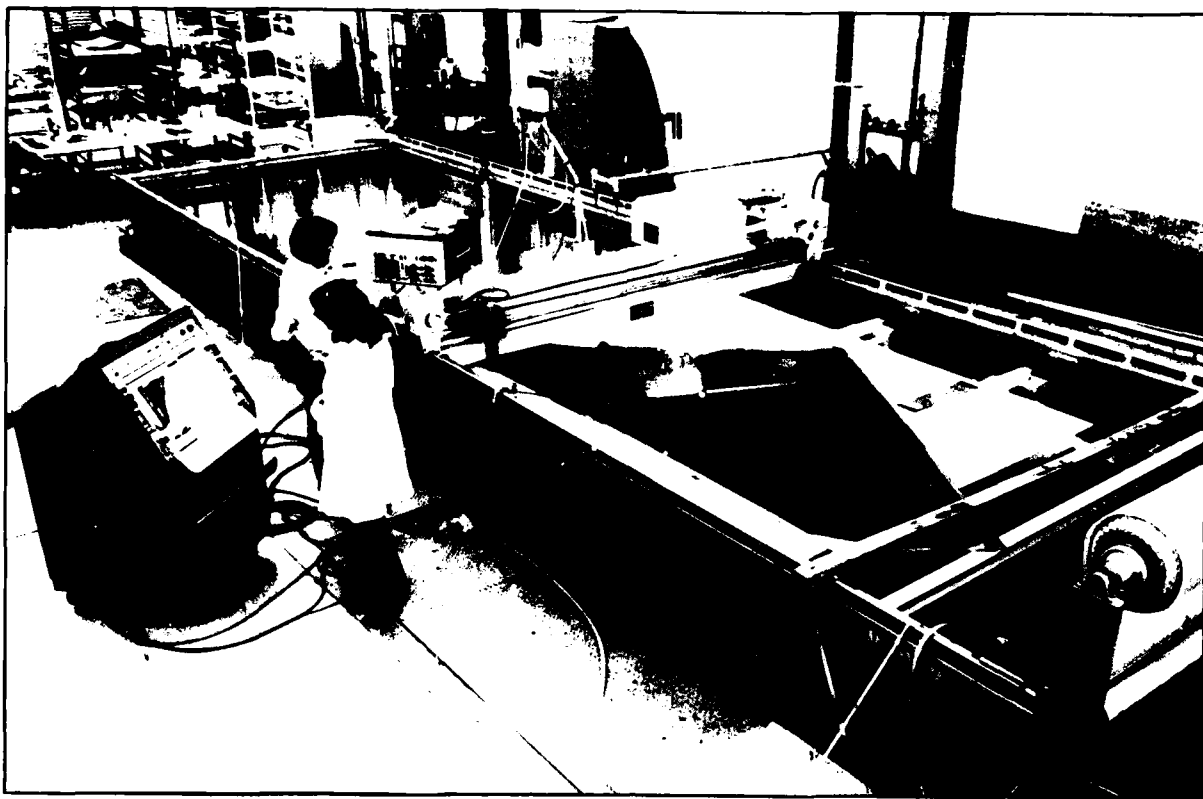
Fig. 21 Ultrasonic Immersion Inspection

X-RAY TUBE

DELAMINATION

X-RAY FILM   VOID IN FILLER MATERIAL
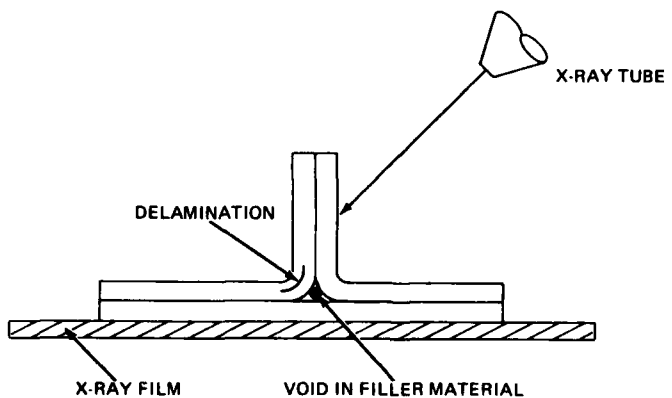
Fig. 22 Schematic Representation of Radiographic Inspection
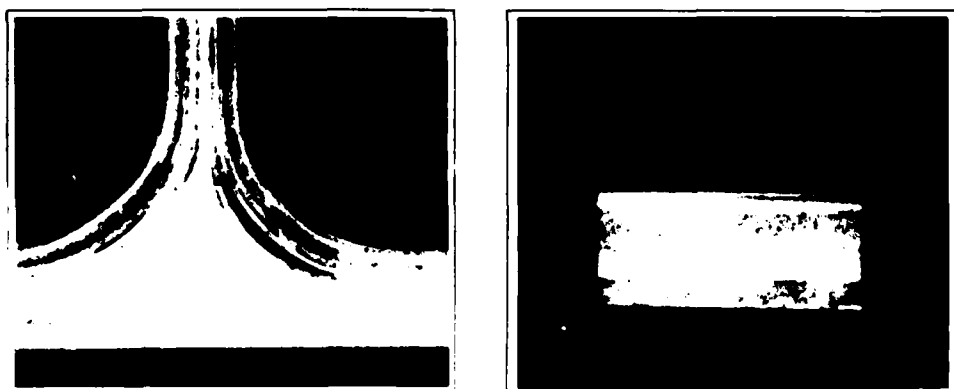
a) CROSS-SECTION OF DELAMINATION   b) RADIOGRAPH OF DELAMINATION SHOWN IN (a)

Fig. 23 Delamination in Radius of Composite Structure

WEIGHT
kg   LB

NOTE: VARIATIONS IN STRUCTURES AND MATERIALS
ONLY. ALL OTHER ADVANCED TECHNOLOGIES
(I.E., AERODYNAMICS AND PROPULSION)
REMAIN UNCHANGED.
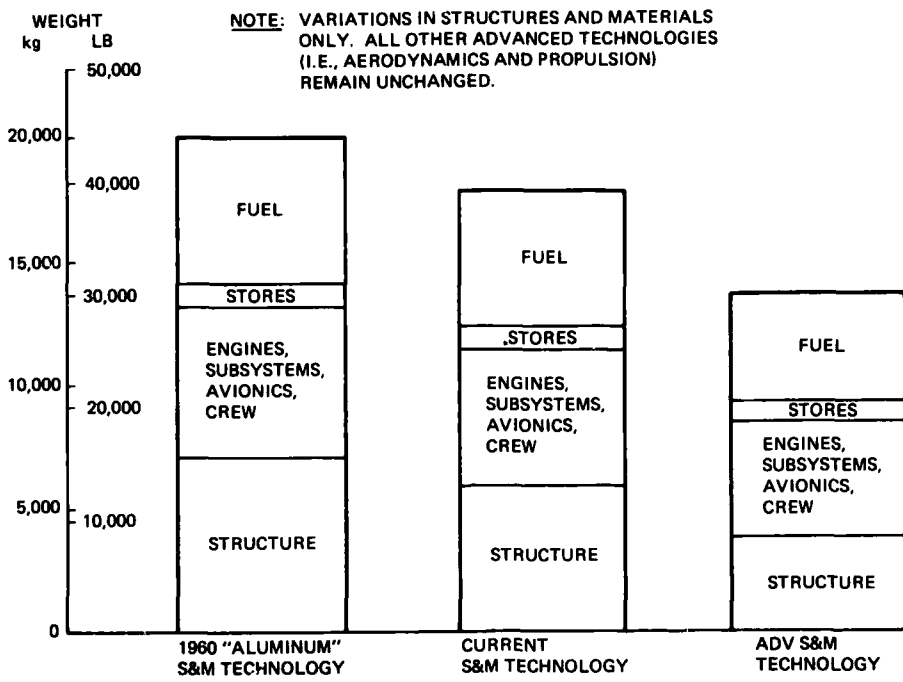
Fig. 24   Effect of Structures and Materials Technology on Aircraft Weight

Comparable production airframe flyaway costs, in constant 1980 dollars, were $115/kg ($250/lb) for the 1960 all-aluminum aircraft and about $170/kg ($370/lb) for the current fighter aircraft. The relative production cost per unit weight of the 1990 tactical fighter would probably be no more than 10% higher than that of the current aircraft, or about $185/kg (410/lb) in 1980 dollars. These costs are based on the material prices shown in Fig. 25 and the assumption that automated production facilities would be available. Since the airframe weight of the resized advanced tactical fighter would be approximately 65% of that of a fighter with the same mission performance (but using current structures and materials technology), the flyaway cost of the advanced technology airframe should be 29% lower. RTD&E costs would be somewhat higher for the advanced aircraft, since more testing would be needed for qualification. Even so, there would be at least a 10 to 15% procurement cost savings for the smaller advanced aircraft. Life-cycle cost savings could be very significant, since the resized smaller aircraft would be considerably more fuel efficient. In terms of 1980 dollars and current fuel prices ($1.38/gallon), fuel savings would add up to $1.1M per aircraft relative to the current technology aircraft and $2.1M over the all-aluminum 1960 technology aircraft over a 15-year life at 300 flight hours per year.

	MATERIAL	PRICE, $/LB	BUY-TO-FLY RATIO (TYPICAL)	FLYAWAY COST, $/LB
CONVENTIONAL TECHNOLOGY	ALUMINUM	1.80-2.2	8.0	15
	STEEL (PH STAINLESS)	2.70	5.0	14
	TITANIUM	16-31	6.0	100
ADVANCED TECHNOLOGY	GRAPHITE/EPOXY TAPE	38-55	1.3	60
	GRAPHITE/EPOXY CLOTH	70-80	2.0	150
	BORON/EPOXY TAPE	242	1.25	300
	TITANIUM-NEAR NET SHAPES	25-40	1.5	53
	TITANIUM-SPF/DB	16-31	2.0	50
	B/B$_4$ C/TITANIUM	600-1000	1.2*	1000
	*WHEN USED AS SELECTIVE REINFORCEMENT			

Fig. 25   Aerospace Material Prices, Fall 1980

REFERENCES

1. Hadcock, R.N., Introduction of New SDM Technology into Production Systems, AIAA Paper No. 79-07119R, September 1980.

2. Post, C.T., Solving the Engineering Problems of Tomorrow's Aircraft Industry, American Machinist, 12 December 1981

3. Vaccari, J.A., Toward the All-Composite Aircraft, American Machinist, 12 December 1981

ASSESSMENT OF STRUCTURAL INTEGRITY OF COMPOSITES

BY NON DESTRUCTIVE METHODS

Bryan Harris

School of Materials Science
University of Bath
Claverton Down
Bath AB2 7AY
UK

SUMMARY

Composite materials, and particularly structural reinforced plastics, often contain defects as a result of normal manufacturing procedures. And during proof-testing or service loading additional defects of other kinds are produced. These defects all affect the mechanical properties of the composites and it is important for designers to be aware of their effects and to allow for their presence. A variety of techniques has been used to evaluate the quality of composite materials and structures and to study the accumulation of damage in composites subjected to stress, creep, fatigue or impact conditions. Optical methods, x-radiography, ultrasonic techniques, thermal imaging, and acoustic emission analysis are all methods which are capable of revealing certain aspects of the development of damaged regions in a composite, but the usefulness of most of these is limited to certain types of material or specific structural situations. It is conceivable that no single technique will prove to be capable of giving a complete picture of the damaged state of a composite so as to permit satisfactory life prediction, and more refined methods of detecting localised damage levels and assessing their effect are probably still required.

1. INTRODUCTION

Many types of composite materials are used in engineering, but for stringent structural applications like those for aerospace purposes low-density composites consisting of high strength fibres like, glass, carbon, aromatic polyamides and, to a smaller extent. boron, in combination with thermoset resins such as polyesters and epoxides are among the materials that are currently of most serious interest. Composites such as chopped glass fibre reinforced thermoplastics. glass/chalk/polyester moulding compounds (SMC and DMC), and glass or steel fibre reinforced concrete are potentially important for less demanding applications. but problems relating to structural defects and damage are less acute in materials of this kind.

When designing an aircraft structure or a pressure vessel in metallic materials the engineer has confidence in available design procedures which have been in use for many years and have improved with experience. These procedures have the backing of a reasonable degree of understanding, at the microstructural level, of the mechanisms of plastic deformation. crack propagation. fatigue crack growth etc.. that are likely to lead to structural failure. Reasonable predictions can be made by means of fracture mechanics or other predictive methods of the life of a structure under conditions of steady or cyclic loads, impact, and even stress corrosion. Design failures do still occur -- all too frequently -- but such incidents are often due, partly or wholly, to a designer's failure to take into account known factors of metallurgical. geometric or environmental significance.

For composites the situation is far less satisfactory. Our experience of their behaviour is limited; effects of long-term exposure to load and environment are not properly known; and our understanding of the microstructural mechanisms of damage is imperfect. As a consequence of their nature and methods of preparation it is difficult to avoid inherent manufacturing defects. And because composites consist of two (or more) materials with highly disparate characteristics it is impossible to avoid creating additional defects during loading or putting into service.

Our uncertainty about how these defects accumulate and grow is reflected in current design procedures or codes of practice. In the case of glass-reinforced plastics (GRP), for example. this uncertainty results in factors of safety as high as 20 for critical applications. The weight and strength advantages of strong fibres are wasted if such large safety factors are enforced and there is therefore an economic disincentive against using reinforced plastics under such conditions. The normal safeguard against unrealistic safety factors is. of course. proof-testing but the proof testing of a composite structure often induces extra damage which therefore weakens the structure.

2. MANUFACTURING DEFECTS IN REINFORCED PLASTICS

Cylindrically symmetric structures such as pressure vessels, tanks, rocket motor casings, centrifuge cylinders, missile launcher tubes, and a variety of pipes are made by winding fibres soaked with pre-catalysed resin onto removable mandrels. Winding patterns may be simple or complex and may be accurately calculated to resist a prescribed stress system. After the resin has hardened the mandrel is removed and the material may be post-cured at an elevated temperature. Since the winding procedure is usually controlled automatically, a high degree of uniformity is possible in the fibre distribution of filament-wound structures, but planes of weakness sometimes occur between winding layers, especially if resin-rich pockets are allowed to form.

Large panels are easily constructed by hot-pressing, between flat or shaped platens, sheets of preimpregnated fibres or cloth. Pressing must be carried out carefully to produce initimate association of the fibres in different layers, accompanied by expulsion of trapped air and excess resin, and the time/temperature cycle must be controlled so as to ensure curing of the resin only when these conditions have been met. Higher fibre contents are obtainable with non-woven laminates than with woven cloth composites, and the characteristics of the two types of material are quite different. The orientation of the fibres in the separate laminations is varied to suit the specific load-bearing characteristics required of the laminate or moulding. Overlapping or defective layers will be a source of weakness in the finished laminate, while failure to control the resin content and curing cycle will result in interlaminar planes of weakness which are resin rich or even regions where the plies remain unbonded.

Lower quality chopped-strand-mat (CSM) reinforcements may also be press-laminated but are most frequently laid up by hand methods, especially for irregularly shaped structures. Large structures, tanks and even pipes are made in this way. The usual procedure is to coat a former with resin, allow it to gel, and then build up the required shape and thickness by rolling on layer upon layer of resin-soaked cloth or mat. A final gel-coat is then applied and the finished structure may be post-cured. The distribution of fibres in such structures will be uneven. Resin pockets and voids are invariably present, and the unreinforced gel-coat itself will be a ready source of cracks. Figure I shows the typical non-uniform structure, revealed in a fracture surface of a hand laid-up pressure vessel of CSM/polyester.

In summary, all practical composites are likely to contain defects of various kinds arising from the processes of manufacture. Indeed, composites are noted for the variability of mechanical properties which they exhibit unless they have been produced under the most rigorously-controlled conditions. The variability of materials produced by hand lay-up methods is clearly likely to be much more marked than that of composites made by highly mechanised processes. The specific nature and severity of the defects found in any manufactured product will also be characteristic of the manufacturing process. The defects which may be present in manufactured composites include:

- incorrect overall fibre volume fraction
- misaligned or broken fibres
- non-uniform distribution of fibres, with resultant matrix-rich regions
- groups of fibres imperfectly wetted by the matrix
- gaps or overlaps in the arrangement of sheets of reinforcement in any given lamination
- inter-laminar debonded regions (delaminations)
- incorrect state of cure of resin
- resin cracks or transverse ply cracks resulting from thermal stresses during cooling
  after manufacture.

Furthermore, since most composites consist of materials of widely different thermal expansion coefficients they may, if heated and cooled during manufacture, develop residual stresses sufficiently high to crack a brittle matrix. High performance carbon fibre laminates are frequently found to have suffered multiple internal cracking unless proper care is taken to control the production cycle.

Any of these defects may locally reduce the strength of the material below the required component design stress and they are also likely to grow under load. They may then act as sites for the initiation of fatigue damage, or may facilitate the growth of a fatigue crack during cyclic loading. A comprehensive assessment of the quality of a composite material prior to putting into service is clearly, therefore, as important as the monitoring of the levels of damage accumulated in a composite structure during service. Most of the well-known non-destructive testing methods have been used on composite materials, but it seems generally to be agreed that there is at present no single NDE technique that can give a complete picture of the manufactured quality or state of damage of fibre composite materials. All have their limitations, and the most common of these is poor resolution.

3. DAMAGE IN COMPOSITES DURING TESTING AND SERVICE

Materials that are not rejected on the basis of normal quality inspection tests may nevertheless contain many small defects which could adversely affect their performance. Composites for high performance applications should therefore, be proof-tested, but any form of loading, whether it be proof-testing or putting into normal service, can result both in the enlargement of existing flaws and in the generation of new defects. Two problems therefore face engineers and users of composites. The first is to know what size and distribution of manufacturing defects can be *tolerated* in the material or structure prior to proof-testing. The second is to know what levels of damage are introduced by given proof or service loads and what effect this damage has on the residual load-bearing ability of the material. At the present time it is not clear how we distinguish between the two types of defect.

Composite materials as a whole are unlike engineering metals in that they are inhomogeneous and anisotropic. They also accumulate damage in a general rather than a localised fashion. The various microstructural mechanisms of damage accumulation occur sometimes indepundently and sometimes interactively, and the predominance of one or another of them may be affected by materials variables and testing conditions.

The structure of a composite and the associated damage processes may be described at several levels. The loading of a unidirectional composite will result in the fracture, first of the weaker fibres (Fig. 2a) and subsequently of the stronger ones, in a fashion determined by the statistics of flaw distribution in the fibres. A fibre break may initiate a crack in the adjacent matrix if the matrix is brittle (Fig. 2b) or the stress concentration caused by the break may be relieved by plastic flow in a ductile matrix (Fig. 2c). If the stress transferred to the matrix at a fibre break is sufficiently high, it may subsequently also lead to failure of neighbouring fibres (Fig. 2d) especially if they are in close proximity, but this form of 'knock-on' mechanism does not usually occur until high composite stresses are reached.

By contrast, a pre-existing crack will be slowed down and may be halted by an intact fibre in its path (Fig. 3a). If the stress concentrated by a matrix crack is sufficiently high the fibre may be broken in due course, but if not the crack will either pass round the fibre (Fig. 3b) if the bond strength is high, or it may propagate along the interface, debonding the fibre from the matrix for some distance (Fig. 3c) before continuing in the matrix on a different plane.

Practical composites are rarely unidirectional because the high degree of anisotropy makes them unsuitable for many engineering purposes. In a laminate containing a proportion of its fibres at some angle to the applied stress direction the relatively weak fibre/matrix interfaces (Fig. 4a) are readily broken at low composite load levels. In composites with randomly-distributed fibres this debonding damage occurs uniformly throughout the material, and in chopped strand mat (CSM) glass/polyester laminates, for example, it manifests itself as a uniform whitening of the material as many light-scattering interfaces are introduced. On the other hand, in a simple 0/90 laminate the debonds in the transverse plies are linked together by small increments of matrix crack to form a regular sequence of transverse ply cracks (Fig. 4b). Cracking of this kind starts at strains as low as 0.2% and continues, the crack spacing decreasing with increasing load, until the transverse plies are fully cracked at strains of 1% or less. The transverse cracks are usually retained within the 90° plies but may also initiate damage over a small distance into the 0° plies. As the load level on a transversely cracked laminate increases, the transverse cracks may turn along the inter-laminar boundaries and propagate as delaminations (Fig. 4c). In a 0/90 laminate, cracking of a similar nature can occur parallel to the fibres in the 0° plies as a result of both thermal strains and Poisson constraint (1) (Fig. 4d).

In complex, multi-ply laminates of the more practical kind, variations in the anisotropic character of adjacent plies leads to shear coupling stresses which may become sufficiently great, particularly in the neighbourhood of holes or notches, to cause delamination cracks which can spread along the interply boundaries, especially in poorly laminated composites with resin-rich zones at these boundaries (Fig. 5a). Prior to delamination, the adjacent plies support each other against substantial in-plane shear deformations, but these constraints are removed when delamination (decoupling) occurs and the resolved shear stresses acting along the fibres in plies inclined at some angle to the tensile stress can easily cause multiple shear splitting within the plies (Fig. 5b).

A particular problem with filament wound vessels is that even though the hoop stresses may be well supported by the fibres, any axial stresses that are present (in a capped-off pipe for example) can cause fibre/resin debonding. If this occurs in each layer of the windings a path may be opened up between the inside and outside surfaces and permit weepage of any fluid contained under pressure in the vessel. Such leakage may occur at stresses below 25% of the pipe bursting stress (2).

From the testing and design point of view, the problem with composite materials in general is that they are inhomogeneous and anisotropic, and reinforced plastics rarely behave in a linear elastic fashion. Crack propagation is not a simple process as it is in metals. Crack paths are highly complex, and even where an identifiable major crack occurs it is usually not the only manifestation of structural damage. All of the microstructural and macroscopic failure processes that we have just discussed may contribute, in a major or minor way, to degrade the mechanical properties of a composite. The damage, in most cases, is widespread and not necessarily localised in a crack tip region, although this is usually where it is most serious. The tendency to lump together under the umbrella terms 'composites' or 'reinforced plastics' a wide range of engineering materials of substantially different character can also be misleading. The process of damage accumulation depends sensitively on the relative strengths and stiffnesses of the fibre/matrix combination, the character of the interfacial bond, and the manner of distribution of the fibres in the composite.

4. NON-DESTRUCTIVE EVALUATION OF COMPOSITES

4.1 Visual Inspection

In translucent (non-pigmented) GRP, inspection by transmitted light can give a good indication of the presence of pores, poor wetting out, delaminations, and gross inclusions. Prakash (3) has also shown that light transmission can, in favourable circumstances, be correlated with the fibre content, V_f. It is a commonly-observed feature of the occurrence of damage in GRP that loss of transparency is associated with the development of fibre resin debonding and resin cracking, the phenomenon being known as stress-whitening.

In non-translucent composites --- most composites in fact --- the only feasible visual inspection techniques relate to observation of surface damage. The detection of surface cracking (which may not necessarily reflect the true state of deterioration of a composite) and of deeper cracks that are open to the surface, may be enhanced by the familiar dye penetrant methods. These methods can be highly sensitive, and can be used to indicate areas where a more detailed study can usefully be carried out. It has been suggested, however, that they give no useful indication of early fatigue damage (4).

For critical components and areas previously identified as being susceptible to damage, especially fatigue damage, Moiré methods may be suitable. Photographic grids are printed on the surface of the composite and irradiated by coherent light. The resulting interference fringes give clear indications of local stress-concentrations and deformation, including those arising from sub-surface damage (5).

Laser holography methods have also been used for inspection of composite vessels (6) and have been shown to be capable of detecting bond failures and early fatigue damage in lined, filament-wound structures. The method appears to have no advantage, in terms of resolution, over ultrasonic C-scan inspection (q.v.) and it is not easily (or cheaply) adapted for dynamic or field investigations.

Conventional brittle lacquer mapping methods for locating potential sources of fatigue arising from stress concentrations have been successfully used in design studies of GRP fan blades (7), and results indicate that the technique gives information consistent with that obtained by the experimentally less-convenient strain-gauging procedures.

4.2 Radiographic Methods

Radiography is not easily applied in the field, but a good deal of information about composite quality can be obtained by x-ray inspection (8). Contact radiography with sources of 50 kV or less yields high contrast photographs from low-density materials like GRP because of their low inherent filtration. The linear absorption

coefficient of glass is about twenty times that of most resins, and film density measurements can therefore be correlated with glass fibre content per unit surface area, provided the material is unpigmented. The fibre distribution, quality of weave, and the presence of large laminating defects can be easily investigated, and there is evidence that failures often occur at manufacturing defects which are revealed by x-rays even when the defects do not appear to reduce the composite strength. Contact radiographs showing fibre distributions have also been analysed by optical diffraction methods to give quantitative information about the fibre distribution that could not otherwise be obtained (9). The sensitivity of contact radiography can be substantially improved, both for surface-opening and sub-surface defects and cracks, by impregnating the composite with a heavy organic liquid such as carbon tetrachloride or tetrabromoethane. Reynolds (10) has suggested that the limiting crack length for detection by contact radiography is about 30 mm, but this depends very much on the orientation and extent of opening of the crack. Contact radiography cannot normally distinguish fibre/resin debonding or fine transverse cracks resulting from thermal contraction mismatch, and it cannot easily identify delamination cracks, even large ones, unless the cracks are filled with a radio-opaque material.

Projection radiographic techniques can be used with advantage to improve resolution(10). Typically, a 15 micron focal spot is used close to the sample, resulting in projection with a primary enlargement of up to 100. The method has the advantage over contact radiography that the non-image-forming scatter which occurs inside the sample, and which is normally recorded on a contact radiograph, is considerably reduced and reduced and resolution is therefore improved. In this way, with primary magnifications of up to 100 and with subsequent further optical enlargement it has been shown to be possible to resolve single carbon fibres in thin sections, and very fine distributions of sub-surface cracks can be seen in damage zones near crack tips (11) (fig.6).

Although not generally useful for NDE of composites, it is noteworthy that neutron radiography, which is particularly sensitive to the presence of hydrogen, may be valuable in specific cases, such as when there is a need to detect the presence of water in a cracked laminate after environmental exposure or to study the efficacy of gluing in certain types of composite structure.

4.3 Microwave Methods

The dielectric constant of glass is much greater than that of resins at microwave frequencies, and a measurement of the average dielectric constant of a GRP composite can therefore be correlated reasonably satisfactorily with the glass content of the material. A typical instrument, such as that described by Torp et al (8) consists of an open-ended coaxial resonator which can be applied to a GRP surface in order to close the resonant cavity. As the instrument is moved over the surface, changes in the local (average) glass content are indicated by variations in the resonant frequency. The shift in resonant frequency depends on penetration, and thickness corrections must be made when thin plates are examined. But when the appropriate calibration has been made, the glass content of a structure can be investigated by scanning from one side only. Good correlations have been obtained with this technique from materials within the same batch, but problems have arisen when attempting to compare materials from different sources. It is therefore essential that materials to be examined are well-characterised. Since any defect which affects the microwave penetration will also cause a resonance shift, the method could also find useful application as a means of monitoring gradual deterioration of a structure once its dielectric response in the undamaged state had been well-established.

4.4 Eddy Current Methods

Eddy current techniques have been relatively little used for composite materials, and do not show great promise for monitoring damage accumulated in service or proof-testing. By means of reactance-sensitive circuitry, Prakash (12) was able to detect changes in fibre volume fraction in CFRP, and with a directional (horse-shoe) probe he was able to distinguish clearly the lay-up geometry of CFRP laminates. Torp et al (8) have used the method as a one sided thickness gauge for GRP by gluing a metal foil to the laminate face remote from the probe. The thickness (in the range 15-30 mm) of GRP interposed between foil and probe determines the induced current and the technique is said to be accurate to 0.1 to 0.2 mm. This compares very favourable with ordinary magnetic thickness gauges which rely on the force of attraction between the probe magnet and a ferromagnetic plate on the back of the laminate, for which an accuracy of 0.5 to 2.0 mm is cited. It is difficult to see how eddy current gauges could respond sensitively to general fatigue damage, although in composites like CFRP or boron/aluminium it seems feasible that delamination damage and sizeable manufacturing defects could be detected.

4.5 Thermographic Methods

When a uniform heat flux is applied to a plate, any anomalous variations in the resulting temperature distribution in the plate are indications of structural flaws in the material. Williams (13) has described how visualisation of these temperature distributions can be achieved by means of temperature-sensitive colour changes in cholesteric liquid crystals. He prepared GRP samples containing air and paper inclusions to simulate manufacturing defects, and after painting the surface of the composite black, he sprayed on a coating of liquid crystal about 0.02 mm thick. The colour changes in the liquid crystals were reproducible over given temperature ranges when the composites were irradiated with quartz-iodine lamps and Williams was easily able to identify his artificial defects.

Thermal imaging, with limiting detection of temperature differences of about $0.2^{\circ}C$, is easily carried out by means of infra-red television photography, colour differentiation analysis giving better resolution than black and white photography. The method has been used to monitor fatigue damage in boron/aluminium composites (14) and has successfully indicated changes in stress patterns near stress concentrators and other damage that results in heat dissipation. Surface temperature was found to be a sensitive indicator of both dispersed and localised damage. Reifsnider and Stinchcombe (15) have also successfully studied heat emission from damaged areas in carbon/epoxy laminates. McLaughlin et al (16) detected damage in glass/epoxy laminates at low stresses and frequencies, but suggest that detection in materials of higher thermal conductivity is more difficult. They indicated that testing frequencies greater than 5 Hz are needed in order to detect fatigue damage in CFRP. An additional limitation is that thermographic methods cannot distinguish between new local damage and heat dissipation at old damage sites.

In a recent study, Pye and Adams (17) investigated experimental and theoretical limits for location of shear cracks in CFRP and GRP by infra red thermography. They refer particularly to 'zero-volume' matrix shear cracks where the faces of the crack may be held together by a residual compressive stress. Material containing such cracks can sustain compressive stresses, small tensile stresses, and also shear stresses which are transferred across the crack faces by friction. As a result, the stresses produced during propagation of an ultrasonic pulse may also be

adequately transferred within the material and cracks of this kind may not be detectable either by ultrasonic or x-ray means. When the crack faces rub together under moderately large stresses, however, heat is dissipated and Pye and Adams show that the temperature rise may be expressed, roughly, as

$$\Delta T \propto \frac{\Lambda \psi \sigma^2 f}{k}$$

where σ is the stress level, f, the frequency, k, the thermal conductivity, and $\Delta \psi$ is the change in specific damping capacity due to the damage, a characteristic which they have also studied independently (see section 4.6). For the specimens which they used, the minimum detectable crack lengths predicted by their theoretical analysis were 28 mm in CFRP and less than 14 mm in GRP, the lower sensitivity in CFRP being due to their higher conductivity. The advantages of this method are that it is quickly carried out and without a great deal of operator training, and that it is a remote monitoring technique. It is highly susceptible to disturbance by air currents, however.

4.6 Dynamic Mechanical Analysis

When stresses and strains can be continuously monitored, during fatigue testing or in service, we might suppose that changes in elastic modulus would give non-destructive indications of deterioration in properties due to accumulation of damage. But the reduction of composite stiffness during fatigue depends sensitively on the type of composite and on the extent to which the matrix and interface are directly loaded by the fluctuating stresses. In unidirectional CFRP containing 40 vol. % of HMU fibre, for example, Fuwa (18) found no evidence of reduction in modulus, even after 10^4 cycles at stresses well over 75% of the tensile fracture stress, whereas it is a common feature of GRP fatigue that the stiffness often falls substantially in the first few cycles (19). In any given laminate, the change in modulus in response to stress will also depend strongly on the orientation of the laminate relative to the major stress axes. An indication of the magnitude of this effect is shown by some results of Harris et al (20) who loaded a 0/90 glass/epoxy plate to gradually increasing fractions of the fracture stress and re-measured the modulus in the unloaded condition after each stress increment (fig. 7). It can be seen that in the 45° orientation there is no observable reduction in modulus almost to the fracture stress, whereas in the 0° orientation transverse ply cracking significantly reduces the modulus even at low stresses. Measurement of the modulus itself by mechanical means may therefore prove to be relatively insensitive to changes in the damaged state of a laminate, although Harris et al showed that measurement of relative changes in the resonant frequency of damaged samples could give more subtle indications of changes in the damaged state.

For NDE purposes attention has been paid more to measurements of damping than of modulus, but there are some important limitations of the normal mechanical techniques that have been employed. In principle, for NDE measurements limited strain amplitudes are possible, and changes in damping judged from small imposed vibrations may not be easily detectable. DiBenedetto et al (21) determined the damping capacity of glass/epoxy composites (V_f = 0.5) with different laminate constructions by superposing a low-amplitude 10 Hz excitation during normal tensile or fatigue testing. They found that damping increased during tensile loading or with number of fatigue cycles, and they showed that sudden changes in the level of damping during tests could be correlated with the occurrence of different, clearly-observed damage modes.

Adams and his collaborators (22) studied variations in specific damping capacity (SDC) in various composites as damage accumulated, but their measurements were usually made at large amplitudes (3-10% of failure). They found that in the shearing of smooth, cracked CFRP bars, large changes in modulus and SDC occurred as a function of strain whereas no such changes occur in uncracked bars. They believe that measurements of shear modulus are a more sensitive indicator of fibre content, fibre type, fibre surface treatment, etc. than SDC in undamaged material, but the SDC is a better indicator of developing damage when cracking is occurring. They found it possible to detect shear cracks longer than about 20 mm in torsion pendulum experiments at about 5% of the failure strain, and they show that this is about the same level of sensitivity as can be achieved in acoustic emission experiments (q.v.).

Georgi (23) has emphasised that large-amplitude damping measurements are capable of detecting frictional damping caused by delaminations only if the defects are well removed from nodal points and if there are strong shear deformations. A crack in the free end of a cantilever, for example, will not affect the damping of the sample. Harris et al (20) have also shown, by contrast with the work of Adams et al, that resonance peak width measurements of damping during longitudinal and flexural vibration of centre-pinned beams of 0/90 glass/epoxy laminate do not register damage caused by step-loading sequences to failure even when values of the dynamic modulus measured simultaneously from the resonant frequency (fig. 7b) show significant changes. By contrast yet again, Gibson and Plunkett (24) believe that damping changes give more significant indications of damage in 0/90 laminates than the corresponding decrease in modulus. In making use of this method it is clearly necessary, therefore, to match the techniques of determining damping with the type of damage causing the damping.

A cracked bell or railway wheel sound dull instead of ringing when tapped, and the railway wheel tapper has long used this simple concept as an easy NDE method. By extension, if any structure can be forced to resonate in a reproducible manner, its frequency spectrum can be rapidly analysed to establish its characteristic 'sound'. Any damage to the structure could then be expected to change this characteristic spectrum in a recognisable way. Nevadunsky et al (4) refer to their use of a simple 'coin-tap' test of this kind to monitor composite fatigue test pieces, but found it to be a poor indicator of early fatigue damage because significant indications were observed only where damage was already visible. Cawley and Adams (25) have used a more elaborate vibration technique for non-destructive evaluation of the integrity of structures. They measured changes in the lower natural frequencies at a single point in a structure at two or more stages in its life and correlated observed changes in these frequencies which result from local or general changes in stiffness, with the severity of damage which had caused the frequency changes. In practical terms, one set of frequencies is measured before the component is put into service and subsequent measurements then reveal whether the structure is still sound. This is an attractive form of NDE testing because the required dynamic characteristics can be measured at a single point of the structure, unlike most other methods which require access to the whole structure. It is also a rapid method since time-consuming scanning is not required. Cawley and Adams were able to detect damage equivalent to the removal of 1% of the cross-sectional area at a given location.

In order to use the method for location of damage sites it is necessary to perform a theoretical dynamical analysis of the structure to predict the mode shapes reasonably accurately. If this can be done, damage sites can be located by measuring the changes in natural frequency resulting from that damage in two vibrational modes. The ratio of these

frequency changes is a function of the location of the damage only and yields a locus of possible damage sites. If several pairs of modes are used the damage site may be unambiguously defined except in symmetric structures.

4.7 Ultrasonic Methods

Taken as a whole, ultrasonic inspection techniques of various kinds are the most widely preferred of the common NDE methods currently being used for quality assessment of composites. It is important to reconise that the subject may be dealt with at two levels, however. In the first place, there has been extensive research on the measurement of ultrasonic velocity and attenuation in a wide variety of composite materials, and reasonably good correlation has been achieved with theoretical models of wave propagation in anisotropic media, like those of Musgrave for example (26). A good deal of this work is naturally intended to provide absolute values of the parameters studied, and in order to overcome the problem of measuring ultrasonic properties of inhomogeneous, anisotropic materials both the equipment required and the analysis of the results are often highly sophisticated, the equipment usually being far from portable. Much of the research described in the technical literature is therefore of considerable interest, but of little direct relevance to the problems faced by an NDE engineer confronted by large composite vessels of complex structure and geometry.

On the other hand, there are available several simple and relatively inexpensive pieces of portable ultrasonic NDE equipment which, with experience, can give reliable results for many types of material -- metals, concrete, etc. Such equipment ought also to be useful for GRP, as long as the user recognises the constraints that are imposed on the interpretation of his measurements by the peculiar character of the composites. He must also accept that experience with one type of composite (or with other materials) cannot necessarily be transferred uncritically to the investigation of another type of composite. In what follows, the emphasis is on what can most simply be achieved by means of non-complicated ultrasonic measurements, but in view of the importance of the subject, reference is also made to theoretical aspects.

Most composite materials are highly dispersive, having, in many cases, a 'regular' structural pattern at several levels of scale (fibre tows, weave of cloth, laminate stacking sequences, etc), an inevitable array of interfaces (fibre/resin interfaces, interlaminar interfaces) and an inherent distribution of defects (pores, voids, etc). Ultrasonic waves in composites are therefore highly attenuated and velocity and attenuation are strongly dependent on frequency. This frequency dependence is also affected by the detailed geometrical construction (lay-up) of the laminate (27). Generally speaking, the propagation of ultrasonic waves will be affected by frequency, wave length, composite structure (even by the dimensions of the fibre 'network'), structural defects, and by damage caused by loading. The problem of high attenuation is reasonably well overcome by using broad band transducers and low wave frequencies which give shorter, more highly penetrating pulses with less pronounced near-field interference effects. As a result of the low pulse intensities used for composites work, however, it is generally necessary to use higher amplification than is needed for other materials. Most of the common ultrasonic techniques have been used, including pulse transit time measurements (with time delay), pulse echo methods, goniometry and ultrasonic interferometry. On the other hand, techniques based on multiple reflections, such as are often preferred for higher sensitivity work in homogeneous materials, cannot generally be used for composites because of their higher attenuation. Pulse transit time is easily measured by simple electronic equipment, and gives highly reproducible measurements of velocity from which, with certain provisos, the elastic modulus of the material can be obtained. The transmitted pulse is highly distorted by its passage through a composite, however, and simple measurements of attentuation often give far from ideal results. Since there is a range of frequency components in each pulse, the pulse shape is distorted by the frequency-dependent attentuation due to a given defect state. This distortion can also lead to time shifts in the cross-over points used to measure delay time, with the result that the measured pulse velocity may be lowered. Dean (28) has also suggested that observation of the change in pulse width can give information about the defect state.

When an ultrasonic source of finite dimension (diameter), D, is placed in good contact with the surface of a homogeneous medium, the beam of plane waves which it emits diverges as a result of diffraction effects beyond the near-field zone. As shown in figure 8 the length, d, of the near-field zone is given by $D^2/4\lambda$, where λ is the wavelength. The beam intensity in the near-field zone is constant, provided no absorption occurs. Clearly, the directivity of the beam increases with size of source, but decreases with wavelength. If the size of the sample under examination is much greater than d, the diffracted waves suffer mode conversion at the sample surfaces and the beam is attenuated. The intensity falls off in this far-field region as the inverse square of distance from the source, as for a point source, and the attenuation due simply to these diffraction effects is approximately 6 dB for each doubling of the distance. Attenuation effects directly due to the character of the material under test must thus clearly be distinguished from the simple geometrical effect. Table I shows some characteristics of two different kinds of GRP, a chopped strand mat/polyester material and a unidirectional glass/epoxy laminate, for transducers typical of those supplied with commercial equipment.

TABLE I. ULTRASONIC CHARACTERISTICS OF GRP

Materials	Density ρ, kgm^{-3}	US velocity (in plane)* V kms^{-1}	Impedance, ρV, $kgm^{-2}s^{-1}$	Wavelength **		Length of Nearfield Zone, d, mm	
				150 kHz	1 MHz	150 kHz	1 MHz
CSM/polyester ($V_f = 0.16$)	1.50	2.9	4.4×10^6	20	3	8	12
Unidirectional glass/epoxy ($V_f = 0.64$)	2.04	4.9	10×10^6	33	5	5	7

* velocity measured in the plane of the laminate as opposed to through the thickness
** probe diameters, D : 150 kHz = 25 mm; 1 MHz = 12 mm.

The velocity of sound normal to the reinforcement (i.e. through the thickness) of GRP materials does not change significantly with glass-content, lay-up etc over a wide-range of common composite types. Indeed, Torp et al(8) have

used the pulse echo method as a means of assessing the thickness of a GRP structure, and this is particularly useful when access can be gained to one side only, although it is difficult to achieve adequate sensitivity in thin plates. Using the average pulse velocity of 2.52 kms^{-1} suggested by Torp et al it appears that the length of the near-field zone for through transmission in most types of GRP at a frequency of 150 kHz is about 9 mm. It is clear, therefore, that only for through-thickness inspection of plates of this dimension or less will ultrasonic measurements on GRP be free from far-field scattering effects. Different considerations will apply to other composites, but for high performance laminates with higher stiffnesses the relevant wave lengths will usually be greater and the near-field zones correspondingly restricted.

4.7.1 Velocity Measurements

Measurements of ultrasonic velocity can easily be made with ordinary commercial equipment. Therefore, provided the wave velocity can be used as a satisfactory control parameter, indicative of, say, composite density or fibre content, and provided the technique is properly calibrated for a series of composites of known character, the method provides a cheap and easy way of revealing obvious deviations from some pre-assessed specification. But the ultrasonic wave samples a large volume of material and only gross (average) variations from point to point in a structure will be detectable. In order to characterise a material more fully (e.g. to determine the elastic modulus) a separate determination of density is also required.

In an anisotropic material the ultrasonic velocity is generally related to the elastic stiffness array, C_{ij}, by

$$V_{ij} = \sqrt{(C_{ij}/\rho)}$$

where ρ is the density, and it is only indirectly related to the elastic compliances, S_{ij}, and to the technical Young's moduli, E_{ij}. Reynolds and Wilkinson (29) have shown that velocity measurements can be correlated with rigorous theoretical models of wave propagation in anisotropic solids, and confirm that, in principle, the velocity can be used to assess details of composite construction, such as fibre alignment, that affect the properties of the material. In measurements on isotropic materials there is a sharp increase in velocity at the transition from rod waves, for which

$$\rho V^2 = E$$

to bulk waves, for which

$$\rho V^2 = \frac{E(1-\nu)}{(1+\nu)(1-2\nu)}$$

(ν being Poisson's ratio). The transition occurs as the ratio of sample size to wavelength approaches unity, and the jump in velocity is about 35% if $\nu \approx 0.3$. For a uniaxial, anisotropic composite material, for which the orthogonal axes are defined as in figure 9, the corresponding transition is from :

$$\rho V^2 = 1/S_{33}$$

to

$$\rho V^2 = C_{33}$$

For a wide range of values of Poisson's ratio, the rod wave expression can be approximated by

$$\rho V^2 = 1/S_{33} \approx (C_{33} - C_{13})$$

and typical experimental results suggest that for uniaxial CFRP the difference between the rod and bulk moduli may be less than 2% (29, 30) although for more isotropic GRP the discrepancy may be as great as 8%.

In off-axis directions, wave propagation is more complex. In uniaxial glass and carbon fibre composites, for example, the longitudinal wave is strongly attenuated by multiple reflexions at fibre/matrix interfaces when the angle of incidence exceeds a small critical angle, about 15° (31). Reynolds and Wilkinson (30) found that measurement of the compressional wave velocity by direct transmission at angles between 20° and 50° to the fibre axis gave significantly lower values than those obtained from goniometric techniques (q.v.) which are therefore preferred. They also point out that for 0/90 laminates the velocity parallel to the fibre directions or along a 45° line of symmetry is governed by the stiffness of the material in the corresponding direction, which is always greater than the Young's modulus. In principle, therefore, we should not expect to obtain accurate values of elastic modulus in any other than very simple composites from longitudinal wave propagation.

For the NDE engineer, the question of absolute accuracy may not be relevant and it is instructive to examine results obtained from a variety of GRP composites with a simple commercial machine -- the "Pundit" ultrasonic tester (CNS Electronics Ltd., U.K.), using 150 kHz probes. Figure 10 shows plots of transit time as a function of path length for several materials. When velocities obtained in this way are converted to stiffnesses, ρV^2, and compared with values of Young's modulus measured by other standard methods the discrepancies are easily assessed. Figure 11 shows such a comparison with Young's modulus values made by dynamic resonance measurements (20). For wave propagation at 0° and 90° in uniaxial and 0/90 laminates the resultant values of C_{33} or C_{11} are of the order of 4% higher than the dynamic Young's modulus for non-woven laminates and 8 to 10% greater for woven cloth laminates. These results are as expected, given the higher shear stiffness of the woven cloth composite relative to that of that of the non-woven material. Since the pultruded material was in the form of a rectangular rod, it is appropriate that the discrepancy in this case is less than 1%. Figure 11 also shows that for compression wave propagation at 45° to the fibre directions in these materials the values of ρV^2 are between 15 and 28% greater than the corresponding dynamic moduli.

In randomly-reinforced composites with almost isotropic properties, like moulding compounds or CSM composites, sound wave transmission is independent of direction and gives a reasonable and reproducible assessment of dynamic modulus and overall glass content. Included in figure 10, for example, are some transit time measurements made on two nominally identical CSM/polyester pressure vessels, one empty, the other filled with water. Even with complex pulse paths taken through curved sections of the vessels, and arbitrarily oriented, the results are to all intents and

purposes identical. Correlations between materials of different kinds cannot be presupposed, and properly calibrated studies must always be carried out, but there seems to be a reasonably good chance of correlating velocity with density (and therefore with glass content) as figure 12 shows, for a wide range of composite compositions and structural types. It should be noted that simple correlations of this kind will not work when, as in the case of the polyester DMC referred to in figure 12, the composite is heavily filled with a material other than glass.

Features of the anisotropy of composites are clearly shown by measurements of wave velocity as a function of orientation. Figure 13, for example, shows on a polar plot the orientation dependence of longitudinal wave velocity for four GRP materials -- a woven cloth glass/epoxy laminate, a non-woven 0/90 glass/epoxy laminate, a unidirectional glass/epoxy laminate, and a polyester DMC. The shapes of the laminate velocity "surfaces", by comparison with the completely isotropic behaviour of the DMC, clearly reflect their different degrees of anisotropy.

Reynolds and Wilkinson[30] have also used velocity measurements to study the void content of composites. They used calculations of the elastic constants of composites containing voids to construct calibration curves by means of which the measurement of two or more ultrasonic wave velocities may be converted to separate estimates of fibre volume fraction and matrix porosity with good accuracy. As we have already indicated velocity measurements transverse to the fibres (e.g. V_{22}, with reference to fig. 9) are also likely to provide a sensitive means of assessing levels of porosity in GRP plates of known thickness, since this velocity is relatively insensitive to fibre content, but highly sensitive to quality.

4.7.2. Attenuation Measurements

In addition to diffraction effects due to beam spreading and mode conversion, attenuation in solids occurs as a result of scattering and absorption of the ultrasonic wave, and there are several mechanisms of scattering and loss in GRP.

When changes in velocity occur at interfaces because of differences in characteristic impedance of the adjacent materials, scattering will occur. These interfaces may be on a fine scale, like the fibre/matrix interface or resin/air boundaries in porous regions, or on a gross scale, like the interlaminar planes. If the ultrasound wavelength is much greater than the size of the imperfections, random (Rayleigh) scattering occurs, with attenuation, a, given by

$$a = Kf^4 L^3 \qquad (L \leqslant 0.1)$$

where f is frequency, L is the 'size' of the scattering centres (assuming a homogeneous distribution) and K is a constant. In GRP the size of fibre bundles or tows is too large to cause significant scattering, but the scale of individual fibres and fine porosity is sufficiently small for them to act as scattering centres. The damage sustained by composites during loading comprises fractured fibres, resin cracks, fibre/resin debonds, transverse ply cracking and interlaminar cracking, all of which could be expected to add to the degree of scattering of ultrasound. Some energy losses will also occur through friction between surfaces of small cracks or other free interfaces in damaged composites, and these should also contribute to the level of attenuation in a damaged composite. But although there are available several sensitive methods of measuring attenuation (32), few can reasonably be applied to practical composites or used in the field. It must also be accepted that most methods are comparative, rather than absolute. The reproducible coupling of probes to the sample surface is difficult to achieve, and the apparent attenuation of a signal is very sensitive to the pressure applied to the probes. The surface contact attenuation may also be greater than the changes in attenuation in the sample, and as a consequence it is usual to carry out measurements in a water bath (or with irrigated probes) and to measure the attenuation of the sample relative to that over an equivalent path in water or relative to that of another sample of known (high) quality.

Through-thickness attenuation measurements, carried out on samples thinner than the near-field dimension in order to eliminate diffraction effects, are likely to have the greatest chance of success. Measurements by Markham (33), for example, have shown that the technique is a sensitive indicator of general quality. Debonded interfaces, delaminations, or distributions of fine resin pores all scattered strongly and were found to raise the attenuation of carbon fibre composites from as little as 1 dB/mm to as much as 40 dB/mm.

Attenuation appears to be little affected by changes of a few percent in fibre content, so that in practice through thickness attenuation measurements can also be used to determine void content even where there are local variations of V_f (34). Prakash and Owston (35) have also shown that measurements of reflected intensity could be made as a function of orientation by rotating a commercial twin-probe transducer against the surface of a laminate. As a result of mode conversions resulting from interactions of probe and laminate geometry the reflected intensity gives a very clear indication of the stacking sequences in laminates.

Although in general it is not the absolute attenuation that is measured in conventional experiments, Hayford et al(36) have described a buffer block technique that does give the absolute attenuation of thin composite samples. They used a pulse echo method, with 5 MHz pulses, and they measured one returning echo from the backface of the sample and two echos from a buffer block. In this way they have been able to show a correlation between the failure load in interlaminar shear tests and the initial attenuation of their samples.

Perhaps the most highly developed ultrasonic NDE method based on measurements of through-thickness attenuation is the C-scan technique which is used routinely for inspecting large panels. Synchronised raster scanning motions of the transmitter and receiver (irrigated or in a water bath) on opposite sides of the plate allow measurements of the intensity of the transmitted wave to be made as a function of position. It is common to use a focussed transmitter, focussing on the back face of the plate, with the receiver as close to the back face as possible. The transmitted intensity is used to modulate the brightness of a visual display spot, or the density of ink on a diagram at the appropriate (x, y) coordinates, so as to build up a picture of plate quality. The resolution of the technique is limited by dispersion in the composite and by the beam dimensions. It is necessary to use something like a focussed 4 MHz probe to detect defects of the order of 1 mm in size, and as a consequence C-scanning is more reliable as an indicator of general quality than as a detector of specific defects. Large voids, distributions of fine porosity, areas of variation in fibre content, and delaminated regions will usually be revealed by a C-scan, but for assessment of the severity of specific defects it is necessary to make standard test plates containing flat-bottomed

drilled holes of various depths and diameters for calibration purposes. A typical black and white photograph of part of a C-scan of a 2.5 mm thick plate of carbon fibre/epoxy laminate is shown in figure 14. The fibre pattern is clearly visible and although there are variations in printing density, the plate quality would be regarded as acceptable. For quality control purposes it is preferable to select a critical attenuation level for writing or not writing, so that defective areas are clearly visible to an unskilled operator.

There is some disagreement about the value of the C-scan method for detecting fatigue damage in composites. Nevadunsky et al (4), for example, report that the method only revealed defects at seams in fatigued GRP laminates, although in carbon/glass hybrid laminates other signs of damage were visible. Sturgeon (37) on the other hand, shows clear evidence of developing fatigue damage in CFRP laminates, and concludes that C-scanning methods are probably the most useful currently available for inspection of dynamic fatigue damage.

It is likely that users of commercial ultrasonic equipment will want to try to use their systems to measure attenuation in the plane of a sheet, vessel or moulding, particulary if access is limited to one side only. The disadvantage of such a procedure is, as already mentioned, that the high (and variable) surface contact attenuation and diffraction effects resulting from the divergent beam are likely to mask any real material effect. For example, in figure 15 are shown measurements of attenuation at 150 kHz, made with the Pundit system previously referred to on several types of GRP, including laminated plates, a pultruded rod, and CSM/polyester pressure vessels. The system has a stepped input attenuator which is used to set to an arbitrary 100% level on an oscilloscope screen the height of a pulse that has passed through a standard aluminium block. The amount of attenuation that must then be 'inserted' to bring the height of a signal from a test sample back to 100% then gives the relative sample attenuation by subtraction. Silicone grease or 'Swarfega' hand cleaner jelly are used as a coupling agents. The results in figure 15 are plotted logarithmically as a function of probe spacing, and despite the difficulty of obtaining reproducible coupling, the crudity of the spacing technique, and the indirect method of transmitting and receiving the pulse, the curves are all reasonably linear and of the same slope. The vertical spacing of the curves seems to reflect the level of surface smoothness rather than any logical effect of composite composition or structure, and the slope gives in each case an increase of approximately 6 dB for each doubling of the probe spacing, as expected for a straightforward far-field scattering effect. The only sample not to show this effect is the pultruded rod which clearly acts as a wave guide for the rod waves and shows a very low level of attenuation independent of path length. The large scatter for this sample results from the subtraction of two approximately equal attenuation readings.

All of these samples were of high quality, and little can therefore be deduced from these results about composite type or quality. On the other hand, if the orientation of the pulse path is altered while keeping the path length constant, variations in attenuation are obtained (fig. 13) which do relate to the laminate structure. The path length for these measurements was (arbitrarily) 20 cm and the results are normalised so that the measured relative attenuation in the 0° direction is taken as 100%. It can be seen that for composites with fibres at 0° and 90° the attenuation is higher at 45°, as would be expected, and that the woven fibre structure causes a greater increase in attenuation at 45° than a non-woven structure. The lobed patterns in these 0/90 laminates are repeated in each quadrant, but for the unidirectional plate the attenuation rises to a maximum at 90°. These features clearly reflect the scattering mechanisms discussed earlier in this section, but do not give the same patterns as those obtained by the through-transmission technique of Prakash and Owston. The attenuation of DMC, like its velocity surface, also reflects its isotropic character.

The effects of deliberately-introduced defects on in-plane attenuation can be seen in figure 16. Three types of glass/polyester laminates, containing chopped strand mat, woven roving, and unidirectional reinforcement, were produced with three types of defect -- dry patches (poor wetting-out of fibres), resin-rich patches, and inserted aluminium foil -- typical of common manufacturing defects. For the woven roving composites, the through-thickness attenuation of the defective plates, relative to that of a high quality control plate produced at the same time, was as follows :

Defect	Attenuation Relative to Control (through thickness) dB/mm
Aluminium foil	0.36
Resin rich patches	1.68
Dry patches	6.63

Thus, in a 4 mm thick sheet, the signal strength was reduced just below half the control level by the most severe defect -- the dry patches. Figure 16 shows that the dry patches can also be detected by in-plane attenuation measurements in the unidirectional and woven roving composites, but not in the CSM material, and that the other defects are unlikely to be undetected in any of the materials by this means. This is a clear indication of the extent to which diffraction and surface contact effects can mask materials effects of substantial severity. All of these defects would be detected by C-scanning.

4.7.3 Ultrasonic Goniometry

For certain applications goniometric methods permit sensitive measurements of ultrasonic characteristics to be made on small samples (38). From measurements of the critical angle of incidence of a beam impinging on a composite sample in a water bath the elastic moduli are accurately determined, and Reynold and Wilkinson (29, 30, 31) have compared results obtained in this way with those measured by direct transmission. It has also been shown by van Dreumel and Speijer (39) that measurements of transmitted intensity during polar scanning with similar apparatus can give direct information on laminate stacking sequences. At angles of incidence away from the critical a transmitted signal is detected as an interference product of several wave modes and their reflections, similar to those described by Prakash and Owston (35). By continuously monitoring the amplitude of the transmitted signal during scanning with the specimen rotating in two axes, and using this amplitude to modulate the intensity of a spot on a screen, diagrams are obtained which give information about both the critical angles of incidence and the structure of the laminate. The authors show diagrams for typical composites which clearly distinguish between unidirectional and angle-ply lay-ups, between carbon, glass and Aramid fibres, and between woven and non-woven reinforcements. As yet, the method gives no quantitative data, but promises a very clear possibility of "finger printing" and laminate identification by pattern recognition.

4.7.4 Other Ultrasonic Methods

Another of the better-established NDE techniques based on ultrasonics is the principle embodied in commercial equipment of the kind exemplified by the Fokker Debond Tester manufactured by Wells-Krautkramer. This machine uses swept frequency probes generating shear waves of constant amplitude and compares the response of the test material with that of a standard. The resonant frequency and amplitude of the transducer response are recorded in contact with the standard and any frequency and amplitude shifts that occur when the probe is subsequently coupled to the test sample are noted. These shifts must then be calibrated against some known (or measurable) property such as the strength of a lap joint, and they can then be used as a predictor of lap strength. By appropriate calibration the technique is said to be able to give more sensitive indications of the presence of flaws, voids, weak bonds, porosity, delaminations, incorrect cure conditions, poor wetting and poor gap-filling in joints, than other ultrasonic methods (40).

In the techninque of ultrasonic spectroscopy, the frequency content of a pulse that has travelled through a material is analysed by spectrum analysis or fast Fourier transform methods, and this has been said to provide information othger than that obtained from velocity and amplitude measurements (41). But although, for example, the frequency spectra of well-bonded and disbonded laminates are quite different the information contained in them cannot easily be correlated with that obtained from simple attenuation measurements, and it is not clear how spectroscopy results might be interpreted in physical terms.

4.8 Acoustic Emission Monitoring

Any sudden structural change within a composite, such as resin cracking, fibre fracture, rapid debonding, or interlaminar cracking, causes dissipation of energy as elastic stress waves which spread in all directions from the source. The technique of detecting of these acoustic emissions (AE) by suitable transducer/amplifier systems is now well established and triangulation methods may be used to locate flaws in large structures and to assess their severity. There are several ways of analysing the information obtained by AE monitoring of structures under load: some may lead to suitable quantitative procedures for realistic proof testing or life prediction, and some may provide deeper insight into the mechanisms of damage accumulation in composites.

Each stress wave reaches the piezoelectric transducer (usually coupled to a free surface) as a complex wave packet, and the wave form of the electrical signal produced by the transducer is made more complex by resonances of the transducer itself. If the signal is amplified and led to a counter that identifies all positive crossings of a given threshold the number of counts recorded will clearly be much greater than the absolute number of microfailure events that have occurred. This type of counting is known as ring-down counting. A better technique is to convert the ring-down signal into a single envelope and id·ntify each envelope as a distinct 'event' by using a counter that recognises a dead-time of, say, 100 μs between events. This kind of counting is called event counting and there should be nearly a 1 : 1 ratio between the number of microfailure events and the number of counts recorded by the equipment. Both types of counting can be used with a time reset system to give an indication of the rate of occurrence of emissions. Alternatively the total number of counts can be plotted as a function of load, number of cycles in a fatigue test, or time in a creep test. Simple counting is less informative than rate mode monitoring in composites from which very large numbers of counts are usually recorded. A further simple modification is to use a root-mean-square meter to give a continuous record of the mean pulse amplitude as a function of elapsed time during a test, which gives a rough guide to the amount of energy being dissipated at any stage during deformation and failure.

None of these simple methods gives information about the nature of specific microfailure events. To obtain more detailed information it is necessary to analyse either the frequency spectrum or the amplitude distribution of the individual pulses. There are inherent difficulties in frequency analysis because of the fact that the electrical pulses are drastically modified by the transducer. Amplitude analysis, on the other hand, is potentially a fruitful source of information that can provide a more complete characterisation of the emission. In a typical system the numbers of pulses, $n(a)$, exceeding a given amplitude, a, are recorded as a function of the amplitude and may be displayed in various ways. A classicial histogram shows the actual distribution of pulse amplitudes as they occur, and changes in the character of the predominant deformation mechanism may be revealed in this way. Alternatively, a logarithmic plot of the cumulative distribution of $n(a)$ against amplitude may be displayed. If the energies of emission events are randomly distributed, the plot will be a smooth curve of the form :

$$n(a) = (a/a_o)^{-b}$$

where a_o and b are constants. When simple (homogeneous) materials are tested, a large value of b indicates emissions from a large number of small events, whereas a small value of b shows that high energy events predominate. If a change in the character of the AE source events occurs during a mechanical test this may be revealed by monitoring b. In complicated materials like composites unique values of b are not anticipated, but critical points of the amplitude spectrum may be identified by discontinuities in the slope of the b-plot. Changes in the relative contributions of different mechanisms to the overall build-up of damage may also be indicated by changes in the amplitude spectrum as a function of stress level, time, number of cycles, etc.

In tests to failure on simple composites the total acoustic emission count, N, often increases with stress or strain in a smooth fashion to failure. The curve is frequently logarithmic, of the form :

$$N = A\epsilon^n$$

(where A and n are constants: ϵ is the strain) and in unidirectional composites tested in the fibre direction there is good evidence that the AE counts recorded relate predominantly to the failure of fibres or fibre bundles (42). In one instance it has been possible to show close correlation between observed AE and that predicted on the basis of statistical failures of brittle fibres (43).

For more complicated laminates other mechanisms occur and the AE pattern may give clear indications of different failure processes in laminates of different construction (44) (figure 17). The transverse cracking, for example, that occurs at low stresses in laminates with non-woven fibres gives rise to low-stress AE peaks which are not found in either unidirectional laminates or in woven cloth composites (figure 18). The AE responses from samples or structures which contain manufacturing defects are also likely to differ from those of higher quality samples and this allows early recognition, during proof testing, for example, of faulty components if the response of the good material is already well characterised (figure 19) (45).

A familiar phenomenon known as the Kaiser effect relates to the fact that damage is irreversible. Once loaded to a given stress level and allowed to stabilise, no further AE should be recorded on unloading or on reloading until the previous maximum stress is exceeded (figure 20). Time-dependence or testing rate effects sometimes prevent ideal Kaiser-like behaviour, but it is now becoming common to use deviations from this ideal as part of a quality acceptance routine. If the stress at which emissions begin again on reloading is below a certain prescribed fraction of the original maximum stress (this fraction being sometimes termed the 'Felicity Ratio') the structure or component is rejected. A related test, which has for some time been used to check the integrity of metallic pressure vessels, is to monitor the acoustic emissions during periodic proof-loading cycles carried out at intervals during service (46). Failure to observe operation of the Kaiser effect during any proof test is an indication that new damage has occurred in the intervening period.

Amplitude distribution analysis has been regarded as a potentially useful tool for elucidating the micromechanisms of failure in composites, but at the present time there is much uncertainty about the implication of some of the information that is obtained from the analysis. Results have been published, for example, showing well-defined peaks in classical histograms that are supposedly related to distinct failure mechanisms in different kinds of composite (47). Elsewhere, it has been claimed that well-defined b-values (slope of the log cumulative distribution) identifiable with specific microfailure obtained from a variety of different composites, with values of b of 0.5 to 0.8 for fibre failure and values of 1.1 to 1.6 for other mechanisms, such as resin cracking and debonding (48). This carries with it the implication that fibre failures are always the events of highest energy. It is clear from our own work at Bath (49), however, that no such simple general correlation can possibly exist, since the amplitude of a fibre failure event depends sensitively on the condition of the local fibre/resin interface, the extent of debonding and the presence of an environment hostile to the fibres --- particularly in GRP --- to name only three factors. An indication of the difficulty of making generalisations can be obtained from the set of amplitude distributions and associated log cumulative plots for three different kinds of GRP shown in figure 21. It can be seen that the slope of the 'b' plot is high for the non-woven laminate, as might be predicted, but is much lower for the woven cloth laminate, despite that fact that fibre failure must dominate composite failure in both cases. The random (CSM) composite fits no easily discernable scheme, and it is only in such materials as this that we have observed such clear-cut multi-modal distributions of AE amplitudes. On the other hand we have observed that both the number of counts and the shape of the amplitude distribution can distinguish between samples of CSM/polyester plates in which the resin cure conditions are different, or between nominally identical samples (from the same plate) whose failure loads are different and which are therefore clearly of different quality (figure 22) (50).

At this stage of our work, however, it seems improbable to us that a single specific microfailure event can be unambiguously identified with an acoustic emission signal of particular amplitude. A more realistic approach seems likely to be based upon a statistical analysis of the amplitude distributions. Furthermore, a proper resolution of the problem of the effect of the attenuation on amplitude distributions of AE in composites is still required.

The use of AE for monitoring the accumulation of fatigue damage in composites has been less intensively studied, and there is no generally applicable model. This also reflects the fact that composites of different kinds accumulate damage in different ways. When unidirectional CFRP composites are cycled in repeated tension the damage that occurs is predominantly fibre failure (51). Figure 23, from the work of Fuwa et al on HMU carbon fibre/epoxy composites, shows that emissions signalling fibre breakage occurred on the first loading cycle and as the peak load was reached during subsequent cycles. The number of emissions per cycle fell as cycling progressed and samples usually became silent within a hundred or so reversals(figure 24). Fuwa et al reported that when this pattern of behaviour occurred the sample did not subsequently fail in fatigue, even at stresses as high as 90%, the tensile strength. On the other hand, in poor material the rate of emission did not fall during cycling and failure was likely to occur within one or two hundred cycles. Emissions began in any one cycle slightly below the peak stress of the previous cycle, the threshold stress for re-emission being somewhat lower the higher the cyclic stress, but never below 94% of the cyclic stress level. Fuwa et al suggested that if after initial loading a sample was cycled only below 94% of the initial load level no new damage would occur and the material would be below a notional fatigue limit. They found no simple correlation between the number of AE counts during cycling and the cyclic stress level, although there was some suggestion that in samples of different tensile strength, cycling at similar fractions of the tensile strength produced roughly similar total numbers of counts. The nature of the damage that occurred in these CFRP during load cycling was of the same kind as that which occurred during ordinary monotonic loading (figure 25) and during constant load experiments at high stress levels when AE counts were monitored as a function of time. Fuwa et al concluded from these experiments that the emissions during both cycling and holding at constant load reflected the same microfailure mechanism, a process in which the matrix gradually responded to the full applied stress level by local viscoelastic flow, thus transferring a gradually increased level of load to the fibres. The final, stabilized state thus represented a condition of equilibrium with many of the weaker fibres having broken at least once at their points of greatest weakness, the composite as a whole then being marginally stronger than it had been before cycling. Fuwa et al (52) also experimented with hoop-wound rings and polar-wound pressure vessels constructed from a similar variety of CFRP, failure in each case again being predominantly fibre-controlled, and obtained almost identical results. They proposed a proof-testing procedure based on AE monitoring that should preclude premature failure in internally-pressurised vessels of similar construction.

Results for other composites, with lower modulus fibres, or of cross-laminated construction for example, would not be expected to be the same as those described above. In a unidirectional GRP laminate, for example, Fuwa et al (53) found that only when the cyclic stress level was below about 25% of the fracture stress did the acoustic emission counting rate fall to a very low level. At higher stresses the curve never flattened and at only 65% of the tensile strength cycling resulted in very noising splitting failures after some hundreds of cycles only (figure 26). It is emphasised that the emissions recorded at stresses up to 50% of the failure stress were not accompanied by any visible sign of damage in these materials, although they were associated with measurable reductions in the elastic modulus. In this kind of material, by contrast with unidirectional CFRP, the rate of damage accumulation during cycling was much higher than that which occurred at constant load as shown in figure 27 (54) which shows AE as a function of time when identical pieces of laminate were either held under a constant tensile load or cycled repeatedly to the same stress level. Although the time scales are not directly comparable, it is clear that in this case there is a genuine fatigue effect, unlike the behaviour of the similar CFRP samples.

In laminated composites we would expect the AE recorded during cycling to reflect the increased availability of damage mechanisms, relative to those available in unidirectional composites. Thus, in a 0/90 laminate cycled at a peak stress of about half the fracture load, the emissions on the first cycle would relate to transverse ply cracking and the next few cycles should not yield any more emissions from this source. Fig. 20 suggests that in 0/90 glass/epoxy laminates this would be so, but on further cycling some of the transverse ply cracks could easily propagate in some other mode, yielding further emissions. Bechi et al (48), testing notched GRP laminates in 3-point bending, found

that large AE activity occurred during the first few cycles and that this was followed by a quiet period which in turn was succeeded by further large activity just prior to failure. They found, however, that the cumulative total number of counts was independent of fatigue life and of the composite lay-up geometry.

Holt and Worthington (55) have recently carried out tests on filament-wound rings of composites containing EHTS and HMS carbon fibres, and E-glass and R-glass fibres (V$_f$ 0.55) in epoxy resin, with both hoop and angle winding. These were tested in repeated tension with AE monitoring. Their results disagree to some extent with those of Fuwa et al described earlier, and in particular they disagree with the view that cessation of AE activity in CFRP after a run-in period guarantees stabilisation and safe operation. Furthermore, they show at that a higher amplifier gain that that used by Fuwa, activity reduces to a very low level but does not cease altogether. Like Fuwa, they show that AE activity gives no warning of impending fatigue failure in CFRP but suggest that fatigue leads to a breakdown of the Kaiser effect in the period immediately prior to failure which may be used as a warning method. For GRP, Holt and Worthington showed that the continued AE activity during fatigue was progressive and roughly according to a reproducible relationship that offered the possibility of predicting fatigue life.

The resistance of a composite to crack propagation clearly relates to the deformation processes that occur in a zone known as the damage zone, near the tip of any propagating crack. It is not surprising therefore that there should be a relationship between the acoustic emissions from a sample and the stress intensity factor, K. A simple correlation has been found (56) for example, between total AE and K for single-edge-notched samples of heat-treated 7075 aluminium alloy with various crack sizes for which

$$N = 3.8 \times 10^{-14} K^4$$

A similar relationship has been obtained for the discontinuous fibre system asbestos/cement, for which the exponent of K was 6 (57). Direct comparisons cannot be made because of the different sample geometries and amplifer gains. Comparable work on cross-plied GRP laminates indicated a change in predominant damage mechanism at high stress levels when straight line plots of log N versus log K changed slope discontinuously (58). The same work gave a very good logarithmic correlation between the total emission count and the observed area of the damaged zone which gradually built up at the crack tip, an important result for those attempting to develop fracture mechanics ideas for use with reinforced plastics.

The use of acoustic emission methods for locating structural defects or localised regions of developing damage is reasonably well established for metallic structures, and has also been applied with some success to composite structures. The principle used is to determine the times of flight for a pulse travelling between pairs of transducers in an array and to use computer triangulation methods to obtain visual plots of the locations of events as they occur. Linear location along a rod or bar can be done with two transducers (59), but for more complicated structures arrays for four, eight or more transducers are needed. Various algorithms exist to cope with mathematically simply structures and it is common to combine these to deal with more complex geometries, but even in simple materials substantial errors may occur (60). Source location requires a knowledge of the structure geometry, the positions of the transducers, the wave velocity, and the relative arrival times. In composite materials, therefore, where both the wave velocity and the degree of dispersion may be anisotropic, the analysis becomes complex. These difficulties may be overcome to some extent by precalibrating the system with pulses of known characteristics from known locations, and some satisfactory results have indeed been obtained for simple structures. But existing spacial location methods must be treated with circumspection at present when applied to composite structures.

A somewhat less rigorous, but still useful, approach to location is the 'zone of interest' approach that is more commonly use at the present time (61). This makes use of the fact that attenuation in composite structures is frequency dependent. A widely-spaced array of low frequency tranducers monitors the behaviour of the entire structure and the summed output from that array indicates overall acoustic activity. Simultaneously, high frequency probes situated in known areas of probable high emission monitor the local behaviour of vulnerable regions, but do not detect events from further afield. A comparison of the difference in response from the two sets of transducers then gives the experienced operator an indication of local damage, always provided the danger zones have been properly identified at the outset.

The use of acoustic emission methods to define acceptance criteria for composites structures is now becoming familiar to manufacturers, largely, it seems, as a result of the experiences of workers at the Monsanto Company (61). In their procedures, a reinforced plastics tank is rejected if it fails any of the following tests in a single loading sequence :

● The total number of AE counts must not exceed 5000(for a prescribed tranducer). This represents almost no damage for a reasonably sized vessel.
● Not more than 10 events with amplitudes in excess of 70 dB must be monitored. Such counts are *assumed* to represent fibre failure.
● During a dwell period under load, no counts must be monitored beyond the first 2 minutes.
● The Felicity ratio must not be less than 0.96.

The last two criteria relate to creep stability. These are rigid rules, easily capable of misuse if applied in a test that does not correspond in every detail to those carried out by the originators of the rules. They also imply an absolute significance of the prescribed parameters, which is unjustified. Identification of such criteria is certainly an important step towards improved design and proof-testing procedures for composites. Nonetheless, slavish application at such an early stage in our understanding of damage mechanisms and their relation to AE characteristics could result in unnecessary rejection of good quality components and an increase rather than decrease in the use of uneconomic designs.

An interesting recent development that combines certain features of acoustic emission analysis with ultrasonic methods is the use of a parameter known as the stress wave factor (SFW) (62). This method uses an AE probe to monitor the content of pulses transmitted over a fixed distance through the material from an ultrasonic transmitter. The stress wave factor is defined as follows :

SWF = (Pulse rate)x(no. of oscillations per pulse)x(time interval).

It is thus a numerical factor that indicates the attenuation of a pulse of predetermined characteristics. By scanning along a structure, the factor is said to give a good indication of future failure sites, provided the response of good quality material is accurately known. The SWF also correlates well with tensile and shear strength of composites, and for a given fibre orientation shows up differences in fibre/matrix bonding, resin content, etc. It seems likely, then, that it will also give reasonable indications of fatigue damage.

It is clear that a good deal of further experimental work is needed, covering a wide range of materials and testing variables, before acoustic emission can be reliably used as a predictor of fatigue life, and indicator of the residual life of a fatigued sample or component, or as a means of delivering a warning of impending failure. But there is good reason to believe, from what has been achieved so far, that suitable NDE routines based on AE analysis will be developed in time at least for certain types of composites.

5. CONCLUSIONS

By comparison with the existing detailed understanding of the working of standard NDE methods for metallic materials, the value of non-destructive inspection methods for composite materials appears to be much less certain. No single method has yet emerged as being universally useful, although it appears that ultrasonic C-scanning, within the known limitations already discussed, is one of the most used and most useful. The use of two or more techniques, especially where the information they give overlaps, is safer than relying on a single method. But it is vital that before any technique is used, it is extensively calibrated in relation to the particular type of composite which it is proposed to monitor, so that the limitations of the method are completely understood. Above all, it is important that interpretation of results is not based on experience with conventional homogeneous materials.

6 ACKNOWLEDGEMENTS

7. REFERENCES

1. J.E. Bailey, P.T. Curtis and A. Parvizi, (1979), Proc. Roy. Soc. Vol. A366, 599-623
2. D. Hull, M.J. Legg and B. Spencer, (1976), Composites, Vol.7, 245.
3. R. Prakash, (1979), private communication.
4. J.J. Nevadunsky, J.J. Lucas and M.J. Salkind, (1975), J. Composite Materials, Vol.9, 394-408.
5. N.J. Wadsworth, (1971), Proc. Conference on *Properties of Fibre Composites* NPL (IPC, London), 59.
6. C. de Floc'h and J.P. Maigret, (1980), Proc. 3rd International conference on Composite Materials (ICCM3), Pergamon Press, Vol.2, 1721-1731.
7. A.J. Wootton, J.A. MacKinnon and W. Paton, (1977), Strain, October 1977, 3-7.
8. S. Torp, O. Førli and J. Malmo, (1977), Proc. 32nd Annual Technical Conference of SPI, paper 9-A.
9. F. Polato, P. Parrini and G. Gianotti, (1980), Proc. ICCM3 (Pergamon), vol.2, 1050-1058.
10. W.N. Reynolds, (1969), Proc. 24th Annual Tech. Conference of SPI, paper 14-B.
11. R.J. Lee, (1982) Private communication from AERE, Harwell.
12. R. Prakash and C.N. Owston, (1976), Composites, Vol.7, 88-92, see also R. Prakash, Mechanics, Bangalore, 250-254.
13. J.H. Williams, S.H. Mansouri and S.S. Lee, (1979), *Thermal Non-Destructive Testing of Fibreglass Laminates using Liquid Crystals*, Report of Composite Materials and Non-Destructive Evaluation Lab., MIT, July 1979.
14. W.W Stinchcombe, K.L. Reifsnider, L.A. Marcus and R.S. Williams, (1975) in *Fatigue of Composite Materials*, STP 596 (ASTM), 115-129.
15. K.L. Reifsnider and W.W. Stinchcombe, (1976), Proc. Infrared Inforamtion Exchange.
16. P.V. McLaughlin, E.V. McAssey and R.C. Dietrich, (1980), NDT International, Vol.13, 56-62.
17. C.J. Pye and R.D. Adams, (1981), J. Phys.D., Applied Physics, Vol.14, 927-941.
18. M. Fuwa, (1974), Ph.D. Thesis, University of Sussex.
19. T.R. Smith and M.J. Owen, (1968), Plastics and Polymers, 33.
20. B. Harris, F.J. Guild and C.R. Brown, (1979), J. Phys.D. Applied Physics, Vol.12, 1385-1407.
21. A.T. DiBenedetto, J.V. Gauchel, R.L. Thomas and J.W. Barlow, (1972), J. Materials, Vol.7, 211-215.
22. R.D. Adams, J.E. Flitcroft, N.L. Hancox and W.N. Reynolds, (1973), J. Composite Materials, Vol.7, 68-75.
23. H. Georgi, (1979) in Proc. AGARD-CP-277, *Damping Effects in Aerospace Structures*, paper 9.
24. R.F. Gibson and R. Plunkett, (1976), J. Composite Materials, Vol.10, 325-341.
25. P. Cawley and R.D. Adams, (1979), J. Composite Materials, Vol.13, 161-175.
26. M.J.P. Musgrave, (1954), Proc. Roy. Soc., Vol.A226, 356.
27. A. Berthault, R. Dormeval and M. Stelly, (1980), Proc. ICCM3, (Pergamon), Vol.1, 635-648.

28.   G. Dean, (1974), in *Composites - Standards, Testing and Design*, (IPC Press), 126-130.

29.   W.N. Reynolds and S.J. Wilkinson, (1974), Ultrasonics, Vol.12, 109-114.

30.   W.N. Reynolds and S.J. Wilkinson, (1978), Ultrasonics, 159-163.

31.   S.J.Wilkinson and W.N. Reynolds,(1974),J.Phys.D:Appl.Phys.,vol.7,50.

32.   R. Truel, C. Elbaum, B.B. Chick, "Ultrasonic Methods in Solids State Phys'.cs" (1969), Academic Press (N.Y.).

33.   M.F. Markham, (1970), Proc. AGARD Conference 63, *Composite Materials*, paper 4.

34.   D.E.W. Stone, (1974), Discussion in Proc. Conference on *Carbon Fibres, Their Composites and Applications*, Plastics Institute (London).

35.   R. Prakash and C.N. Owston, (1971), Composites, Vol.8, 100-102.

36.   D.T. Hayford, E.G. Hennecke, W.W. Stinchcombe, (1977), J. Composite Materials, Vol.11, 429-44.

37.   J.B. Sturgeon, (1978), British J. of NDT, November 1978, 303-309.

38.   J.G. Elliot, (1973), *An Investigation of Ultrasonic Goniometry Methods Applied to Carbon Fibre Composite Materials*, AERE (Harwell) Report NDT/64.

39.   W.H.M. van Dreumel and J.L. Speijer, (1981), Materials Evaluation, Vol.39, 922-925.

40.   D.F. Smith and C.V. Cagle, (1966), Applied Polymer Symposia, No.3, 411-434.

41.   O.R. Gericke, (1976), in *Non-Destructive Evaluation of Materials*, eds. J.J. Burke and V. Weiss, 299-320.

42.   M. Fuwa, A.R. Bunsell and B. Harris, (1975), J.Materials Sci., 10, 2060-2070.

43.   D.O. Harris and H.L. Dunegan, (1972), in *Testing for Prediction of Materials Performance in Structures and Components*, STP 515 (ASTM), 158-170.

44.   F.J. Guild, M.G. Phillips and B. Harris, (1980), NDT International, Vol.13, 209-218.

45.   M.G. Phillips and B. Harris, (1980), in *Reinforced Plastic Constructed Equipment in the Chemical Process Industry*, I.Mech.E./I.C.E., Manchester, paper 7.

46.   H.L. Dunegan, (1975), Metals Engineering Quarterly, (February).

47.   J.T. Ryder and J.R. Wadin,(1979),*Acoustic emission monitoring of a quasi-isotropic graphite/epoxy laminate under fatigue loading*, Report from Dunegan Endevco Inc.

48.   J. Becht, H.J. Schwalbe and J. Eisenblaetter, (1976), Composites, Vol.7, 245.

49.   M.G. Phillips, F.J. Guild, P.J. Ackerman and B. Harris, (1981), Proceedings of the Institute of Acoustics conference on Acoustic Emission and Photoacoustic Spectroscopy. London.

50.   M.G. Phillips and B. Harris, (1980), Proceedings ofICCM3, Paris, Pergamon Press, Vol.2, 998-1014.

51.   M. Fuwa, B. Harris, A.R. Bunsell, (1975), J. Phys.D. : Appl. Phys., Vol.8, 1460-1471.

52.   M. Fuwa, A. R. Bunsell and B. Harris, (1976), J. Strain Analysis, Vol.11, 97-101.

53.   M. Fuwa, A.R. Bunsell and B. Harris, (1974), in *Composites: Standards , Testing and Design*, NPL Conference, April 1973, (IPC London), 77-79.

54.   B. Harris, (1977), Composites, Vol.8., 213-220.

55.   J. Holt and P.J. Worthington, (1981), Int. J. Fatigue, Vol.3, 31-35.

56.   H.L. Dunegan, D.O. Harris and C.A. Tatro, (1968), Engineering Fracture Mechanics, Vol.1, 105.

57.   J.C. Lenain, (1976), *Etude de la Resistance a la Fissuration d'un Materiau Composite Matrice Fragile et Fibres Discontinues : L'Amiante-Ciment*, These, Ecole des Mines, Paris.

58.   J.T. Barnby and T. Parry, (1976), J. Phys. D. : Appl. Phys., Vol.9, 1919.

59.   J.H. Williams and S.S. Lee, (1979), NDT International, (February), 5-7.

60.   H.J. Rindorf,(1981), Bruel and Kjaer Technical Review, no.2, 3-42.

61.   T.J. Fowler and E. Gray, (1979), Proc. ASCE Convention, Boston, preprint no.3593, see also T.J. Fowler, (1977), Proc. ASCE Convention San Fransisco, preprint no. 3092.

62.   A. Vary and R.F. Lark, (1979), J. Testing and Evaluation, Vol. 7, 185-191.

Fig. 1. Structure of hand laid-up CSM/polyester pressure vessel, showing resin-rich regions, uneven fibre distribution, and voids. The gel coat layer is at the top of the photograph (x60).
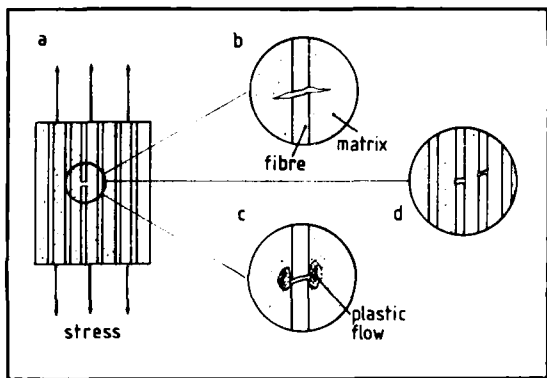

Fig.2. Microfailure mechanisms in fibre composites : I.
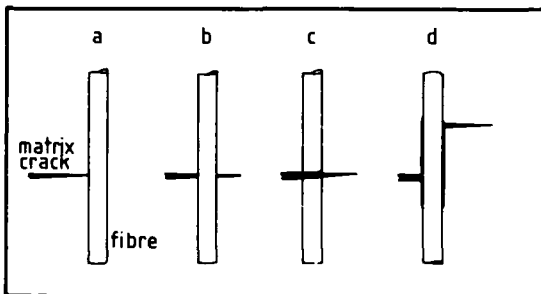
Fig. 3. Microfailure mechanisms in fibre composites : II.
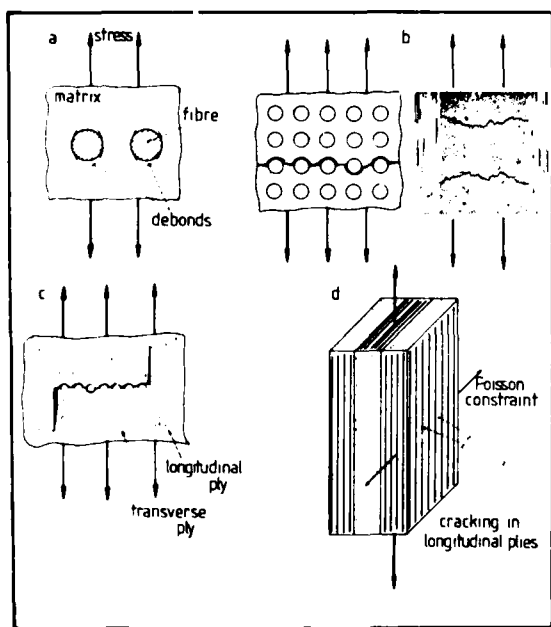

Fig. 4. Laminate failure mechanisms : I.
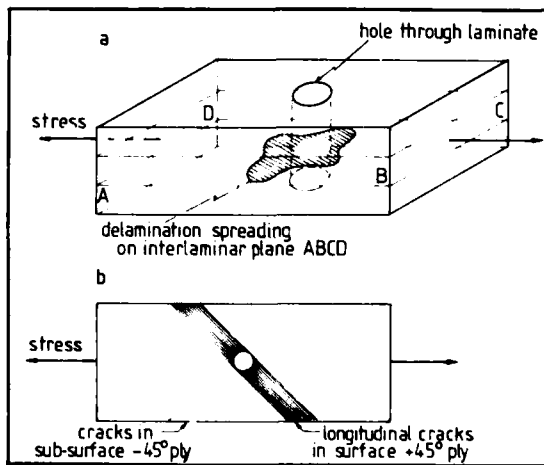
Fig. 5. Laminate failure mechanisms : II.

Fig. 6. X-radiograph of fracture CFRP laminate
showing extensive multiple cracking and
development of damage parallel to fibres.
(carbon/epoxy; $[0, 0 \pm 45]_s$)
Courtesy of Mr R.J. Lee, AERE, Harwell [11].
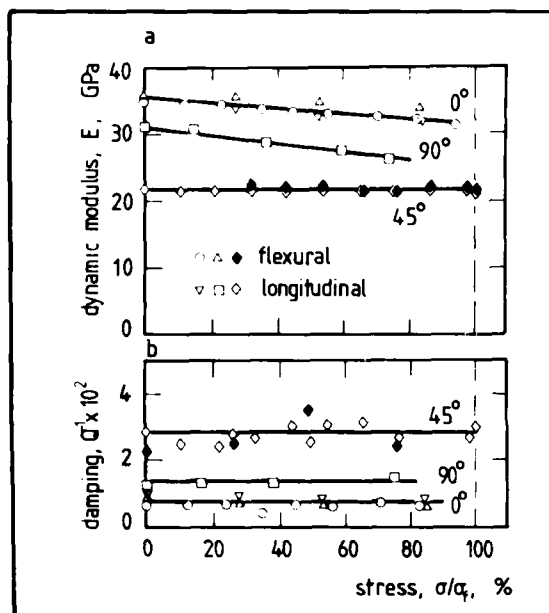
Fig. 7. (a) Elastic modulus of a non-woven
glass/epoxy laminate (Permaglass XE-6) as a
function of pre-stress (20).
The modulus is measured by dynamic resonance in
the unloaded state following loading to the
stress indicated. The pre-stress level is
normalised by dividing by the composite failure
stress, σ_f.

(b) Dynamic damping of Permaglass XE-6 as a
function of normalised pre-stress, σ/σ_f.

Fig 8. Divergence of an ultrasonic beam in an
infinite medium.

Fig. 9. Definition of orthogonal axes with
reference to geometry of a unidirectional
composite lamina.
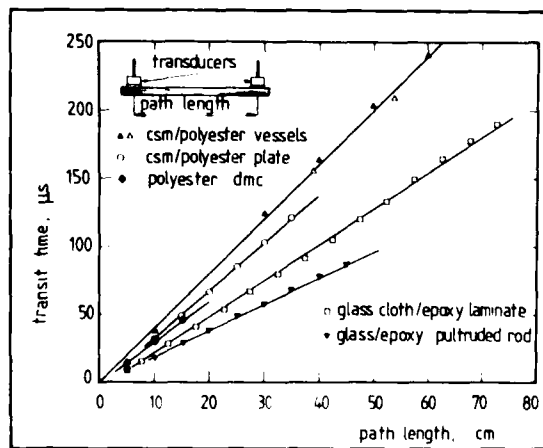
Fig. 10. Measurement of ultrasonic pulse tran-
sit time versus path length for a variety of
types of GRP. The measurements are made with a
simple commercial system, the 'Pundit' (CNS
Electronics Ltd). Frequency = 50 kHz.
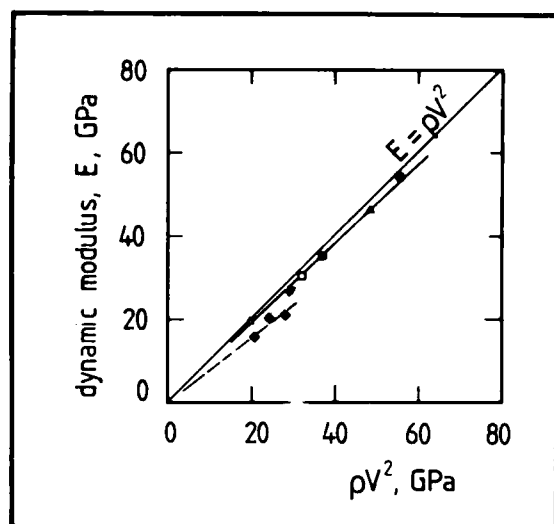
Fig.11. Comparison of moduli, ρV^2, obtained from ultrasonic velocity measurements, with measurements of Young's modulus obtained from dynamic resonance experiments.

● Pultruded rod (glass/epoxy)
▲△Unidirectional glass/epoxy laminate, 0° and 90° to fibres.
■□0/90 Non woven glass/epoxy laminate; 0° and 90° directions.
▼▽0/90 Woven glass/epoxy laminate; 0° and 90° directions.
◆ 0/90 laminates tested at 45° to orthogonal axes.
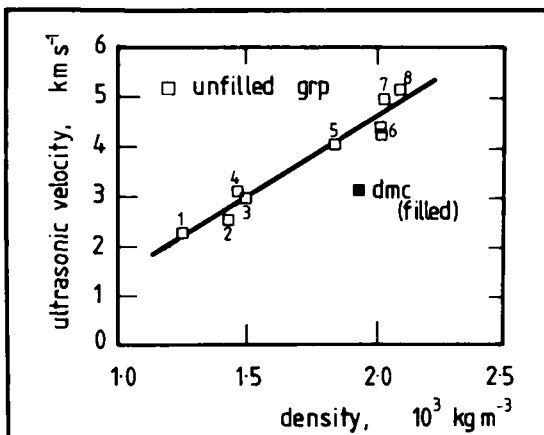
Fig.12. Relationship between ultrasonic pulse velocity (150 kHz) and GRP density for various composites. 1 - polyester resin; 2 - CSM/polyester pressure vessel; 3 - CSM/polyester plate; 4 - CSM + WR/polyester slab (from CEGB waterbox); 5 - Permaglass 22FE25 (woven glass/epoxy laminate); 6 - Permaglass XE6 (0/90 non-woven glass/epoxy laminate) 7 - Permaglass XE5 (unidirectional glass/epoxy laminate) 8 - Glass/epoxy pultruded rod.
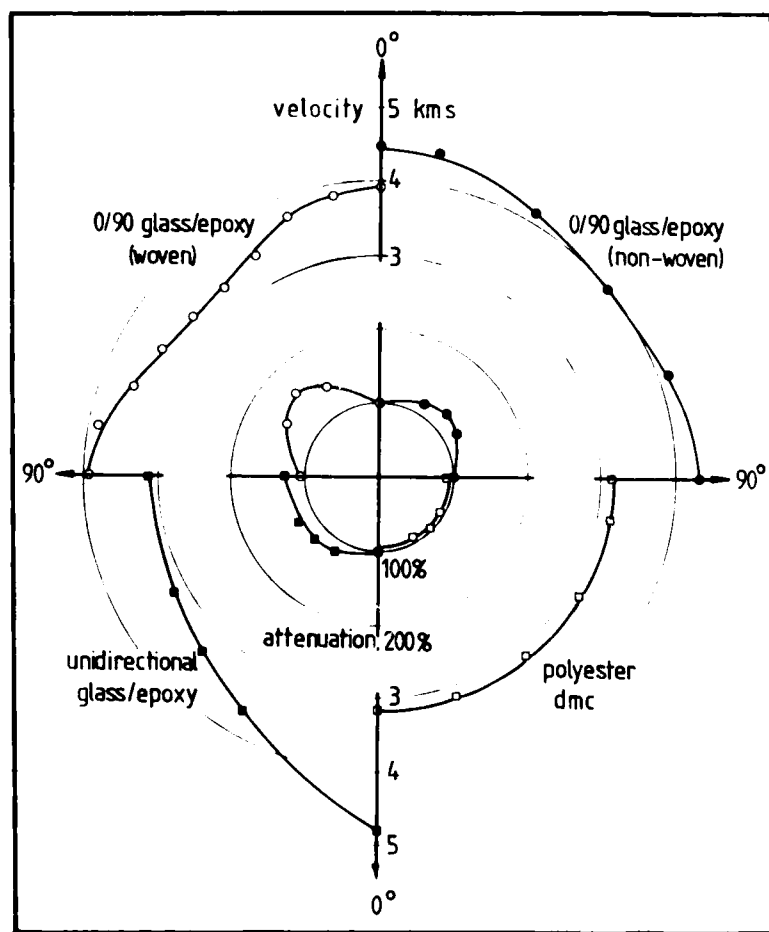
Fig.13. Ultrasonic velocity and attenuation as functions of orientation in the plane of the plate for four varieties of GRP composite. The measurements were made with a standard path length of 20 cm at 150 kHz. The attenuations are plotted relative to the values in the 0° direction as 100%.

○Permaglass 22FE25, woven glass cloth/epoxy (V_f = 0.47);
●Permaglass XE6, non-woven 0/90 glass/epoxy laminate (V_f = 0.62);
■Permaglass XE5, unidirectional glass/epoxy (V_f = 0.63);
□Polyester DMC (V_f = 0.10).
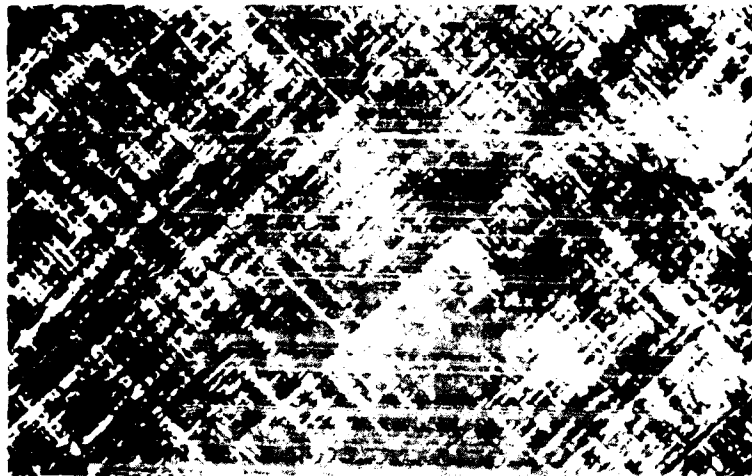
Fig.14. Part of a C-scan print of a CFRP plate
(2.5 mm thickness).
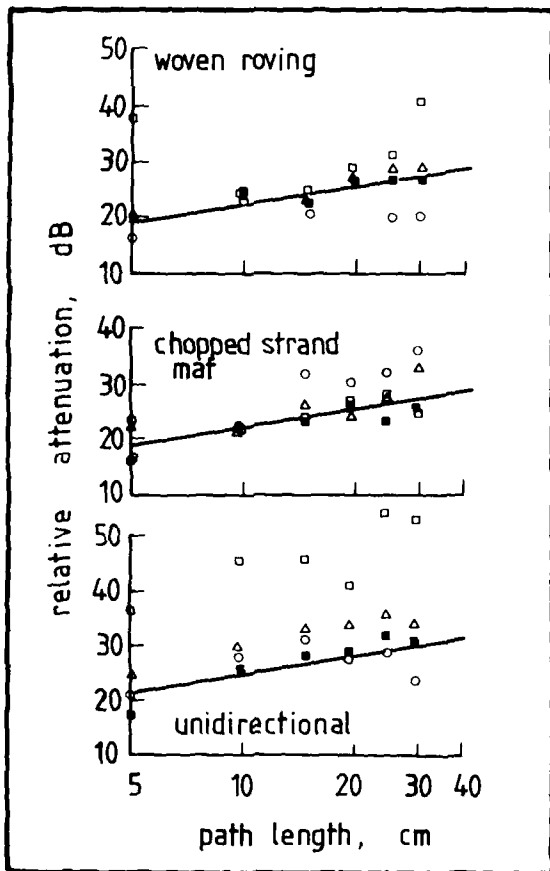
Fig.15. In-plane attenuation measurements on
several GRP materials, attenuation relative to
a standard being plotted as a function of path
length. Measurements were made at 150 kHz with
the Pundit instrument.

▲ 0/90 glass/epoxy plate;
■ Unidirectional glass/epoxy plate;
○ CSM/polyester plate;
▼ woven cloth glass/epoxy plate;
□△CSM/polyester pressure vessels;
◆ pultruded glass/epoxy rod.
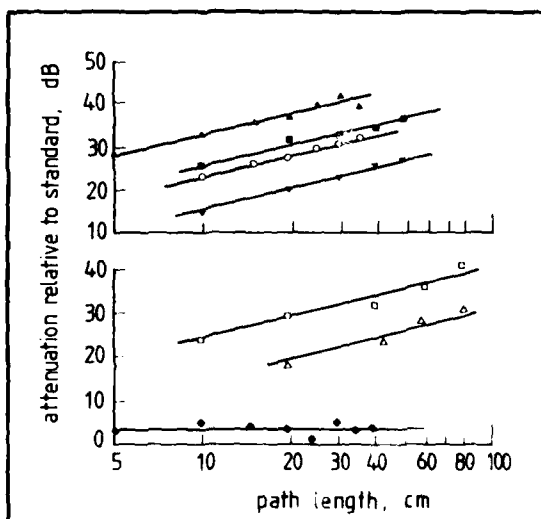
Fig.16 In-plane attenuation measurements on
glass/polyester plates containing deliberately
introduced defects. Three types of plate are
represented, with unidirectional, woven roving
and CSM reinforcement, and they contain three
types of defects —— dry patches, resin rich
patches and aluminium foil laminated into
the plates.

■ control laminate of good quality;
△ aluminium foil inserts;
○ resin rich regions;
□ dry patches.
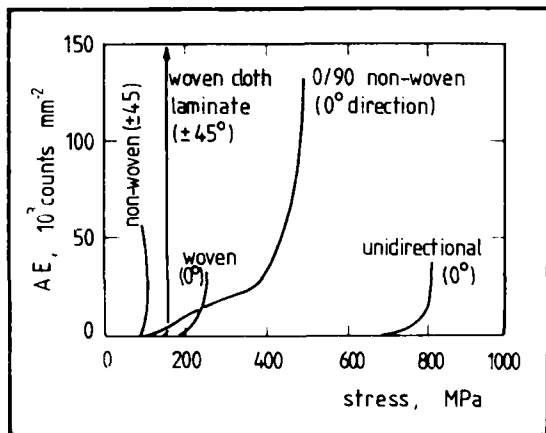
Fig. 17 Acoustic emission (ring-down counts) as a function of stress during tensile testing of some glass/epoxy composites. The number of counts is normalised relative to the cross-sectional area of the sample [20]
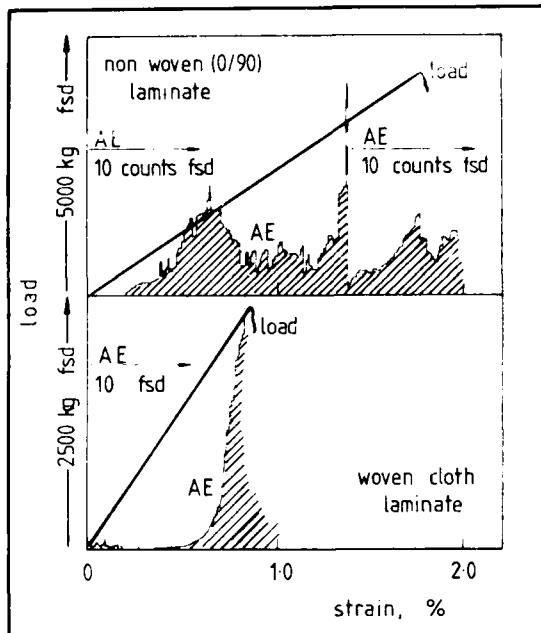
Fig. 18. Load and AE versus strain plots for identical sized samples of glass/epoxy laminates: top; Permaglass XE6, non-woven laminates, bottom; Permaglass 22FE25, woven cloth laminate. The height of the AE plot at any point represents the number of ring-down counts per second [20]
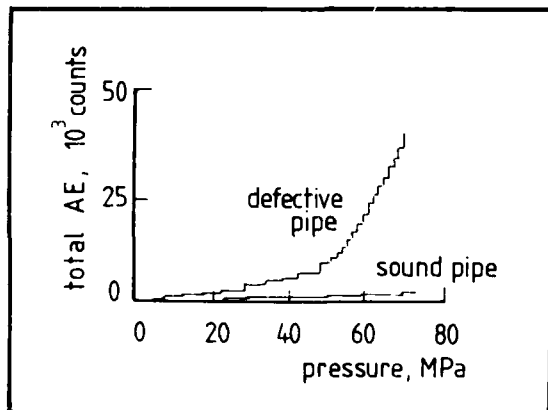
Fig. 19 Acoustic emissions during pressurisation of "sound" and "defective" pipes. After Becht et al (48).
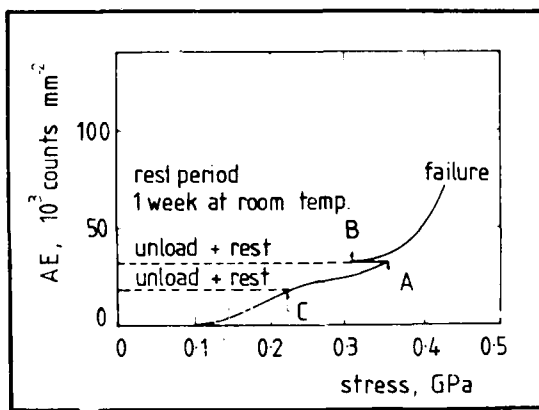
Fig.20. Illustrating Kaiser effect and Felicity ratio. Acoustic emission recommences at point C on reloading after a rest period; Kaiser effect is observed. After loading to A and unloading, AE recommences at B upon reloading; Felicity ratio =(stress at B)/ (stress at A). The curve relates to a 90 degree crossply non woven glass-epoxy laminate.

histogram (linear scale)   log(cumulative)

STRESS LEVELS
1 — 78 % σ_f
2 — 95% σ_f
3 — failure
          (268MPa)

GLASS/EPOXY LAMINATE
Woven cloth (V_f=0.47)

1 — 17% σ_f
2 — 34% σ_f
3 — 51% σ_f

σ_f = 610MPa

GLASS/EPOXY
Non woven (V_f=0.67)

CSM/POLYESTER
failure
$q_{max.}$
80% $q_{max.}$
60%
20% 40%

A.E.,   1024 events full scale per channel

amplitude level,   50 channels, 1.2dB per channel
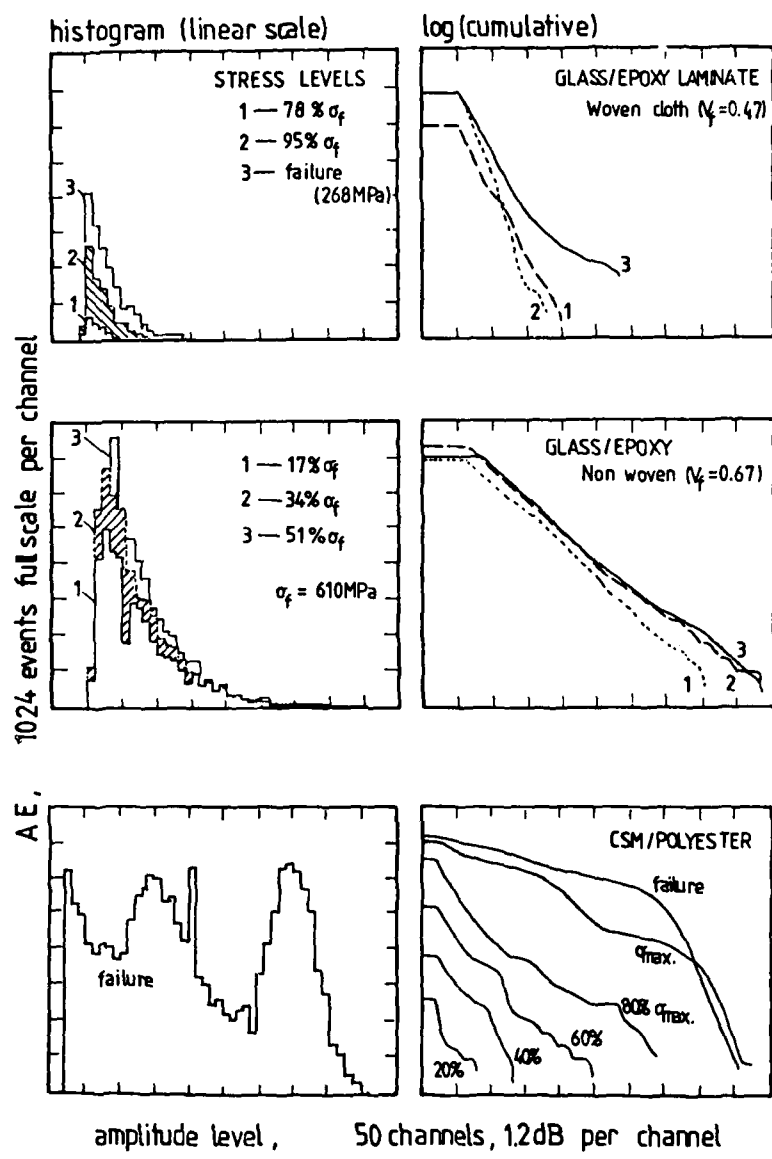
Fig.21. AE amplitude distributions from tensile loading of three grp laminates. On the left, the classical histogram display. On the right logarithmic plots of the cumulative distribu-tions. Numbers on the curves indicate the stress level at which the distribution was recorded. Upper curves relate to a woven cloth laminate, middle curves to an unwoven orthogonal crossply laminate, and lower curves to a CSM/polyester composite(44).
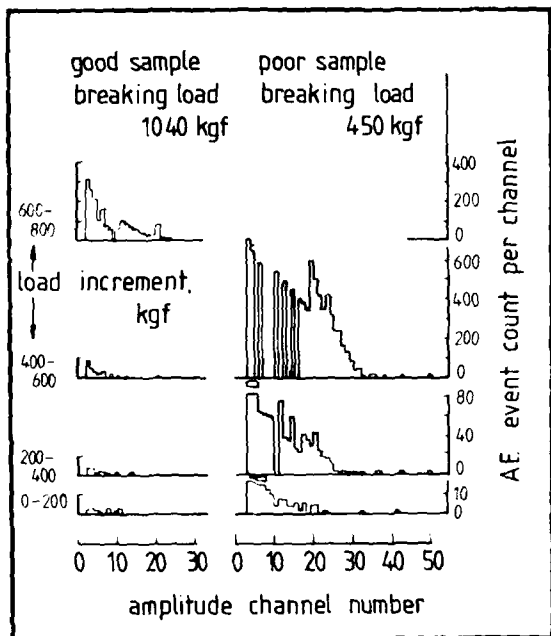
Fig.22. AE amplitude distributions, following identical tensile load increments, for two nominally identical samples of CSM/polyester plate. Note the difference in failure load. Statistical comparison of the distributions enabled these samples to be distinguished at a low stress level.(50)
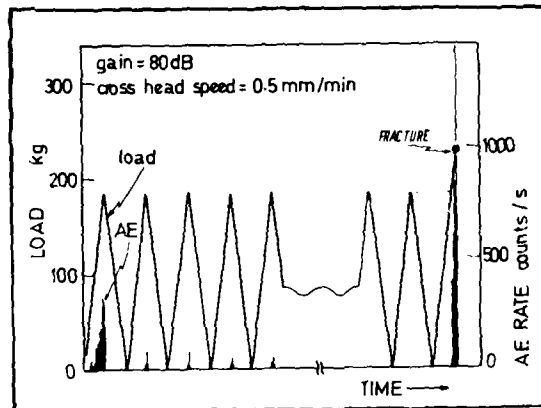
Fig. 23. Acoustic emission recorded during zero-tension fatigue cycling of unidirectional HMU carbon fibre/epoxy composite. (51)
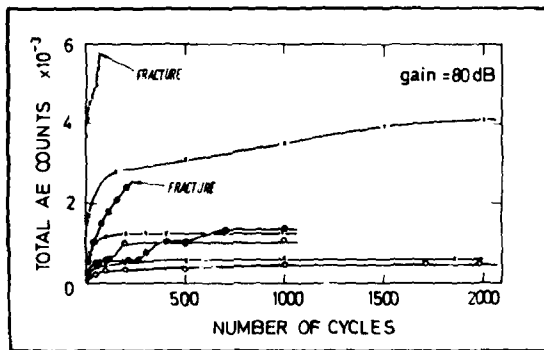
Fig.24. Accumulated acoustic emission counts as a function of number of cycles during zero-tension fatigue cycling of CFRP samples. (51)
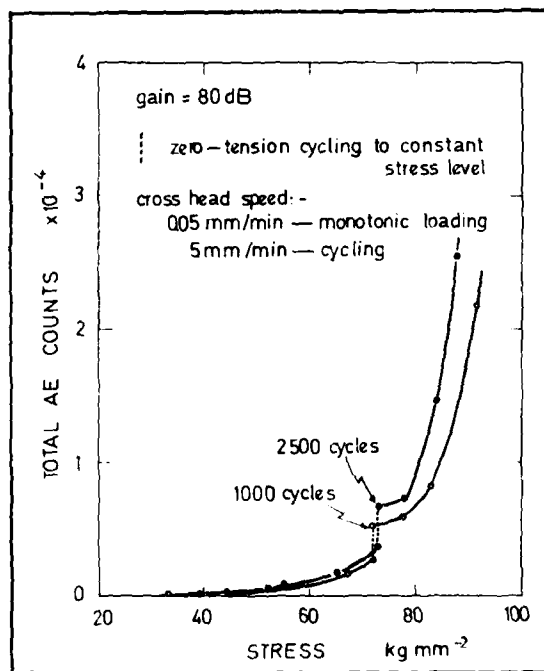
Fig.25. Acoustic emission recorded when a sample of CFRP is monotonically loaded to a given stress, cycled between that stress and zero load, and subsequently reloaded monotonically(53).
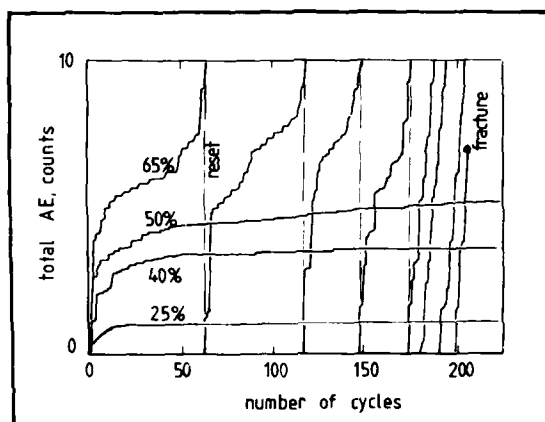
Fig.26. Acoustic emission recorded during
zero-tension cycling a unidirectional glass/epoxy
composite to successively greater fractions of
its static tensile failure stress (53).
Amplifier gain ≠ 60 dB. The numbers on the
curves represent the stress level as a percentage
of the failure stress.
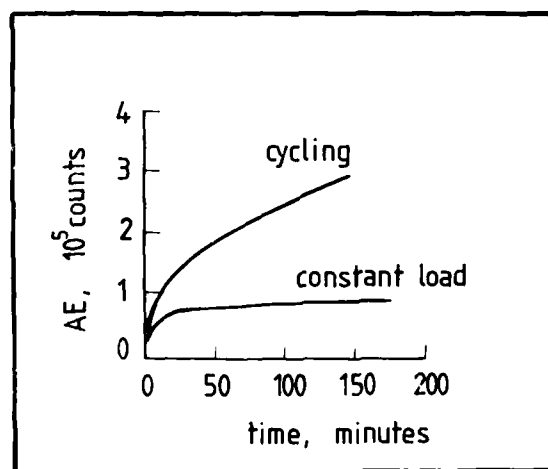
Fig.27. Acoustic emission from GRP during cyclic
loading or holding at constant load. The GRP,
a unidirectional polyester/glass composite
(V_f 0.60) is loaded in the fibre direction at
60% of its tensile failure stress. Larger numbers
of emissions are recorded during cycling than
when the load is held constant. AE amplifier
gain = 60 dB (54)

BIBLIOGRAPHY ON FIBRE COMPOSITE MATERIALS

Compiled by

Mrs J Hart B.Sc.

Defence Research Information Centre
Procurement Executive, Ministry of Defence, UK

in collaboration with

Professor B. Harris
School of Materials Science
University of Bath, Claverton Down, Bath, UK

B

SELECTIVE BIBLIOGRAPHY

The Bibliography which follows is a compilation
of references selected to suit this particular
Lecture Series; it is not intended to be
comprehensive. The references are presented in
reverse chronological order according to the date
of publication of the document. An author index
is included.

It is regretted that AGARD cannot undertake to
provide copies of the documents listed. These
should be sought through National Library Centres
or from the organisations which published them.

1. 82A11525 NASA Issue 2 Category 24
   ENVIRONMENTAL EFFECTS OF COMPOSITE MATERIALS - BOOK
   Springer, G. S.
   810000 Westport, CT, Technomic Publishing Co., 1981. 210 p
   AA(Michigan, University, Ann Arbor, MI) 210 p. $28

2. 82A10546 NASA Issue 1 Category 37
   RF CURING OF EPOXY COMPOSITES
   Ritter, L. C.
   810000 ManTech Journal, Vol. 6, No. 1, 1981, p. 7-13, Army-supported Research
   AA(Boeing Vertol Co., Philadelphia, PA) 7 p, Jpn. 63

3. 82A10548 NASA Issue 1 Category 23
   ORGANIC MATERIALS LAB IN FOREFRONT
   Thomas, G. R.
   810000 ManTech Journal, Vol. 6, No. 1, 1981, p. 17-22.
   Army-supported research. AA(U.S. Army, Organic Materials Laboratory,
   Watertown, MA) 6 p, Jpn. 23

4. 82A11229 NASA Issue 1 Category 39
   INTERLAMINAR STRESS SINGULARITIES AT A STRAIGHT FREE EDGE IN
   COMPOSITE LAMINATES
   Raju, I. S.; Crews, J. H., JR.
   National Aeronautics and Space Administration. Langley Research
   Center, Hampton, Va. (ND210491)
   810000 NSG-1449 Computers and Structures, Vol. 14, No. 1-2, 1981, p. 21-28
   AA(NASA, Langley Research Center; Joint Institute for Advancement
   of Flight Sciences, Hampton, Va) AB(NASA, Langley Research Center,
   Hampton, Va) 8 p. Refs. 6 Jpn. 75

5. 82A11243 NASA Issue 1 Category 39
   ANALYSIS OF LAMINATED COMPOSITE SHELL STRUCTURES BY FINITE ELEMENT
   METHOD
   Panda, S.; Natarajan, R.
   810000 Computers and Structures, Vol. 14, No. 3-4, 1981, p. 225-230.
   AA(Regional Engineering College, Rourkela, India) AB(Indian Institute
   of Technology, New Delhi, India) 6 p, Refs. 13 Jpn. 77

6. 82A11976 NASA Issue 2 Category 23
   JAPAN CONGRESS ON MATERIALS RESEARCH, 24TH, KYOTO, JAPAN, SEPTEMBER 1980,
   PROCEEDINGS
   Kunugi, M.
   810000 Congress sponsored by the Science Council of Japan, Society of
   Materials Science, Society of Naval Architects of Japan, et al Kyoto,
   Society of Materials Science, 1981, 364 p (For individual items see
   A82-11977 to A82-11985) 364 p. $40

7. 82A11982 NASA Issue 2 Category 24
   VIBRATION CHARACTERISTICS OF HYBRID COMPOSITE LAMINATES
   Fukuda, T.; Fughii, T.
   810000 In: Japan Congress on Materials Research, 24th, Kyoto, Japan,
   September 1980, Proceedings. (A82-11976 02-23) Kyoto, Society of
   Materials Science, 1981, p. 306-309. AB(Osaka City University, Osaka,
   Japan) 4 p.

8. 82A11983 NASA Issue 2 Category 24
   THE EFFECT OF THE FIBER ORIENTATION ANGLE ON THE FAILURE OF SHORT
   FIBER COMPOSITES
   Hayashi, I.; Shibanuma, K.; Kawata, H.; Kawada, H.
   810000 In: Japan Congress on Materials Research, 24th, Kyoto, Japan,
   September 1980, Proceedings. (A82-11976 02-23) Kyoto, Society of
   Materials Science, 1981, p. 310-317. AA(Waseda University, Tokyo,
   Japan) AB(Nippon Genshiryoku, Japan) 8 p. Refs. 6

9. 82A10701 NASA Issue 1 Category 24
    COMPOSITE MATERIALS - RUSSIAN BOOK
    Kompozitsionnye materialy
    Manokhin, A. I.
    810000 Moscow, Izdatel'stvo Nauka, 1981. 304 p. In Russian. (For
    individual items see A82-10702 to A82-10746 304 p. Jpn. 23

10. 82A10705 NASA Issue 1 Category 24
    ORGANIC-FIBER COMPOSITES
    Kompozitsionnye materialy na osnove organicheskikh volokon
    Mashinskaia, G. P.; Perov, B. V.
    810000 In: Composite materials. (A82-10701 01-24) Moscow,
    Izdatel'stvo Nauka, 1981, p. 29-35. In Russian. 7 p. Jpn. 23

11. 82A10706 NASA Issue 1 Category 24
    HIGH-TEMPERATURE COMPOSITE MATERIALS
    Vyzokotemperaturnye kompozitsionnye materialy
    Karpinos, D. M.; Tuchinskii, L. I.
    810000 In: Composite materials. (A82-10701 01-24) Moscow,
    Izdatel'stvo Nauka, 1981, p. 35-40. In Russian. 6 p. Refs. 5 Jpn. 23

12. 82A10724 NASA Issue 1 Category 39
    PRINCIPLES OF THE CALCULATION OF THE DEFORMATION PARAMETERS OF FIBER-
    REINFORCED COMPOSITE MATERIALS
    Osnovy rascheta parametrov deformatsii voloknistykh kompozitsionnykh
    materialov
    Tikhonov, A. S.; Manuilov, V.F.; Arefev, B. A.; Galakhov, A. V.
    810000 In: Composite materials. (A82-10701 01-24) Moscow,
    Izdatel'stvo Nauka, 1981, p. 140-143. In Russian. 4 p. Refs. 7 Jpn. 69

13. 82A10735 NASA Issue 1 Category 24
    THE INFLUENCE OF SURFACE TREATMENT OF HIGH-MODULUS FIBERS ON THEIR
    COMPATIBILITY WITH POLYMER BINDERS
    Vliianie poverkhnostnoi obrabotki vysokomodul nykh volokon na
    sovmestimost s polimernymi sviazuiushchimi
    Kobets, L. P.
    810000 In: Composite materials. (A82-10701 01-24) Moscow,
    Izdatel'stvo Nauka, 1981, p. 201-206. In Russian. 6 p. Refs. 13 Jpn. 24

14. 82A10736 NASA Issue 1 Category 24
    AUGMENTATION OF THE STIFFNESS OF A POLYMER MATRIX AND ITS INFLUENCE ON
    THE MECHANICAL PROPERTIES OF COMPOSITE MATERIALS
    Povyshenie zhestkosti polimernoi matritsy i ee vliianie na mekhanicheskie
    svoistva kompozitsionnykh materialov
    Trostianskaia, E. B.; Babaevskii, P. G.; Bukharov, S. V.
    810000 In: Composite materials. (A82-10701 01-24) Moscow,
    Izdatel'stvo Nauka, 1981, p. 207-210. In Russian. 4 p. Jpn. 25

15. 82A10738 NASA Issue 1 Category 24
    EFFECT OF THE EPOXY MATRIX COMPOSITION ON THE PROPERTIES AND
    WORKABILITY OF CARBON PLASTICS
    Vliianie sostava epoksidnoi matritsy na svoistva i tekhnologichnost
    ugleplastikov
    Guniaev, G. M.; Khoroshilova, I. P.
    810000 In: Composite materials. (A82-10701 01-24) Moscow,
    Izdatel'stvo Nauka, 1981, p. 214-218. In Russian. 5 p. Jpn. 25·

16. 82A10739 NASA Issue 1 Category 24
    BEHAVIOR OF CARBON PLASTICS UNDER THE COMBINED EFFECT OF ENVIRONMENT
    AND STRESS
    Povedenie ugleplastikov pri kompleksnom vozdeistvii sredy i nagruzki
    Sorina, T. G.; Surgucheva, A. I.; Buianov, G. I.; Finogenov, G. N.;
    Iartsev, V. A.
    810000 In: Composite materials. (A82-10701 01-24) Moscow,
    Izdatel'stvo Nauka, 1981, p. 218-223. In Russian. 6 p. Jpn. 25

17. 82A10740 NASA Issue 1 Category 24
    OPTIMIZATION OF THE COMPOSITION AND REINFORCEMENT STRUCTURE
    OF TWO- AND THREE-COMPONENT COMPOSITE MATERIALS
    Optimizatsiia sostava i struktury armirovaniia bi- i
    trekhkomponentnykh kompozitsionnykh materialov
    Guniaev, G. M.; Rumiantsev, A. F.; Fedkova, N. N.; Mitrofanova, E.
    A.; Chekina, Z. F.; Stepanychev, E. I.; Makhmutov, I. M.
    810000 In: Composite materials. (A82-10701 01-24) Moscow,
    Izdatel'stvo Nauka, 1981, p. 223-227. In Russian. 5 p. Jpn. 25

18. 82A14050 NASA Issue 3 Category 38
    NDT CHRONOLOGY OF ADVANCED COMPOSITES AT GRUMMAN AEROSPACE
    Collins, R. M.
    811100 Materials Evaluation, Vol. 39, Nov. 1981, p. 1126-1129.
    AA(Grumman Aerospace Corp., Advanced Composite Development Dept.,
    Bethpage, NY) 4 p. Refs. 7 Jpn. 384

19. 82N12142 NASA Issue 3 Category 24
    IN-SERVICE INSPECTION METHODS FOR GRAPHITE-EPOXY STRUCTURES ON
    COMMERCIAL TRANSPORT AIRCRAFT
    Final Report
    Phelps, M.L.
    Boeing Commercial Airplane Co., Seattle, Wash. (BR798021)
    NASA-CR-165746 811100, Nov. 1981, NAS1-15304 105 p. Jpn. 304 HC A06/MF A01

20. 82A12738 NASA Issue 2 Category 24
    THE RESIN MATRIX - ITS INFLUENCE ON SHEET MOLDING COMPOUND
    MECHANICAL PROPERTIES
    Pritchard, G.; Rhoades, G. V.
    811000 Polymer Composites, Vol, 2, Oct. 1981, p. 179-184
    AB(Kingston Polytechnic, Kingston-on-Thames, Surrey, England) 6 p.
    Refs. 18

21. 82A12739 NASA Issue 2 Category 39
    STRESS INTENSITY FACTOR MEASUREMENTS IN COMPOSITE LAMINATES WITH
    VARIOUS NOTCH CONFIGURATIONS
    Roman, I.; Harel, H.; Marom, G.
    811000 Polymer Composites, Vol. 2, Oct. 1981, p. 199-203.
    AC(Jerusalem, Hebrew University, Jerusalem, Israel) 5 p.

22. 82A12741 NASA Issue 2 Category 24
    THE RHEOLOGY AND MOLD FLOW OF POLYESTER SHEET MOLDING COMPOUND
    Lee, L. J.; Marker, L. F.; Griffith, R. M.
    811000 Polymer Composites, Vol. 2, Oct. 1981, p. 209-218. AC(General
    Tire and Rubber Co., Akron, OH) 10 p. Refs. 26

23. 82N12141 NASA Issue 3 Category 24
    BIAXIAL TESTS OF FLAT GRAPHITE/EPOXY LAMINATES
    Final Report, 1 Feb. 1976 - 31 Dec. 1980
    Liebowitz, H.; Jones, D. L.
    National Aeronautics and Space Administration. Langley Research
    Center, Hampton, Va. (ND210491)
    NASA-CR-165793 811000, Oct. 1981, NSG-1289 106 p. Jpn. 304 HC A06/MF A01

24. 82A11176 NASA Issue 1 Category 24
    SUB-T/g/ ANNEALING STUDIES OF ADVANCED EPOXY-MATRIX GRAPHITE-FIBER-
    REINFORCED COMPOSITES
    Kong, E. S. W.
    National Aeronautics and Space Administration. Ames Research Center,
    Moffett Field, Calif. (NC473657)
    811000 NCC2-103 Journal of Applied Physics, Vol. 52, Oct. 1981, p.
    5921-5925. AA(NASA, Ames Research Center, Materials Science and
    Applications Office, Moffett Field; Stanford Joint Institute for
    Surface and Microstructural Research, Stanford, CA) 5 p. Refs. 24 Jpn. 25

25. 82N11117 NASA Issue 2 Category 24
NOVEL IMPROVED PMR POLYIMIDES
Pater, R. H.
National Aeronautics and Space Administration. Lewis Research
Center, Cleveland, Ohio. (ND315753)
NASA-TM-82733; E-1045 810000 Presented at the 13th Natl. SAMPE
Tech. Conf., Mt. Pocono, Pa., 13-15 Oct. 1981 18 p. Jpn. 158
HC AO2/MF AO1

26. 82N12140 NASA Issue 3 Category 24
THE EFFECT OF RESIN ON THE IMPACT DAMAGE TOLERANCE OF GRAPHITE-
EPOXY LAMINATES
Williams, J. G.; Rhodes, M. D.
National Aeronautics and Space Administration. Langley Research
Center, Hampton, Va. (ND210491)
NASA-TM-83213, Oct. 1981, 811000 Presented at the 6th ASTM Conf.
on Composite Mater.: Testing and Design, Phoenix, Ariz., May 1981
46 p. Jpn. 304 HC AO3/MF AO1

27. 82A10307 NASA Issue 1 Category 5
SOME POSSIBILITIES FOR COMPOSITE LIGHT AIRCRAFT CONSTRUCTION
Webb, J. H.
810900 (Royal Aeronautical Society, Symposium on Developments in
Structures and Manufacturing Techniques, London, England, Apr. 14,
1981.) Aeronautical Journal, Vol. 85, Sept. 1981, p. 328-331.
AA(Cranfield Institute of Technology, Cranfield, Beds., England)
4 p. Jpn. 9

28. 82A10308 NASA Issue 1 Category 5
LIGHT AIRCRAFT STRUCTURAL DESIGN IN NON-METALLICS - USE OF
COMPOSITE HONEYCOMB FOR LIGHT AIRCRAFT
Woodley, G. E.
810900 (Royal Aeronautical Society, Symposium on Developments in
Structures and Manufacturing Techniques, London, England, Apr. 14,
1981.) Aeronautical Journal, Vol. 85, Sept. 1981, p. 332-333.
AA(Ciba-Geigy Plastics and Additives Co., Duxford, Cambs., England)
2 p. Jpn. 9

29. 82N12139 NASA Issue 3 Category 24
HYBRIDIZED POLYMER MATRIX COMPOSITE
Final Report
Stern, B. A.; Visser, T.
Composites Horizons, Pomona, Calif. (CZ198003)
NASA-CR-165340, Sept. 1981, 810900 NAS3-21384 85 p. Jpn. 304
HC AO5/MF AO1

30. 82N12645 NASA Issue 3 Category 44
WEST EUROPE REPORT: SCIENCE AND TECHNOLOGY, NO. 72 - COMPOSITE
MATERIALS AND ENERGY TECHNOLOGY
Joint Publications Research Service, Arlington, Va. (J1957394)
JPRS-78876, 1 Sept. 1981, 810901 Transl. into ENGLISH from various
West European articles 49 p. Jpn. 374 HC AO3/MF AO1

31. 81A43974 NASA Issue 20 Category 23
MATERIALS WITH SUPERIOR CHARACTERISTICS AND THEIR AVAILABILITY IN
THE FUTURE
Superwerkstoffe und ihre Verfuegbarkeit in der Zukunft
Hauffe, K.
810800 Metall, Vol. 35, Aug. 1981, p. 737-744. In German.
AA(Goettingen, Universitaet, Goettingen, West Germany) 8 p. Refs. 53

32. 82A11547 NASA Issue 2 Category 24
ON THE RELATIONSHIP BETWEEN ENGINEERING PROPERTIES AND DELAMINATION
OF COMPOSITE MATERIALS
Herakovich, C. T.
810700 NAS1-15080; NCC1-15; NASA TASK 14 Journal of Composite
Materials, Vol. 15, July 1981, p. 336-348. 13 p. Refs. 9

33. 82A11548 NASA Issue 2 Category 24
     A RAPIDLY CONVERGENT SCHEME TO COMPUTE MOISTURE PROFILES
     IN COMPOSITE MATERIALS UNDER FLUCTUATING AMBIENT CONDITIONS
     Weitsman, Y.
     810700 F33615-79-C-5517; F49620-78-C-003 Journal of
     Composite Materials, Vol. 15, July 1981, p. 349-358.
     AA(Texas A & M University, College Station, TX) 11 p. Refs. 10

34. 82N11119 NASA Issue 2 Category 24
     THE INDUSTRIAL PROCESSING OF UNIDIRECTIONAL FIBER
     PREPREGS
     Laird, B.
     National Aeronautics and Space Administration,
     Washington, D.C. (NC452981)
     NASA-TM-76599 810600, June 1981, NASW-3199 Transl.
     into ENGLISH from Plastiques Renforces, Fibres de
     Verre Textile v. 19, Jul.-Aug. 1980 p 9-16
     Original language document announced as A80-44924
     Transl. by Kanner (Leo) Associates, Redwood City,
     Calif. Original doc. prep. by Ciba-Geigy France,
     S. A. 18 p. Jpn. 158 HC A02/MF A01

35. 82N11136 NASA Issue 2 Category 24
     THE EFFECTS OF JET EXHAUST BLAST IMPINGEMENTS ON
     GRAPHITE-EPOXY COMPOSITES - F-18 AIRCRAFT
     M.S. Thesis
     Hampey, J. M.
     Naval Postgraduate School, Monterey, Calif.
     (NS368219) AD-A104622 810600, June 1981, 134 p.
     Jpn. 161 HC A07/MF A01

36. 81A35697 NASA Issue 15 Category 34
     EFFECTIVE THERMAL CONDUCTIVITIES OF FIBROUS COMPOSITES
     Han, L. S.; Cosner, A. A.
     810500 AF-AFOSR-78-3640 ASME, Transactions, Journal
     of Heat Transfer, Vol. 103, May 1981, p. 387-392. AB
     (Ohio State University, Columbus, Ohio) 6 p. Refs. 16
     Jpn. 2525

37. 81A39675 NASA Issue 18 Category 38
     APPLICATIONS OF ACOUSTIC EMISSION TO NONDESTRUCTIVE
     TESTS OF FIBER COMPOSITE INDUSTRIAL APPARATUS
     Applications de l'emission acoustique au controle non
     destructif des structures industrielles en materiaux
     composites
     Lenain, J. C.
     810400 Plastiques Renforces, Fibres de Verre Textile,
     Vol. 21, Apr. 1981, p. 15-18. In French. AA(Endevco
     France, Paris, France) 4 p. Refs. 5

38. 81A44326 NASA Issue 21 Category 23
     MATERIAL AND PROCESS APPLICATIONS - LAND, SEA, AIR,
     SPACE; PROCEEDINGS OF THE TWENTY-SIXTH NATIONAL SYMPOSIUM
     AND EXHIBITION, LOS ANGELES, CA, APRIL 28-30, 1981
     810000 Symposium and Exhibition sponsored by the Society
     for the Advancement of Material and Process Engineering.
     Azusa, CA, Society for the Advancement of Material and
     Process Engineering (Science of Advanced Materials and
     Process Engineering Series. Volume 26), 1981. 891 p
     (For individual items see A81-44327 to A81-44398) 891 p.
     Jpn. 3644 $60

39. 81A44339 NASA Issue 21 Category 24
    ELECTRICAL CHARACTERISTICS OF CARBON/GRAPHITE FIBER
    COMPOSITES
    Delmonte, J.
    810000 In: Material and process applications - Land,
    sea, air, space; Proceedings of the Twenty-Sixth
    National Symposium and Exhibition, Los Angeles, CA,
    April 28-30, 1981. (A81-44326 21-23) Azusa, CA, Society
    for the Advancement of Material and Process Engineering,
    1981, p. 179-185. 7 p. Refs. 6 Jpn. 3645

40. 81N24183 NASA Issue 15 Category 24
    CATALYZED COMBUSTION OF CARBON FIBERS FROM CARBON
    FIBER-RESIN COMPOSITES
    Final Report, Oct. 1977 - Oct. 1980
    Ganjei, J.; Dominguez, D.; Mackey, J.; Murday, J.
    Naval Research Lab., Washington, D.C. (NS999791)
    AD-A098046; NRL-MR-4486 810422, 22 April 1981,
    WF61542001 76 p. Jpn. 2026 HC A05/MF A01

41. 81N26126 NASA Issue 17 Category 5
    HELICOPTER FATIGUE LIFE ASSESSMENT
    Advisory Group for Aerospace Research and
    Development, Neuilly-Sur-Seine (France) (AD455458)
    AGARD-CP-297; ISBN-92-835-0289-2 810300, March 1981,
    Partly in ENGLISH and FRENCH Proc. of 51st meeting
    held in Aix-en-Provence, France, 14-19 Sep. 1980
    261 p. Jpn. 2299 HC A12/MF A01

42. 81N26132 NASA Issue 17 Category 5
    COMBAT DAMAGE ASSESSMENT
    Carper, C. H., Jr.
    Army Aviation Research and Development Command,
    Fort Eustis, Va. (AZ143130)
    810300, March 1981, Applied Technology Lab. In
    AGARD Helicopter Fatigue Life Assessment 20 p
    (SEE N81- 26126 17-05) 19 p. Jpn. 2299 HC A12/MF A01

43. 82N12143 NASA Issue 3 Category 24
    EFFECT OF FIGHTER ATTACK SPECTRUM ON COMPOSITE
    FATIGUE LIFE
    Final Report, Sep. 1978 - Oct. 1980
    Badaliance, R.; Dill, H. D.
    McDonnell Aircraft Co., St. Louis, Mo. (MP532498)
    AD-A105034; AFWAL-TR-81-3001 810300, March 1981,
    F33615-78-C-3218; AF PROJ. 2401 126 p. Jpn. 304
    HC A07/MF A01

44. 80A38727 NASA Issue 16 Category 12
    MATERIALS AND PROCESSES FOR USE IN SPACE TECHNOLOGY -
    Russian Book Materialy i protsessy kosmicheskoi tekhnologii
    Okhotin, A. S.
    800000 Moscow, Izdatel'stvo Nauka, 1980. 232 p. In
    Russian. (For individual items see A80-38728 to A80-38762) 232 p.

45. 80A38759 NASA Issue 16 Category 24
    ELASTIC RIBBONS BASED ON THERMALLY STABLE LOW-MODULUS FIBERS
    FOR THE AUTOCLAVELESS FORMING OF GLASS-PLASTIC AIRCRAFT
    COMPONENTS
    Elastichnye lenty na osnove termostoikikh nizkomodul nykh
    volokon dlia bezavtoklavnogo formovaniia stekloplastikovykh
    izdelii letatel nykh apparatov
    Kuzmin, V. V.; Kernasovskii, I.S.
    800000 In: Materials and processes for use in space
    technology. (A80-38727 16-12) Moscow, Izdatel'stvo Nauka,
    1980, p. 203-207. In Russian. 5 p.

46. 80A52999 NASA Issue 24 Category 39
    BUCKLING OF ANTISYMMETRIC CROSS- AND ANGLE-PLY LAMINATED PLATES
    Sharma, S.; Iyengar, N.G.R.; Murthy, P. N.
    800000 International Journal of Mechanical Sciences, Vol. 22,
    No. 10, 1980, p. 607-620. AA(Punjab Engineering College,
    Chandigarh, India) AC(Indian Institute of Technology, Kanpur,
    India) 14 p. Refs. 20 Jpn. 4367

47. 81N27208 NASA Issue 18 Category 24
DEVELOPMENT OF A CFC WINDOW FRAME, USING SHORT FIBER PRESSING TECHNOLOGY -
JET AIRCRAFT CABIN WINDOWS
Final Report
Heinze, F.; Stemmer, G.
Messerschmitt-Boelkow-Blohm G.m.b.H., Hamburg (West Germany). (MT615389)
BMFT-FB-W-80-032; ISSN-0170-1339, Dec. 80, 801200 Unternehmensbereich.
Sponsored by Bundesministerium fuer Forschung und Technologie. In German;
English summary 123 p. Bonn Bundesministerium fuer Forschung und Technologie
Jpn. 2450 HC A06/MF A01

48. 82A10867 NASA Issue 1 Category 38
AN ACOUSTIC EMISSION ENERGY ANALYSIS AND ITS USE TO STUDY DAMAGE IN
LAMINATED COMPOSITES
Mohan, R.; Prathap, G.
801200 Journal of Nondestructive Evaluation, Vol. 1, Dec. 1980, p. 225-233.
AB (National Aeronautical Laboratory, Bangalore, India) 9 p. Refs. 14 Jpn. 65

49. 82A10871 NASA Issue 1 Category 38
STRESS-WAVE ATTENUATION IN THIN STRUCTURES BY ULTRASONIC THROUGH-TRANSMISSION
Lee, S. S.; Williams, J.H. JR.
Massachusetts Inst. of Tech., Cambridge. (MJ700802)
801200 Journal of Nondestructive Evaluation, Vol. 1, Dec. 1980, p. 277-285.
NASA-supported research. AB (MIT, Cambridge, MA) 9 p. Refs. 21, Jpn. 65

50. 82A12646 NASA Issue 2 Category 24
KEVLAR COMPOSITES; PROCEEDINGS OF THE SYMPOSIUM, EL SEGUNDO, CA. DECEMBER 2,
1980
800000 Symposium sponsored by the Technology Conferences. El Segundo, CA,
Technology Conferences, 1980. 96 p. (For individual items see A82-12647 to
A82-12650) 96 p. $24

51. 82A12648 NASA Issue 2 Category 54
KEVLAR ARAMID COMPOSITES IN LIFE-SAVING EQUIPMENT - HELMETS FOR FIGHTER AIRCRAFT
CREWS
Van Haastert, J.A; Rosenberg, I.
800000 In: Kevlar composites; Proceedings of the Symposium, El Segundo, CA,
December 2, 1980. (A82-12646 02-24) El Segundo, CA, Technol Conferences,
1980, p. 52-57. AB (A-T-O, Inc., Scott Aviation Div., Sierr dre, CA) 6 p.

52. 82A12649 NASA Issue 2 Category 37
KEVLAR ARAMID COMPOSITES IN PRESSURE VESSELS/TANKS
Morris, E. E.
800000 In: Kevlar composites; Proceedings of the Symposium, El Segundo, CA,
December 2, 1980. (A82-12646 02-24) El Segundo, CA, Technology Conferences,
1980, p. 58-84. AA (Structural Composites Industries, Inc., Azusa, CA) 27 p.
Refs. 11

53. 81A19300 NASA Issue 6 Category 5
HINGELESS TAILROTOR IN FIBER COMPOSITE CONSTRUCTION AND VIBRATION-ISOLATION
SYSTEMS /ARIS, ASIS/ FOR HELICOPTERS
Gelenkloser Heckrotor in Faserverbund-Bauweise und Schwingungs-Isolations-
systeme /ARIS, ASIS/ fuer Hubschrauber
Reichert, G.
MBB-UD-311-80-O 801000 Bundesministerium fuer Forschung und Technologie,
Statusseminar zur Luftfahrtforschung und Luftfahrttechnologie, Garmisch-
Partenkirchen, West Germany, Oct. 8, 9, 1980. Paper. 35 p. In German.
AA (Messerschmitt-Boelkow-Blohm GmbH, Munich, West Germany) 35 p. Refs. 8

54. 81N27206 NASA Issue 18 Category 24
ANALYSIS OF COMPOSITE LAMINATES AND FIBER COMPOSITE REPAIR SCHEMES
Jones, R.
Aeronautical Research Labs., Melbourne (Australia). (AF441057)
AD-A099629; ARL/Struc-Note-465; Oct 80, AR-002-236 801000 17 p. Jpn.
2449 HC A02/MF A01

55. 81N16144 NASA Issue 7 Category 24
ELECTROMAGNETIC EFFECTS OF (CARBON) COMPOSITE MATERIALS UPON AVIONICS SYSTEMS
Stringer, F.S.
Advisory Group for Aerospace Research and Development, Neuilly-Sur-Se_ne
(France). (AD455458)
AGARD-CP-283; ISBN-92-835-0277-9 801000, Oct 1980, Partly in English and
French. Conf held at 39th Tech. Meeting of the Avionics Panel of AGARD,
Lisbon, 16-19 Jun. 1980. AA(RAE, Farnborough, England) 369 p. Jpn. 872
HC A16/MF A01

56. 81N16154 NASA Issue 7 Category 24
THE UK MINISTRY OF DEFENCE PROGRAMME ON THE ELECTROMAGNETIC PROPERTIES OF
CARBON FIBER COMPOSITES
Thomson, J.M.; Evans, R.H.
Royal Aircraft Establishment, Farnborough (England). (R2785060)
801000, Oct. 1980, In AGARD Electromagnetic Effects of (Carbon) Composite
Mater. Upon Avionics Systems 9 p (See N81-16144 07-24) 9 p. Jpn. 874
HC A16/MF A01

57. 81N16153 NASA Issue 7 Category 24
THE ELECTRICAL EFFECTS OF JOINTS AND BONDS IN CARBON FIBER COMPOSITES
Brettle, J.; ! dge, K.J.; Poole, R.
Allen Clark Research Centre, Towcester (England). (AM808939)
801000, Oct. 1980, In AGARD Electromagnetic Effects of (Carbon) Composite
Mater. Upon Avionics Systems 17 p (See N81-16144 07-24) AC (Plessey
Electronic Systems Research, Havant, England) 17 p. Jpn. 874 HC A16/MF A01

58. 80A34840 NASA Issue 14 Category 5
CURRENT AND PROJECTED USE OF CARBON COMPOSITES IN UNITED STATES AIRCRAFT
Leonard, R.W.; Mulville, D.R.
National Aeronautics and Space Administration. Langley Research Center,
Langley Station, Va. (ND210491)
800600 NATO, AGARD, Specialists Meeting on Electromagnetic Effects of Carbon
Composite Materials upon Avionics Systems, Lisbon, Portugal, June 16-19, 1980,
Paper. 31 p. AA(NASA, Langley Research Center, Hampton, Va.) AB (U.S. Navy,
Naval Air Systems Command, Washington, D.C.) 31 p. Refs. 19 Jpn. 2492

59. 80A36547 NASA Issue 15 Category 24
COMPOSITES IN FUTURE TRANSPORTS. I - NON-METALLICS
Cole, R.T.; Meade, L.E.
800800, Aug. 1980, Lockheed Horizons, Summer 1980, p. 3-12. AB (Lockheed-
Georgia Co., Marietta, Ga.) 10 p. Jpn. 2695

60. 80A51486 NASA Issue 23 Category 24
COMPOSITES IN FUTURE TRANSPORTS. II - METALLICS
Cole, R.T.; Meade, L.E.; Bates, W.F.
801100, Nov. 1980, Lockheed Horizons, Fall 1980, p. 31-36. AC(Lockheed-Georgia
Co., Marietta, Ga.) 6 p. Jpn. 4197

61. 82A12026 NASA Issue 2 Category 39
EMERGING TECHNOLOGIES IN AEROSPACE STRUCTURES, DESIGN, STRUCTURAL DYNAMICS
AND MATERIALS; PROCEEDINGS OF THE AEROSPACE CONFERENCE, SAN FRANCISCO, CA
AUGUST 13-15, 1980
Vinson, J.R.
800000 Conference sponsored by the American Society of Mechanical Engineers,
New York, American Society of Mechanical Engineers, 1980. 333 p. (For
individual items see A82-12027 to A82-12045) AA(Delaware, University, Newark, DE)
333 p. $20.

62. 82A12028 NASA Issue 2 Category 39
IMPACT-INITIATED DAMAGE THRESHOLDS IN COMPOSITES
Sharma, A.V.
North Carolina Agricultural and Technical State Univ., Greensboro. (N346518)
800000 NSG-1296 In: Emerging technologies in aerospace structures, design,
structural dynamics and materials; Proceedings of the Aerospace Conference,
San Francisco, CA, August 13-15, 1980. (A82-12026 02-39) New York, American
Society of Mechanical Engineers, 1980, p. 11-26. AA(North Carolina Agricultural
and Technical State University, Greensboro, NC) 16 p. Refs. 10

END

FILMED

DTIC
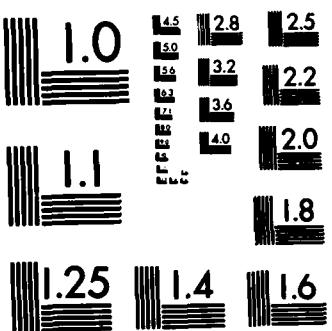
MICROCOPY RESOLUTION TEST CHART

NATIONAL BUREAU OF STANDARDS-1963-A

63. 82A12029 NASA Issue 2 Category 24
MECHANICAL BEHAVIOR OF HYBRID COMPOSITES
CHOU, T.W.
800000 In: Emerging technologies in aerospace structures, design
structural dynamics and materials; Proceedings of the Aerospace
Conference, San Francisco, CA, August 13-15, 1980. (A82-12026 02-39)
New York, American Society of Mechanical Engineers, 1980, p. 27-36.
AA(Delaware, University, Newark, DE) 10 p. Refs. 7

64. 82A12030 NASA Issue 2 Category 24
SIZE EFFECT ON STRENGTH AND FATIGUE OF A SHORT FIBER COMPOSITE MATERIAL
Wang, A.S.D.; Tung, R.W.; Sanders, B.A.
800000 In: Emerging technologies in aerospace structures, design
structural dynamics and materials; Proceedings of the Aerospace
Conference, San Francisco, CA, August 13-15, 1980. (A82-12026 02-39)
New York, American Society of Mechanical Engineers, 1980, p. 37-52.
Research supported by the General Motors Corp. AA (Drexel University,
Philadelphia, PA) AC (GM Technical Center, Warren, MI) 16 p. Refs. 9

65. 82A12032 NASA Issue 2 Category 39
ON THE STATE OF TECHNOLOGY IN ADHESIVELY BONDED JOINTS IN COMPOSITE
MATERIAL STRUCTURES
Vinson, J.R.
800000 In: Emerging technologies in aerospace structures, design,
structural dynamics and materials; Proceedings of the Aerospace
Conference, San Francisco, CA, August 13-15, 1980. (A82-12026 02-39)
New York, American Society of Mechanical Engineers, 1980, p. 67-85
AA (Delaware, University, Newark, DE) 19 p. Refs. 62

66. 80N28436 NASA Issue 19 Category 24
SELECTED NASA RESEARCH IN COMPOSITE MATERIALS AND STRUCTURES
National Aeronautics and Space Administration. Langley Research
Center, Hampton, Va. (ND210491)
NASA-CP-2142; L-13915 800000 Presented at the 2d Ind. Rev. of the NASA
Aircraft Energy Efficiency (ACEE) Composite Programs, Seattle, 11-13
Aug. 1980 237 p. Jpn. 2534 HC A15/MF A01

67. 81N11128 NASA Issue 2 Category 24
EFFECT OF SERVICE ENVIRONMENT ON COMPOSITE MATERIALS
Advisory Group for Aerospace Research and Development, Neuilly-Sur-Seine
(France). (AD455458)
AGARD-CP-288; ISBN-92-835-0273-6, Aug. 1980, 800800 In English; partly in
French. Presented at the 50th Meeting of the AGARD Struct. and Mater. Panel,
Athens, 14-17 April 1980 326 p. Jpn. 170 HC A15/MF A01.

68. 81N11129 NASA Issue 2 Category 24
THE IMPLICATIONS OF LABORATORY ACCELERATED CONDITIONING OF CARBON FIBRE
COMPOSITES
Edge, E.C.
British Aerospace Aircraft Group, Preston (England). (BX275659)
800800, Aug 1980, Advanced Structural Applications Dept. In AGARD Effect of
Serv. Environ. on Composite Mater. 17 p. (See N81-11128 02-24) 17 p.
Jpn. 170 HC A15/MF A01

69. 81N11137 NASA Issue 2 Category 24
RELATIONSHIPS BETWEEN IMPACT RESISTANCE AND FRACTURE TOUGHNESS IN ADVANCED
COMPOSITE MATERIALS
Dorey, G.
Royal Aircraft Establishment, Farnborough (England). (R2785060)
800800, Aug. 1980, Materials Dept. In AGARD Effects of Serv. Environ. on
Composite Mater. 11 p. (See N81-11128 02-24) 11 p. Jpn. 171 HC A15/MF A01

70. 81N11145 NASA Issue 2 Category 24
FATIGUE AND DAMAGE PROPAGATION IN COMPOSITE ROTOR BLADES
Barnard, A.J.
Westland Helicopters Ltd., Yeovil (England). (WW895582)
800800,Aug. 1980, In AGARD Effect of Serv. Environ. on Composite Mater.
17 p. (See N81-11128 02-24) Sponsored by Ministry of Defence, England 17 p.
Jpn. 172 HC A15/MF A01

71. 81A27885 NASA Issue 11 Category 5
APPLICATIONS OF CARBON FIBRE COMPOSITES TO MILITARY AIRCRAFT STRUCTURES
Sharples, T.
800700 (Royal Aeronautical Society, Symposium on Large Scale Composite
Structures, London, England, Apr. 22, 1980) Aeronautical Journal, Vol. 84,
July 1980, p. 177-182. AA (British Aerospace, Aircraft Group, Preston,
Lancs., England) 6 p. Jpn. 1750

72. 81N15108 NASA Issue 6 Category 27
COUPLE-STRESS EFFECTS IN THE TWO-DIMENSIONAL PROBLEM FOR CROSS-PLY
LAMINATES
Partsevskii, V.V.
Royal Aircraft Establishment, Farnborough (England). (R2785060)
RAE-LIB-TRANS-2046 800600,June 1980, Transl. into English from Mekhan.
Kompozitnykh Materialov (USSR), No. 1, 1979, p 46-50 12 p. Jpn. 727 HC
A02/MF A01

73. 80A37289 NASA Issue 15 Category 39
DETERMINING STRESS INTENSITY FACTORS IN COMPOSITE STRUCTURAL
ELEMENTS
Grishin, V.I.; Medvedev, B.M.
800600 (Problemy Prochnosti, Oct. 1979, p. 61-64) Strength of Materials,
Vol. 11, No. 10, June 1980, p. 1134-1137. Translation. AB(Tsentral'nyi
Aerogidrodinamicheskii Institut, Moscow, USSR) 4 p. Refs. 6. Jpn. 2764

74. 80A34993 NASA Issue 14 Category 39
Structures, Structural Dynamics, and Materials Conference, 21st, Seattle,
Wash., May 12-14, 1980, Technical Papers Parts 1 and 2.
800000 Conference sponsored by AIAA, ASME, ASCE and AHS. New York, American
Institute of Aeronautics and Astronautics, Inc., 1980. Pt.1, 535 p.
Pt.2, 523 p. (For individual items see A80-34994 to A80-35107) 1058 p.
Jpn. 2559 Members $75.; Nonmembers $100.

75. 80A35077 NASA Issue 14 Category 5
AEROELASTIC TAILORING OF FORWARD SWEPT COMPOSITE WINGS
Weisshaar, T.A.
AIAA 80-0795 800000 F33615-79-C-3224; AF-AFOSR-77-3423D In:
Structures, Structural Dynamics, and Materials Conference, 21st Seattle,
Wash., May 12-14, 1980, Technical Papers. Part 2. (A80-34993 14-39)
New York, American Institute of Aeronautics and Astronautics, Inc., 1980,
p. 761-770. AA (Virginia Polytechnic Institute and State University,
Blacksburg, Va.) 10 p. Refs. 12 Jpn. 2494

76. 80A47200 NASA Issue 20 Category 37
FABRICATION TECHNIQUES FOR ADVANCED REINFORCED PLASTICS; PROCEEDINGS OF
THE SYMPOSIUM, UNIVERSITY OF SALFORD, SALFORD, LANCS., ENGLAND, APRIL 22, 23,
1980.
800000 Symposium sponsored by James Carr and Sons, Courtaulds, Ltd.,
Fothergill and Harvey, Ltd., et al. Guildford, Surrey, England, IPC
Science and Technology Press, Ltd., 1980. 122 p. (For individual items
see A80-47201 to A80-47211) 122 p.

77. 80A35771 NASA Issue 14 Category 24
TECHNOLOGY OF GRAPHITE-RESIN COMPOSITE MATERIALS AND THEIR APPLICATION IN
THE AERONAUTICAL INDUSTRY
Tecnologia dei materiali compositi grafite-resina'e loro applicazioni
nell'industria aeronautica
Romeo, G.
800400 (AIAS, Convegno Nazionale, 7th, Cagliari, Italy, Sept. 1979)
Ingegneria, Mar.-Apr. 1980, p. 80-101. In Italian. AA (Torino,
Politecnico, Turin, Italy) 22 p. Jpn. 2511

78. 80N18106 NASA Issue 9 Category 24
APPLICATION OF COMPOSITE MATERIALS TO TURBOFAN ENGINE FAN EXIT GUIDE
VANES
Smith, G.T.
National Aeronautics and Space Administration. Lewis Research Center,
Cleveland, Ohio. (ND315753)
NASA-TM-81432; E-356 800000 Presented at 35th Ann. Conf. of the Reinforced
Plastics/Composite Inst., New Orleans, 4-8 Feb. 1980; sponsored by Soc.
of Plastics Industries 19 p. Jpn. 1103 HC A02/MF A01

79. 80N18439 NASA Issue 9 Category 39
LITERATURE REVIEW ON THE MECHANICAL BEHAVIOR OF FIBER COMPOSITE MATERIALS.
ANALYSIS OF THE STATE-OF-THE-ART, VOLUME I
Schrifttumsrecherche zum festigkeitsverhalten von-faserverbundwerkstoffen
analyse des standes der-technik - band 1
Gerharz, J. J.; Schuetz, D.
Laboratorium fuer Betriebsfestigkeit, Darmstadt (West Germany). (LD064856)
LBF-TB-145-VOL-1 790000 1979, 436 p. Jpn. 1150 HC A19/MF A01
(81N14003 NASA Issue 5 Category 24
Royal Aircraft Establishment, Farnborough (England). (R2785060)
RAE-LIB-TRANS-2045; BR76376; TB-145 800900, Aug 1980, Transl. into English)

80. 80N18440 NASA Issue 9 Category 39
LITERATURE REVIEW ON THE MECHANICAL BEHAVIOR OF FIBER COMPOSITE MATERIALS.
ANALYSIS OF THE STATE-OF-THE-ART, VOLUME 2: APPENDIX
Schrifttumsrecherche zum festigkeitsverhalten von-fasterverbundwerkstoffen
analyse des standes der-technik - band 2: anhang
Gerharz, J.J.
Laboratorium fuer Betriebsfestigkeit, Darmstadt (West Germany). (LD064856)
LBF-TB-145-VOL-2-APP 790000 1979, 519 p. Jpn. 1150 HC A22/MF A01

81. 80N26405 NASA Issue 17 Category 24
EFFECT OF DEGREE OF ABRASION OF CARBON FIBER COMPOSITE SURFACES ON STRENGTHS
OF ADHESIVE BONDED JOINTS
Stone, M.H.
Royal Aircraft Establishment, Farnborough (England). (R2785060)
RAE-TM-MAT-327; BR71986, Dec. 79, 791200 10 p. London HMSO Jpn. 2239 HC A02/MF
A01

82. 80A34751 NASA Issue 14 Category 23
NEW HORIZONS - MATERIALS AND PROCESSES FOR THE EIGHTIES; PROCEEDINGS OF THE
ELEVENTH NATIONAL CONFERENCE, BOSTON, MASS., NOVEMBER 13-15, 1979
790000 Conference sponsored by the Society for the Advancement of Material and
Process Engineering. Azusa, Calif. (National SAMPE Technical Conference
Series, Volume 11), 1979, 1064 p (For individual items see A80-34752 to
A80-34820) Jpn. 2506

83. 80A34818 NASA Issue 14 Category 24
ADVANCED MISSILE MATERIAL RESPONSE - AERODYNAMIC HEATING AND DEBRIS IMPACT ON
COMPOSITES
Giedt, D.C.; Cohen, L.J.
790000 In: New horizons - Materials and processes for the eighties;
Proceedings of the Eleventh National Conference, Boston, Mass., November
13-15, 1979. (A80-34751 14-23) Azusa, Calif., Society for the Advancement of
Material and Process Engineering, 1979, p. 985-992. AB (McDonnell Douglas
Astronautics Co., Huntington Beach, Calif.) 8 p. Jpn. 2510

84. 81A14251 NASA Issue 3 Category 32
INTERNATIONAL SYMPOSIUM ON ELECTROMAGNETIC COMPATIBILITY, 21ST, SAN DIEGO,
CALIF., OCTOBER 9-11, 1979, PROCEEDINGS.
790000 Symposium sponsored by the Institute of Electrical and Electronics
Engineers. New York, Institute of Electrical and Electronics Engineers, Inc.,
1979. 469 p. (For individual items see A81-14252 to A81-14294) 469 p. Jpn.
310 $26.25

85. 81A14263 NASA Issue 3 Category 32
THE RAE RESEARCH AND DEVELOPMENT PROGRAM ON EMC FOR AIRCRAFT AND
FLIGHT WEAPONS SYSTEMS
Thomson, J.M.
790000 In: International Symposium on Electromagnetic Compatibility,
21st, San Diego, Calif., October 9-11, 1979, Proceedings. (A81-14251
03-32) New York, Institute of Electrical and Electronics Engineers,
Inc., 1979, p. 118-123. AA (Royal Aircraft Establishment, Farnborough,
Hants., England) 6 p. Refs. 12 Jpn. 310

86. 80N18145 NASA Issue 9 Category 25
CARBON AND GRAPHITE. PART 1: CARBON AND GRAPHITE FIBERS AND FIBER
COMPOSITES, VOLUME 4. A BIBLIOGRAPHY WITH ABSTRACTS
Progress Report, Sep. 1977 - Oct. 1979
Reed, W.E.
National Technical Information Service, Springfield, Va. (NM881438)
PB80-802366; NTIS/PS-78/1050; NTIS/PS-77/0844; NTIS/PS-76/0685;
NTIS/PS-75/613; COM-74-11527 791200 Supersedes NTIS/PS-78/1050;
NTIS/PS-77/0844; NTIS/PS-76/0685; NTIS/PS-75/613; COM-74-11527 249 p.
Jpn. 1108 HC $30.00/MF $30.00

87. 80N18144 NASA Issue 9 Category 25
CARBON AND GRAPHITE. PART 2. CARBON AND GRAPHITE COMPOSITES -
EXCLUDING CARBON FIBER COMPOSITES. A BIBLIOGRAPHY WITH ABSTRACTS
Progress Report, 1964 - Oct. 1979
Reed, W.E.
National Technical Information Service, Springfield, Va. (NM881438)
PB80-802374; NTIS/PS-78/1051; NTIS/PS-77/0845; NTIS/PS-76/0686;
NTIS/PS-75/614; COM-74-11527 791200 Supersedes NTIS/PS-78/1051;
NTIS/PS-77/0845; NTIS/PS-76/0686; NTIS/PS-75/614; COM-74-11527 262 p.
Jpn. 1108 HC $30.00/MF $30.00

88. 80A36863 NASA Issue 15 Category 39
OPTIMAL DESIGN STUDIES ON COMPOSITE WINGS WITH STATIC AND DYNAMIC
CONSTRAINTS
Venkayya, V.B.; Harris, T.; Khot, N.S.
AAAF Paper NT 79-29 790600 Association Aeronautique et Astronautique
de France, Congres International Aeronautique, 14th, Paris, France,
June 6-8, 1979, 39 p. AC (USAF, Flight Dynamics Laboratory,
Wright-Patterson AFB, Ohio) 39 p. Jpn. 2762

89. 80A36867 NASA Issue 15 Category 5
CURRENT DEVELOPMENTS IN AIRCRAFT FATIGUE EVALUATION PROCEDURES
Buxbaum, O.; Schuetz, D.
AAAF Paper NT 79-33 790600 Association Aeronautique et Astronautique
de France, Congres International Aeronautique, 14th, Paris, France,
June 6-8, 1979, 32 p. AB (Fraunhofer Gesellschaft zur Foerderung der
angewandten Forschung, Institut fuer Betriebsfestigkeit, Darmstadt,
West Germany) 32 p. Refs. 24 Jpn. 2676

90. 80A36876 NASA Issue 15 Category 5
FIBER STRUCTURES ON THE MIRAGE 2000 AND MIRAGE 4000
STRUCTURES FIBRES SUR MIRAGE 2000 ET MIRAGE 4000
Peyrony, M.
AAAF Paper NT 79-44 790600 Association Aeronautique et Astronautique
de France, Congres International Aeronautique, 14th, Paris, France,
June 6-8, 1979, 34 p. In French. AA(Avions Marcel Dassault-Breguet
Aviation, Vaucresson, Hauts-de-Seine, France) 34 p. Jpn. 2676

91. 80A36878 NASA Issue 15 Category 24
SPACE STRUCTURE - TODAY AND TOMORROW - CARBON FIBER COMPOSITES FOR
AEROSPACE STRUCTURES
Brunsch, K.
AAAF Paper NT 79-46 790600 Association Aeronautique et Astronautique
de France, Congres International Aeronautique, 14th, Paris, France,
June 6-8, 1979, 11 p. AA(Messerschmitt-Bolkow-Blohm GmbH, Ottobrunn,
West Germany) 11 p. Jpn. 2695.

AUTHOR INDEX

AUTHOR	REFERENCE NO.
Babaevskii, P.G.	14
Badaliance, R.	43
Barnard, A.J.	70
Brettle, J.	57
Brunsch, K.	91
Buxbaum, O.	89
Carper, C.H. Jr.	42
Chou, T.W.	63
Cohen, L.J.	83
Cole, R.T.	59, 60
Collins, R.M.	18
Cosner, A.A.	36
Crews, J.H. Jr.	4
Delmonte, J.	39
Dill, H.D.	43
Dominguez, D.	40
Dorey, G.	69
Edge, E.C.	68
Evans, R.H.	56
Fughii, T.	7
Fukuda, T.	7
Ganjei, J.	40
Gerharz, J.J.	79, 80
Giedt, D.C.	83
Grishin, V.I.	73
Guniaev, G.M.	15, 17
Hampey, J.M.	35
Han, L.S.	36
Harel, H.	21
Harris, T.	88
Hauffe, K.	31
Hayashi, I.	8
Heinze, F.	47
Herakovich, C.T.	32
Iyengar, N.G.R.	46
Jones, D.L.	23
Jones, R.	54
Karpinos, D.M.	11
Kernasovskii, I.S.	45
Khoroshilova, I.P.	15
Kobets, L.P.	13
Kong, E.S.W.	24
Kunugi, M.	6
Kuzmin, V.V.	45
Laird, B.	34
Lee, L.J.	22
Lee, S.S.	49
Lenain, J.C.	37
Leonard, R.W.	58
Liebowitz, H.	23
Lodge, K.J.	57
Manokhin, A.I.	9
Manuilov, V.F.	12
Marker, L.F.	22
Mashinskaia, G.P.	10
Meade, L.E.	59, 60
Medvedev, B.M.	73
Mohan, R.	48
Morris, E.E.	52
Mulville, D.R.	58
Natarajan, R.	5
Okhotin, A.S.	44
Panda, S.	5
Partsevskii, V.V.	72
Pater, R.H.	25
Perov, B.V.	10
Peyrony, M.	90
Phelps, M.L.	19
Prathap, G.	48
Pritchard, G.	20
Raju, I.S.	4
Reed, W.E.	86, 87
Reichert, G.	53
Rhoades, G.V.	20
Rhodes, M.D.	26

AUTHOR	REFERENCE NO.
Ritter, L.C.	2
Roman, I.	21
Romeo, G.	77
Rosenberg, I.	51
Rumiantsev, A.F.	17
Schuetz, D.	79, 89
Sharma, A.V.	62
Sharma, S.	46
Sharples, T.	71
Shibanuma, K.	8
Smith, G.T.	78
Sorina, T.G.	16
Springer, G.S.	1
Stemmer, G.	47
Stern, B.A.	29
Stone, M.H.	81
Stringer, F.S.	55
Surgucheva, A.I.	16
Thomas, G.R.	3
Thomson, J.M.	56, 85
Tikhonov, A.S.	12
Trostianskaia, E.B.	14
Tuchinskii, L.I.	11
Tung, R.W.	64
Van Haastert, J.A.	51
Venkayya, V.B.	88
Vinson, J.R.	61, 65
Visser, T.	29
Wang, A.S.D.	64
Webb, J.H.	27
Weisshaar, T.A.	75
Weitsman, Y.	33
Williams, J.G.	26
Williams, J.H. Jr.	49
Woodley, G.E.	28

REPORT DOCUMENTATION PAGE

1. Recipient's Reference	2. Originator's Reference	3. Further Reference	4. Security Classification of Document
	AGARD-LS-124	ISBN 92-835-1436-X	UNCLASSIFIED

5. Originator	Advisory Group for Aerospace Research and Development North Atlantic Treaty Organization 7 rue Ancelle, 92200 Neuilly sur Seine, France

6. Title	PRACTICAL CONSIDERATIONS OF DESIGN, FABRICATION AND TESTS FOR COMPOSITE MATERIALS

7. Presented at a Lecture Series under the sponsorship of the Structures and Materials Panel and the Consultant and Exchange Programme of AGARD on 11–12 October 1982 in Oporto, Portugal, 14–15 October 1982 in London, UK, and 18–19 October 1982 in Ankara, Turkey.

8. Author(s)/Editor(s)	9. Date
Various	September 1982

10. Author's/Editor's Address	11. Pages
Various	206

12. Distribution Statement	This document is distributed in accordance with AGARD policies and regulations, which are outlined on the Outside Back Covers of all AGARD publications.

13. Keywords/Descriptors

Composite materials	Stress analysis
Design criteria	Quality assurance
Fabrication	Inspection
Manufacturing	Test procedures
Tooling	

14. Abstract

The lectures are directed to the practical application of composites to structures. The scope includes a lecture on design considerations involving material selection, fabrication techniques, and tooling concepts. Stress analysis is covered including knockdown factors, load transfer concepts and analytical techniques. The Lecture Series concludes with a lecture on qualification requirements and practical consideration in inspection and testing techniques. These lectures are not geared to the day-to-day developments at the very forefront of technology, but rather to state-of-the-art concepts, techniques, and materials that when combined will assure a high probability of success in achieving design goals for cost as well as weight savings.

AGARD Lecture Series No.124 Advisory Group for Aerospace Research and Development, NATO PRACTICAL CONSIDERATIONS OF DESIGN, FABRICATION AND TESTS FOR COMPOSITE MATERIALS Published September 1982 206 pages The lectures are directed to the practical application of composites to structures. The scope includes a lecture on design considerations involving material selection, fabrication techniques, and tooling concepts. Stress analysis is covered including knockdown factors, load transfer concepts and analytical techniques. The Lecture Series concludes with a lecture on qualification P.T.O.	AGARD-LS-124 Composite materials Design criteria Fabrication Manufacturing Tooling Stress analysis Quality assurance Inspection Test procedures
AGARD Lecture Series No.124 Advisory Group for Aerospace Research and Development, NATO PRACTICAL CONSIDERATIONS OF DESIGN, FABRICATION AND TESTS FOR COMPOSITE MATERIALS Published September 1982 206 pages The lectures are directed to the practical application of composites to structures. The scope includes a lecture on design considerations involving material selection, fabrication techniques, and tooling concepts. Stress analysis is covered including knockdown factors, load transfer concepts and analytical techniques. The Lecture Series concludes with a lecture on qualification P.T.O.	AGARD-LS-124 Composite materials Design criteria Fabrication Manufacturing Tooling Stress analysis Quality assurance Inspection Test procedures
AGARD Lecture Series No.124 Advisory Group for Aerospace Research and Development, NATO PRACTICAL CONSIDERATIONS OF DESIGN, FABRICATION AND TESTS FOR COMPOSITE MATERIALS Published September 1982 206 pages The lectures are directed to the practical application of composites to structures. The scope includes a lecture on design considerations involving material selection, fabrication techniques, and tooling concepts. Stress analysis is covered including knockdown factors, load transfer concepts and analytical techniques. The Lecture Series concludes with a lecture on qualification P.T.O.	AGARD-LS-124 Composite materials Design criteria Fabrication Manufacturing Tooling Stress analysis Quality assurance Inspection Test procedures
AGARD Lecture Series No.124 Advisory Group for Aerospace Research and Development, NATO PRACTICAL CONSIDERATIONS OF DESIGN, FABRICATION AND TESTS FOR COMPOSITE MATERIALS Published September 1982 206 pages The lectures are directed to the practical application of composites to structures. The scope includes a lecture on design considerations involving material selection, fabrication techniques, and tooling concepts. Stress analysis is covered including knockdown factors, load transfer concepts and analytical techniques. The Lecture Series concludes with a lecture on qualification P.T.O.	AGARD-LS-124 Composite materials Design criteria Fabrication Manufacturing Tooling Stress analysis Quality assurance Inspection Test procedures

requirements and practical consideration in inspection and testing techniques. These lectures are not geared to the day-to-day developments at the very forefront of technology, but rather to state-of-the-art concepts, techniques, and materials that when combined will assure a high probability of success in achieving design goals for cost as well as weight savings.

The material in this publication was assembled to support a Lecture Series under the sponsorship of the Structures and Materials Panel and the Consultant and Exchange Programme of AGARD presented on 11–12 October 1982 in Oporto, Portugal, 14–15 October 1982 in London, UK, and 18–19 October 1982 in Ankara, Turkey.

requirements and practical consideration in inspection and testing techniques. These lectures are not geared to the day-to-day developments at the very forefront of technology, but rather to state-of-the-art concepts, techniques, and materials that when combined will assure a high probability of success in achieving design goals for cost as well as weight savings.

The material in this publication was assembled to support a Lecture Series under the sponsorship of the Structures and Materials Panel and the Consultant and Exchange Programme of AGARD presented on 11–12 October 1982 in Oporto, Portugal, 14–15 October 1982 in London, UK, and 18–19 October 1982 in Ankara, Turkey.

requirements and practical consideration in inspection and testing techniques. These lectures are not geared to the day-to-day developments at the very forefront of technology, but rather to state-of-the-art concepts, techniques, and materials that when combined will assure a high probability of success in achieving design goals for cost as well as weight savings.

The material in this publication was assembled to support a Lecture Series under the sponsorship of the Structures and Materials Panel and the Consultant and Exchange Programme of AGARD presented on 11–12 October 1982 in Oporto, Portugal, 14–15 October 1982 in London, UK, and 18–19 October 1982 in Ankara, Turkey.

requirements and practical consideration in inspection and testing techniques. These lectures are not geared to the day-to-day developments at the very forefront of technology, but rather to state-of-the-art concepts, techniques, and materials that when combined will assure a high probability of success in achieving design goals for cost as well as weight savings.

The material in this publication was assembled to support a Lecture Series under the sponsorship of the Structures and Materials Panel and the Consultant and Exchange Programme of AGARD presented on 11–12 October 1982 in Oporto, Portugal, 14–15 October 1982 in London, UK, and 18–19 October 1982 in Ankara, Turkey.

FILMED

2-83

DTIC